ARISTOTLE UNIVERSITY OF THESSALONIKI
FACULTY OF SCIENCES
SCHOOL OF GEOLOGY

IOANNIS ALEXANDRIDIS
MSc Geologist

CONTRIBUTION TO THE UNDERSTANDING OF THE GEOLOGICAL STRUCTURE AND PETROLEUM SYSTEMS OF EPIRUS WITH INTEGRATION OF FIELD GEOLOGY AND ORGANIC GEOCHEMISTRY METHODS

DISSERTATION THESIS

THESSALONIKI
2023

ΑΡΙΣΤΟΤΕΛΕΙΟ ΠΑΝΕΠΙΣΤΗΜΙΟ ΘΕΣΣΑΛΟΝΙΚΗΣ

ΣΧΟΛΗ ΘΕΤΙΚΩΝ ΕΠΙΣΤΗΜΩΝ
ΤΜΗΜΑ ΓΕΩΛΟΓΙΑΣ

ΙΩΑΝΝΗΣ ΑΛΕΞΑΝΔΡΙΔΗΣ
MSc Γεωλόγος

ΣΥΜΒΟΛΗ ΣΤΗΝ ΚΑΤΑΝΟΗΣΗ ΤΗΣ ΓΕΩΛΟΓΙΚΗΣ ΔΟΜΗΣ ΚΑΙ ΤΩΝ ΠΕΤΡΕΛΑΪΚΩΝ ΣΥΣΤΗΜΑΤΩΝ ΤΗΣ ΗΠΕΙΡΟΥ ΜΕ ΣΥΝΔΥΑΣΜΟ ΜΕΘΟΔΩΝ ΓΕΩΛΟΓΙΑΣ ΠΕΔΙΟΥ ΚΑΙ ΟΡΓΑΝΙΚΗΣ ΓΕΩΧΗΜΕΙΑΣ

ΔΙΔΑΚΤΟΡΙΚΗ ΔΙΑΤΡΙΒΗ

ΘΕΣΣΑΛΟΝΙΚΗ
2023

ΙΩΑΝΝΗΣ ΑΛΕΞΑΝΔΡΙΔΗΣ
MSc Γεωλόγος

CONTRIBUTION TO THE UNDERSTANDING OF THE GEOLOGICAL STRUCTURE AND PETROLEUM SYSTEMS OF EPIRUS WITH INTEGRATION OF FIELD GEOLOGY AND ORGANIC GEOCHEMISTRY METHODS

Εκπονήθηκε στον Τομέα Ορυκτολογίας-Πετρολογίας-Κοιτασματολογίας του Τμήματος Γεωλογίας Α.Π.Θ. Υποβλήθηκε στο Τμήμα Γεωλογίας Α.Π.Θ. τον Νοέμβριο του 2023

Ημερομηνία Προφορικής Εξέτασης: 15/11/2023

Αριθμός Παραρτήματος Επιστημονικής Επετηρίδας Τμήματος Γεωλογίας N°: 244

[λαμβάνεται από το Γραμματεία]

<u>Τριμελής Συμβουλευτική Επιτροπή</u>

Καθηγητής Ανδρέας Ν. Γεωργακόπουλος, Επιβλέπων
Καθηγητής Δημήτριο Γουρνής, Μέλος Τριμελούς Συμβουλευτικής Επιτροπής
Επικ. Καθηγήτρια Σοφία Πεχλιβανίδου, Μέλος Τριμελούς Συμβουλευτικής Επιτροπής

<u>Εξεταστική Επιτροπή</u>

Καθηγητής Ανδρέας Ν. Γεωργακόπουλος
Καθηγητής Δημήτριος Γουρνής
Επικ. Καθηγήτρια Σοφία Πεχλιβανίδου
Αναπλ. Καθηγητής Σταύρος Καλαϊτζίδης
Καθηγητής Βασίλειος Μέλφος
Επικ. Καθηγητής Ερνέστος Σαρρής
Καθηγητής Lorenz Schwark

Citation:

Alexandridis I., 2023. – Contribution to the understanding of the geological structure and petroleum systems of Epirus with integration of field geology and organic geochemistry methods. Ph.D. Thesis, School of Geology, Aristotle University of Thessaloniki, Annex Number of Scientific Annals of the School of Geology No 244, 235 pp.

Αλεξανδρίδης Ι., 2023. – Συμβολή στην κατανόηση της γεωλογικής δομής και των πετρελαϊκών συστημάτων της Ηπείρου με συνδυασμό μεθόδων γεωλογίας πεδίου και οργανικής γεωχημείας. Διδακτορική Διατριβή, Τμήμα Γεωλογίας Α.Π.Θ., Αριθμός Παραρτήματος Επιστημονικής Επετηρίδας Τμ. Γεωλογίας Νο 244, 235 σελ.

Οι απόψεις και τα συμπεράσματα που περιέχονται σε αυτό το έγγραφο εκφράζουν το συγγραφέα και δεν πρέπει να ερμηνευτεί ότι εκφράζουν τις επίσημες θέσεις του Α.Π.Θ.

Εικόνα Εξωφύλλου: «Pantokrator Shale» στην περιοχή των ορέων του Σουλίου.

Table of contents

Table of Figures

Acknowledgements

The completion of this thesis would be unattainable without the support and contribution by several people and the overload of the quest would be unbearable without them.

To all those and each one separately, I express my deepest gratitude.

First, to my life partner, Maria, who relentlessly supported me with limitless love, faith, reassurance, and fortitude. She stoically endured the duty burden I added on her shoulders during my countless hours of absence on the mountains and in front of the laptop screen.

To my supervisor and mentor, professor emeritus Andreas Georgakopoulos who became a heart friend, and supporter of my scientific hypostasis. The fieldwork with him was always a great joy and winding-up in meaningful memories and scientific results.

To the professor Lorenz Schwark, who generously shared his expertise and offered me his valuable companionship during long fieldwork days.

To the professor Kimon Christanis, who taught me to work methodically and stick to the detail and to accuracy. To the associate professor Stavros Kalaitzidis who offered his valuable advice and friendship. To the professors Vasileios Melfos and Dimitrios Gournis, the assistant professors, Sofia Pechlivanidou and Ernestos Sarris, for their meticulous and high-quality review of the thesis.

To Dr. Ioannis Oikonomopoulos, Dr. Thomas Gentzis and Dr. Humberto Carvajal-Ortiz, whose assistance with the analytical laboratory work with the source rock samples comprised the core of this study. Their overall guidance was more than essential in completing this thesis.

To Annie Rassios, whose scholarship supported the pilot field work that led to the formulation of the proposal of this Ph. D thesis.

To the professor Lambrini Papadopoulou who provided guidance with the SEM microscope analyses.

To the Geological Science that motivated me and kept me going in serving it with the highest academic and ethical standards.

Last but not least, to Thanos, who looked after me in difficult times on the mountains and not only, and made me his successful mentor and proudest big brother. To my mother Calliope, my father Thodoris and grandfather "pappous Thanasis", who raised me to be down to earth and fight my battles with uncompromising integrity and dignity.

And,

to my sons, Thodoris and Christos who taught me everything I know.

To all these people, who made me a better person and scientist, this thesis is heartfully dedicated.

Preface

This thesis is the result of a detailed petroleum geological study of Epirus. It is a well-known fact that Epirus exhibits hydrocarbon potential attested by the widespread oil seeping. The present thesis aim is to increase and improve the understanding of the geological structure and petroleum geology of Epirus and the associated hydrocarbon potential. To this end, an extensive fieldwork survey was carried out throughout Epirus in order to collect and evaluate novel data.

The Chapter 1 provides the study rationale, scope and background, as well as a review of the basic principles in the sedimentary basin and petroleum system analysis.

The Chapter 2 provides a brief outline of the geotectonic, geological and petroleum geological background of the study.

The Chapter 3 exhibits the study strategy and the methods used, i.e., field geology, organic petrography and organic geochemistry.

The Chapter 4 provides the study results, namely the detailed lithostratigraphy, the structural elements, the analytical results on the source rocks and bitumens.

In the Chapter 5, the results are synthesized into basin analysis and petroleum system insights and the Chapter 6 summarizes the main conclusions of the study.

The findings provide valuable insights into the petroleum system function and basin evolution, while the discovery of a new source rock of world-class hydrocarbon potential (i.e., the Pantokrator Shale; up to 270 mg HC/g rock) comprise a breakthrough in the understanding of the area, proving that the unlocked potential of the area might be substantial.

Acronyms and Abbreviations

Acronym – abbreviation	Term
HC	Hydrocarbon
PS	Petroleum System
OM	Organic Matter
IZ	Ionian Zone
IZ-I	Ionian Zone – Internal
IZ-C	Ionian Zone – Central
IZ-E	Ionian Zone – External
TOC	Total Organic Carbon
RE6	Rock Eval 6
RE7S	Rock Eval 7S
Fm.	Formation (lithostratigraphic)
Mt.	Mountain
Bbl.	Barrel
BB	Billion Barrels
OIIP	Oil Initially in Place

Acronym – abbreviation	Formation
Brdg.	Burdigalian
Fl.	Flysch
Mrl.T	Transitional Marl
Ls.P-E	Paleocene – Eocene Limestones
Ls.Sen	Senonian Limestones
Sh.V	Vigla Shales
Ls.V	Vigla Limestones
Dol.V	Vigla Dolomites
Sh.PU	Upper Posidonia Shales
Ls.Fil	Filamentous Limestones
Sh.PL	Lower Posidonia Shales
Mrl.B	Basal Marl
Ls.Sin	Siniais Limestones
Ls.P	Pantokrator Limestones
Sh.P	Pantokrator Shales
Dol.P	Pantokrator Dolomites
Ls.Fp	Foustapidima Limestones
TCB	Triassic Collapse Breccias
TG, TA	Triassic Gypsum, Triassic Anhydrite
T.Ev	Triassic Evaporites

Chapter 1 – Introduction

1.1 Hydrocarbons in the energy mix

It is arguably the energy that thrusts societal progress forward. Human achievements historically resulted from the First (approximately 1750–1830), Second (approximately 1870–1915), and Third (approximately 1970–present) Industrial Revolutions prove that energy resource abundance and efficacy—dominantly, amongst other parameters—dictate the rate of progress. While the First Industrial Revolution was greatly based upon the waterpower and steam power from coal combustion, the Second and Third were primarily based upon hydrocarbons—especially oil—to generate electric power. Figure 1 shows the timeseries (1971–2019) of the global energy supply (GES) by source (IEA, 2023) in exajoules (EJ). It is clearly demonstrated that hydrocarbons (oil and natural gas) are the primary energy resource, accounting for 62.3% of the GES in 1973 and 54.1% in 2019 (IEA) (Figure 2). The proportion of the HC contribution to GES relatively to the second most used energy resource (coal) is steadily running at ~2:1 ratio and higher. Combined together, coal and HC (fossil fuels) account for the 85% of the GES in 1973 and for the 80.1% in 2019.

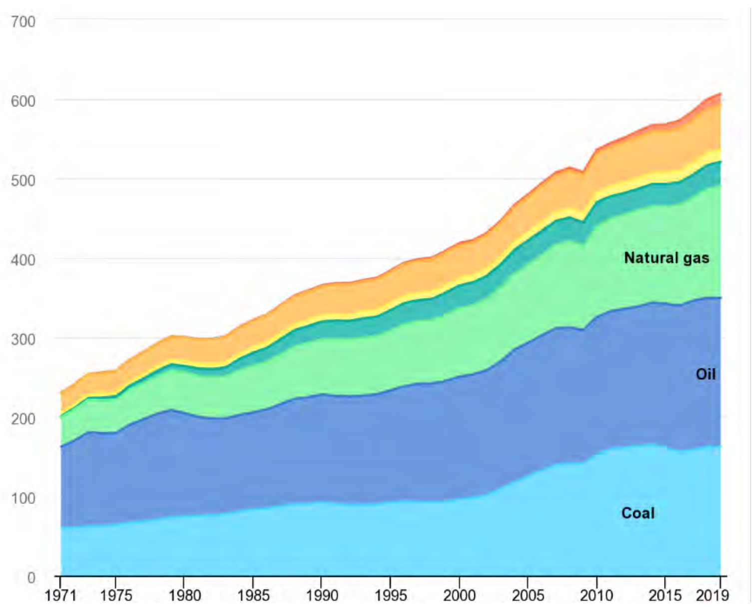

Figure 1. World total energy supply by source in exajoules (1971-2019). Source: IEA, 2022

These data show the dependency of humanity on fossil fuels, especially HC, as energy resources. However, in recent years, renewables (solar, geothermal, biofuel, wind, and hydropower) tend to occupy an increasingly higher proportion of the GES. This trend is called "green transition." It is led by the increasing concerns over climate change, whose cause has been firmly ascribed to the gases released into the atmosphere by the combustion of fossil fuels for energy. Hence, humanity turns to more seemingly environmentally friendly energy solutions, whose efficiency and overall environmental impact are not accurately constrained so far.

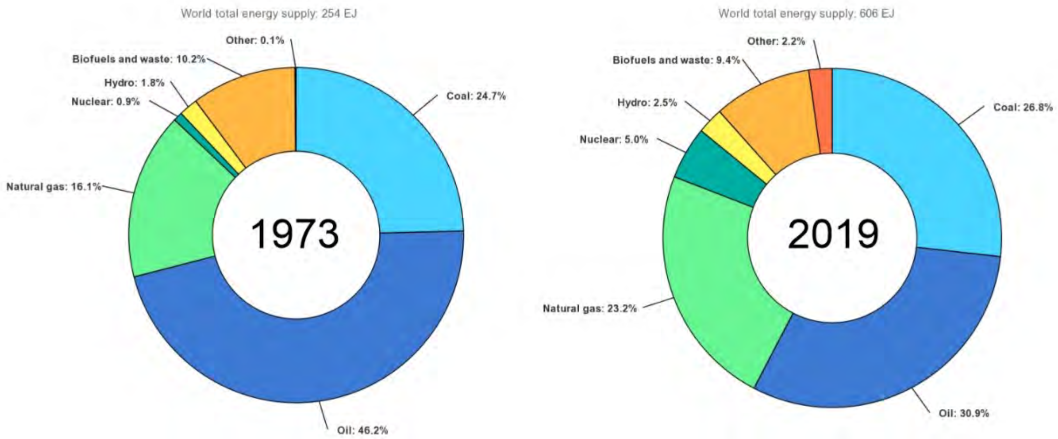

Figure 2. Global share of total energy supply by source in 1973 and 2019. Source: IEA, 2022

Currently (end of 2019, IEA), renewable contribution proportion to the GES is running at a ~15% rate on a global scale. Renewable contribution to electric energy generation is running at a ~30% rate on a global scale in 2020 (IEA). However, green goals' (steps to the Green Transition) achievement depends on the availability of natural resources such as metals and REEs (rare-earth elements) demanded for energy-harvesting machinery construction as well as for energy storage and distribution. Moreover, hydrocarbon-based, traditional fuel-combustion transportation means replacement, which demands time up to its total completion as there is no technology broadly used to replace the existing one. At the same time, global energy demand steadily increases. Therefore, despite the huge investments in renewables due to divestments in hydrocarbons, inevitably, hydrocarbon consumption will accompany Green Transition efforts over the coming decades. Natural gas, instead of oil, is preferred and promoted as a 'clean' fuel solution.

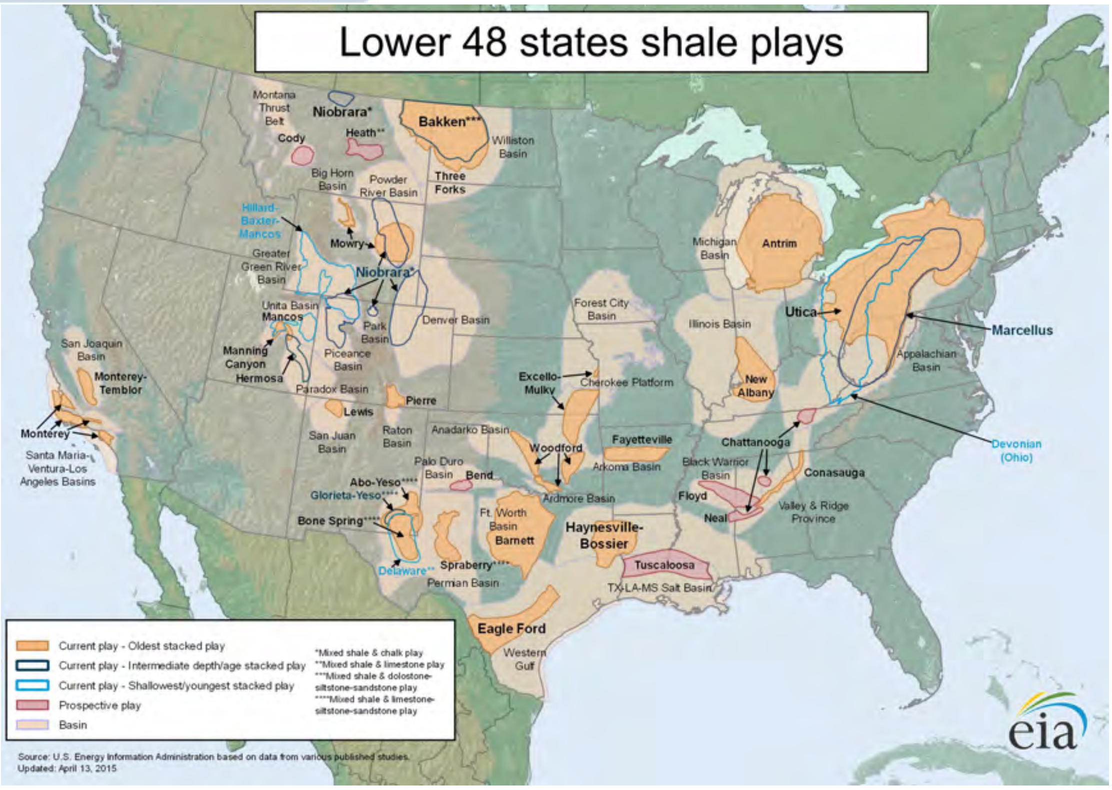

Figure 3. Lower 48 States shale plays. Source: U.S. Energy Information Administration, 2015

The recent war outbreak between Russia and Ukraine led political decisions for efforts to be made towards a redistribution of the hydrocarbon markets, in the direction of less dependency on the Russian oil. This underscores a maintained, strong interest in the oil and gas industry, which contradicts the prevalent green transition rhetoric. Moreover, important discoveries of oil and gas fields still being made in frontier areas such as in Africa, Australia, Alaska, Eastern Mediterranean etc. New technologies are developed and implemented for enhanced oil recovery (EOR) from giant oil fields holding BB of OIIP. Currently, the USA leads the global oil production, by unconventionally exploiting its vast oil-shale plays (i.e., Niobrara, Eagle Ford, Marcellus, Permian, Bakken, Barnett, Monterey Fm. etc.) with hydraulic fracturing and horizontal drilling (Figures 3&4).

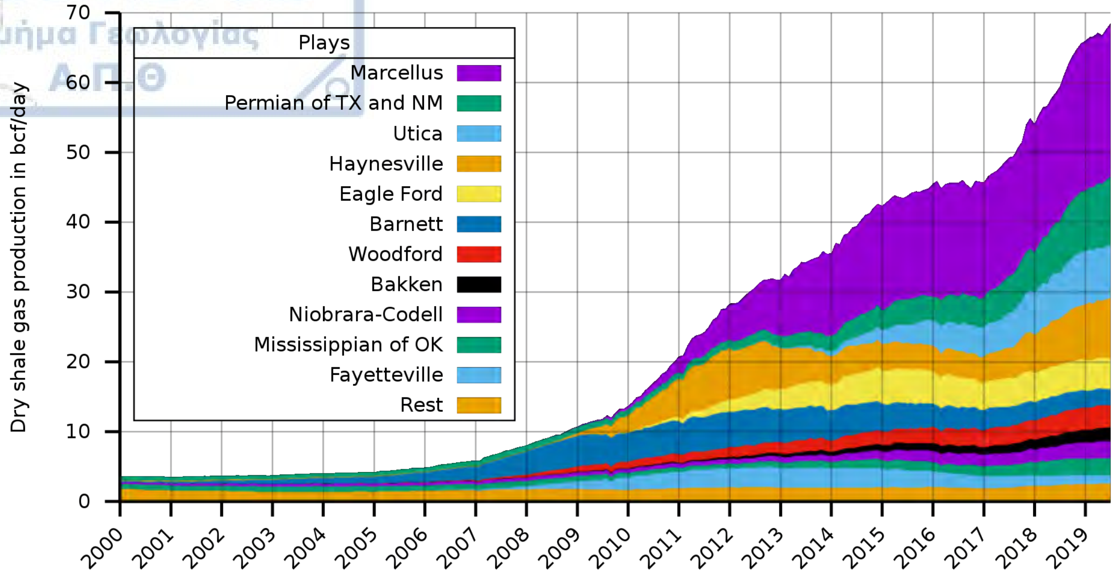

Figure 4. Natural gas production in bcf/d from the U.S. shale plays as estimated by the U.S. Energy Information Administration (EIA)

Oil occurs in Epirus and broader western Greece. This is evident by the numerous oil (bitumen) seeps (Figure 5), which have been known and documented since the Classical Era (Herodotus, 484–430 B.C.). HC exploration activities in western Greece date back to the first decades of the 20th century, whereas pioneering drilling attempts date back to the beginning of WWII. Albanian counterparts of the Ionian Zone (IZ) host numerous prolific oil fields, producing large HC quantities for almost a century. Italian oil fields which demonstrate striking geological similarities with the IZ in Greece and Albania, have produced HC from numerous oil fields for more than 70 years.

Figure 5. Solid bitumen (asphalt) seepage from fractured Miocene clastics (flyschoid) in the area of Dragopsa

Despite the promising geology and the proof for commercial oil accumulations (discovery of Katakolon oil and gas field in 1981), exploration has practically ceased for more than 15 years, following the sealing of the Demetra-1 well in 2001, which, although drilled a very promising buried anticlinal structure, eventually terminated at 3,966 m due to technical difficulties (formation overpressure).

Recent (April 2022) political announcements, set a clearer orientation of the greek hydrocarbon exploration and exploitation sector in the near future, encouraging these activities. The main aim is to promote the energy security of the country by discovering and developing new technologies while exploiting the current energy resources.

1.2 Hydrocarbon exploration

Hydrocarbon exploration's ultimate target is an integrated attempt to assess whether economically viable hydrocarbon accumulations occur in a given area. It is performed in stages, reflecting the maturity of the overall operation. The initial stage is called "frontier", the middlemost growth," and the final "mature" exploration. In the first stage, the effort demands, among others, the co-evaluation of multiple factors controlling hydrocarbon accumulation, such as the geology (presence of a trap, source, seal, and reservoir rocks of adequate efficiency). The next, more advanced exploration steps include drilling, well logging, advanced seismic surveys, and reservoir simulations. All three exploration stages should take place in tandem (Rønnevik, 2015).

Hydrocarbon exploration in frontier areas is accompanied by significant risks, including geopolitical, environmental, and investment cost challenges.

The present work aims to provide a novel perception of the petroleum potential of Epirus. To achieve this, it analyzes and discusses the initial and most fundamental steps of hydrocarbon exploration, namely, the evaluation of the geological elements and processes as they were originally defined by Magoon & Dow (1994) and adapted and further modified by Dembicki (2017) (Table 1). It is broadly accepted that these elements and processes control the occurrence of possible hydrocarbon accumulations.

Table 1. Table of the Petroleum System elements and processes. Dembicki (2017) adds the "expulsion" after generation which is reasonable as not every expulsion leads to migration. Also, Dembicki (2017) adds the preservation after accumulation, which is critical for a meaningful Petroleum System characterization.

Petroleum System			
Magoon and Dow 1994		**Dembicki 2017**	
Elements	Processes	Elements	Processes
Source Rock	Trap formation	Source Rock	Trap formation
Reservoir Rock	Generation	Reservoir Rock	Generation
Seal Rock	Migration	Seal Rock	Expulsion
Overburden	Accumulation	Overburden	Migration
		Migration pathway	Accumulation
		Trap	Preservation

1.3 Study area

The study area (Figure 6) is located in Epirus, NW Greece, extending ~6,000 km^2, roughly covering the area among the boundaries of the Greek-Albanian borders to the north, the Arta-Preveza basin to the south, the Epirus-Akarnania syncline to the east, and the shore to west. Within the study area occur several mountains, mountain ranges and hill ranges such as the Mitsikeli Mt (1,810 m), Tomaros Mt (1,974 m), Kassidiaris Mt (1,329 m), Souli Mt (1,615 m), Paramythia Mt (1,658 m), Chionistra Mt (1,639 m), Xirovouni Mt (1,614 m) and Thesprotiko Mt (1,250 m).

The terrain is generally rugged, and steep cliffs occur in many locations. These are related either to thrust fault fronts or to deep erosion/dissolution of the carbonate rocks. Karst landforms with sinkholes and dolinas are prominent in many mountains such as in the Xirovouni Mt. Vegetation is generally dense and mainly consists by Kermes oaks (*Quercus coccifera*) and other conifer species as well as with numerous broadleaf plants species. Wildlife thrives and consists of numerous avian, mammal and reptile species.

The study area stretches in all five drainage basins of Epirus that supply water the homonymous large rivers. These are the hydrological basins of Aoos, Kalamas, Acheron, Louros and Arachthos. Two large lakes are found in the study area, the natural "Pamvotis" lake and a part of the artificial "Pournari" lake in the Arachthos drainage basin.

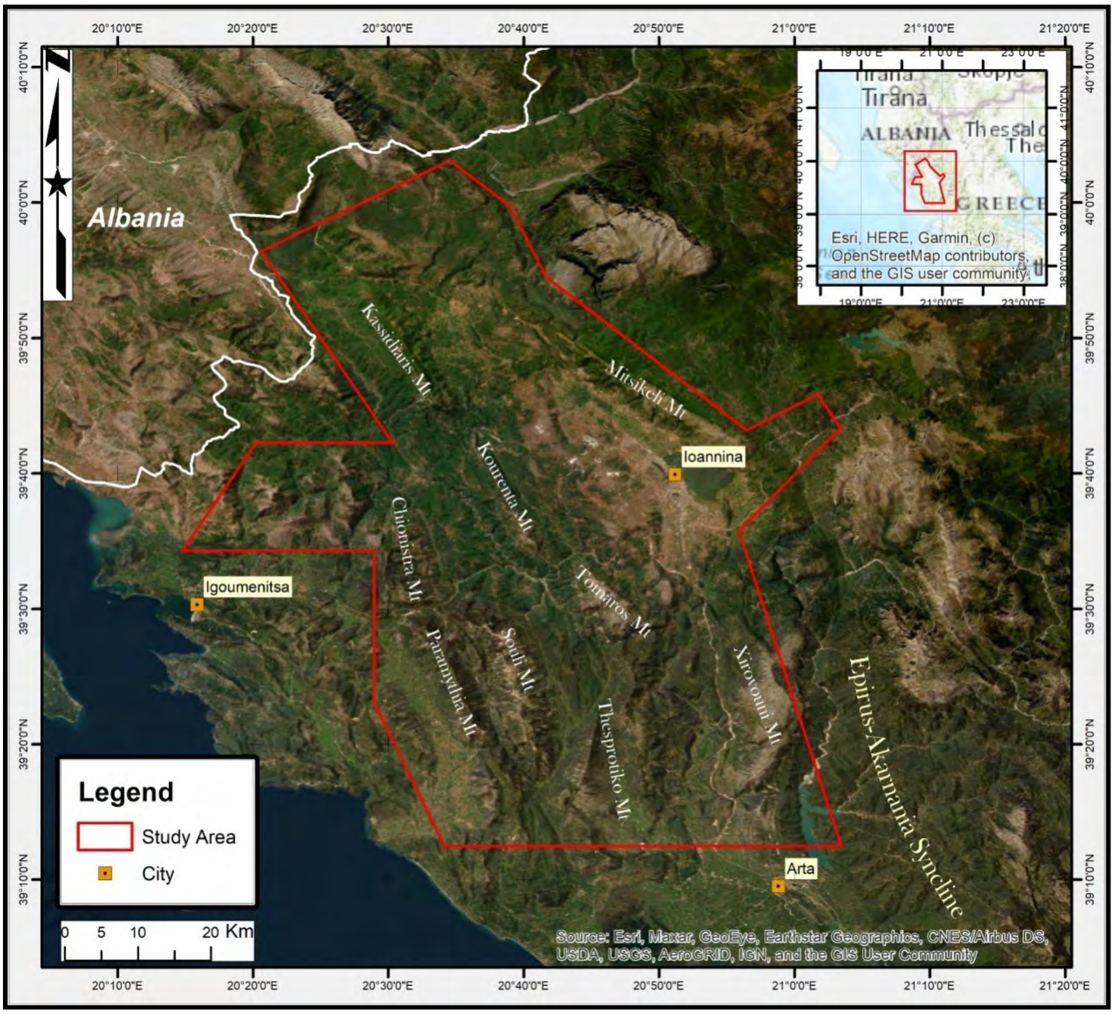

Figure 6. The study area (enclosed with the bold red line). The main mountains included in the area and referred in the text are annotated. The three main cities are also shown for reference.

In the Figure 7 the studied locations are enclosed within the study area over a satellite image background.

1.4 Study background

From a geological point of view, the study area pertains to the Ionian Zone (IZ). The IZ geologic evolution unravelling is a remarkably complex task. This has a major impact on the petroleum system (PS) evolution and function study as well. From an economic point of view and despite the numerous HC indications, areas with such entangled geo-history do not appeal attractive as the total geological uncertainty and risk increase.

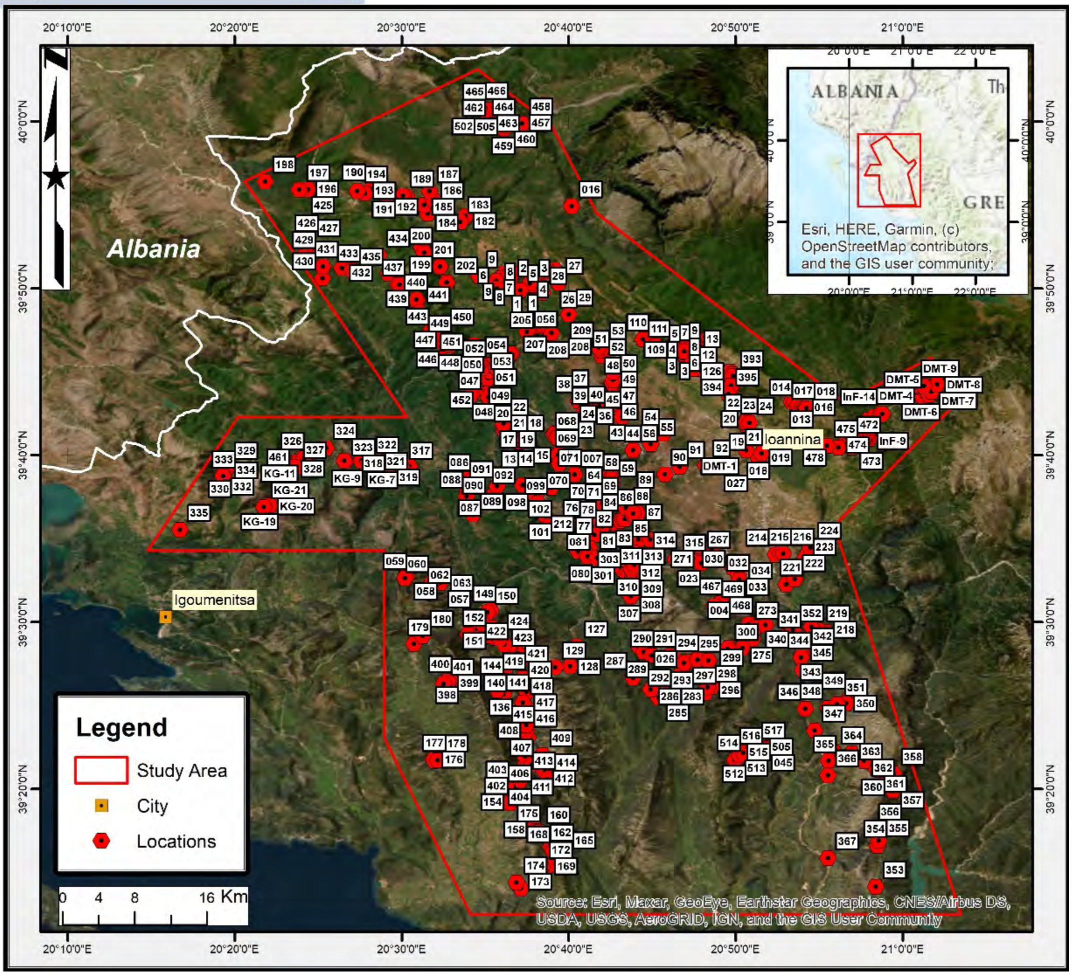

Figure 7. Labeled (location identities) studied locations shown in red hexagons.

The Ionian Zone's geological complexity is a consequence of the long-lasting basin history that underwent different geodynamic settings, resulting in a suite of basin configurations, as paleogeographic reconstruction suggests (e.g., van Hinsbergen et al., 2020). The presence of the thick(?) Triassic evaporite layer makes the geological evolution even more complex, as it has possibly impacted—in ways and magnitudes difficult to fully assess—all the aspects that control the basin structure and function. These are related to evaporite's physical properties, such as density, shear strength, and thermal conductivity, which differ significantly from the underlying and overlying rocks. Furthermore, the Tertiary continental collision caused squishing and westward transposition of the rock units, as well as differential block tilting and rotations bearing all the pre-existing tectonic-stratigraphic features. Diapirism, normal, and strike-slip faulting modified all the preexisting tectonosedimentary features, leading to the complex present setting.

The inhomogeneous assemblage of the geological features reflects in the petroleum system elements and processes, which exhibit high inhomogeneity among the various parts of the basin.

Previous studies in Epirus and broader western Greece resulted to the establishment of geological explanatory concepts, many of which were applicable to the petroleum-geological aspects. Cross-examination of these works, as well as testing them against the most recent advances in sedimentary basin analysis, raises important questions on the geological models applied to address the geological issues from a petroleum-geological perspective. For instance, the control of the Triassic evaporites in the basin (and, by extension, in the petroleum systems) is underestimated and poorly constrained. In the following table (Table 2) are summarized some of the petroleum geological-related problematic aspects, grouped in categories.

Table 2. Categories of hydrocarbon exploration-related problematic aspects regarding Epirus' petroleum geology

Category	Problem	This study*
Geotectonics/Tectonics	Timing, duration and strain partitioning of rifting event(s) (REs)	A
	Far-field stress effects from adjacent plate motions	I
	Length/displacement ratio of rift-related faults	I
	Opening/spreading time of the Mediterranean Tethys	C
	Heat flow rates associated to REs	A
	Basin configuration evolution throughout the Mesozoic-Cenozoic	A
Salt Tectonics/Salt thermal influence	Triggering mechanism and initiation of salt movements	C
	Tectonostratigraphic and thermal scenarios of early salt expulsion	I
	Response of basin configuration to salt movements	C
	Salt Thermal Effect over the overlying potential SRs	C
Source Rocks	Organic matter type characterization	A
	Thermal maturation characterization	A

Lithology/Reservoirs	Bulk source rock thickness and extent	A
	Improvement of the understanding of lithostratigraphy	A
	Dolomitization model(s)	C
*It refers to the degree of completeness that this study reached concerning a given project. I: initiation C: conceptualization A: answer		

This thesis is an integrated study based on an extensive field survey, aiming to assess geological aspects of the basin evolution and the petroleum potential tied to it. It is primarily based on extensive and detailed fieldwork following a pilot fieldwork program conducted in aiming to identify basic geologic characteristics such as the structural style, the lithologic composition and basic petroleum-geological elements such as potential source rocks and reservoir rocks.

The main aim of the thesis is to answer questions about the parameters controlling Ionian Zone PS's function namely generation, expulsion and migration timing, type and quantity of the organic matter, main stratigraphic and structural characteristics as well as the physical processes that govern them.

Unravelling the manifold of the integrated PS study demanded a consistent terminology system in order to communicate the results in a precise, coherent and effective way. Therefore, this work follows some of the most broadly accepted and commonly used terms and nomenclature of pioneering and impactful previous landmark works, dealing with the subjects of structural geology, tectonics, stratigraphy, salt-tectonics, and Ionian Zone lithostratigraphy, among others.

1.5 Basics of sedimentary basin analysis

Sedimentary basins are areas on the crust that have undergone subsidence that led to development of accommodation space and sediment deposition. There are two geodynamic mechanisms that induce subsidence and create sedimentary basins. The one is the crustal stretching accompanied by the subsequent crustal cooling and the other is the crustal flexure (McKenzie, 1978;

Bally & Snelson, 1980). de V. Klein (1987) summarized the most pioneering studies on the basin origins.

1.5.1 Lithostratigraphic aspects

1.5.1.1 Carbonates

The carbonate classification scheme based on the depositional texture proposed by Dunham (1962) (Figure 8) was employed to characterize the carbonate sediment texture. Dunham's scheme of five carbonate rock classes was selected as it provides a simple and handy tool for the description of the carbonate rocks of Ionian Zone. However, the terms "micrite" for the lime mud and "sparite" for the crystalline calcite where adapted from Folk (1959). This is because the term "micrite" has been extensively used in the literature for the Ionian Zone and the "sparite" matrix characterizes the extensive Lower Jurassic Pantokrator Limestone.

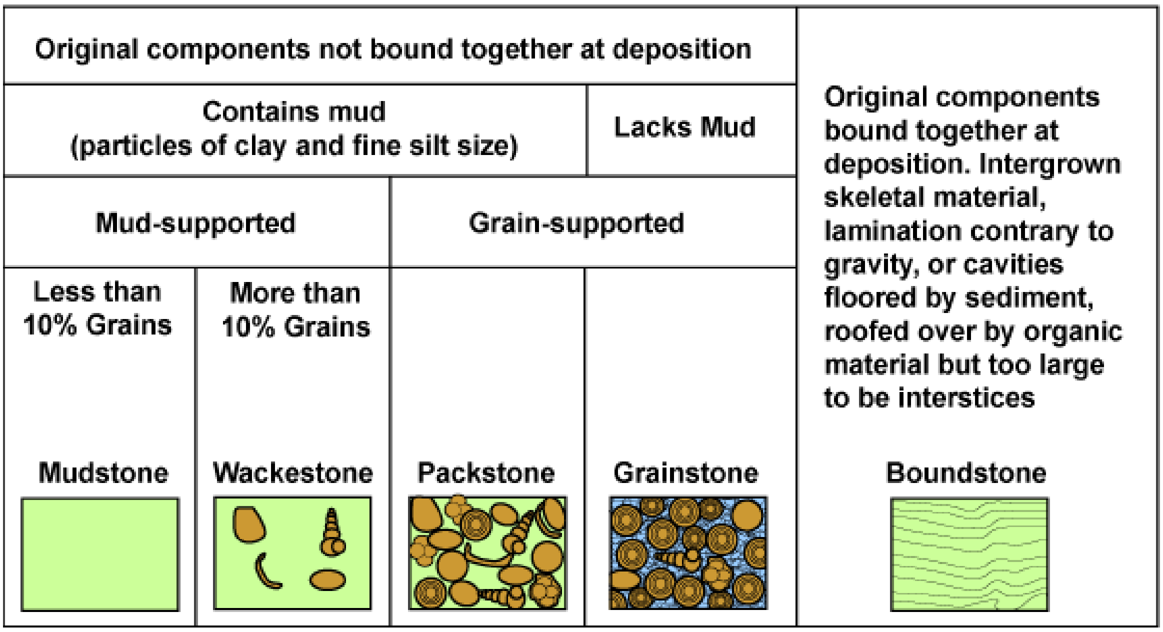

Figure 8. Dunham's (1962) carbonate lithology classification based on texture.

Carbonate factories are classified into shelves, platforms, and ramps based on their geometry (Figure 9). All can be further classified into two categories: rimmed and non-rimmed.

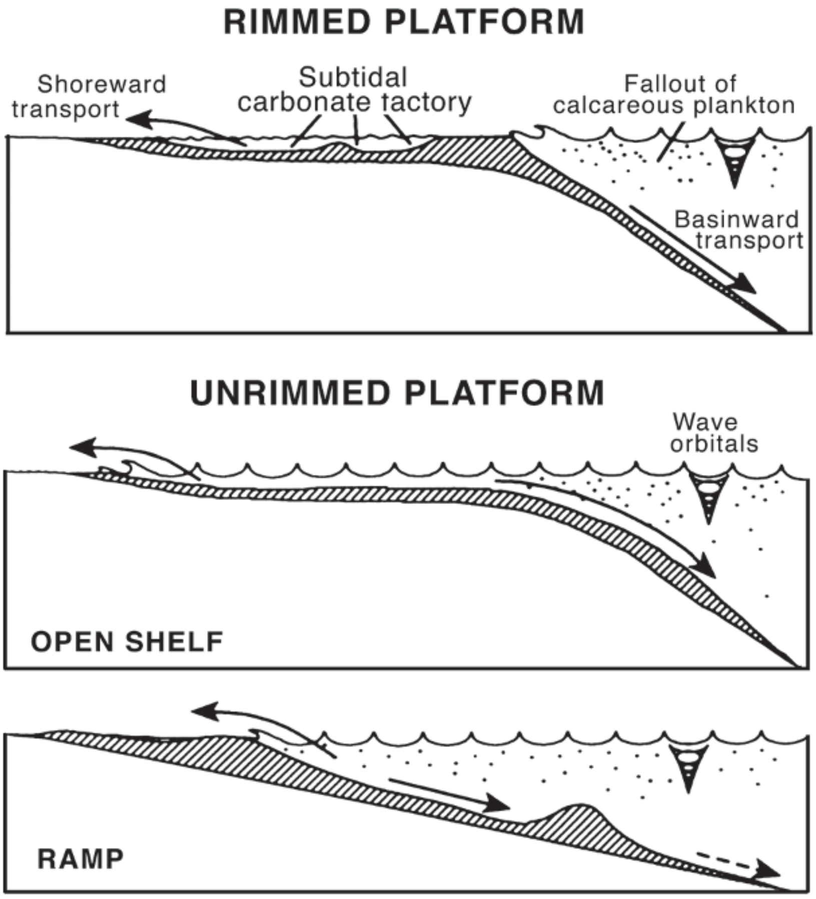

Figure 9. The three main types of carbonate platforms

Rimmed carbonate shelves or platforms are characterized by a steep shelf margin or rim, which acts as a barrier to sediment transport and promotes the deposition of carbonate sediment within the shelf area. These shelves are commonly found in areas with high energy conditions, such as oceanic islands and continental margins. Great Barrier Reef in Australia and the Bahamas are examples of rimmed carbonate platforms. Ramps can also have barriers rimming the lagoon.

Non-rimmed carbonate shelves or platforms are characterized by a gradual slope and lack a distinct rim or barrier. These shelves are typically found in low energy conditions, such as shallow seas and continental shelves. Examples of non-rimmed carbonate platforms include the Persian Gulf and the Gulf of Mexico.

The zonal distribution of the carbonate depositional facies is a crucial aspect of carbonate sedimentary geology that is broadly used in interpreting the evolution of ancient marine environmental conditions. Carbonate ramps are features that connect non-rimmed carbonate shelves to deeper water environments. These ramps are characterized by a gradual slope and are typically composed of mixed sediment types, including carbonate and clastic sediments.

The depositional facies zones in carbonate ramps are primarily controlled by the interplay of four major factors: water depth, energy, sedimentation rate, and water chemistry (Flügel, 2010). Deeper water environments are generally characterized by lower energy conditions and finer-grained sediments. Conversely, shallower water environments have higher energy, resulting in coarser-grained sediment deposition. Energy is transferred through wave and tidal action. Water chemistry controls the types of carbonate minerals that are precipitated. The presence of magnesium and bicarbonate ions leads to the deposition of aragonite and calcite, respectively.

Four depositional facies zones in carbonate ramps have been classified (Figure 10): inner ramp, mid-ramp, outer ramp and basin. Inner ramp facies are characterized by shallow water conditions with high energy levels where wave action is high and low energy in protected areas. These include reefs, shoals, and lagoons. Mid-ramp zone includes environments with lower energy in greater water depths and high energy in areas affected by waves. These are typically characterized by fine-grained sediments such as grainstones and wackestones, while mud mounds are frequently developed. Outer ramp facies are found deeper in the ramp in low-energy environments. Sedimentations is generally characterized by thin-grained sediments, often bioturbated and laminated. High-energy event-beds regularly occur. Basin facies occur in less inclined bottom, deeper water environment and consist of fine-grained sediments, often laminated.

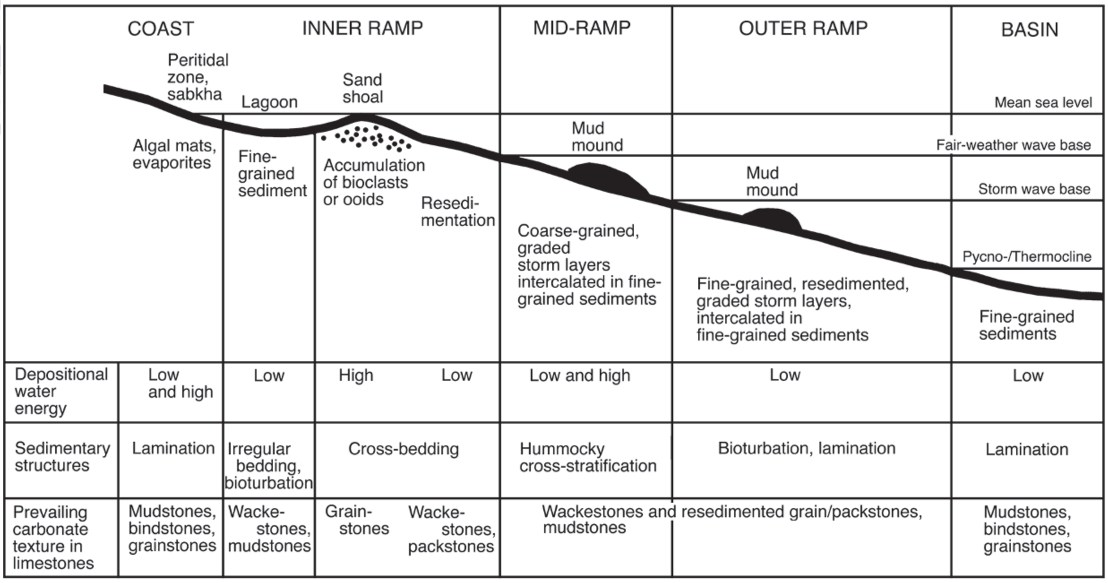

Figure 10. Generalized subdivision of carbonate ramps (Flügel, 2010)

1.5.1.2 Gravity-driven deposits

Pilot field work in the study area prior to the main field work phase resulted in the identification of various lithofacies typically associated to gravity-induced deposits, such as turbidites, slumps and debris flows (Figure 11).

Figure 11. Mass transport deposits in the Vikos gorge. Fragments of laminated dolomites, dolomitic sandstones and black chert with reaction rims.

Especially the “flysch”, which is synorogenic clastics deposited with turbidity currents, is well known throughout western Greece and particularly Epirus (Figure 12).

Figure 12. Typical image of the flysch in Epirus, with successive alternations of sandstone (or calcarenite) and siltstone/shale.

Turbidites is a very common type of deep-water clastic sediment facies. They are characterized by the deposition of graded beds that are typically composed of sand, silt and clay. Formation mechanism involves the downslope movement of hyperpycnal sediment currents known as turbidity currents. They are initiated by sediment resuspension on the continental shelf that flow into the deep basin (Shanmugam, 2020). Turbidites are characterized by a distinct sequence of layers, with coarser-grained sediment deposited first followed by finer-grained sediment, resulting in graded bedding. These deposits are widely known as “flysch”.

Flysch deposits are a type of deep water clastic sediment facies, which are typically found in collisional orogenic settings. They are usually consisting of alternating layers of sandstone and shale. Clastic material is provided by the erosion of mountain ranges and subsequently transported into the adjacent basin. Flysch deposits are typical in synorogenic flexural foreland basins.

Turbiditic facies can be used to assess past paleogeographic conditions, relative water depth and energy level. Also, they provide information on sediment transport processes and sediment provenance. The presence of turbidites or flysch deposits can also provide important clues to the tectonic history of a region, such as the location of ancient mountain ranges or the presence of active plate boundaries.

Slumping is quite common at various stratigraphic intervals and scales throughout Epirus. Slumping occurs when gravity induces slope failure in poorly lithified sediments. These sediments are plastically deformed developing characteristic folded structures (Figure 13), even with sub-isoclinal and sheath-like folds which are known to occur in strongly deformed metamorphic rocks.

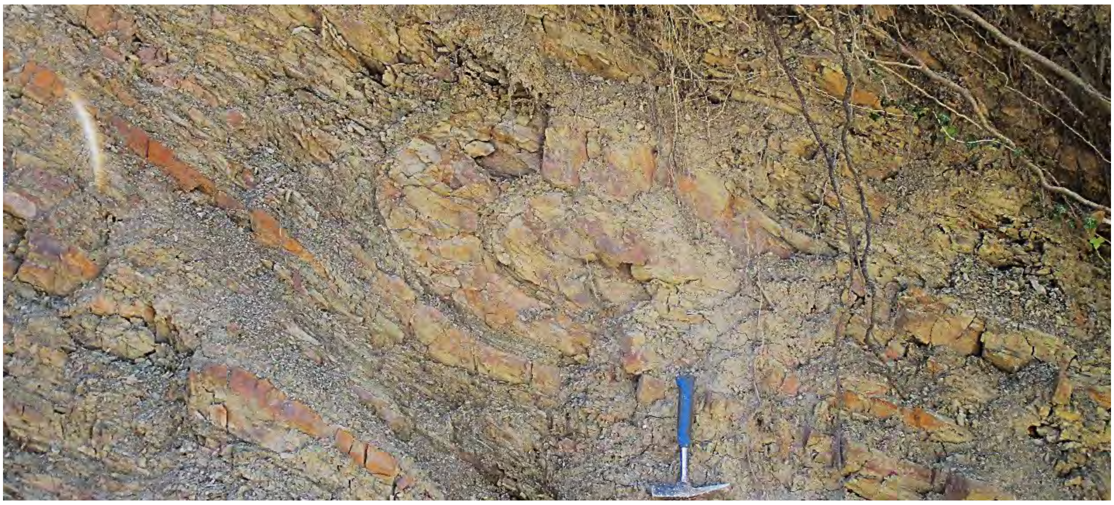

Figure 13. An isoclinal slump fold of a sandstone bed within the flysch

This work follows the simple gravity-induced deposit classification scheme (Figure 14) that is proposed in Moscardelli & Wood (2008) and references therein.

GRAVITY INDUCED DEPOSITS			Genetic Classification Transport Mechanism	Descriptive Classification Sedimentary Structures	Seismically Recognizable Features (Moscardelli et al., 2006; this work)
Mass Transport Complex	Slide	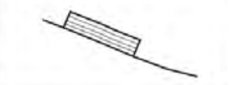	Shear failure along discrete shear planes with little or no internal deformation or rotation	Essentially undeformed, continuous bedding	Continuous blocks without apparent internal deformation. High-amplitude, continuous reflections.
	Slump		Shear failure accompanied by rotation along discrete shear surfaces with various degrees of internal deformation	Plastic deformation particularly at the toe or base. Plow structures, folds, tension faults, joints, slickensides, grooves, rotational blocks	Compressional ridges, imbricate slides, irregular upper bedding contacts, duplex structures, contorted layers. Low- and high-amplitude reflections geometrically arranged as though deformed through compressive stresses.
	Debris Flow	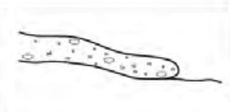	Shear distributed throughout the sediment mass. Strength is principally from cohesion due to clay content. Additional matrix support may come from buoyancy. Plastic rheology and laminar state.	Matrix supported, random fabric, clast size variable, matrix variable. Rip ups, rafts, inverse grading and flow structures possible.	Mega rafted and/or detached blocks, irregular upper bedding contacts, lateral pinch-out geometries, oriented ridges and scours. Low-amplitude, semitransparent chaotic reflections.
Turbidity Current	Turbidite		Supported by fluid turbulence (newtonian rheology)	Normal size grading, sharp basal contacts, gradational upper contacts.	Lobate features Laterally continuous

Figure 14. Classification of gravity-induced deposits (adopted form Moscardelli and Wood, 2008)

1.5.2 Structural geological aspects

Detailed structural studies for the Epirus are limited. Only a few regional studies occur, mostly dealing with the general structural style and tectonostratigraphic aspects (e.g., Karakitsios, 1995). This likely depends on factors such as the steep terrain, the heavy vegetation and the particularly complex structure that is characterized by strongly deformed strata with successive compressional, extensional, and strike-slip-related tectonic elements. Structural style is primarily deduced by seismic profiles (e.g., Monopolis and Bruneton, 1982; Makris and Papoulia, 2011; Makris and Papoulia, 2019;).

The study of rock deformation is an important aspect of hydrocarbon exploration as it provides a range of data that can aid in the unraveling of the petroleum potential of an area. Deformation of the rocks can be measured and evaluated on various scales, from the sub-millimeter to the multiple-kilometer scale. Hydrocarbon exploration and production stages, from the initial evaluation of a sedimentary basin to production, implement different structural geological methods. During the initial evaluation, the overall structural style and general tectonic setting of a basin are usually investigated in order to obtain a primary image of the geological evolution of the area as well as of the possible hydrocarbon-bearing structures, such as the anticlines. Moreover, tectonically complex areas such as the fold-and-thrust belts do not appear as attractive exploration targets due to the increased geological uncertainties, which in turn elevate the economic risk. On the other hand, more detailed studies on the outcrop scale, such as fracture evaluation, are conducted during more advanced exploration stages or during production in order to aid in engineering, hence commercial decisions.

Often, deformation can reflect a very complex geological history. Signatures of translation, rotation, fracturing, folding, shearing, and volume change can coexist. In this cases, deformation history unravelling and attribution of different structural features to different tectonic stages, as well as their relative succession, are crucial in exploration.

1.5.2.1 Folding

Unravelling folding mechanisms and evaluating of its implications is essential for assessing geological histories. Folding of rocks can be either developed under tectonic stresses or due to gravitational force.

Tectonically induced folding is primarily driven by the stress developed by plate tectonics. Tectonic plate movements and interaction, exerts compressional, extensional, or shear stress on the rocks. Compressional stress is commonly account for folding. The geometry and orientation of folds depend on factors including the direction of the principal stress axis, the stress magnitude and rheological properties (e.g., Ramberg, 1963; Ramsay and Huber, 1987).

On the other hand, folds can be developed in soft sediment regimes, when unconsolidated sediments are forced in sliding due to gravity over inclined basin floor. These folds can provide information about paleo-slope orientations as their b-axis lie approximately perpendicular to the slope dip (e.g., Alsop et al., 2014). They can also serve as indicators of seismic activity (e.g., Spalluto et al., 2007) or rapid sedimentation events.

For the description of the folds the following nomenclature was followed (Figure 15) for both tectonic (i.e., lithospheric stress applied on hard rock) and gravitationally-induced folds (semi-lithified rock mass sliding on slope).

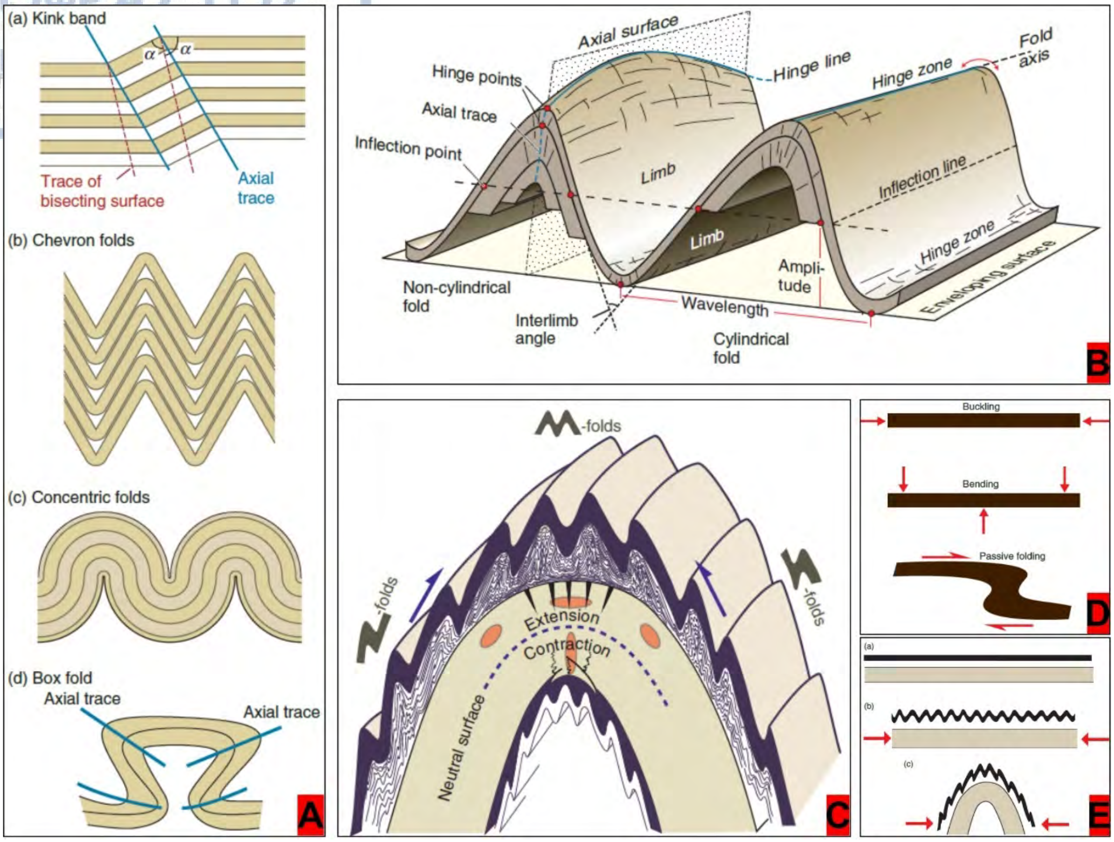

Figure 15. A) Fold nomenclature based on hinge shape, B) Geometric elements of folds, C) Parasitic folds and contraction/extension regimes, D) Fold classification based on folding mechanism, E) Folding initiation and evolution differences between thin and thin beds. A-E figures adopted from Fossen, 2010

1.5.2.2 Fracturing

Fractures in rock include structures such as joints and faults. Joints are discontinuities within the rock mass where astride blocks do not exhibit dislocation. Faults are discontinuities in a rock mass where astride blocks exhibit relative dislocation. Both types of fractures can originate from tectonic stress applied on a rock mass in the brittle state. In the Figure 16 the main fracture types and associated attributes are presented (Fossen, 2010 and references therein).

Brittle deformation kinematics can be assessed by the orientations of the various discontinuities such as faults and joints (e.g., Ramsay & Huber, 1987). Other elements associated with the discontinuity development and function such as the slip lineations can further assist in kinematic analysis (e.g., Marrett & Allmendinger, 1990).

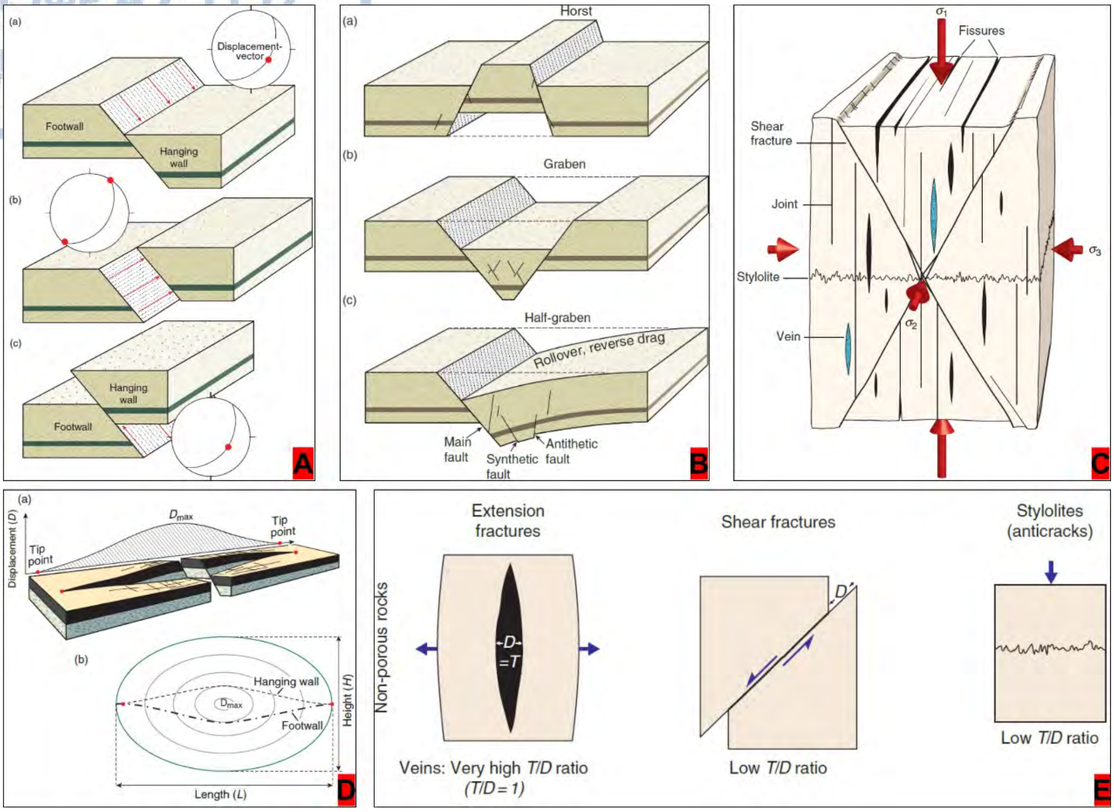

Figure 16. A) The three main fault type end-members. Intermediate types typically occur, B) typical faulting-related structures, C) typical fracture types and the associated stress orientation tensors (i.e., σ1, σ2, σ3), D) illustration of an idealized fault plane and the associated dislocation, E) the three main fracture types. A-E figures adopted from Fossen, 2010

1.5.3 Hydrocarbon exploration in fold-and-thrust belts

Excluding from the dataset the Zagros fold-and-thrust belt (FTB), which accounts for 49% of global FTB hydrocarbon reserves, Cooper (2007) concluded that FTBs do not significantly differ from the other hydrocarbon provinces in terms of oil/gas/condensate ratio. Moreover, USGS (2000) calculated that the undiscovered reserves in FTBs account for 15% of all undiscovered reserves. This percentage is almost identical to the percentage of actual oil reserves (14%) of the total global reserves. These findings point out that FTBs represent an average proportion of the global hydrocarbons (Figure 17).

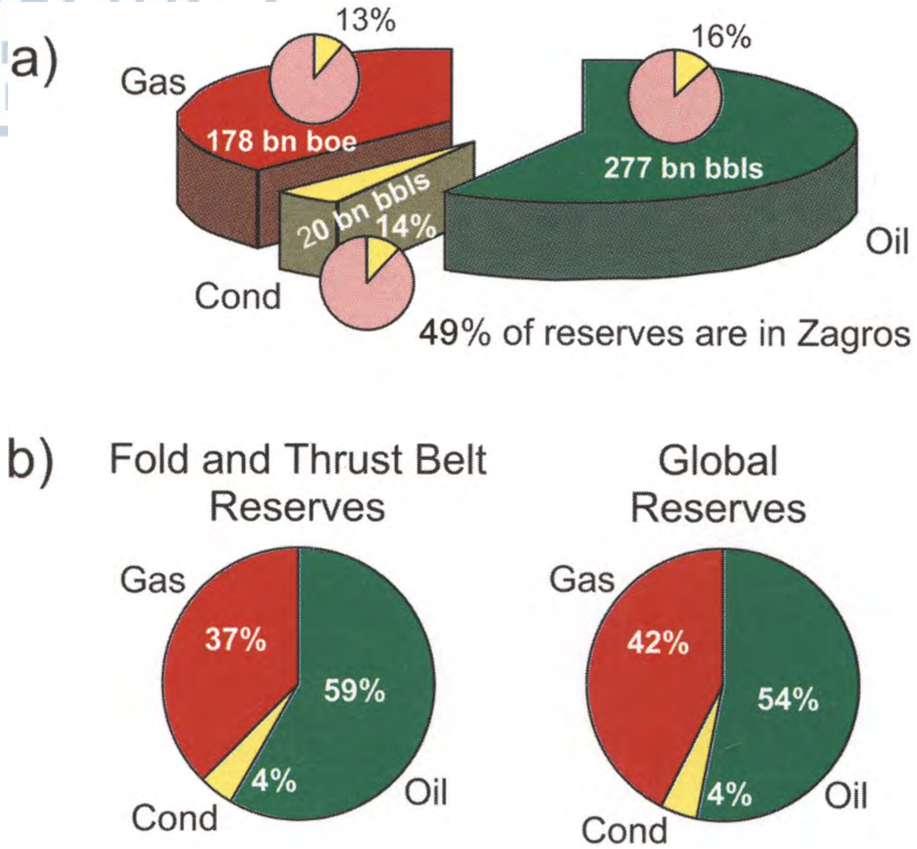

Figure 17. a) HC type distribution in FTB's. 49% of the total reserves are located in Zagros FTB. The total volume per each HC type are indicated. b) HC type split comparison of between FTB's and global reserves (Cooper, 2007).

1.5.4 Salt tectonics

The term "salt-tectonics" is used to describe the structures related to the presence of an evaporite layer in a basin that induces a variety of characteristic structures in the overlying rock layers due to its significantly different physical and mechanical characteristics, such as density and shear strength, respectively. The presence of such a layer interbedded in the stratigraphy of a given area reduces the overall mechanical homogeneity, and this is prone to destabilizing the entire system. The main triggering factor for salt movement initiation is widely considered to be differential loading (Hudec & Jackson, 2007). Buoyancy (a lower density layer below a higher density layer), which was extensively considered as a main factor, plays a secondary role in the salt movement initiation (Hudec & Jackson, 2007). Buoyancy (a lower density layer below a higher density layer), which was extensively considered as a main factor, plays a secondary role in the salt movement initiation (Hudec & Jackson, 2007).

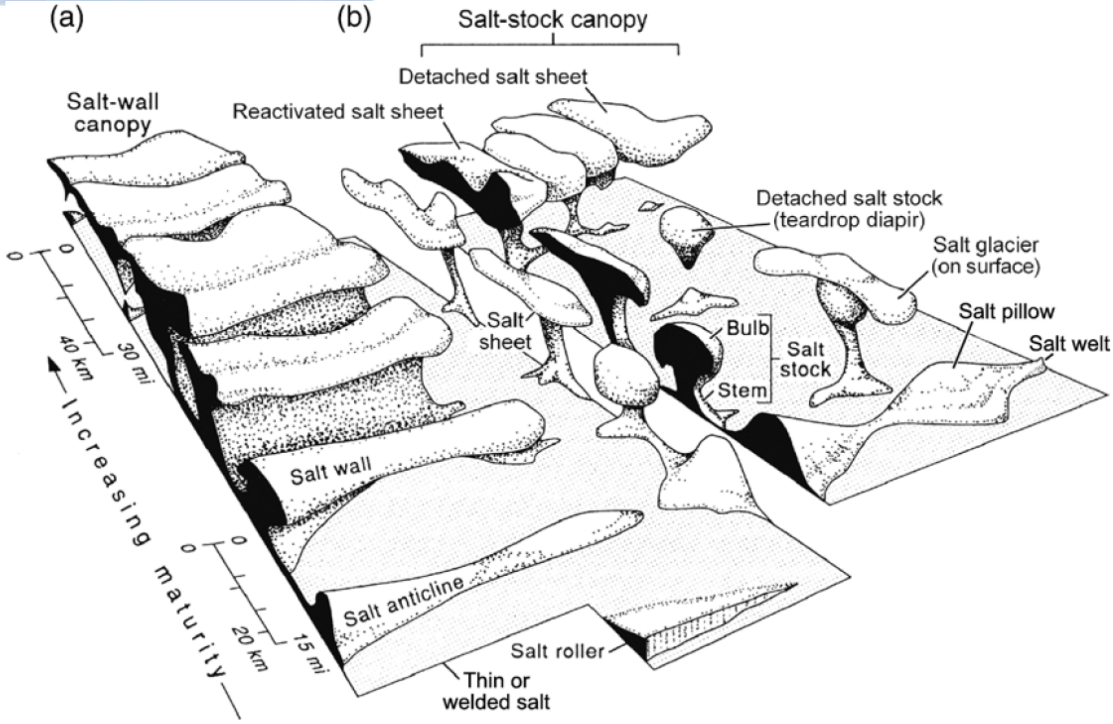

Figure 18. Simplified block diagram (after Jackson and Talbot, 1991) with shapes of the salt structures. (a) Elongated structures rising from linear feeders. (b) Structures rising from point feeders.

Salt-bearing basins, irregardless of the pre- and syn-salt deposition tectonic evolution, can further (post-salt-deposition) be subjected to tectonic stresses either extensional (and/or transtensional) or compressive (and/or transpressional). During these stages, salt movements are initiated, resulting in a large variety of salt structures (Figure 18). Moreover, salt movements can also occur without significant tectonism. This phenomenon is called “halokinesis”.

Evolving salt structures can affect the sedimentary basin in terms of sedimentation, thermal evolution and overall structure (e.g., Callot et al., 2016; Rowan et al., 2016; Duffy et al., 2018).

It is well understood that structural style in salt-bearing basins is strongly controlled by salt’s attributes such as composition (mineral facies dominating, e.g., halite, dolomite, anhydrite, etc.), thickness, water content, etc.

1.5.5 Salt thermal effect

Besides the structural style, salt layers in a basin also affect the thermal regime around them. This is a very important implication for the petroleum geology as it controls the kerogen maturation degree and distribution in a petroleum system domain. Mello et al. (1995) simulated the thermal regime around various size and shape diapirs (Figure 19).

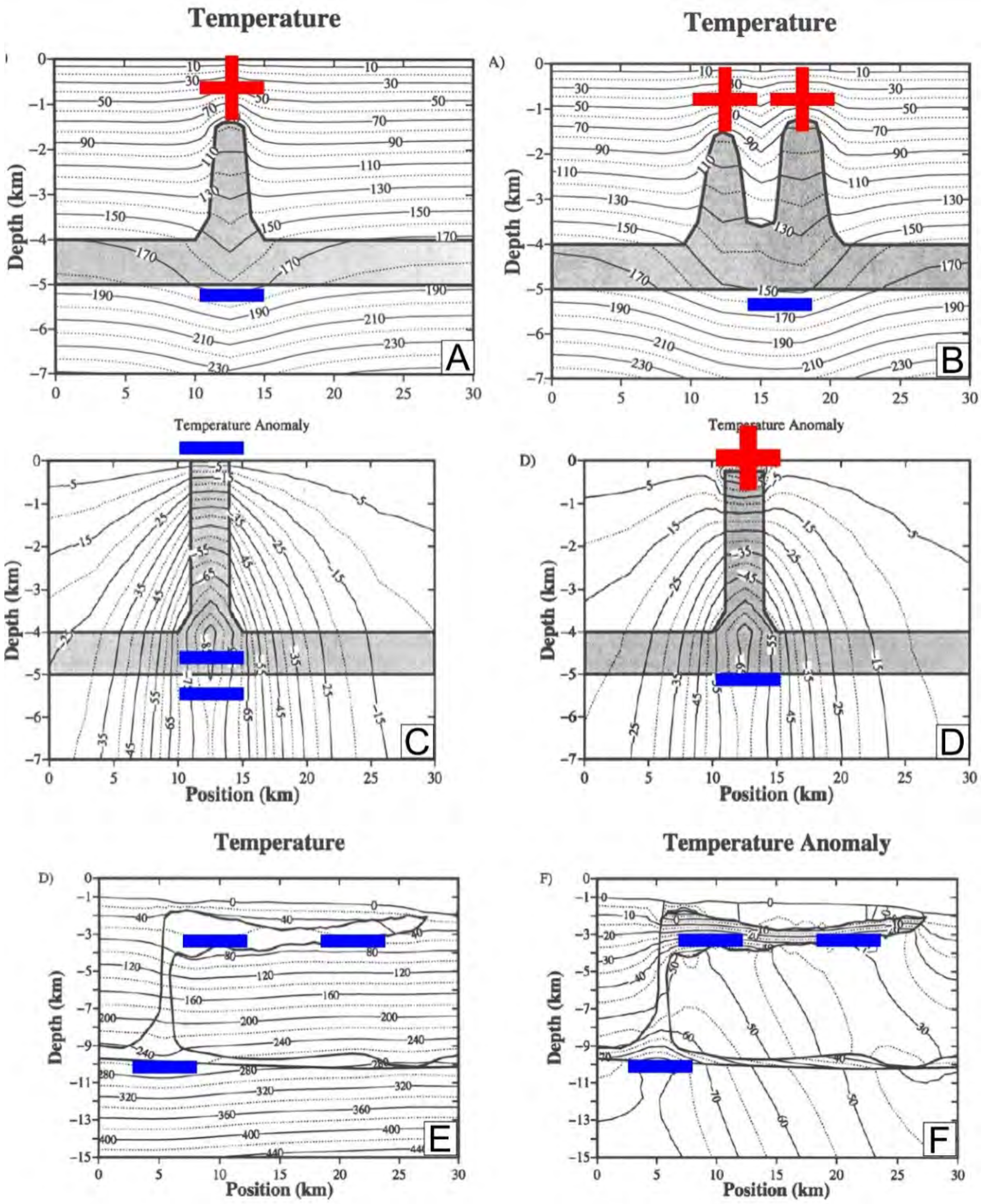

Figure 19. A-F) Heat distribution and temperature anomalies around salt bodies of various shapes. A, B, D) the typical dipole of temperature above and below salt plugs, C) the collapse of the dipole to a monopole in the case where the salt reaches the surface, E. F) blanketing effect below salt canopies (modified after Mello et al., 1995).

The results indicated a dipole in the thermal regime, namely a positive anomaly above the salt dome and a negative anomaly below the salt dome. One interesting finding is that heat is abducted outside the basin when the diapir pierces through the surface.

Because of this thermal restraining effect, deep salt-bearing basins tend to be more oil prone than deep basins that do not contain salt layer(s). This has important implications for hydrocarbon exploration.

1.5.6 Fate of the organic matter in sediments

The organic matter in sediments occurs in two forms: a) the kerogen and b) the bitumen. Kerogen is the insoluble fraction of sedimentary organic matter in organic solvents. It is derived from breakdown and subsequent diagenetic alteration of animal, plant, and bacterial remnants. Kerogen composition depends on the original composition of the organic matter and the diagenetic processes inducing its polymerization (e.g., Horsfield et al., 1994). The bitumen is soluble in organic solvents and can either be part of the preserved organic matter in thin-grained rocks or a product of hydrocarbon generation (e.g., Sanei, 2020). The latter can be also termed solid bitumen, tar or asphalt and is usually found in coarse grained sediments, filling pores and fractures in various distances (sub-mm to km) from the source. In the diagram of Figure 20, the fate of the organic matter during and after deposition is illustrated.

The organic matter (OM) that sinks into sediments in aquatic environments may either be preserved or diminished. The OM origin may be terrestrial (e.g., trees, land animals etc.) or aquatic (e.g., algae, bacteria, fecal pellets, marine organisms etc.) whole organisms, or debris. The preservation or not of the OM depends on factors such as the sedimentation rate, the water column dissolved oxygen content, the clastic particle size at the bottom and the presence of organisms.

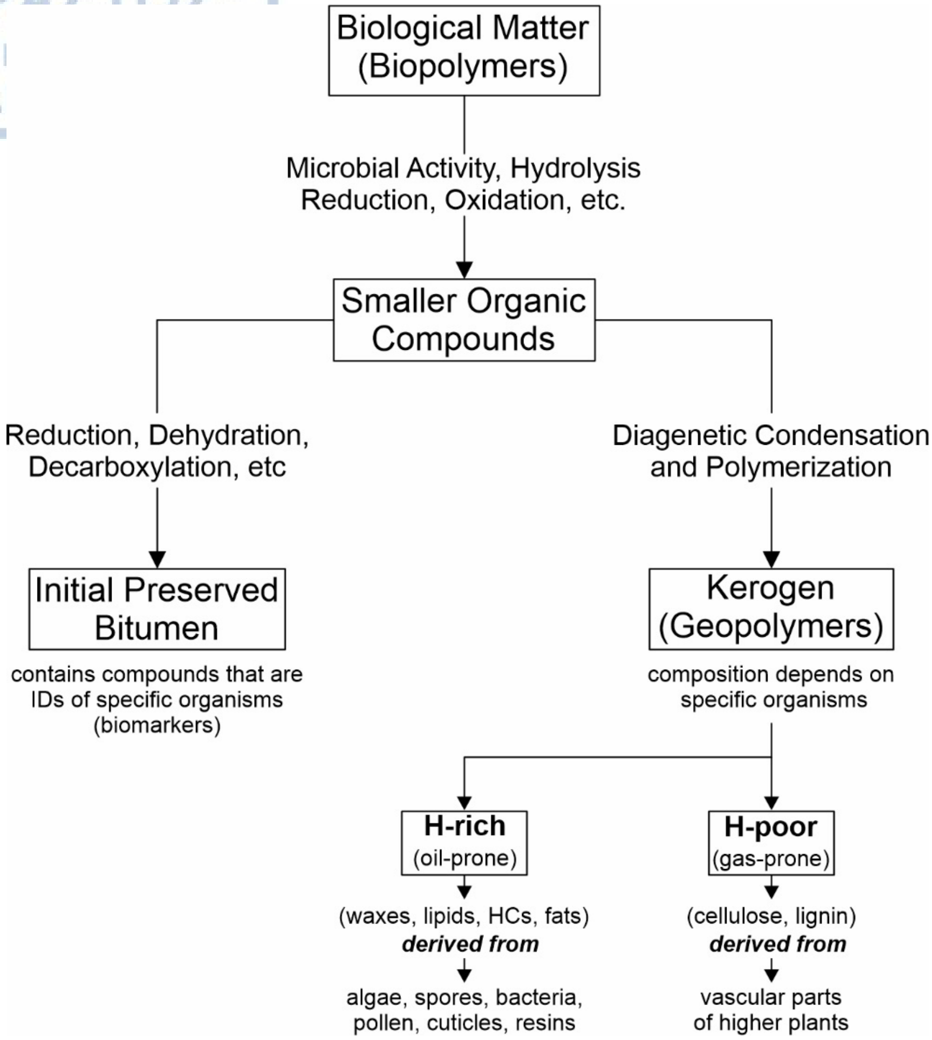

Figure 20. Schematic diagram showing the evolution of the organic matter from the original biopolymer stage to kerogen as well as the physicochemical processes involved at each stage. Notice that the fraction of the organic matter containing the biomarkers, useful in the identification of specific organisms, is the bitumen.

The well-oxygenated waters, either oxidize the OM or sustain OM-fed organisms. In oxygenated bottom waters, coarse-grained sediments tend to allow oxygen-rich water to circulate among clasts. This either oxidizes the OM, or allows scavenging organisms to feed on the sinking OM. On the contrary, thin-grained sediments (i.e., clay and mud) do not allow water circulation, hence, partial OM preservation can be expected even in muds of oxygenated water columns (Figure 21). In that case, rapidly sinking OM (such as the fecal pellets having a hydrodynamic shape, leaving less time for OM oxidation) favors OM preservation.

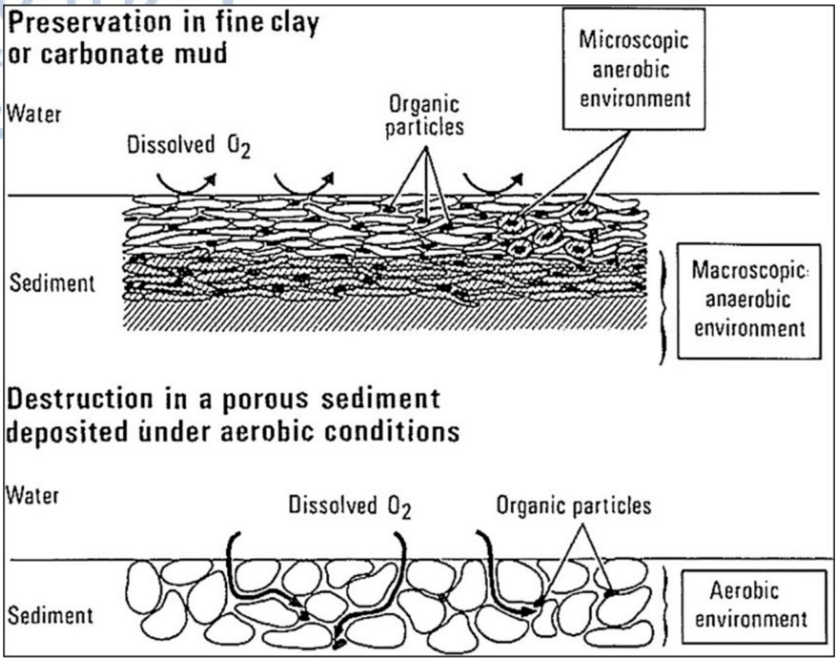

Figure 21. Conceptual sketch comparing the organic matter preservation in fine-grained sediments (upper part) versus coarse-grained sediments (lower part) shortly after deposition. From Tissot, B.P., Welte, D.H., 1984. Petroleum Formation and Occurrence. New York, Springer-Verlag, 699 p.

1.5.7 Water column oxygenation

Bottom water anoxia is considered a much more efficient parameter that favors OM preservation, as it lacks life, therefore, biological sequestration of the OM. Demaison & Moore (1980) provided a comprehensive guide to the anoxic aquatic environments, classifying the anoxic depositional settings in 4 main categories:

- Large anoxic lakes
- Anoxic silled basins
- Anoxic layers caused by upwelling
- Open ocean anoxic layers

Oxygenation in shallow water depends on surface primary productivity whereas in deep waters on water circulation. Anoxia occurs when oxygen demand surpasses supply (Demaison and Moore, 1980). More specifically, high surface productivity demands high oxygen amounts that eventually lead to anoxia. In deeper settings, water circulation may bring cool, well-oxygenated and nutrient-rich bottom water that boosts productivity and consequently, anoxia (Figure 22).

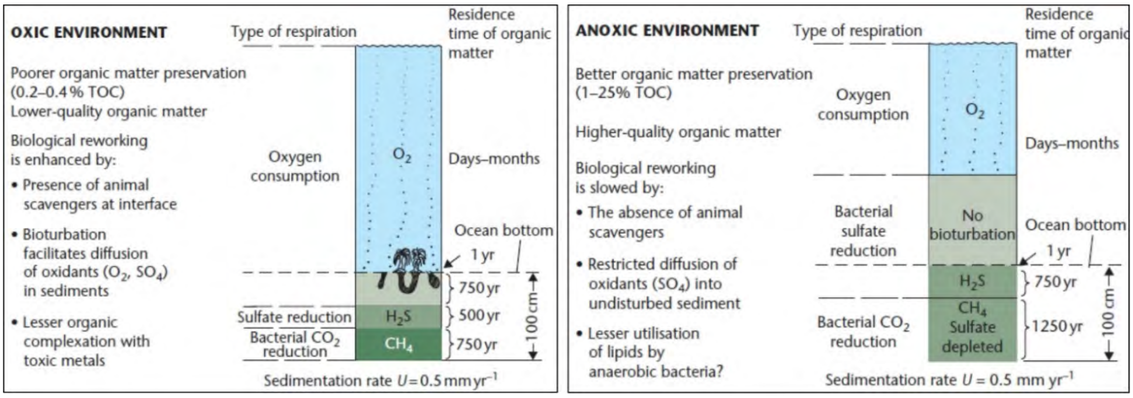

Figure 22. Comparison of the organic matter degradation under oxic and anoxic conditions [modified from Allen & Allen (2013) after Demaison and Moore (1980)].

1.5.8 Sedimentation rate

Sedimentation rate has been indicated as a key factor for optimal source rock deposition. Low sedimentation rates leave the OM exposed on the basin floor to keep degrading and/or be consumed by organisms (Johnson Ibach, 1982). High sedimentation rates may dilute the OM in the large sediment volume; thus, the TOC content remains low (Johnson Ibach, 1982). This low TOC might not surpass the cut-off value of a SR to be considered of adequate quality to produce commercial HC quantities. The cut-off values suggested in various studies are shown in the following Table 3. A schematic correlation of the sedimentation rate and the TOC content is given in Figure 23. The sedimentation rate of 1mm per year is considered as the value for optimal OM preservation and SR development (e.g., Johnson Ibach, 1982; Bohacs et al., 2005).

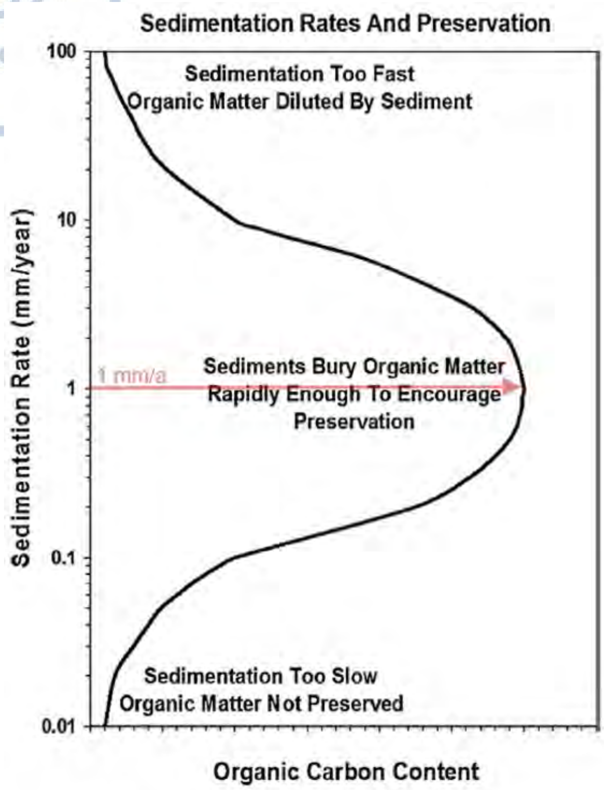

Figure 23. Relation of the sedimentation rate and the preservation of the OM. (Modified from Fleet, A.J., Kelts, K., Talbot, M.R. (Eds.), Lacustrine Petroleum Source Rocks. Geological Society of London Special Publication 40, p. 3–26.)

1.5.9 Kerogen type

Arguably, the kerogen type, quantity, and thermal maturity play the most important role in the type of generated HCs (oil, gas, and their mixtures). However, whether the kerogen is capable of generating quantities that may lead to exploitable oil accumulations or not is strongly controlled by the TOC (wt.%) content. Several authors (e.g., Ronov, 1958; Meyer and Nederlof, 1984; Lewan, 1987; Cooper, 1990, p. 20; Jarvie, 1991; Peters and Moldowan, 1993, p. 51) argue that it is unlikely for a source rock to expel exploitable oil quantities at TOC<1.0 to 1.5 wt.% (Table 3).

Table 3. Cut-off TOC values suggested from various geochemical studies

Reference	***Cut-off TOC (wt.%)***
Ronov (1958)	1.4
Meyer & Nederlof (1984)	1.5

Lewan (1987)	1.5
Cooper (1990)	1
Jarvie (1991)	0.5 to 1
Peters & Moldowan (1993)	1

Kerogen undergoes chemical and structural alteration during thermal maturation. Chemical changes have been studied by van Krevelen and structural changes by Behar and Vandenbroucke (1987), respectively. What is being seen is that during thermal maturation, kerogen becomes less H-rich (Figure 21A), and the structure tends to be dominated by more stable aromatic structures (Figure 21B). The H-rich aliphatic structures in the original kerogen are rapidly depleted, while the kerogen is enriched in carbon. Shortly after the oil window initiation, Types I and II are practically indistinguishable. At the wet gas zone, any original kerogen type (I, II, or III) is indistinguishable.

Liquid HCs might be preserved as bitumen up to the catagenesis onset. Methane (C1) can also be present at this stage. Oil generation from kerogen thermal cracking initiates at the onset of the catagenesis stage. The chemical composition of the generated oil changes during the thermal maturation stages. This reflects the change in kerogen. Along with liquid HCs, wet gas (C2-C4) is formed, which peaks around the oil peak. After the oil peak, condensate and wet gas are formed, whereas in the last HC-generation stage, only methane is formed. Moreover, oil and gas tend to thermally crack over time, forming methane. These steps are shown schematically in Figure 24C.

These observations, from a practical exploration perspective mean that an oil-prone SR (e.g., Type II) will produce oil in lower thermal maturity while progressively the generated HCs will become gaseous in more progressive phase (Figure 24C), reflecting the chemical and structural composition of the kerogen in any stage.

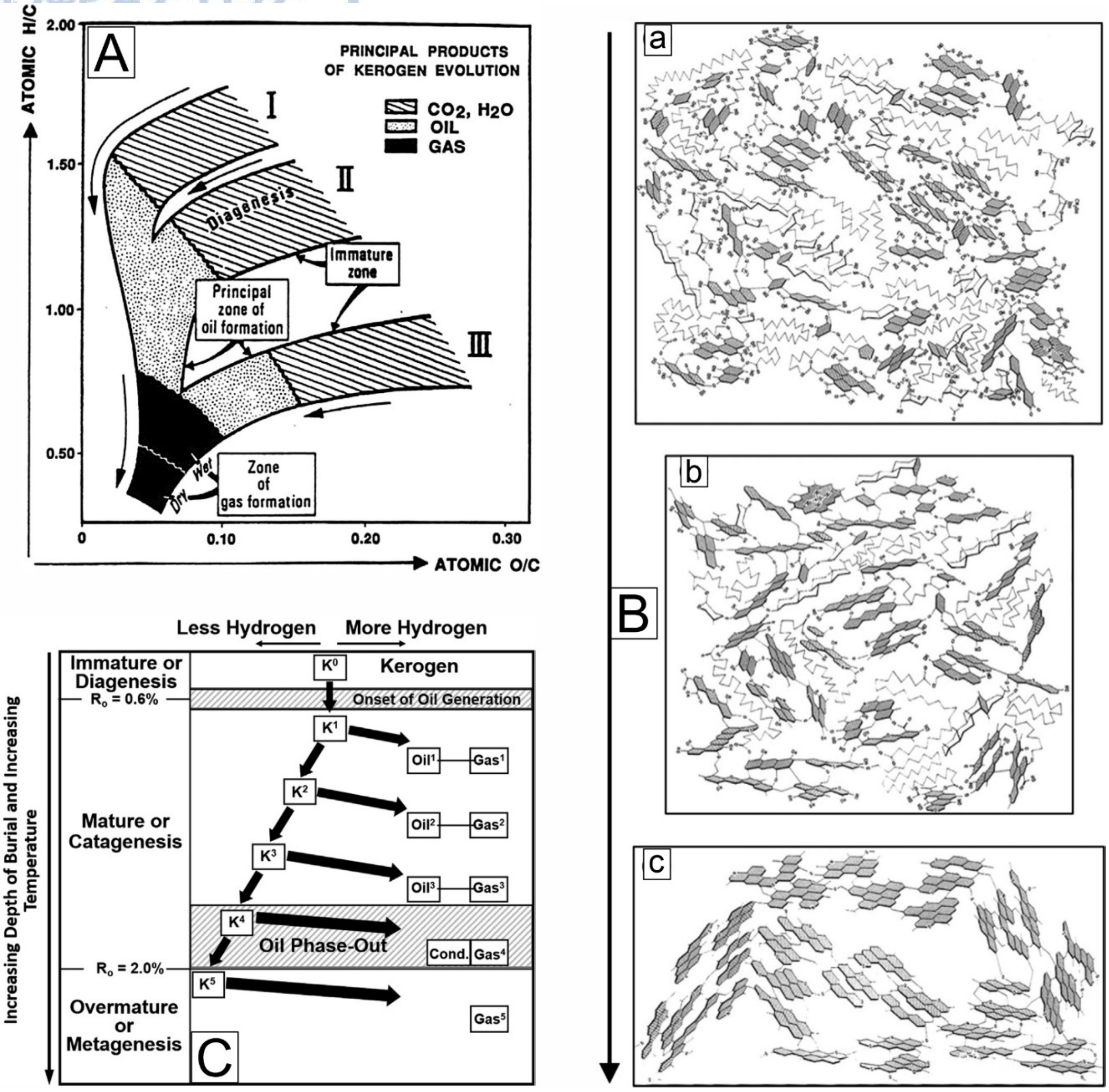

Figure 24. [A] van Krevelen diagram (*From Tissot, B.P., Welte, D.H., 1984. Petroleum Formation and Occurrence. New York, Springer-Verlag, 699 p*.), [B] structural and compositional evolution of a type II kerogen in three stages (a, b, c) of thermal evolution (*Adapted from Behar, F., Vandenbroucke, M., 1987. Chemical modelling of kerogens. Organic Geochemistry 11, 15–24*.), [C] evolution of the kerogen and its products at each stage of the thermal evolution (*Modified after Horsfield B., Rullkotter, J., 1994. Diagenesis, catagenesis, and metagenesis of organic matter. In: Magoon, L.B., Dow, W.G. (Eds.), The Petroleum System–From Source to Trap, vol. 60. American Association of Petroleum Geologists Memoir, p. 189–199.*)

Single-type kerogen in a source rock is rather uncommon. Mixtures in various proportions of the various kerogen types within a source rock are most common. This practically means that any well-preserved HC accumulation is expected to be composed by various liquid and gaseous hydrocarbons (Figure 25).

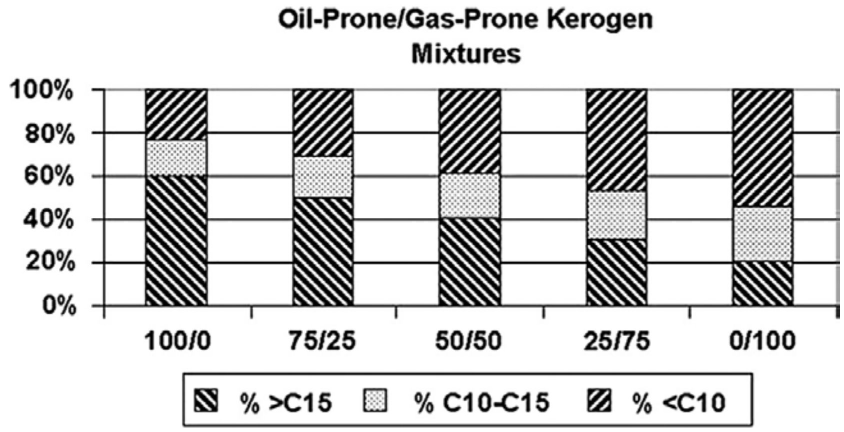

Figure 25. Pyrolysis–GC results demonstrating the progressive changes resulting from the mixture of oil-prone Type I or II kerogen with gas-prone Type III kerogen (from Dembicki, 2009) .

1.5.10 Kerogen kinetics

Kerogen kinetics analysis is an important method to understand the kerogen behavior in thermal stress by assessing its thermal transformation. It refers to the chemical changes the kerogen undergoes during heating, leading to progressive generation of various hydrocarbons. It is used to assess the hydrocarbon generation history within a basin with respect to temperature and time. This is critical when it comes to the petroleum system (Magoon and Dow, 1994) evaluation. Temperature influence in kerogen conversion is much higher than the time's (Figure 26). Apart from temperature and time, kerogen kinetics depend on its composition and in the presence of mineral catalysts (e.g., Dembicki, 1992; Rahman et al., 2017; 2018).

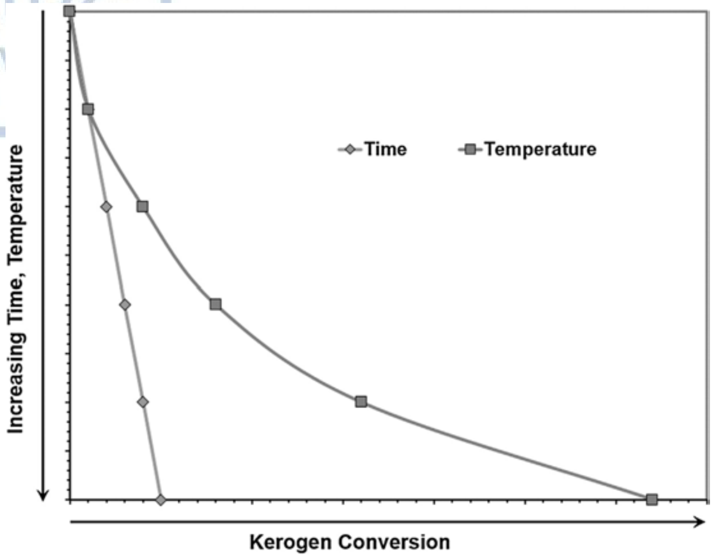

Figure 26. Comparison of the progress of the kerogen conversion reaction between linear time increase versus linear temperature increase (from Dembicki, 2017).

Figure 27 shows the kinetic parameters of the kerogen types. Type I and IIS kerogens show single activation energies (53 and 50 kcal/mol, respectively), and their peak transformation temperature windows are very narrow (~5 and ~10 oC, respectively). The Type IIS kerogen activation energy is the lowest among kerogens, likely reflecting the predominance of the more labile C-S-C cross-linking bonds. This has important implications in petroleum system analysis as this kerogen type is expected to generate oil with much lower thermal maturities than the anticipated "typical" oil window VR: 0.6% (Orr, 1986; Lewan et al., 1998). It has been shown (Baskin and Peters, 1992; Jarvie and Lundell, 2001) that source rocks Formations with high organic sulfur content, such as the Monterey, Bazhenov, Kimmeridgian, etc., have generated oil with significantly lower thermal maturities (at ~0.30-0.35% VR or ~410-415^{o}C T_{max}) (e.g., Baskin and Peters, 1992).

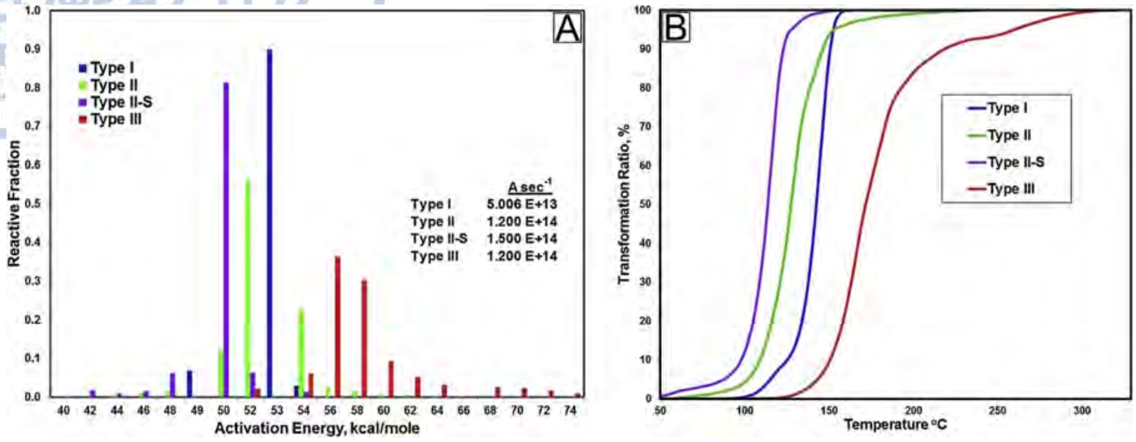

Figure 27. A) Activation energies for each kerogen Type, B) Transformation ratio versus temperature curves for each kerogen Type (from Dembicki, 2017).

Intervals or areas where the OM preservation was inadequate due to biological and geological factors such as oxidative conditions are not attractive exploration targets. A rapid and inexpensive means to screen whether a rock holds HC potential is the Rock Eval pyrolysis method which provides parameters (among others) such as the total organic carbon (TOC) and the hydrogen index (HI), crucial in source rock evaluation.

1.5.11 Integrated hydrocarbon exploration

Multidisciplinary studies combining "basic" geology (e.g., geological mapping, stratigraphy, petrography, structural geology, etc.) with geophysical surveys and organic geochemical studies arguably comprise the very core of frontier exploration activities. The importance of each one of them for a successful outcome has been quantified by Sluijk & Parker (1986) (Figure 28), where the importance of combined methods is reflected in the immense cost-effectiveness. All these efforts being put into reduce the risk, but they are unable to diminish it.

1.6 Research questions

Pilot field work for the present study started in 2014. Since the first days of field work, it was obvious that although the available published literature had achieved significant progress in the understanding of the Ionian Zone geology and petroleum geology specifically, there were unsettled issues outflowing from the particularly complex tectonic and stratigraphic setting.

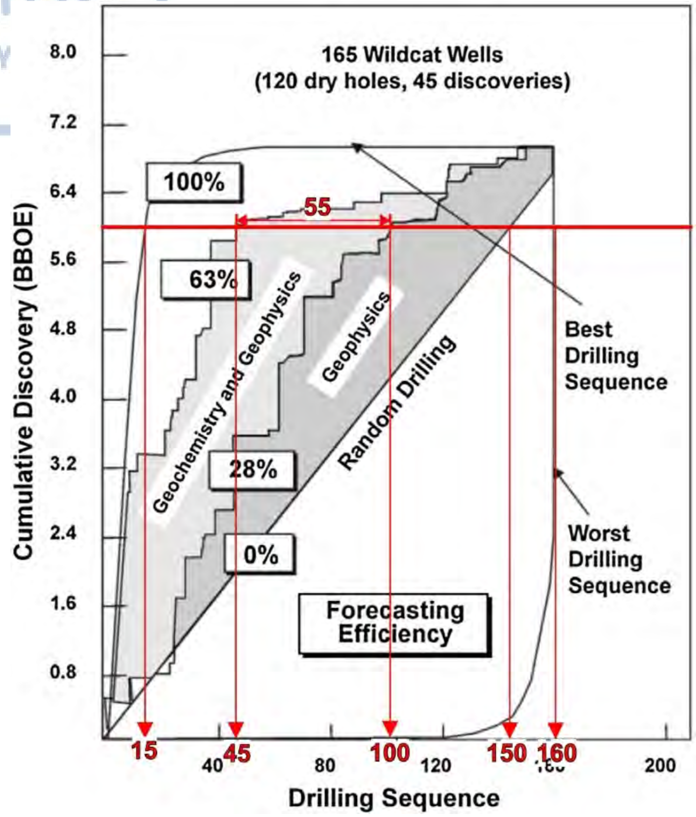

Figure 28. Cumulative discovery versus drilling sequence diagram in which the importance of integrated exploration methods is highlighted. Taking as a base scenario the 6 BBOE cumulative discovery, it is observed that this figure is achieved with 150 randomly placed drills, or 100 drills solely based on geophysical survey suggestions, or 45 drills after joint geophysical and geochemical survey suggestions.

The study of the literature had partially answered important questions concerning basin evolution and the large gaps identified in the section study. Some of these questions, among others, deal with a) the identification and characterization of the quality characteristics and the extent of the source rock intervals; b) the geotectonic and thermal evolution of the basin; c) the basin configuration evolution; and d) the influence of the Triassic evaporites on the petroleum systems. These questions were attempted to be addressed by means of field-geological investigations, organic geochemical studies, and basin modeling.

Chapter 2 – Geology and petroleum systems of Epirus

2.1 Geotectonic evolution and geological setting

The Ionian Zone is a NW-SE-oriented belt of deformed Mesozoic – Cenozoic sedimentary rocks. It shapes the westernmost parts of the Greek peninsular mainland and Peloponnese, as well as the southwestern parts of Albania. It also forms the Ionian Island of Corfu whereas it partially shapes the eastern parts of the Kefallinia and Zakynthos islands (Figure 29). Along with the Gavrovo-Tripolis to the east and the Paxoi (or Pre-Apulian) Zone to the west, they comprise the External Hellenides . All these three Zones represent the remnants of a wide sedimentary basin of Mesozoic – Cenozoic age (Aubouin et al., 1963; Smith and Moores, 1973).

The general geotectonic evolutionary scheme of the basin involves a) a stage where the area was part of the rifted, northern Gondwanan passive continental margin (Triassic – Jurassic), b) a stage where the continental block (Adria plate) detached from the Gondwana and drifted northwards up to late Cretaceous where eventually, c) progressively collided and accreted over the Eurasian margin (final stage) (e.g., Dercourt et al., 1986; Robertson and Mountrakis, 2006; Robertson, 2007; Papanikolaou, 2013; van Hinsbergen et al., 2019).

The known stratigraphy of the Ionian Zone involves sedimentary sequences spanning from the Lower Triassic to the Pliocene. The Triassic is lithologically dominated by evaporites and dolomite, indicating a shallow marine basin setting and arid climatic conditions. Within this sequence, organic-rich deposits occur in shale, carbonate, clay, and occasionally in chert. The high thickness of these units shows persistent basin subsidence. The onset of the Jurassic is marked by a shift in sedimentation, with limestone becoming the dominant lithology up to the Eocene in most parts of the basin. Within the limestone-dominated section relatively thin shaly, siliciclastic and detrital limestone input occur at various stratigraphic levels. The detrital limestone dominates the formations deposited from the Senonian to the Eocene. Thin beds of detrital limestone also occur in Filamentous Ls., at the base of the Lower Posidonia Beds, locally within the Upper Posidonia Beds.

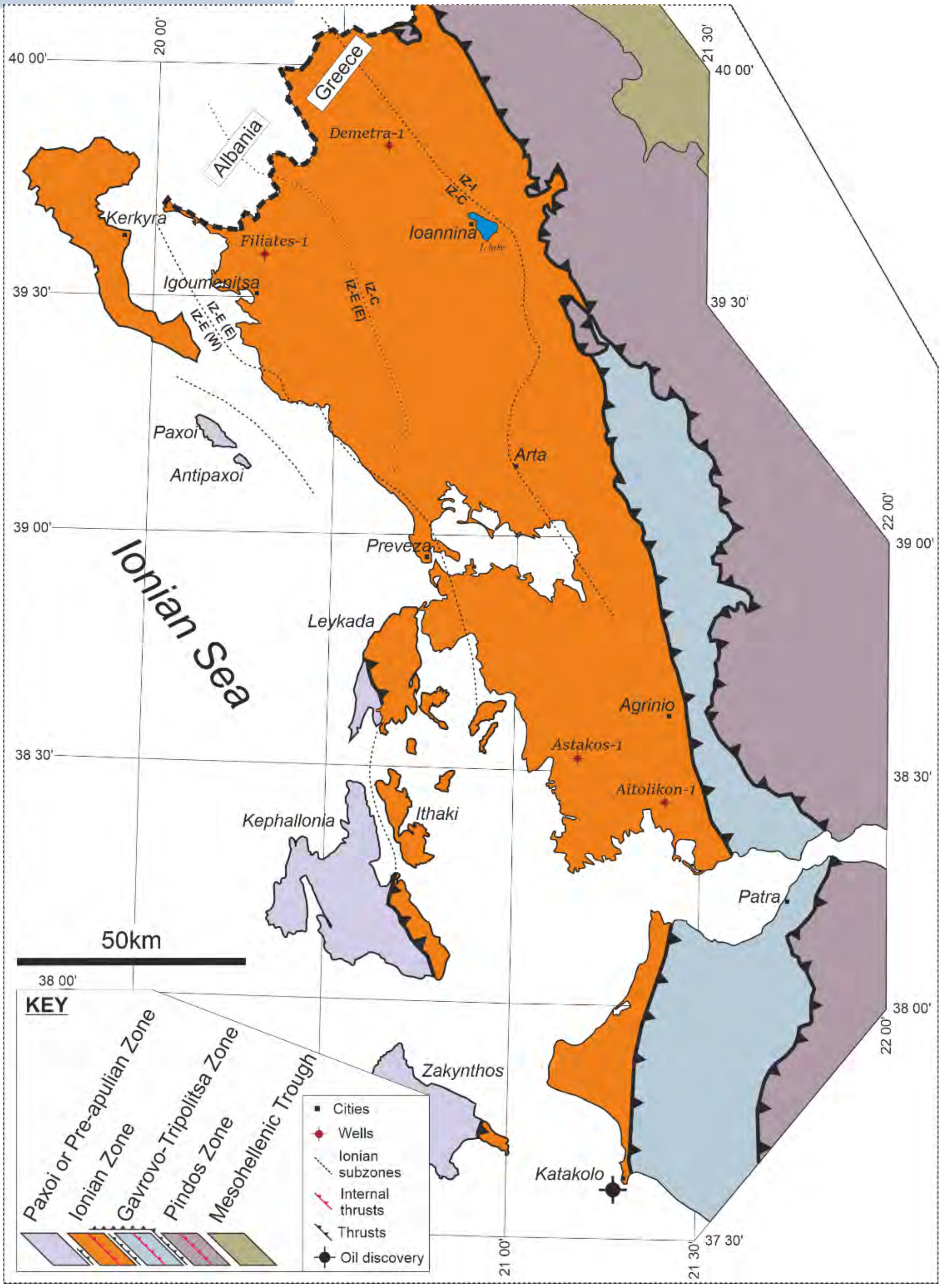

Figure 29. Map of the geotectonic zones of western Greece. Modified from Alexandridis et al. (2022a).

Organically rich intervals occur within the thin shaly/siliciclastic sequences. Basin setting variability reflects in the lithology, which varies from massive limestone in the Liassic to pelagic limestone from the Berriasian onwards. The end-Eocene is marked by the establishment of the clastic sedimentation related to the formation of a foreland basin. Organic-rich deposits occur around the Triassic/Jurassic boundary (Alexandridis et al., 2022a), in the Toarcian-Tithonian sequence (Karakitsios and Rigakis, 1996; Rigakis and Karakitsios, 1998), in Aptian-Cenomanian, and in various levels of the Oligocene-Pliocene clastic section.

The present structure of the Ionian Zone reflects its complex tectonosedimentary evolution, partially attributed to the presence of a thick salt layer at its base as well as the intense deformation of its units during Cenozoic continental collision. In Epirus, complete or partial packages of the stratigraphic units of Mesozoic and Cenozoic ages are well exposed in the folded, faulted and eroded successive thrust sheets. The thrusts and the thrusting-associated anticlines and synclines are generally oriented in NNW-SSE direction. Triassic formations outcrop at the base of various thrust sheets.

2.2 Petroleum Systems in Epirus

In order for a petroleum system to be substantiated, several geological elements must co-occur, and processes must be fulfilled. The occurrence of the petroleum system in Epirus is proven by the numerous oil seeps throughout the region. This fact led to more elaborated exploration efforts, with numerous studies to be conducted, mainly targeting in the stratigraphy and source rock properties (e.g., Karakitsios and Rigakis, 1996; Rigakis and Karakitsios, 1998). These studies resulted to the identification and characterization of various source rock intervals, which are mainly found in the: a) late Triassic (shales within the evaporite succession); b) late Lower Jurassic (*Lower Posidonia Fm*., consisting of shales of Toarcian-Aalenian age); c) Upper Jurassic (*Upper Posidonia Fm*., consisting of shales and bedded cherts); and d) Aptian-Albian (*Vigla Shales Fm*., consisting of shales and cherts). Other intervals of minor extent and/or negligible HC potential occur at the AR basal marls and at the Pliocene (e.g., Maravelis et al., 2014).

Recent outcrop studies (Alexandridis et al., 2021a) have shown that a minor gas potential might be accounted for in the Oligocene flysch and in the Burdigalian flyschoids. Moreover, organic geochemical results from outcrops of the Upper Posidonia beds show that cannot account for any HC generation

(Alexandridis et al., 2021a). However, the most important recent contribution to source rock understanding was materialized with the discovery of a new source rock interval within the Pantokrator platform carbonates (Alexandridis et al., 2021b; Alexandridis et al., 2022a). The organic matter content (up to 39% TOC wt.), the hydrocarbon potential (up to 270 kg HC/ton rock), as well as the extent, indicate a highly oil-prone source rock. Later studies in the area indicated that Pantokrator Shale is an effective source rock, as it was shown that solid bitumen migrated kilometers away from the mature source (Alexandridis et al., 2022b). Biomarker studies pointed to a lagoonal depositional setting (Alexandridis et al., 2022b; 2023a; 2023c). This is an important discovery, as it proves the occurrence of this type of source in the Greek part of the Ionian Zone. Organic-rich formations of analogous age, geological setting and geochemical characteristics are considered to constitute the main oil-prone source rocks in the Italian and Albanian oil fields, accounting for the vast oil volume proportion found in carbonate reservoirs. Table 4 shows the main organic-geochemical characteristics of the potential source rocks found in Epirus.

Table 4. Table of the potential source rocks and their main attributes in Epirus

Fm. name	***Age***	***Lithology***	***max. TOC wt.%***	***max. HI***	***max. GP (kg HC/tn)***	***Ref.***
Pliocene	Pliocene	Mdst	9.16	374	32.81	1
Burdigalian	Burdigalian	Sst, Slt	1.59	197	1.43	2
Rhadovizi	U. Oligocene	Mdst. Sh	13.71	681	17.74	2
Rammia	Oligocene	Sst, Slt	36.63	346	138.85	2
Flysch	Oligocene	Mrl, Mdst, Sh	0.47	268	1.66	2
Vigla shales	Aptian - Cenomanian	Sh, Cht, Slt	44.5	529*	153.8*	3
Upper Posidonia	U. Jurassic	Sh, Cht, Slt	3.34	405	17.5	4
Lower Posidonia	Toarcian - Aalenian	Sh, Mdst	19.12	760	125.85	4
Pantokrator Shale	U. Triassic – L. Jurassic	Sh, BSst, BSlt	38.68	269.79	790	5
Triassic shales	U. Triassic	Sh	16.12	685	98.8	6
1: Maravelis et al., 2014 2: Alexandridis et al., 2021a 3: Karakitsios et al., 2004; *Tsikos et al., 2004 4: Karakitsios and Rigakis, 2007 5: Alexandridis et al., 2022a 6: Karakitsios and Rigakis, 1996						

The main reservoir is considered the Senonian to Eocene limestones, which, although lacking high primary porosity, flexure and folding-induced fractures increase total porosity and permeability (e.g., Kontakiotis et al., 2020). This interval comprises the main reservoir in many Albanian oil fields, which comprises the northward continuation of the Ionian Zone. The Oligocene flysch comprises the regional effective seal, restraining the further upward movement of both liquid (e.g., Patos-Marinza oilfield) and gaseous (e.g., Delvina gas and condensate field) hydrocarbons.

It has been shown that the HC generation of the supra-Triassic organic rich formations is attributed to the Tertiary continental collision and the rapid burial under kilometers of flysch, as well as the overthrusting of the internal nappes over the more external ones (e.g., Karakitsios 2013; Rigakis et al., 2013). Hydrocarbon migration pathways from source to trap have not been studied in detail and only Nikolaou (2001) highlighted the effectivity of the thrust faults as tertiary migration pathways, directly linked to numerous surficial oil shows in western Greece.

Limited work has been performed on the source-oil correlation. Seifert et al. (2020) suggested that the oils in western Greece belong to three groups, I, II, and III, with Group II subdivided into IIa and IIb sub-groups. Palacas et al. (1986) suggested that the oils in western Greece belong to three groups, I, II, and III, with Group I subdivided into the Ia and Ib sub-groups. The results of these two studies were not well related. Oils of the same provenance were placed in different groups. Rigakis (1999), implementing numerous samples of oils, suggested that the western Greek oils belong to four groups (Α to Γ). His results are in better agreement with those of Palacas et al. (1986). In general, Epirus' oils belong to groups A1 and A2, W. Katakolon, Kyllini, and Tryfos belong to group B, and S. Katakolon and Aitoliko belong to group Γ. A recent study by Alexandridis et al. (2023a), showed that solid bitumen occurrences across Epirus can be correlated to the Lower Posidonia Shale and the Pantokrator Shale, or similar source rocks.

2.3 Geotectonic evolution and associated basin configurations

Paleogeographic reconstructions (e.g., Bosellini et al., 1973; Gealey, 1988; Kazmin and Natapov, 1998; Dercourt et al., 2000; Catalano et al., 2001; Barrier et al., 2018; Le Pichon et al., 2019; van Hinsbergen et al., 2020; Schmidt et al., 2020; Scotese 2016) of the Tethyan realm in the Permian-Triassic place the Ionian basin (precursor of the Ionian Zone) at the northern margin of the Gondwana supercontinent. All of these reconstructions agree on the Ionian basin affinity and location. Nevertheless, constraining the exact timing and rift mechanism (McKenzie, 1978; Issler et al., 1989; Gawthorpe and Leeder, 2000; Withjack et al., 2002; Kim and Sanderson, 2005; Reston, 2005; Ingersoll, 2012; Finch and Gawthorpe, 2017; Brune et al., 2018; Peron-Pindivic et al., 2019) of the rifting phase(s) raises variations among the various interpretations.

Partial tectonic recycling of the basin due to the Tertiary compression, intense gravitational normal faulting in co-occurrence with the ongoing compression in depth, evaporite diapirism, and block rotations have masked the preexisting tectonosedimentary features in a particularly complex manner. Confirmation and/or rejection of parts of the reconstructed domains might occur after more detailed seismic, gravitational, and—perhaps—drilling surveys performed in parts of the Mediterranean Sea. This will shed light on the structure of the entire Mediterranean convergent system, possibly re-calibrating the paleogeographic reconstructions as well.

2.3.1 Mechanisms controlling basin setting

Intense extension of the northern Gondwana plate, break-up and drifting of the continental fragments, and their collision-accretion over the Eurasia plate are typified by various basin configurations. Basin types typically reflect Wilson cycle stages, which have been generally concluded by somehow simplistic interpretations of the stratigraphic sequences. However, this study suggests that important local basin configuration differentiations were concluded by the sedimentary infill, indicating potentially regional geodynamic conditions common among large distances (Italy, Albania, Greece). For example, the discovery of the Pantokrator Shale in the IZ-C and its geological, petrographic, and geochemical similarity with time-equivalent formations in Albania and Italy show that the assumed uniform carbonate platform of the Upper Triassic–Lower Jurassic age incorporated deeper basinal parts. This is also evident in wells, where anomalously high thickness ratios of Siniais Ls (deep basin carbonates)/Pantokrator Ls (shallow water carbonates) occur (e.g., Demetra-1 well).

Basins are areas with topographic relief lower than its surroundings and therefore tend to accommodate sediments. Various mechanisms can be responsible for the subsidence, depending mainly in the geotectonic status of the area. Therefore, mantle flow and associated plate motions are the main geological background of basin formation and configuration. Coupled with tectonics, climate plays a major role in basin infill, controlling the source-to-sink mechanisms.

Chapter 3 – Materials and methods

3.1 Study strategy

For the purpose of the study, particular importance was primarily attached to the field work. An extensive pilot field work round was implemented beforehand of the main study in order to obtain a general geologic overview of the area. This pilot stage helped the main study strategy be scheduled on a more pragmatic basis, referring to the time, effort, area/geological disciplines overlap, expenses, and laboratory analysis timing.

3.2 QA/QC Field work-sampling-logging protocols

Table 5 shows the field work-logging protocol that was developed to ensure the quality and homogeneity of the data obtained during field work.

Table 5. Sampling and sample storage protocol

Sample type	***Sample obtainment***	***Sample storage***
Potential source rock	• Sample depth 10-40 cm • Fresh outcrops (e.g., roadcuts) • Less weathered (e.g., away from plant roots, water streams etc.) • Up to 300g per sample	• 18-22oC • 40-60 % RH • Dark room • Paper wrapped • Plastic bag (open) • <6 months storage

3.3 Field studies

An extensive fieldwork survey was scheduled in order to achieve a comprehensive logging of the Ionian Zone formation outcrops, with special focus on the petroleum geological aspects. Sampling of the potential source rocks was performed following a predefined QA/QC protocol (Table 5). The basic fieldwork routine included a lithological and macroscopic sedimentological description, the structural description, and measurements of the structural elements (bedding planes, lineations, faults), while a detailed logging of the joints was also implemented. The sections and locations visited and logged were either predetermined based on their stratigraphic importance, inclusiveness or complexity, or they were studied based on their interesting features that they across during field work. Characteristic representative field photos of sedimentary, stratigraphic, structural and petroleum-geological features were captured, and cartoon sketches of such structures were drawn, both at various scales.

More than 100 days were spent in the field resulted in the obtainment of >80 samples of potential source rocks and the logging of more than 600 locations throughout an area extending in >6000 km^2 throughout Epirus in all four prefectures (Ioannina, Arta, Thesprotia and Preveza). Several stratigraphic sections were studied in detail, and several samples of various fossil remnants were collected in order to be further studied.

The following stratigraphic sections (Table 6) were studied in detail (the stratigraphic range and thicknesses are annotated):

Table 6. Stratigraphic sections studied in detail

Section name/area	***Stratigraphic range/formation***	***Studied thickness (m)***
Kefalovryso – Vassiliko	Triassic – Tithonian	~1100
Souli – Paramythia Mt	Triassic – Tithonian	~1500
Mavroudi	Pliensbachian – Toarcian	~100
Kouklesi	Pliensbachian – Tithonian	~200
Koukoulioi	Triassic – Tithonian	~700
Elataria	Vigla Shales	~90
Chionistra	Liassic – Senonian	~600
Lithino	Pliensbachian – Tithonian	~100
Kastri	Vigla Shales	~80
Igoumenitsa	Triassic – Tithonian	~500?
South Souli	Pliensbachian – Tithonian	~100

Moreover, several sections demonstrating important information concerning the structural geology of the area were also studied in detail.

3.4 Geological mapping

Geological mapping was performed on selected, important unmapped lithological units, combining the direct observation of the lithological unit boundaries in the field with satellite imagery. This method aided the mapping of many outcrops, mainly of the Vigla Shales (which is a known but unmapped lithostratigraphic unit in Epirus) especially those that were difficult to approach (steep, dangerous terrain, dense vegetation, wildlife threats, shepherd dogs, properties, blocked rural roads etc.). The best time to conduct fieldwork in Epirus is the October, November, late February, March, and April, when weather conditions, wildlife, and vegetation have the least negative effect in fieldwork-related activities.

3.4.1 Satellite imagery-aided mapping

This method integrates the classic field work, the usage of the existing geological maps, and the observation of high-resolution satellite imagery available. It is optimally applied in areas that show relatively low vegetation or shifts in vegetation, providing rapid results (geological maps). Georeferenced geological maps help by providing the bulk geological boundaries, which, when compared to satellite imagery, can be tremendously improved in terms of accuracy, even at very large scales (depending on the imagery quality and resolution). Field work is of critical importance as it provides direct and detailed observation of the formations of interest and their contacts. Field work confirms or rejects the drawn geological boundaries over the satellite imagery, and vice versa.

This method is implemented in a circular workflow, as it can start from the fieldwork observations, which will be properly spatially expanded with the satellite imagery analysis, or it can start from the satellite imagery analysis, which, in comparison to the available geological maps, will show the possible formation boundaries (Figure 30). In both workflow directions, a final confirmation of the predicted formation boundaries should always be performed in the field in order to validate the accuracy of the process and the map.

This method significantly reduces the effort of traditional geological mapping, during which a geological boundary should be walked along. Also, this method can provide geological maps of supreme accuracy, especially where the lithological differences between the formations are sharp or these differences induce discrete and spatially consistent vegetation shifts.

Figure 30. Geological mapping circular workflow. Mapping can start either ways. Number of full mapping rounds depend on the project specifications and demands.

In Figure 31, an example of the method is provided. The area selected demonstrates a rather complex structure with synclines, anticlines, and faults. The stratigraphy is dominated by limestone, whereas the formations of interest consist of relatively thin clay-shale and chert-rich intervals lying at various stratigraphic levels. In Figure 31A, the geological map of the area is shown, and in Figure 31B, the satellite imagery is shown. Field work in the area confirmed the following:

a) The boundary between the Ls.V and the Ls.Sen is characterized by a shift in lithology which is physically expressed as a consistent topographic ledge.

b) The formation of interest Sh.V consists by three distinct clay-shale-chert-rich intervals over which the vegetation thrives.

c) The outcrops of the formations of interest Sh.PL and Sh.PU are heavily vegetated as well.

Details of the contacts are given in Figures 31a-f. On this base, it was possible to compose a high-precision geological map (Figure 32) of the formations of interest throughout the particular area over the satellite imagery base map.

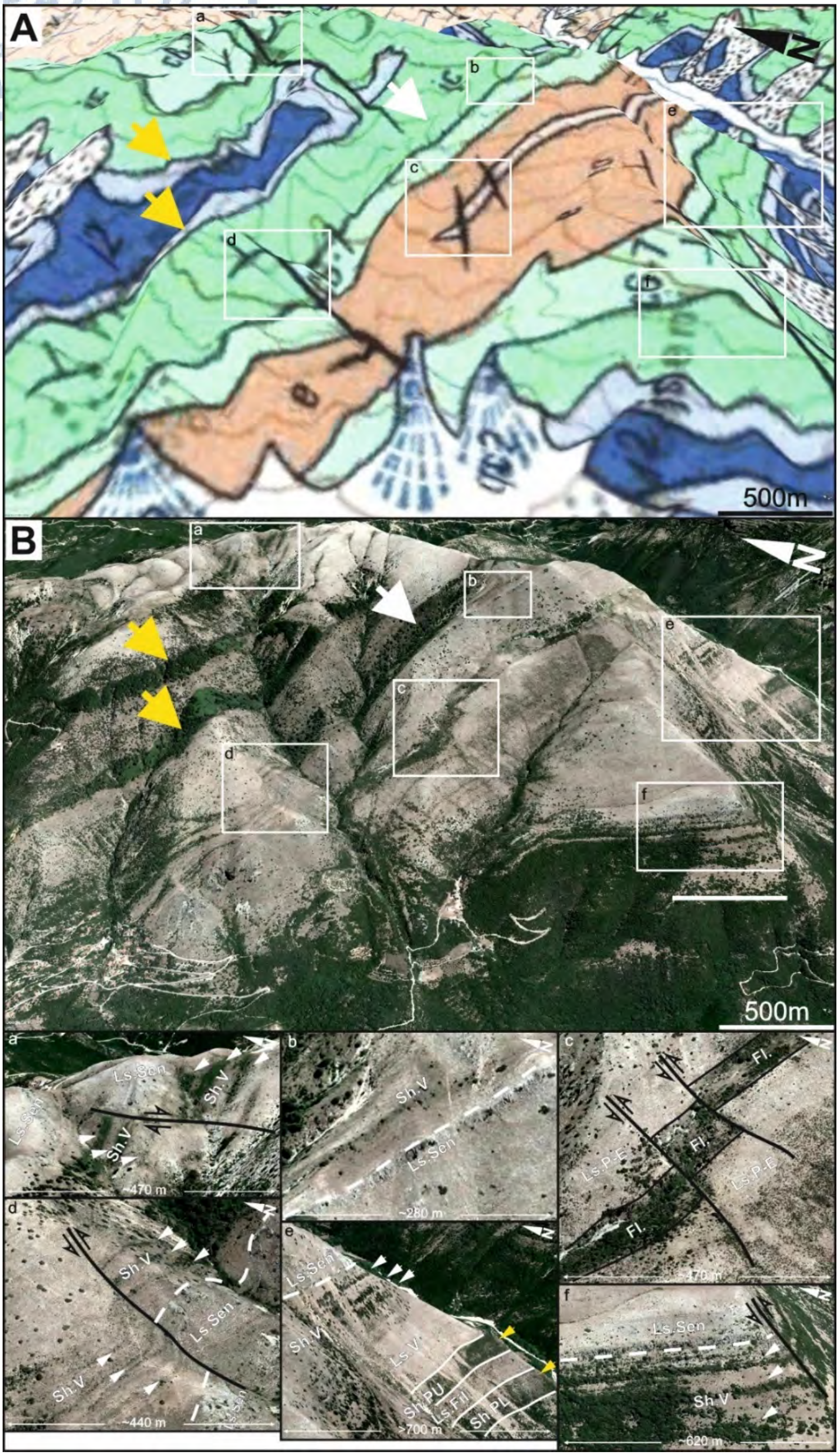

Figure 31. A) Geological map, B) Satellite imagery, oblique view of the area shown in geological map [A], a-f) details of the geological contacts and boundaries.

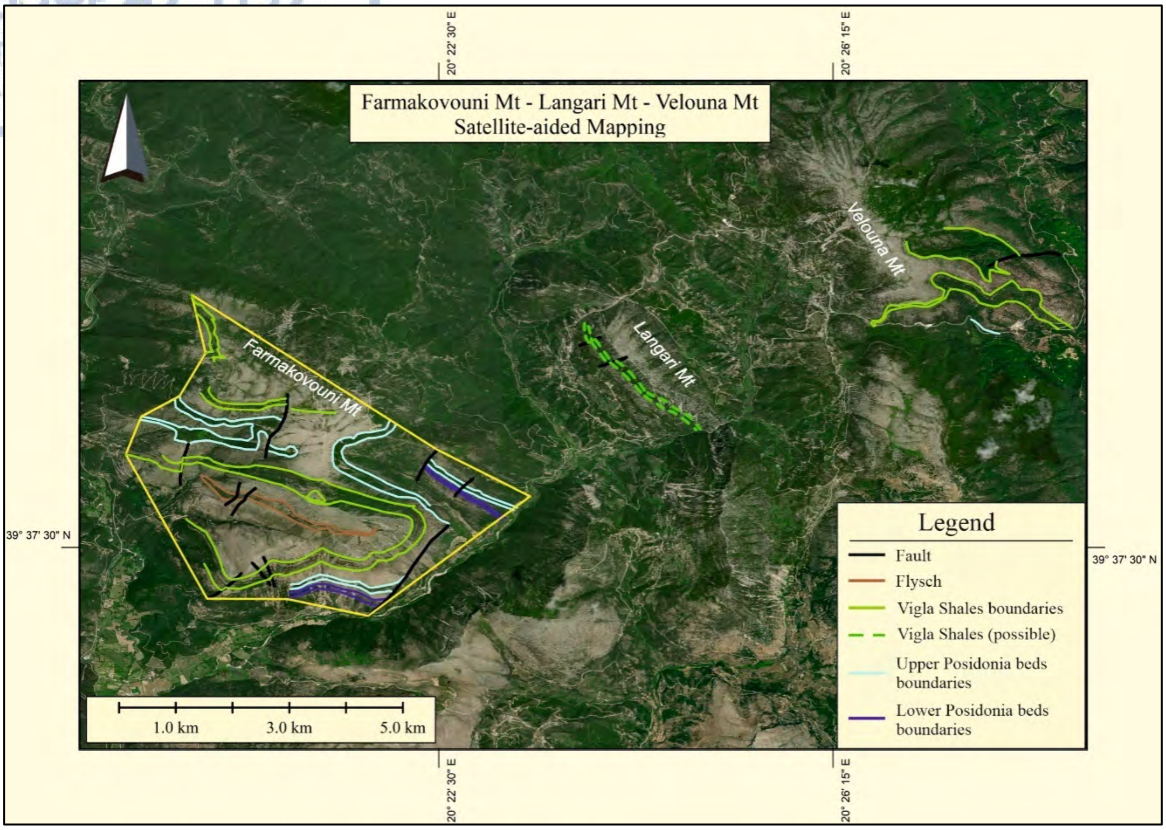

Figure 32. Geological boundaries drawn with high precision over satellite imagery base-map.

3.5 Programmed Open System Pyrolysis – Rock-Eval 6

Rock-Eval 6® (RE6) by Vinci Technologies, France (Lafargue et al., 1998) is an apparatus performing temperature-programmed open system pyrolysis on bulk rock samples. It is broadly used in the O&G industry for basic, fast, and cost-effective source rock screening instead of the expensive and laborious wet chemistry techniques. Implementing the Basic/Bulk-Rock method (Behar et al., 2001), various parameters were acquired (see Table 7), such as the S1 peak of the pyrogram (the amount of free hydrocarbons in mg HC/g rock) and the S2 peak (the amount of hydrocarbons the sample can generate in mg HC/g rock), whereas several other useful parameters were calculated (Table 8), such as the total organic carbon (TOC in wt.%), the hydrogen index (HI, mg HC/g TOC), and the oxygen index (OI, mg HC/g TOC). Moreover, insights on the maturity degree of the OM are acquired by the temperature of the S2 peak (TpS2, commonly referred to as Tmax in ^{o}C). The Analyses were performed in Core Laboratories, Texas, USA.

Table 7. Rock-Eval acquisition parameters

Acquisition parameters	Detector/Oven	Unit	Name
S1	FID/Pyrolysis	mg HC/g rock	Free hydrocarbons
S2	FID/Pyrolysis	mg HC/g rock	Oil potential
TpS2	–	°C	Temperature of peak *S2* maximum
S3	IR/Pyrolysis	mg CO_2/g rock	CO_2 organic source
S3'	IR/Pyrolysis	mg CO_2/g rock	CO_2 mineral source
TpS3'	–	°C	Temperature of peak *S3'* maximum
*S3*CO	IR/Pyrolysis	mg CO/g rock	CO_2 organic source
*TpS3*CO	–	°C	Temperature of peak *S3*CO maximum
*S3'*CO	IR/Pyrolysis	mg CO/g rock	CO organic and mineral source
*S4*CO_2	IR/Oxidation	mg CO_2/g rock	CO_2 organic source
S5	IR/Oxidation	mg CO_2/g rock	CO_2 mineral source
TpS5	–	°C	Temperature of peak *S5* maximum
*S4*CO	IR/Oxidation	mg CO/g rock	CO organic source

Table 8. Rock-Eval calculated parameters

Calculated parameters	Unit	Formula	Name
Tmax	°C	$TpS2 - \Delta Tmax^{*}$	*Tmax*
PI		$\frac{S1}{(S1+S2)}$	Production index
PC	wt%	$\frac{[(S1+S2)\times 0,83]+\left[S3\times\frac{12}{44}\right]+\left[\left(S3CO+\frac{S3'CO}{2}\right)\times\frac{12}{28}\right]}{10}$	Pyrolysable org. carbon
RC CO	wt%	$\frac{S4CO\times\frac{12}{28}}{10}$	Residual org. carbon (CO)
RC CO_2	wt%	$\frac{S4CO_2\times\frac{12}{44}}{10}$	Residual org. carbon (CO_2)
RC	wt%	RC CO + RC CO_2	Residual org. carbon
TOC	wt%	PC + RC	Total organic carbon
S1/TOC	mg HC/g TOC	$\frac{S1\times 100}{TOC}$	
HI	mg HC/g TOC	$\frac{S2\times 100}{TOC}$	Hydrogen index
OI	mg CO_2/g TOC	$\frac{S3\times 100}{TOC}$	Oxygen index
OI CO	mg CO/g TOC	$\frac{S3CO\times 100}{TOC}$	Oxygen index CO
PyroMinC	wt%	$\frac{\left[S3'\times\frac{12}{44}\right]+\left[\left(\frac{S3'CO}{2}\right)\times\frac{12}{28}\right]}{10}$	Pyrolysis mineral carbon
OxiMinC	wt%	$\frac{S5\times\frac{12}{44}}{10}$	Oxidation mineral carbon
MinC	wt%	PyroMinC + OxiMinC	Mineral carbon

The seminal work of Peters (1986) provided a context for the RE6 screening by associating value ranges with potential source rock attributes. Peters and Cassa (1994) further sophisticated the screening parameters, providing a widely used framework (Tables 9, 10 and 11).

Table 9. "Geochemical Parameters Describing the Petroleum Potential (Quantity) of an Immature Source Rock" from Peters and Cassa (1994).

Petroleum Potential	Organic Matter: TOC (wt. %)	Rock-Eval Pyrolysis: S_1[a]	Rock-Eval Pyrolysis: S_2[b]	Bitumen[c] (wt. %)	Bitumen[c] (ppm)	Hydrocarbons (ppm)
Poor	0–0.5	0–0.5	0–2.5	0–0.05	0–500	0–300
Fair	0.5–1	0.5–1	2.5–5	0.05–0.10	500–1000	300–600
Good	1–2	1–2	5–10	0.10–0.20	1000–2000	600–1200
Very Good	2–4	2–4	10–20	0.20–0.40	2000–4000	1200–2400
Excellent	>4	>4	>20	>0.40	>4000	>2400

Table 10. "Geochemical Parameters Describing Kerogen Type (Quality) and the Character of Expelled Products" from Peters and Cassa (1994).

Kerogen Type	HI (mg HC/g TOC)	S_2/S_3	Atomic H/C	Main Expelled Product at Peak Maturity
I	>600	>15	>1.5	Oil
II	300–600	10–15	1.2–1.5	Oil
II/III[b]	200–300	5–10	1.0–1.2	Mixed oil and gas
III	50–200	1–5	0.7–1.0	Gas
IV	<50	<1	<0.7	None

Table 11. "Geochemical Parameters Describing Level of Thermal Maturation" from Peters and Cassa (1994).

Stage of Thermal Maturity for Oil	Maturation: R_o (%)	Maturation: T_{max} (°C)	Maturation: TAI[a]	Generation: Bitumen/TOC[b]	Generation: Bitumen (mg/g rock)	Generation: PI[c] $[S_1/(S_1 + S_2)]$
Immature	0.2–0.6	<435	1.5–2.6	<0.05	<50	<0.10
Mature						
Early	0.6–0.65	435–445	2.6–2.7	0.05–0.10	50–100	0.10–0.15
Peak	0.65–0.9	445–450	2.7–2.9	0.15–0.25	150–250	0.25–0.40
Late	0.9–1.35	450–470	2.9–3.3	—	—	>0.40
Postmature	>1.35	>470	>3.3	—	—	—

Dembicki (2009) brought out the importance of the integrated evaluation of the RE6 parameters, providing pragmatic examples of common pitfalls in RE6 result screening. Important screening parameters depend upon the thermal maturity of the formation; for example, with increasing thermal maturity, hydrogen and TOC consumed produce HC, thus RE6 is not representative of the original state of the OM. Moreover, high-quality marine samples might fall into the Type I kerogen curve area in a pseudo-van Krevelen plot (HI vs. OI). This kerogen is likely a Type IIS kerogen, as Type I kerogen is of lacustrine origin. This work followed with care all the widely accepted methods of RE6 parameter screening.

3.6 Organic petrography

Five polished blocks of potential source rocks were prepared following ISO 7404-2 (2019). One sample belonged to the TCB, one to the Sh.P., one to the Sh.PL, and two to the Sh.V. These samples have the highest TOC wt% content among all the samples analyzed with RE6. They originate from various locations, including lithological variations (Table 12). The dispersed OM composition was examined with the LEICA DMRX coal-petrography microscope. Observations were performed under a white light source (Halogen 200 W) and with a blue light source (UV) excitation in fluorescence mode (Mercury HBO 100 W/2). The objective magnification was ×50 (total x 500), and the samples were oil-immersed. Random reflectance (%Rr) measurements were performed with the LEICA MPV-SP microspectrophotometer. The identification of dispersed OM as well as the reflectance measurements were both determined based on ASTM D7708-14 (2014) and ISO 7404-5 (2009). The analyses were performed in Patras University.

Table 12. Table of the samples studied by organic petrography. Age, formation, area, lithology and basic RE6 parameters are shown.

Age	***Formation***	***Area***	***Lithology***	***TOC***	***HI***	***T_{max}***
Cret.	Sh. V	Vasilopoulo	Black chert	0.59	444	419
Cret.	Sh. V	Elataria	Black chert/shale	2.34	353	422
Low. Jur.	Sh.	Elataria	Black chert	0.65	360	422
Tr./Jur.	Sh. P	Souli Mt.	Black shale	27.2	790	417
Trias.	TCB	Stavrodromi	Black carbonate	0.85	442	417

3.7 GC/MS – Biomarkers

Gas Chromatography/Mass Spectrometry (GC/MS) stands as the basic analytical wet chemistry tool for the analysis of hydrocarbon biomarkers. GC/MS is a method suitable for the identification, quantification, and source determination of hydrocarbons. The application begins with sample preparation, involving bitumen extraction, purification, and concentration steps to isolate target compounds. Subsequently, the gas chromatography component separates individual compounds based on their chemical properties, effectively separating complex mixtures. These compounds are then introduced into the mass spectrometer, where they are ionized, fragmented, and detected, producing mass spectra that serve as molecular fingerprints. The resulting data analysis involves comparison of these spectra to reference libraries and known standards, facilitating the identification and quantification of biomarkers. GC/MS allows for a deep understanding of hydrocarbon systems and environmental implications of the source rock depositional settings.

Presence of specific biomarkers compounds and specific biomarker abundance ratios are utilized as proxies for depositional settings attributes and environmental conditions (e.g., water depth, salinity, photic zone). A summary of such proxies are shown in Table 13.

Table 13. Table of biomarker tools and their utilization in the environmental conditions assessment

TOOL	***Proxy for:***
Bitumen yield	HC generation potential
C_{27} 2-Methyl-trisnorhopane	Cyanobacteria indicator
Pristane/Phytrane ratio (Pr/Ph)	Oxygen content
C_{31}-hopane isomerization at C22: S/(S+R)	Thermal maturity
Long/short chain alkanes & thio-analogs	OM origin
Thioaromatic HCs: P[1], MP[2], DBT[3], MDBT[4]	Thermal maturity, Fe-lean dep. sett.
Alkylated 2methyl-trimethyltridecyclchromans (MTTCs)	Salinity
Hopane/sterane	OM origin /oil stain origin
C29/ C31 hopanes ratio	OM origin / oil stain origin
[1] : Phenanthrene [2] : Methylated phenanthrene [3] : Dibenzothiophene [4] : Methylated dibenzothiophene	

Bitumen extracts from Lower Posidonia Shale and Pantokrator Shale bulk rock samples were examined for their molecular properties. Lower Posidonia samples were obtained from Petousi and Elataria sections, and Pantokrator Shale samples were obtained from Souli Mt area. Moreover, three solid bitumen samples were obtained from three locations; Petousi, Elataria and Vassiliko.

3.8 Scanning Electron Microscopy (SEM)

The scanning electron microscope (SEM) is a versatile apparatus that is broadly used in rock characterization in terms of geochemical and mineralogical composition, as well as for detailed depiction of the surface structure on the scale of a few μm. A focused electron beam impinges on the sample surface, and various receptors collect the emitted signal (backscattered and secondary electrons). The automatic processing of these signals provides various types of imaging of the examined surface as well as a semi-quantitative elemental analysis.

Seven (7) samples were selected at an early stage of the sampling procedure in order to provide helpful insights concerning the Ionian formations under study and to guide the further steps of the field work. The selected samples were studied in two phases. In the first phase, three (3) unpolished and carbon-coated samples were studied (samples 15, 29, and 39), and several images and spectra were obtained. In the second phase, polished and carbon-coated samples (3, 6, 11, 15, 29, 31, 39) were prepared, and several images and spectra were obtained. Details about the samples are presented in Table 14. The analyses were performed in Aristotle University Thessaloniki in a FESEM JSM 7610 FPlus (JEOL) type apparatus.

Table 14. Table of samples examined by SEM.

ID	***Age***	***Formation***	***Lithology***	***Area***	***Type***	***CC***	***Img.***	***Spectr.***	***Phase***
3	Sen.	Ls.Sen	Limestone	Chrysorachi	P	yes	yes	yes	2
6	Tr.	TCB	Carbonate	Repetista	P	yes	yes	yes	2
11	Cret.	Sh.V	Shale/chert	Vasilopoulo	P	yes	yes	yes	2
15	Eoc.	Ls.P-E	Ls./Sh. Oil-impregnated	Soulopoulo	U, P	yes	yes	yes	1, 2
29	U. Jur.	Sh.PU	Shale/chert	Kouklesi	U, P	yes	yes	yes	1,2
31	Sen.	Ls.Sen	Limestone	Despotiko	P	yes	yes	yes	2
39	Cret.	Sh.V	Shale/chert	Elataria	U, P	yes	yes	yes	1,2
Polished (P) and Unpolished (U) sample CC: Carbon Coated samples Sen.: Senonian, Tr.: Triassic, Cret.: Cretaceous, Eoc.: Eocene, U. Jur.: Upper Jurassic Ls.: Limestone, Sh.: Shale									

Chapter 4 – Results

4.1 Lithostratigraphic units

In this study, twenty (20) lithostratigraphic formations are identified in outcrops throughout the Epirus. Their macroscopic lithological, sedimentological, and stratigraphic characteristics are described in detail. The time frame for the majority of the units generally follows the stratigraphic column suggested by Karakitsios (2013).

The locations of the photos are provided in the map and table of locations of the ANNEX.

4.1.1 Burdigalian

The Burdigalian mixed terrigenous and marine clastic and carbonate deposits are an elongated, NNW-SSE-directed lithostratigraphic unit outcropping in the IZ-C sub-zone. To the greatest extent, it is characterized by its resemblance to the flysch lithology. Turbidite successions of alternating sandstone and marlstone/shale beds often dark-colored (Figures 33a and 33e) occur in the majority of the formation outcrops. Thick (>200m) marlstone members also occur. A characteristic, up to 4 m-thick calcarenite bed (Figure 33b) is observed in the western parts of the formation. In one location in the eastern parts of the formation, a thick, dense accumulation of cauliflower oncoids is observed within a gray marl matrix (Figure 33c).

Thick-shelled benthic fauna is rich in calcarenite beds. Large (>5cm) coalified phytoclasts are often observed in the lower parts of sandstone beds (Figure 33d). These phytoclasts are progressively becoming thinner upwards within sandstone individual beds. Glauconite-rich calcarenite is observed in one location. In the area of Zallongo Mountain, Triassic evaporites are found piercing the formation (Figure 33f) to an extent of a few tens of meters.

Figure 33. Field photographs of various lithologies of the Burdigalian flyschoids formation. a) typical turbidite-style successive alternations of sandstone/mudstone beds, b) 3 m of stiff calcarenite, apparent bedding corresponds to slight lithological variation resulting to variations in weathering resistance, c) a "cauliflower" oncoid from the easternmost parts of the Burdigalian deposits, d) large coalified phytoclasts in calcareous sandstone, e) alternations of black clay/marl and sandstone, f) Triassic salt intrusion in the Burdigalian deposits in the Zallongo Mt area.

4.1.2 Flysch

The Flysch Fm. of the Ionian Zone demonstrates important variations in the lithology and thickness throughout the Epirus. The typical form of sandstone/mudstone alternating beds is the dominant lithology throughout the Epirus (Figure 34a).

The presence of coarse-grained (sandstone and conglomerate) members is characteristic at various stratigraphic levels within the flysch sequence of the IZ-I, especially in its easternmost parts. The conglomerate bodies reach thicknesses of up to 100 m or more (Figure 34b). Often, fining upward cycles are recognized. The sorting of the particles is generally poor. The granule-to-boulder (up to 0.5 m in diameter)-sized clasts are well-rounded with various degrees of sphericity (Figure 34d). The main lithology of the clasts is of the ophiolitic suite and of limestone. A sheared granitic gneiss pebble was also observed. The basal contacts of the conglomerate members vary from lithologically gradual to abrupt. In the abrupt contacts, signs of tectonic transposition are identified (sheared contact, truncated beds). Stacking patterns (Figure 34c) of the clasts are frequently observed, revealing the paleocurrent directions. Very thick successions (>500 m) of marl and marly sandstone as well as sandstone are present. Both marl and sandstone bodies frequently contain sparse, coarse-grained clasts distributed parallel to bedding. Bioturbation and various ichnofossils are frequently observed.

In the IZ-C, pebble-sized, well-rounded, sparsely distributed clasts of ophiolites are observed in a few locations. A coral reef fragment was also found in one location. A possible dewatering structure (tepee structure) was observed in one location. A thick (>300 m) marl-dominated member occurs in the upper stratigraphic levels of the flysch sequence in IZ-C, containing a few 2-3 m thick, pebble-sized clast-supported conglomerate beds.

Figure 34. Field photographs of various lithologies of the Flysch formation. a) the typical lithology of the Flysch Epirus with alternations of sandstone/mudstone beds, b) a thick conglomerate member lying in the uppermost parts of the Flysch of IZ-I, within the Potamia Marls, c) well-developed stacking pattern of well-rounded boulder-sized sandstone clasts of IZ-I (water flow direction towards the 220°), d) boulder-size well-rounded clasts within marl matrix in the IZ-I.

Concerning the presence of organic material within the flysch, black vitreous seams of mm-thickness and a few meters in length (Figure 35a) are observed within the transitional sandstone of the base of a conglomerate body in the IZ-I, as well as within a marl-dominated flysch member of the IZ-C. Also, dispersed coalified phytoclasts (sub-mm to cm-sized in diameter) at the base of sandstone beds (Figure 35b) are commonly observed in several sections in IZ-I and IZ-C. Dispersed organic material also occurs within dark-colored marls in the form of sub-mm dark-colored particles. In several outcrops of the IZ-I and IZ-C, structures revealing high accommodation of compressional strain (successive tight folds) are frequently observed.

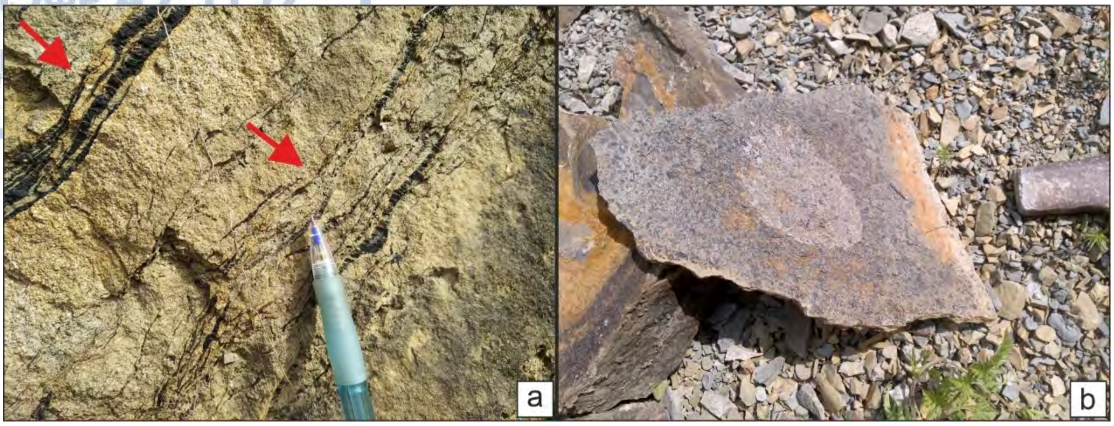

Figure 35. a) thin, black, vitreous seams shown with the red arrows interbedded within the sandstone base of a conglomerate member in IZ-I, b) mm-scale dispersed coalified phytoclasts are often observed in the bottom of individual sandstone beds.

4.1.3 Transitional marl

Between the underlying Paleocene-Eocene limestones and the overlying Oligocene flysch, a 10–30 m-thick formation (Figure 36d) of an intermediate lithology occurs. It is observed throughout Epirus. It consists of brownish and grayish marl and marly limestone, whereas in many sections it appears in greenish and reddish colors (Figure 36a). Occasionally, it shows mm-scale forms of ferrous oxides and, rarely, sparse signs of bioturbation (Figure 36b). In two locations, one in IZ-I and one in IZ-C, these transitional beds were observed interbedded within the upper few tens of m of the Eocene limestones (Figure 36c). The interbedded beds reach 15 m in the IZ-I, whereas in the IZ-C they are a few tens of cm thick.

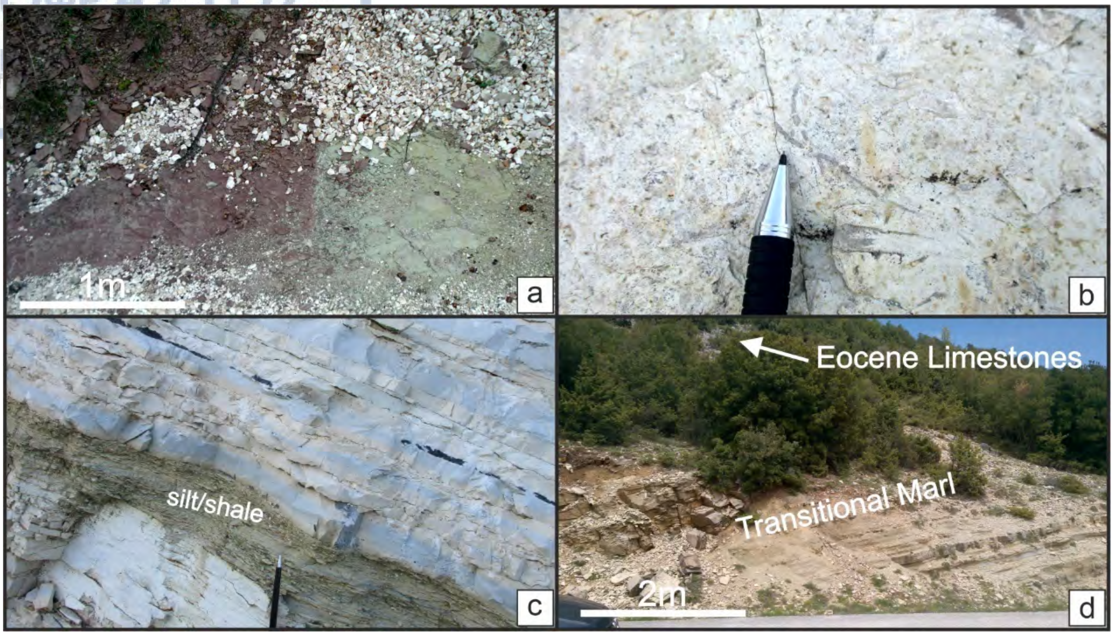

Figure 36. a) this characteristic reddish and greenish marly limestone is observed in numerous outcrops of the Transitional Marl Fm., b) bioturbation ichnofossils, c) shale/silt intercalations within the upper parts of the Eocene Limestones, a few meters below the Transitional Marl, d) a thick transitional succession ~50 m from the base of the Transitional Marl, within the Eocene Limestones.

4.1.4 Paleocene – Eocene limestones

Paleocene-Eocene Limestones consist of white-beige alternating micritic (mudstone) and clastic and bioclastic limestone beds (wackestone and packstone) (Figure 37a). Chert nodules, mostly white-beige and occasionally black-colored, are frequently observed (Figures 37b1 and 37b2). Bed thicknesses vary from a few mm or cm up to several meters (>20m). These particularly thick beds (Figure 37c) are commonly observed in the IZ-I, frequently demonstrating mm-to-cm macroscopic interparticle pores (Figure 37d). Micritic beds often host rudist fragments, Nummulites sp. fragments, and whole individuals at various sizes (1 mm to 4cm in diameter).

Very tightly packed Nummulite-bearing beds are observed in IZ-I. Ferrous oxides are observed in some sections as mm-scale brown (oxidized) masses or crystals. Their distribution is even along the bedding surface (Figure 37e), or they are linearly apposed. Wedge-shaped strata are occasionally observed (Figure 37f).

The thickness of the formation varies throughout the IZ. Maximum thicknesses are observed in the IZ-I. The contact with the underlying Senonian Limestones is conformable. The grain-supported beds are of calciturbiditic and calcidebritic origin.

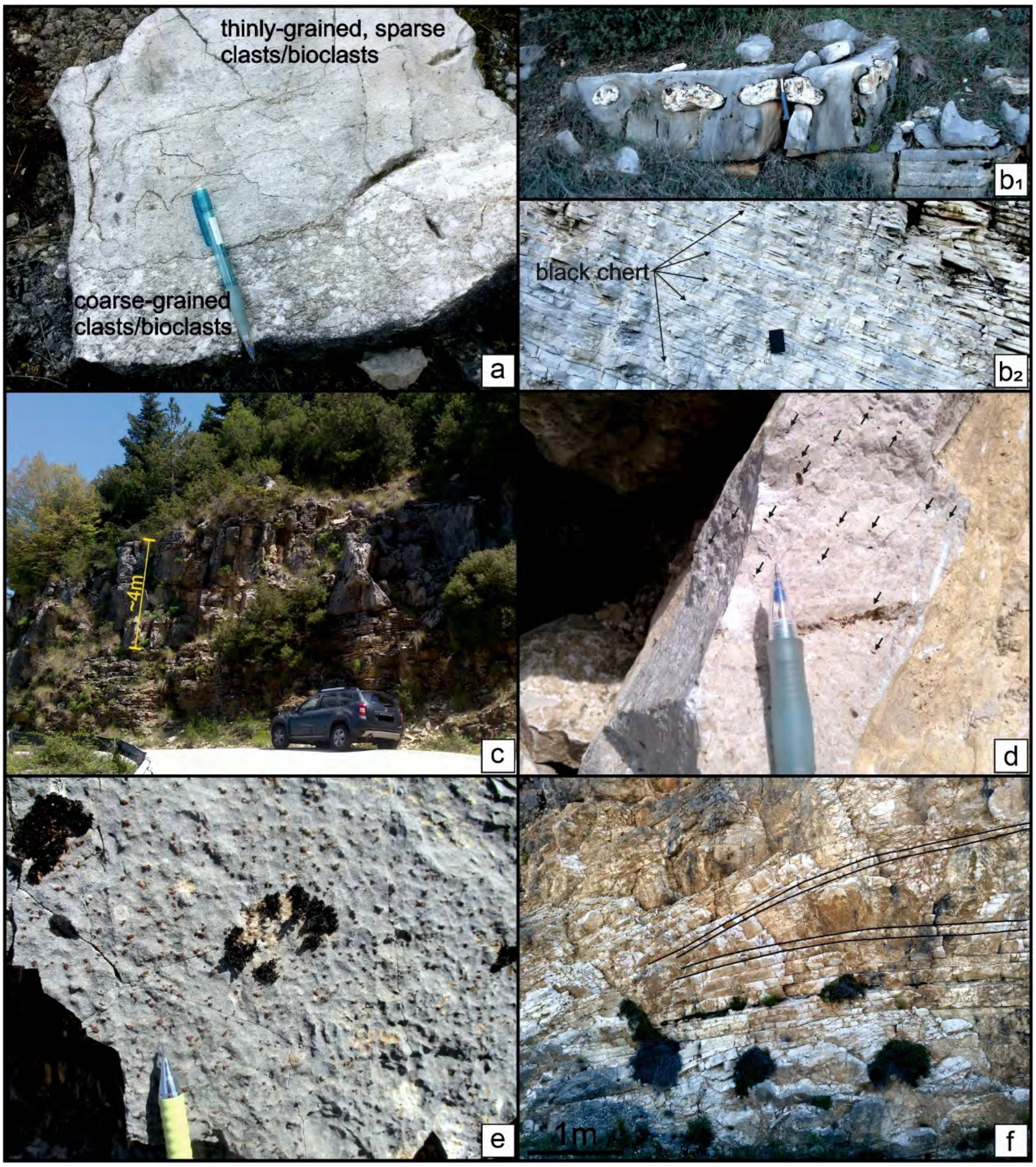

Figure 37. a) finely-grained packstone with sparse larger grains (upper part) in abrupt contact with coarse-grained packstone, b1) thick micritic limestone bed with large chert nodules, b2) thin micritic limestone beds and regularly spaced black chert beds, c) 4 m thick packstone bed in the IZ-I, d) packstone with large vugs containing skeletal and rock grains, e)oxidized euhedral pyrite on bedding plane, f) wedge-shaped bed (IZ-I).

4.1.5 Senonian limestones

Senonian limestones are conformably overlying the Vigla limestones. The boundary (Figure 38a) is usually marked by a shift in thickness (Senonian beds are thicker) as well as in lithology, as the Senonian commences with clastic and bioclastic limestone.

Its overall lithology resembles that of Paleocene-Eocene limestones (alternating beds of micritic and clastic limestone and chert nodules or lenses); nevertheless, the clastic particles are considerably larger (up to 15 cm across or more) in many sections, while the fragmented fauna involves rudists (Figures 38b, e).

Frequently, cross-cutting relations are observed in the stratification within the beds (Figure 38c). Slumped successions reaching 20 m in thickness are observed in various sections (Figure 38d).

Bed thicknesses vary from a few cm up to tens of cm up to 3–4 m. Slump folds are common in many sections. In various locations, e.g., Xirovouni Mt. and Langari Mt., the lowermost 2-3 m of the formation demonstrate a dense network of small normal faults (a few cm up to 1 m) with throws of a few centimeters (Figure 38f).

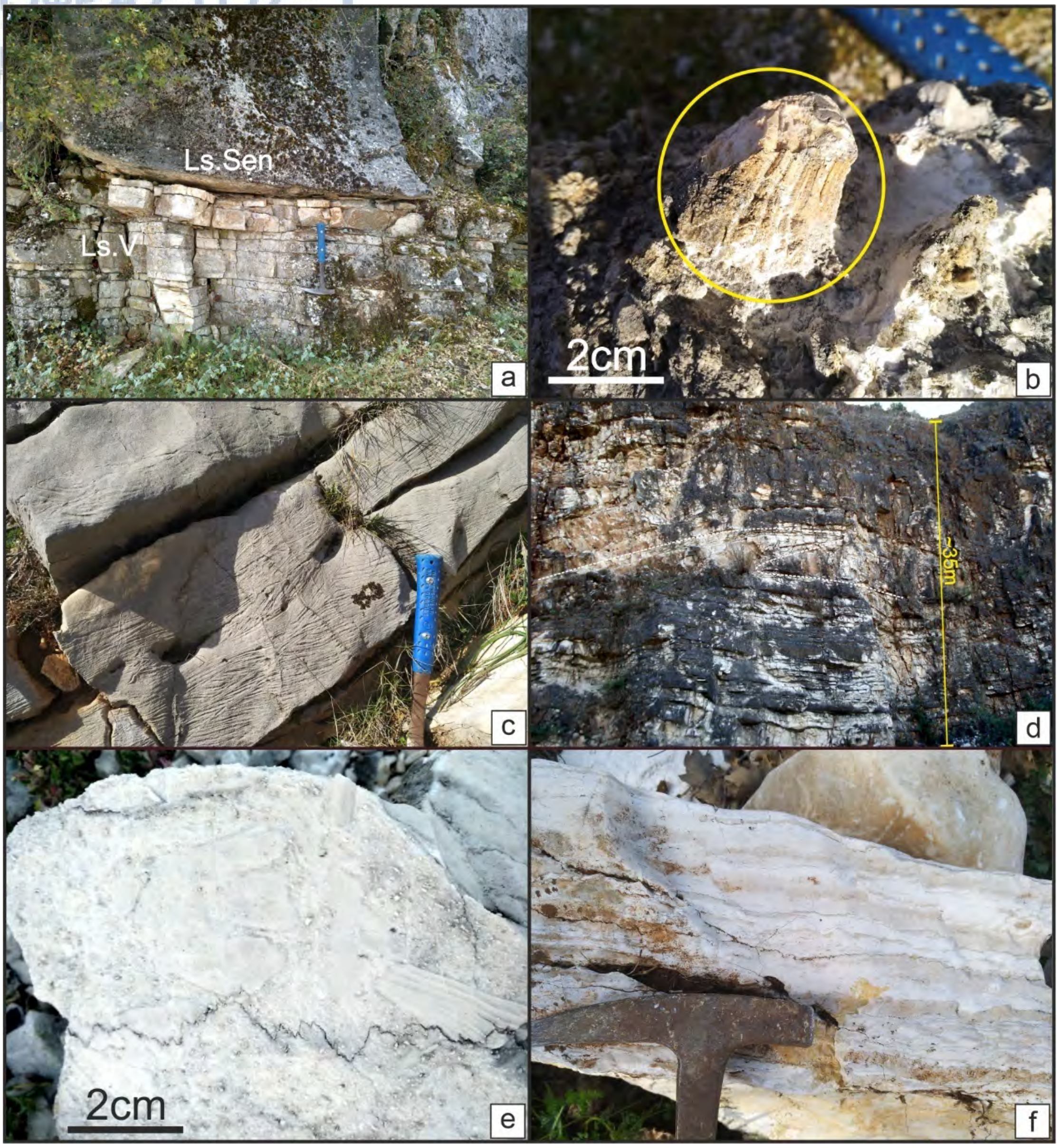

Figure 38. a) abrupt stratigraphic contact of the thin-bedded Vigla Limestones (underlying) and a thick (~3m) massive basal bed Senonian Limestones (overlying), b) a relatively complete larger rudist fragment, c) cross-bedding relations, d) tight slump fold (annotated with white dashed line), e) various rudists fragments and burial stylolite, f) very small syn-sedimentary faults from the base of the formation.

4.1.6 Vigla Shale

The "Vigla Shale" name has been given to a stratigraphic member that is locally located in the upper part of the Vigla Limestones and consists of alternations of thin (~1-2cm) beds of bedded chert, siliceous limestone, siliceous marl, clay, and shale. In sections where the formation is developed in its typical form (cherty, shaly, or marly) the overall color shade is brownish to beige. The colors of the chert vary from grey to black, red to brown, and occasionally greenish. Clay is usually black, brown, and very often green. The abundant green clay (reductive environment) is a characteristic sedimentary feature of this formation (Figure 39a).

In some sections, such as Chionistra Mt., Thesprotiko Mt., Kassidiaris Mt., and Xirovouni Mt., the formation is divided into 2-3 cherty-shaly-marly intervals by 1-2, respectively, cherty limestone beds. The overall thickness of the formation in these sections is ~60–70 m.

In the Chionistra Mt. section (nearby Elataria village), the formation commences with ~3m of black shale and chert with a bitumen smell, overlined by ~15m of cherty limestone, and overlined by >35m of brown, black, green, and red thin bedded marl chert, shale, and clay. In the upper part of the section, a meter-scale slice of cherty limestone appears slumped parallel to bedding, whereas above it, the formation shows extensive slump folding.

The thickness and exact stratigraphic position of the formation vary significantly among the various sections. The example at Pentolakkos village is characteristic of this. In the western parts of the hill, the thick (~40m) Vigla Shales formation lies 1-2 meters below Senonian limestones, whereas in the eastern part of the hill (2 km away), a thin (1-2m) pinch-out of the formation is located >30m below the Senonian limestones (Figure sketch).

In other sections, such as Mitsikeli Mt., the formation is represented by a thick (>80m) interval with thin bedded to laminated limestone and bedded chert. Outcrops of the formation lying in the IZ-C and in the IZ-I show at their upper parts a characteristic lithology that is attributed to the depositional conditions of phosphorite. This phosphorus-rich part up to 10 m thick has been observed in direct contact with the Vigla Shales (Figure 39c) in various locations; nevertheless, the majority of the outcrops lie within the Vigla Limestones at a stratigraphic level more or less equivalent to the Vigla Shales.

In many sections, the Vigla Shales formation appears to accommodate high amounts of compressional strain, as is evident by the successive tight folds (Figure 39b). Also, on numerous hill slopes, the occurrence of the formation is frequently evident by the thriving vegetation, which appears as linear bands.

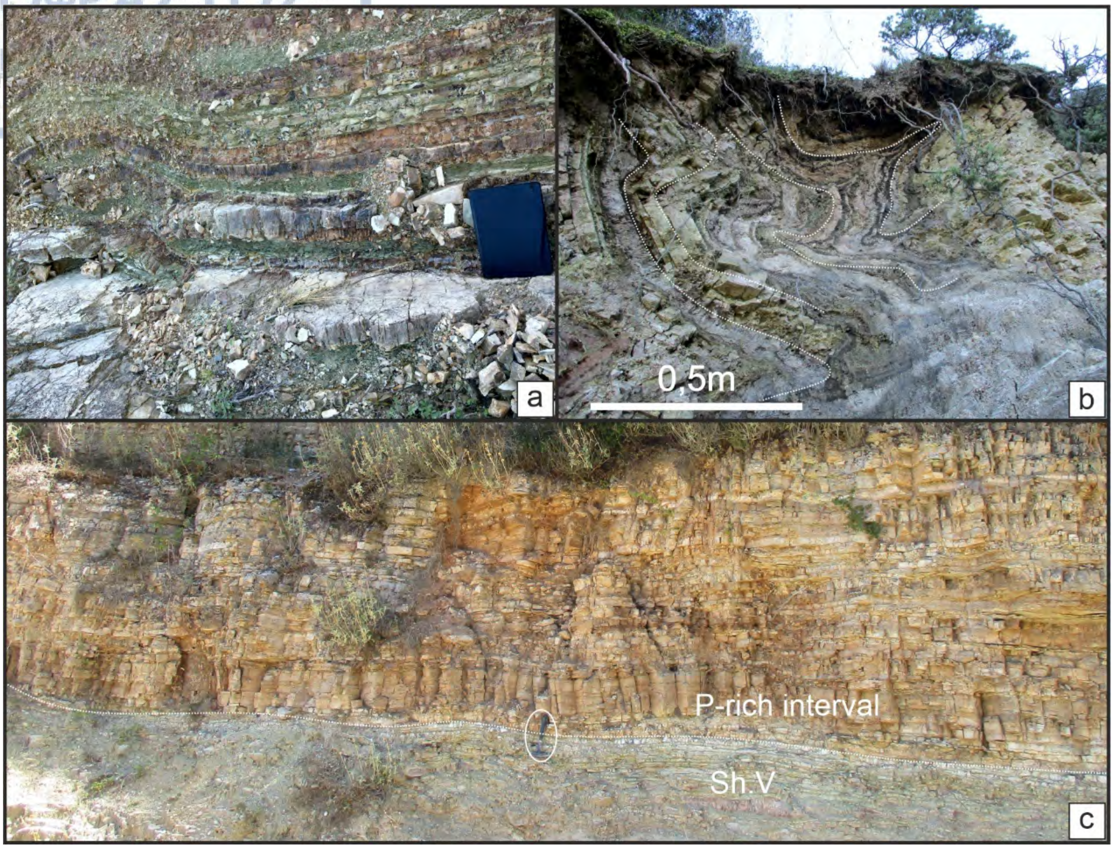

Figure 39. a) lower parts of the Vigla Shales in the Pentolakkos section, green clays are abundant, b) strongly folded (disharmonic folds) in the Kastri section c) the P-rich interval on top of Vigla Shales.

4.1.7 Vigla Limestone

The Vigla Limestones consist of thin-bedded, light grayish to beige micritic limestone and bedded chert and nodules, mostly of light-cream color (Figure 40a). Frequently, the limestone beds contain cm-long, brown chert (or silicified limestone) nodules, often elongated and lying parallel to the bedding (Figure 40b). The lower few tens of meters of the formation demonstrate similar lithology (Figure 40c) in the majority of the studied sections, consisting of alternations of thin-bedded limestone and white-bedded chert with a regular (apparent cyclicity) spacing between the successive chert beds (~ 0,5–0,7 m). Slump folds are frequently observed within various stratigraphic levels of the formation (Figure 40d). The stratigraphic transition from the Upper Posidonia Beds appears conformal in the majority of the outcrops (Figure 40e).

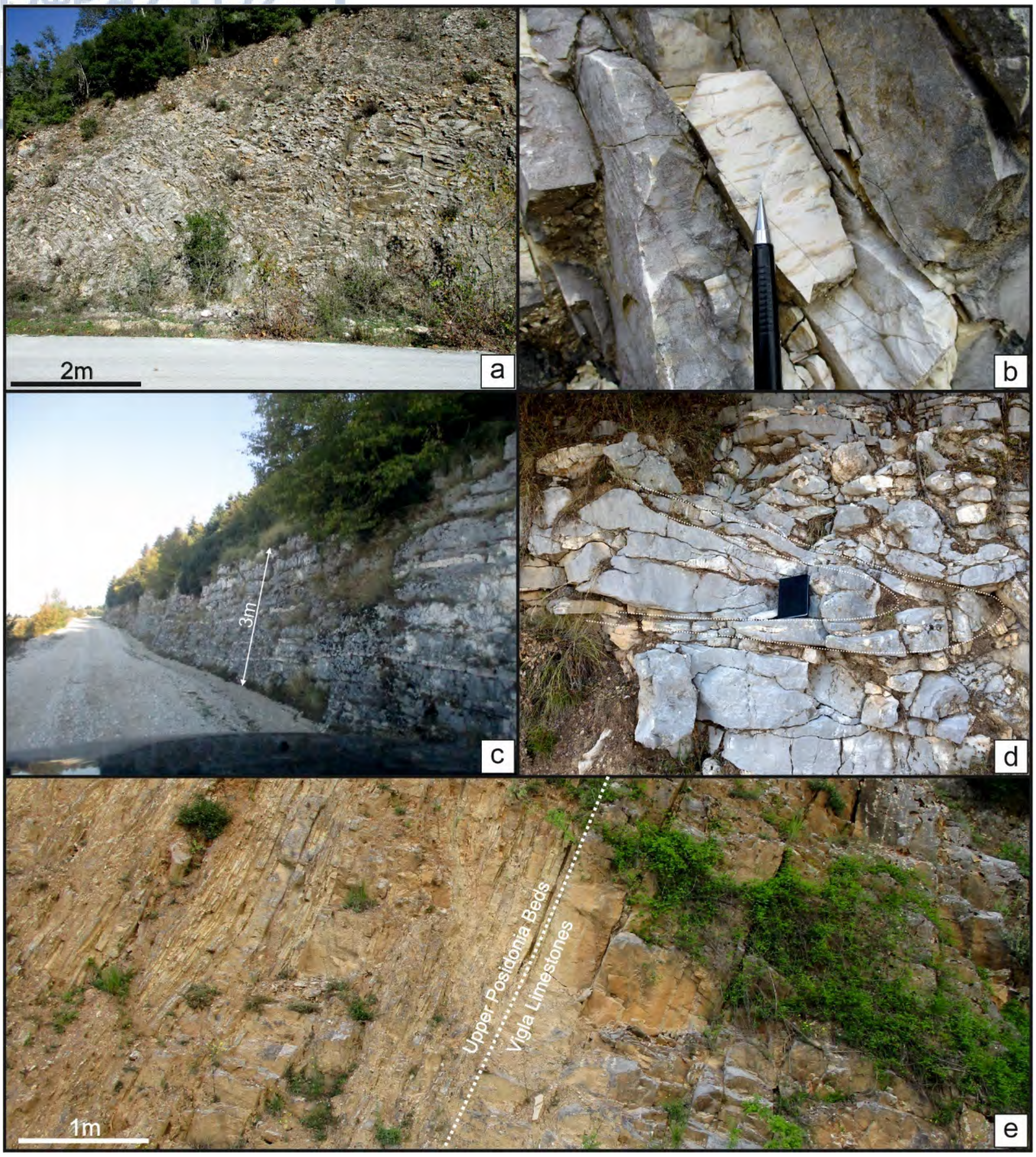

Figure 40. a) typical image of the Vigla Limestones consisting of white thin-bedded limestone and bedded chert, b) brown siliceous patches within the limestone, c) lower parts of the Vigla Limestones in the Mitsikeli Mt., d) a sub-isoclinal slump fold, e) an overturned contact between the Upper Posidonia Beds and the Vigla Limestones (Kefalovryso section).

4.1.8 Vigla dolomites

The dolomitized Vigla Limestones are called Vigla Dolomites and are mainly observed in IZ-I as well as in outcrops nearby Syvota Town (IZ-E). They are mainly gray-colored (Figure 41a), exhibiting the sedimentary features of the Vigla Limestones (bed thickness, chert beds, etc.). Dolomitization appears to be more intensive in the lower parts of the formation (Figure 42b), as these are revealed in the back-thrust-related anticline of the eastern flanks of Xirovouni Mt.

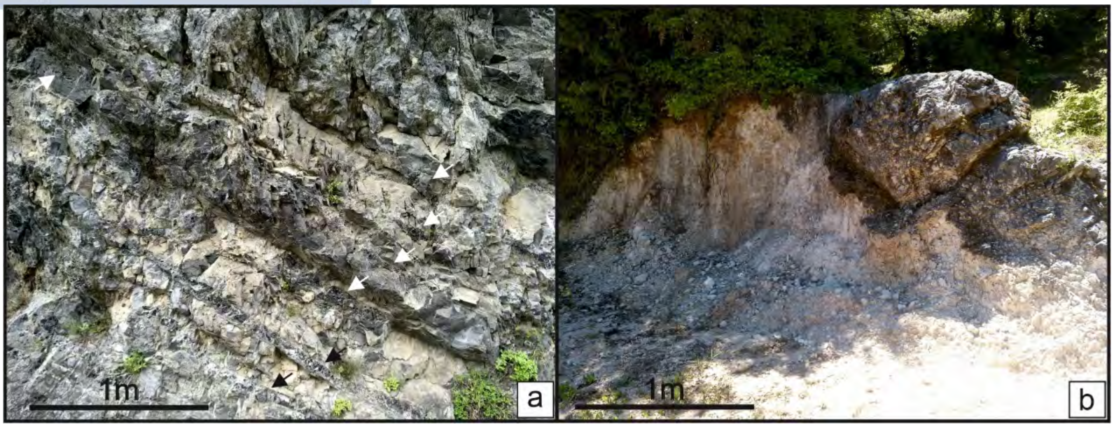

Figure 41. a) gray dolomite and black bedded chert (Aoos gorge, nearby Konitsa village), b) friable dolomite in the exposed core of the Xirovouni anticline.

4.1.9 Upper Posidonia beds

The Upper Posidonia Beds are lithologically similar to the Vigla shales. They consist of thin beds of chert, diatomite, siliceous marl, siliceous limestone, clay, and shale (Figure 42a). The overall color of the formation is light brownish to ochre, whereas the various lithological types (i.e., clay, shale, chert, and marl) have black, red, brown, beige, cream, ochre, and occasionally green. In the Souli Mt. section, the formation demonstrates light ochre to light turquoise shades, whereas in the Chionistra section, the formation shows a deep red shade.

White clay is observed in the lower parts of the formation, near Kaitsa village. The thickness of the formation is highly variable, ranging from a few up to ~100 m (e.g., nearby Ieromnimi and Kaitsa villages).

Large (up to 3cm across) Posidonia shell imprints are found nearby the Elataria and Frosyni villages (Figure 42b), usually on the top of chert beds. Slump folds and syn-sedimentary extensional and contractional faulting are occasionally observed at various locations (Figure 42c).

Areas involving this formation are frequently detected by large distances (or even from the satellite imagery), as it induces mass-rejection phenomena appearing as multi-meter-wide brownish/ochre elongated patches, especially when outcrops are on steep slopes. Moreover, vegetation can be denser comparing to the surrounding limestone.

At the Kassidiaris Mt., the Vigla Limestones are directly overlying the Upper Posidonia Beds which appear eroded (Figure 42d). High amounts of strain are accommodated within the formation, being evident by the intense low-wavelength folding, similar to Vigla shales.

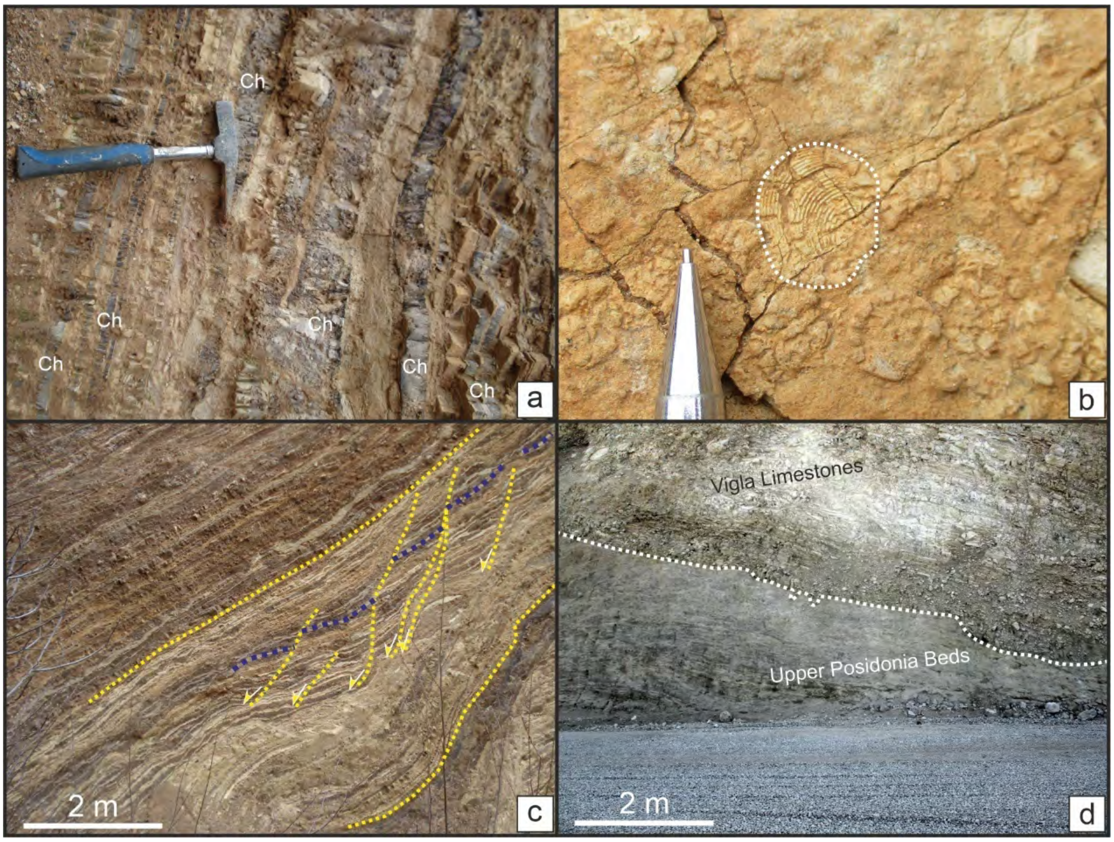

Figure 42. a) typical image of the formation, alternations of black, brownish and dark ochre beds of chert, shale, clay, silt and marl, often siliceous, b) Posidonia shells, c) minor normal syn-sedimentary faults, f) a disconformity between the Upper Posidonia Beds and the Vigla Limestones (Kassidiaris Mt.)

In Kouklesi section, blocks of various sizes (meter to several meters) of the Siniais Limestones (Figure 43a, 43b) are observed within the Upper Posidonia Beds. Smaller white limestone fragments are commonly observed (Figure 43c). Ferromanganese nodules are abundant in some areas (Figure 43d, e).

Figure 43. a-e) images from the Ano Kouklesi area. a, b, c) blocks of various size (up to >1 m3) of deep water limestone likely of Siniais limestone origin, d, e)ferromanganese nodules of various size and shape.

4.1.10 Filamentous limestones

Filamentous limestone is a thin (up to 20 m) formation that locally lies between the Upper and Lower Posidonia Beds (Figure 44a). It consists of thin to medium-bedded limestone and bedded chert. In the Souli Mt. section, the lower parts of the formation contain black bedded chert, whereas the basal strata are truncated. In many outcrops of the formation, a pseudo-microbreccious limestone (Figure 44e) lithology is observed, characteristic of the formation. These microbreccia are similar to others occurring in the lower parts of the Lower Posidonia Beds in the Chionistra Mt. as well as interbedded in the Pliensbachian argillaceous limestone in the Mavronoros Mt. Stromatolite-derived breccia occur in the Souli Mt. section (Figure 44f).

The Souli Mt section demonstrates characteristic shallowing upwards facies characteristics from black chert to the bottom to reef buildups (Figure 44b) in the middle and upper levels up to stromatolites and microbialites to the 3–4 top meters (Figure 44d).

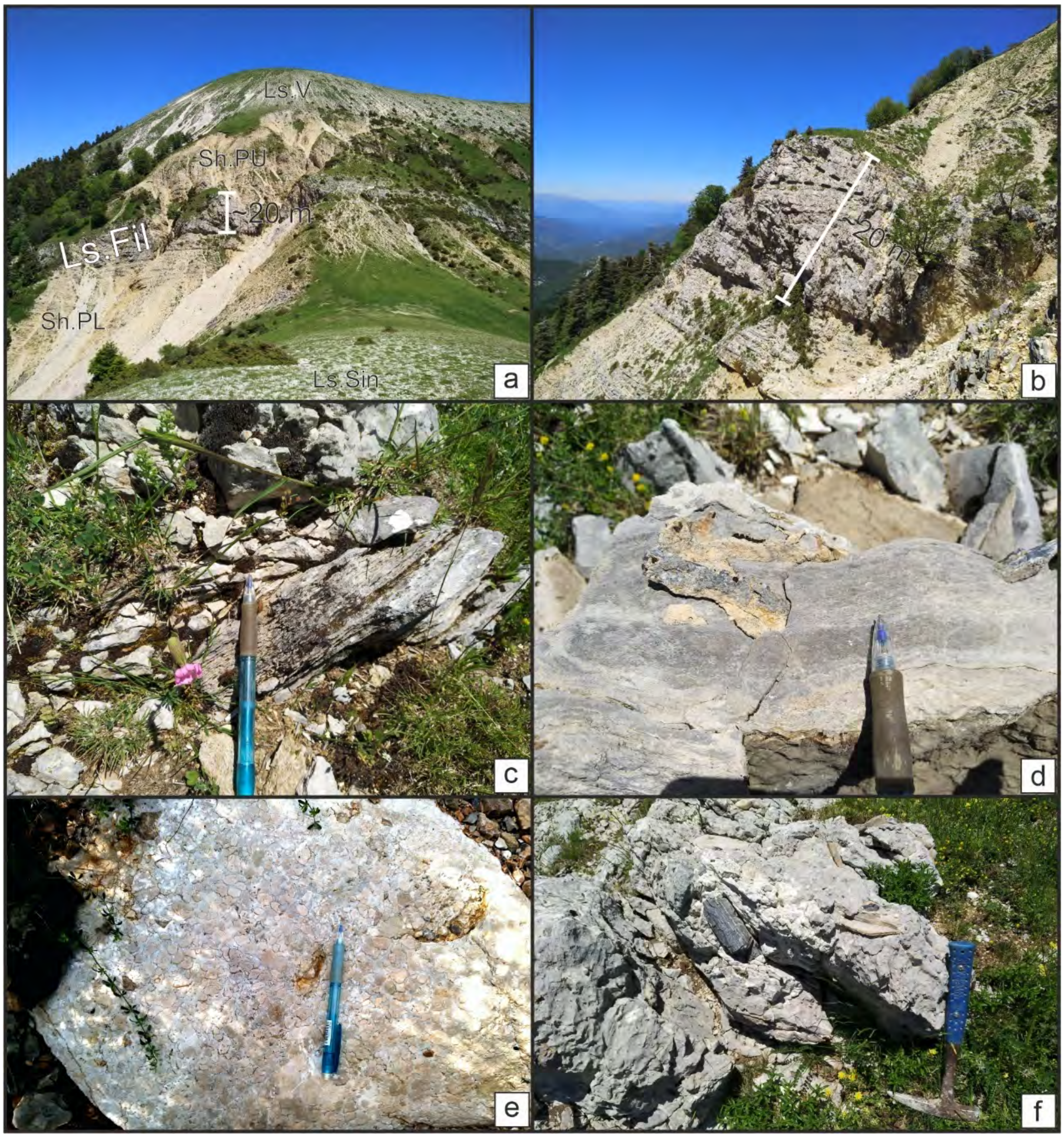

Figure 44. a) a ~20 m-thick bed of the Filamentous limestone (middle part of the photograph) sandwiched between Lower and Upper Posidonia beds, b) a possible build-up within Filamentous limestones (enclosed with bold dashed black line) c) laminated limestone, d) laminated and silk-glowing limestone, e) breccious/conglomeratic limestone, f) breccia and cobbles from the underlying units (black bedded-chert, limestone).

4.1.11 Lower Posidonia beds

The Lower Posidonia Beds are well developed in the western parts of the IZ-C and in the IZ-E. Some sections are particularly favorable for detailed observation of the formation. These are: nearby the Mavroudi village, in the Souli Mt., and in Chionistra Mt. The main and most distinctive lithology of the Lower Posidonia Beds is the bluish laminated marly shale (Figure 45a). Black shale (Figure 45b) is also observed. Black chert is abundant in the upper parts of the formation.

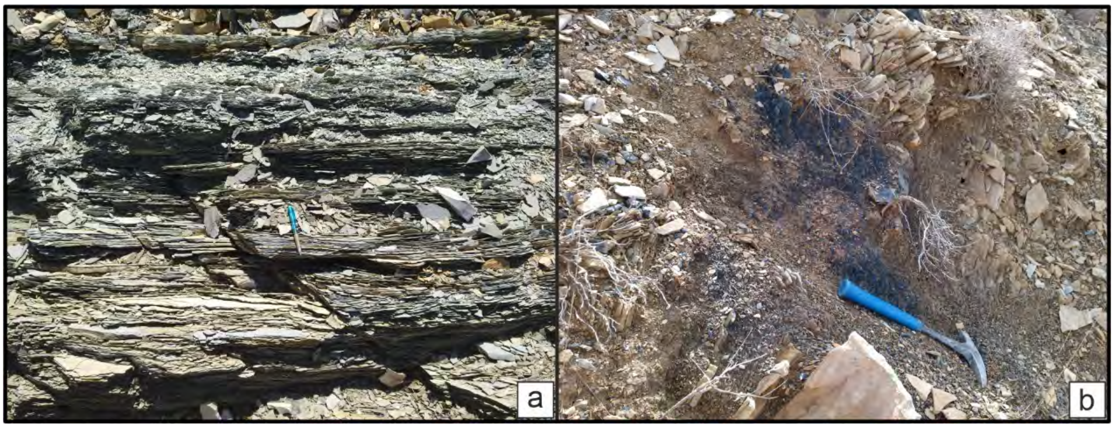

Figure 45. a) Typical image of the lower part of the Lower Posidonia Beds with bluish laminated marly shales, b) black shale

More detailed, in the Souli Mt. section, the formation lies conformably over the Basal Marl (Figure 46a) and commences with 8 m of bluish and black/dark gray laminated shale/marl (Figure 46b). The next 20 m of the formation are dominated by brown marl and shale, with a few intervals of black shale. In this sequence, three (3) horizons of black bedded chert are observed. The lower of these horizons lies at ~15 above the base of the formation, the second lies ~8 above it, and the third lies ~7 above the second. The uppermost ~8–10 m of the formation show distinctive lithology and are dominated by alternations of limestone and black bedded chert. The total thickness of the Lower Posidonia Beds in this section is >40 m. Abundant Posidonia shell imprints (Figure 46c) are located at various levels within the formation. Ammonite aptychi were also observed. Polymictic (carbonate, shale, and chert) breccia in siliceous marl matrix as well as limestone conglomerate in chert matrix are observed.

Figure 46. a) Base of the Basal Marl. The transition towards the marly lithology is also attested by morphological retreat of the slope. b) bluish-dark gray marly shale, c) casts of Posidonia

The base of the Lower Posidonia Shales in the Mavroudi section was difficult to exactly determine due to the lithological similarity with the upper parts of the Siniais Limestones, namely thinly laminated carbonates. The studied section starts with ~10 m of thin-bedded to laminated limestone and white-bedded chert. The next 1, 5 m consists of beige-gray limestone with microbreccious texture. Above it, 12 m of laminated, thin, and thicker limestone beds are alternated with bedded chert. Some clay films are also observed. Above it lies a 2 m-thick microbreccious limestone with chert nodules. The next 3 m include thick bedded limestone. Above lies a 30 m-thick sequence with laminated calcareous shale, chert, and limestone in alternations. In the upper part of this sequence, a small conifer branch fragment was discovered (Figure 47a). On the top of this sequence, a 3 m-thick beige micritic limestone bed occurs, showing intense internal slumping (Figure 47b) and chert injections perpendicular to bedding. The next ~40 m contain the most characteristic formation lithology, this of the laminated bluish and black calcareous and silicified shales (Figure 47c). A few thin limestone beds were intercalated in this sequence, while on its upper part, a 20-cm-thick calcarenite bed is found. Thin black chert nodules occur sparsely. No Posidonia imprints are detected in this section, while a poorly preserved ammonite cast was encountered (Figure 47d).

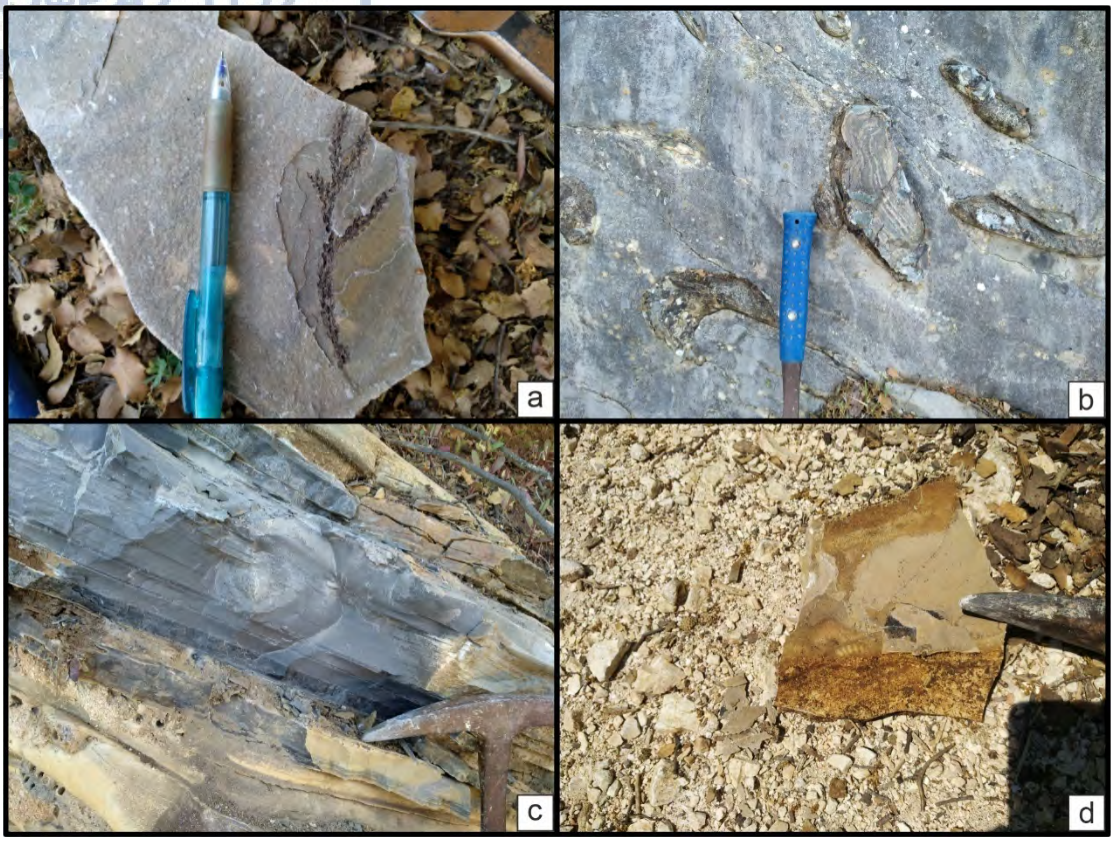

Figure 47. a) conifer branch, b) slumped chert lenses chaotically incorporated within carbonate mud, c) dark gray laminated silicified shaly limestone, d) poorly preserved Ammonite cast

The Chionistra section contains a thick (>80 m) Lower Posidonia Beds sequence. Filamentous limestones do not outcrop in the area; therefore, the upper limit of the formation is not defined. In one of the locations, the sequence commences with 1-3 meters of a mélange composed of chaotically incorporated fragments of limestone, shale, and chert within a black to gray carbonate mud matrix (Figure 48a). In another location, the sequence starts with 30 m of the typical bluish and brownish lithology with no chert detected (Figure 48b). A fault interrupts the continuous observation, bringing in direct contact with a black chert-dominated part of the formation. Higher stratigraphic levels demonstrate a progressively increasing chert content. The black chert of the upper part of the formation emits an intense bitumen smell after hammer beating. Posidonia shell imprints are abundant and large (up to 4 cm across) relative to other outcrops. Some sparse brownish or beige-thin nodular limestone beds bearing ammonite fauna also occur. An ammonite aptychus and shell and a Posidonia shell imprint are observed on a single bed surface at a distance of a few cm. Locally in the broader area, a microbreccious limestone is observed below the formation.

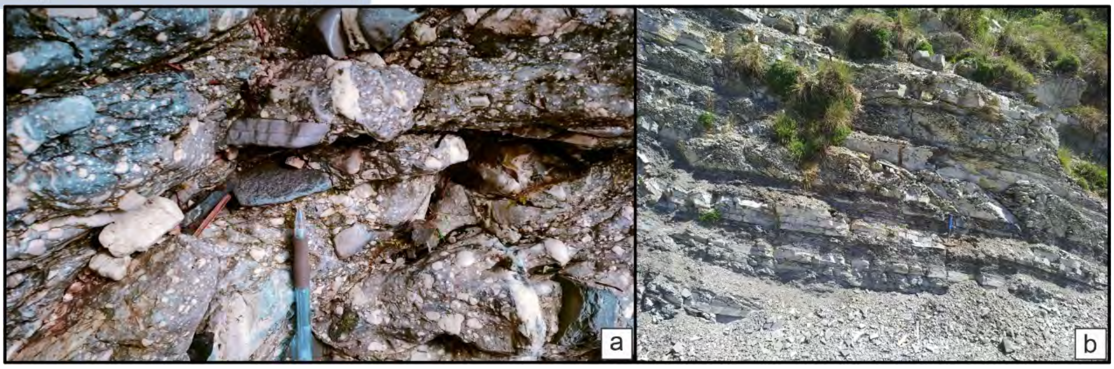

Figure 48. a) Mélange of rounded limestone, shale and chert fragments within a black lime mud matrix, b) bluish laminated marly shales.

Consequently, the main lithological characteristics of the Lower Posidonia Beds include:

1) the basal mélange or conglomerate;
2) the black laminated shale and marly shale of the first ~10 m;
3) the very limited presence (if not absence) of siliceous lithologies at the first ~10 m;
4) the very gradual onset of siliceous oozes at >15-20 m above the base;
5) the gradual lightening of shades in the middle part with brownish shales and marly shales;
6) the back bedded chert-dominated lithology at the higher ~10 m;
7) the possibly rhythmical occurrence of carbonate concretion in the form of carbonate-dominated banks;
8) silicification is observed locally;
9) the lower boundary can be abrupt or gradual;
10) the upper boundary with the filamentous limestone is abrupt;
11) The upper boundary with the Upper Posidonia Beds is gradual.

4.1.12 Ammonitico Rosso

The Ammonitico Rosso Fm. consists of reddish/pinkish and cream-colored nodular limestone (Figure 49a). In the area of Kouklesi, the base of the formation is a ~10 m-thick red marl (Basal Marl, Figures 49b, e) with green marl intercalations, and at its base, a 2 m-thick black shale succession is exposed in a very restricted outcrop.

Frequently, it includes grayish to beige, well-bedded limestone, whereas at transitional sections with the laterally equivalent Lower Posidonia Beds, it appears in brownish/ochre shades and thinner beds. The bed thickness is typically 10–25 cm in the nodular parts. Thin red clay beds also occur. Bodily ammonite shells and aptychi (Figures 49c, d) are observed in several outcrops of the formation.

In the Kouklesi section, a Belemnite rostrum and an ammonite were observed in the same outcrop at a 30 cm stratigraphic distance (Figure 49c). Bioturbation indications also occur (Figure f). The formation thickness is typically around 5–10 m. The thickest (>35 m) accumulations are found nearby the Skandalo village, at the eastern flanks of the Margariti Mt. In some fully exposed sections, the Basal Marl Fm. is observed below the Ammonitico Rosso Fm.

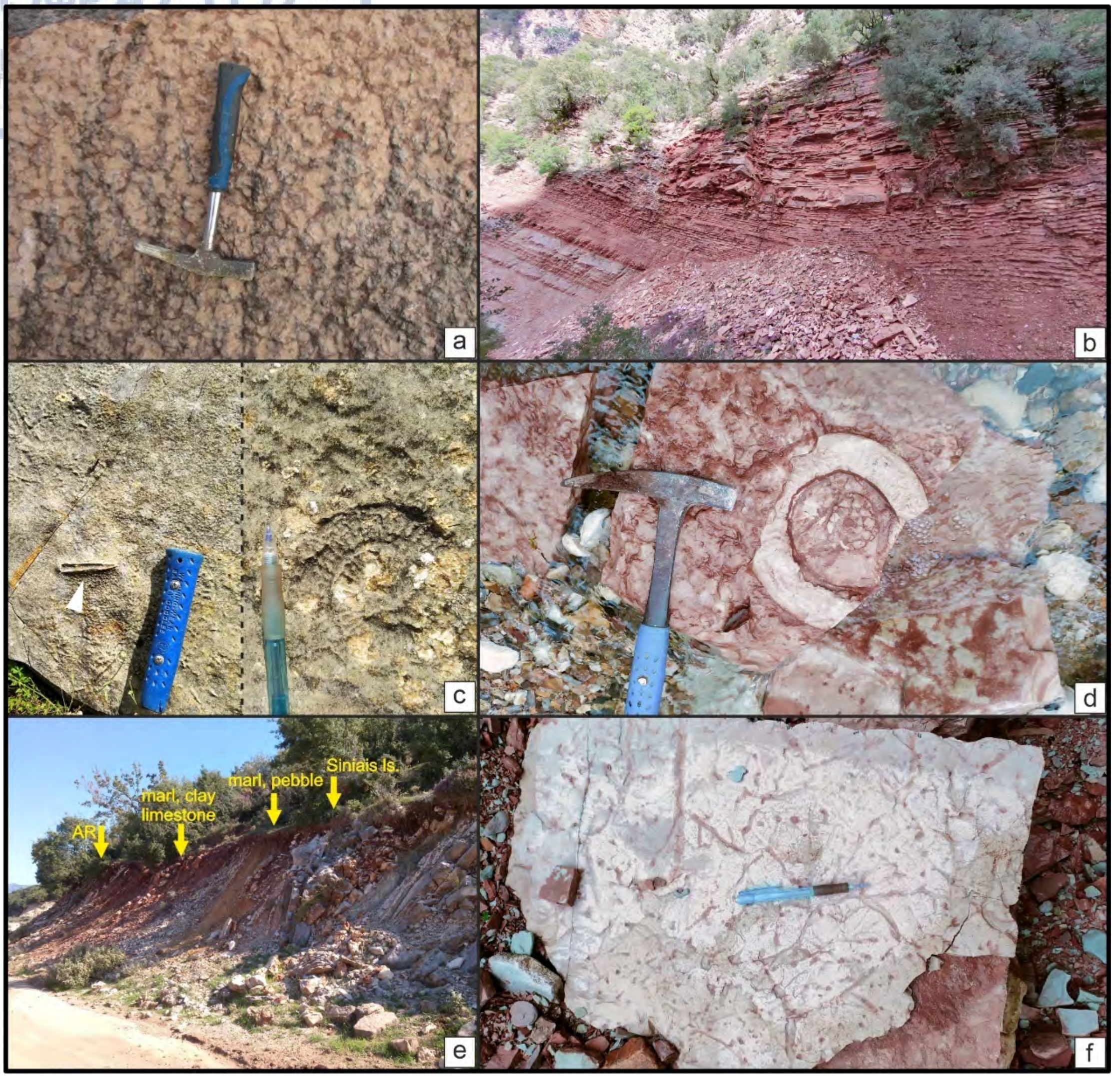

Figure 49. a) pinkish nodular limestone, b) Basal Marl (red and green marls) and the main Ammonitico Rosso formation represented by medium c) Belemnite and Ammonite, d) Ammonite in nodular limestone, e) Basal Marl transition, f) Bioturbation (ichnofossils) over bedding surface of pink limestone.

4.1.13 Basal Marl

Basal marl is a formation that is introduced for the first time in this study. It involves a thin (up to 8 m) marl formation that lies locally over Pliensbachian limestone and is observed in some locations directly below Ammonitico Rosso (e.g., Kouklesi section, Figure 50a) and below Lower Posidonia Beds (e.g., Petousi section, Figure 50b). In the Souli Mt. section, the Basal Marl lies conformably over Siniais limestones. Its thickness is ~7-8 m. It consists of brown marl, which appears laminated at some levels. In the Karvounari section, the Basal Marl consists of brownish-reddish marl, two thin

(~25 cm each) intervals with pebble-sized rounded limestone clasts, and a 1 m-thick intermediate laminated marly limestone bed (Figure 50b). The overall thickness in this section is ~4,5 m.

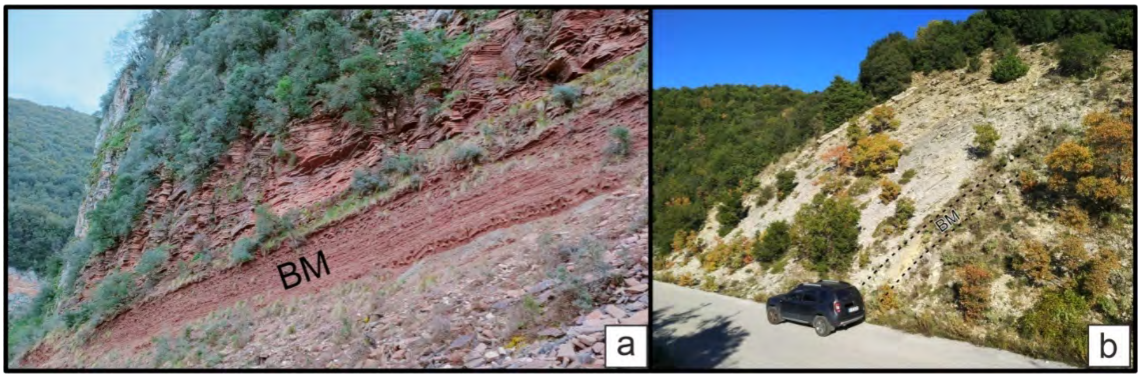

Figure 50. a) Basal Marl (BM) below Ammonitico Rosso (Kouklesi) b) Basal Marl below Lower Toarcian black shales (Petousi)

4.1.14 Siniais limestones

Siniais limestones conformably lie over Pantokrator limestones (Figure 51a). They mainly consist of thin-to-medium-bedded limestone and bedded chert (Figure 51b); nevertheless, some sections contain no chert. Chert nodules also occur. In the Mavroudi and Mavronoros Mt. sections (IZ-E), the color of the chert beds is usually white in the lower parts of the formation, becoming black at higher stratigraphic levels. Formation thickness greatly varies among the various parts of the basin, while it is missing in some sections. In the Mavronoros section, the pelagic limestone that lies above the Pantokrator Limestones and below the Lower Posidonia Beds contains thick (up to ~80 cm) beds (Figure 51c) of black argillaceous limestone with a bituminous smell, as well as microbreccious limestone beds (Figure 51d). A few meters above the contact with the Pantokrator limestones, an ammonite shell (Figure 51e) was observed within the brecciated limestone. Plastic-like intra-strata deformation (slumping) is observed as well (Figure 51f). The lithological resemblance to the Vigla Limestone is evident in the majority of the outcrops.

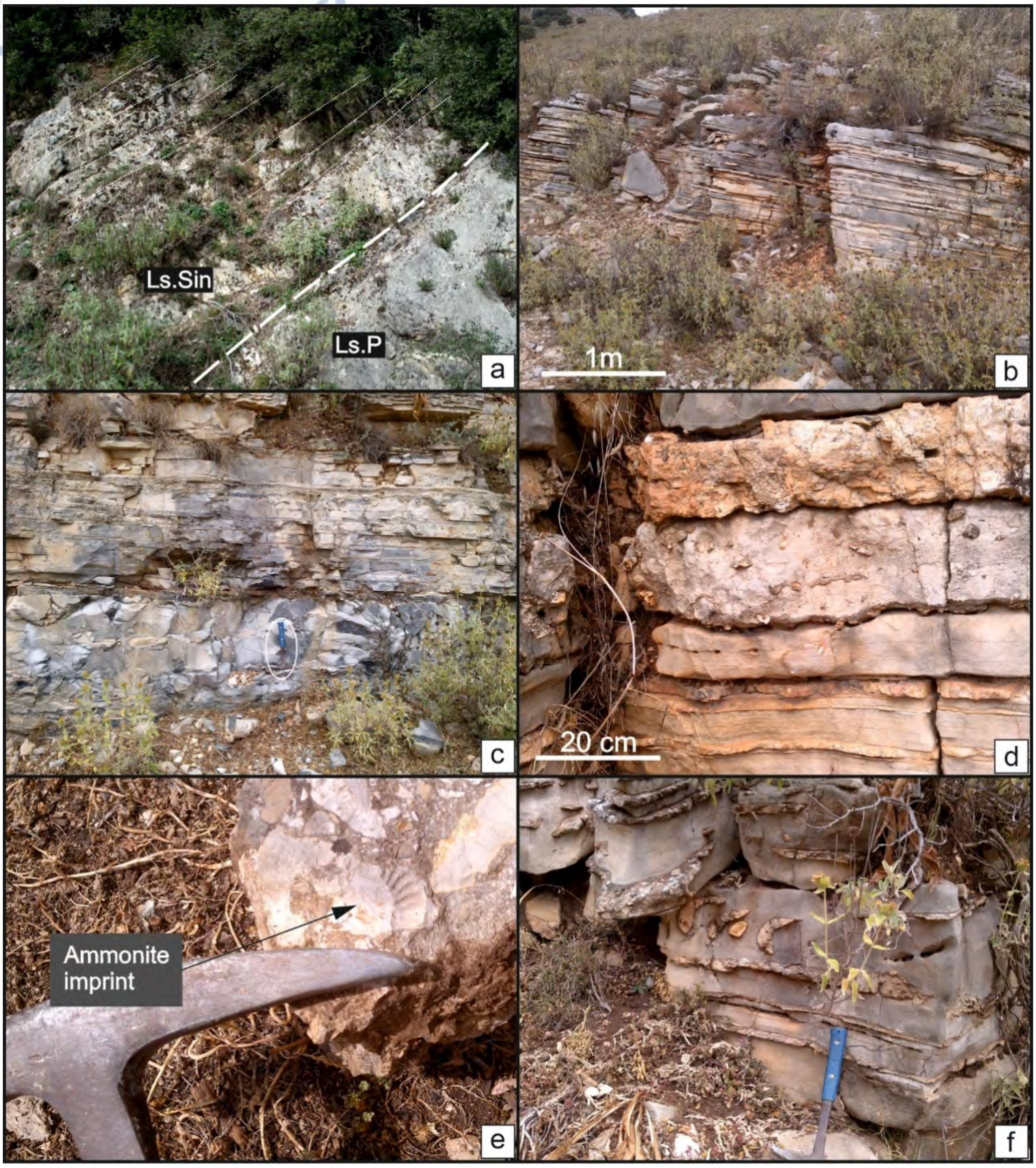

Figure 51. a) Normal Stratigraphic contact of the underlying Pantokrator Limestones and the Siniais Limestones (Lithino village), b) argillaceous limestone and chert bed alternations (Mavronoros Mt.), c) 0.5 m thick dark-gray colored argillaceous limestone with bitumen smell (Mavronoros Mt.), d) nodular/microbreccious limestone bed (Mavronoros Mt.), e) breccia of reworked Siniais Limestones with Ammonite imprint, f) crescentic-shaped chert lenses (slumping)

4.1.15 Pantokrator Limestone

The formation of Pantokrator limestone exhibits various limestone lithologies corresponding to different depositional settings. Nevertheless, in the majority of its outcropping parts, it appears as white or beige massive limestone with no obvious bedding surfaces (Figure 52a). Within this lithotype are macroscopically recognized oolites and pisolites (Figure 52b), oncolites (Figure 52c), as well as stromatolites (Figure 52d). Very large (>1 cm) primary pores of various types (fenestral, intra-fossil, shelter) are regularly observed (Figure 52e), as well as pores up to 4 cm in diameter, probably related to organisms colonizing hardgrounds (Figure 52f).

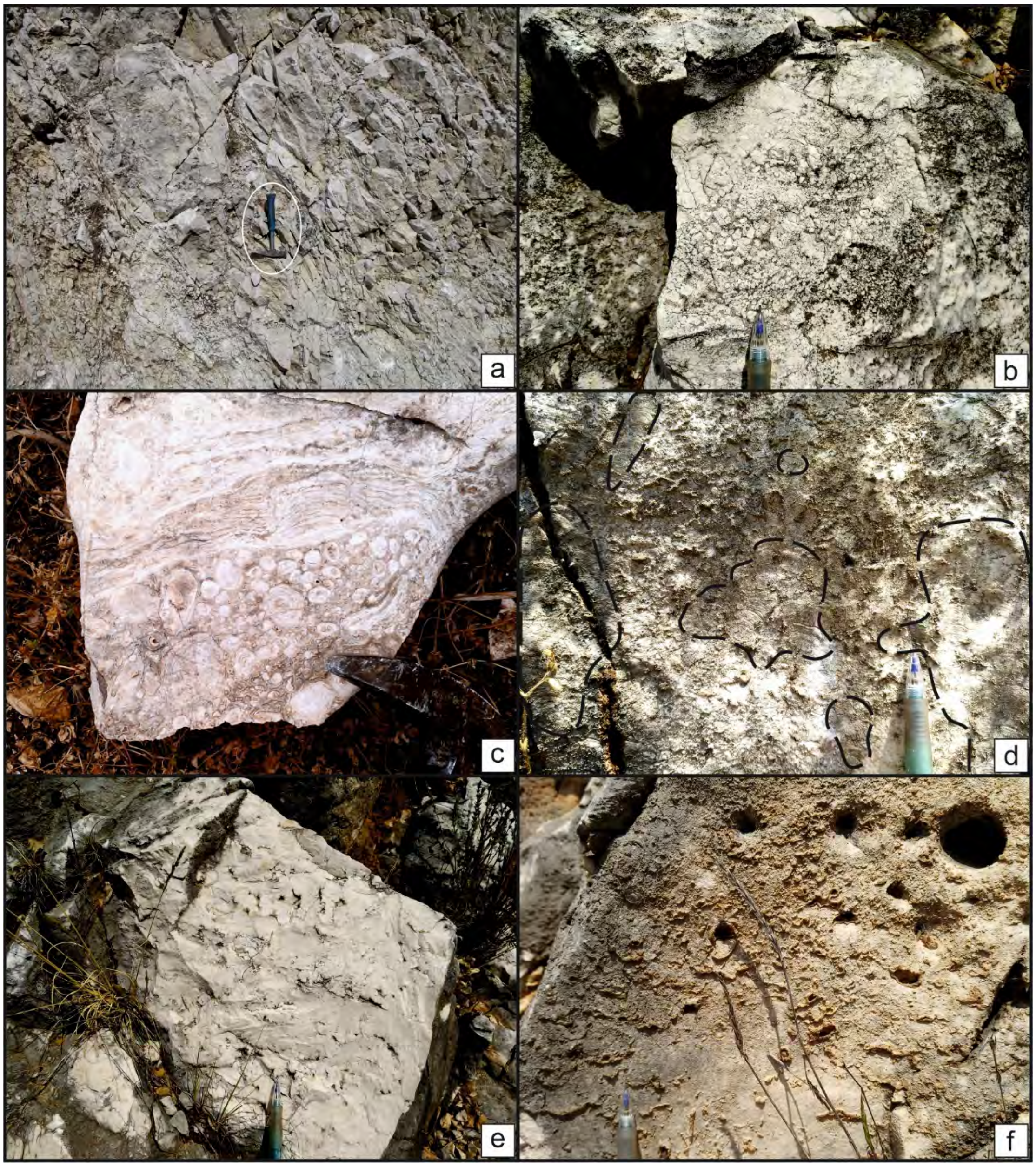

Figure 52. Field photographs of the Pantokrator Limestones Fm. a) Massive limestone, b) ooids and pisoids, c) ooids, pisoids, oncoids and stromatolites, d) columnar stromatolites enclosed with black dashed bold line, e) large open vugs of intrafossil origin, f) eroded large pores related to horizontal burrows in hardground.

Fractures healed by incrementally-developed fibrous calcite in a syntaxial mode (from the fracture walls towards the void) are often observed (Figure 53a). Neptunian dikes filled with limestone breccia (Figure 53b) were also observed in some locations. Thick-shelled mollusk fauna is regularly observed in many locations (Figure 53c). A section of a coral (Figure 53d, possibly *Thecosmillia sp*.) is observed in one location.

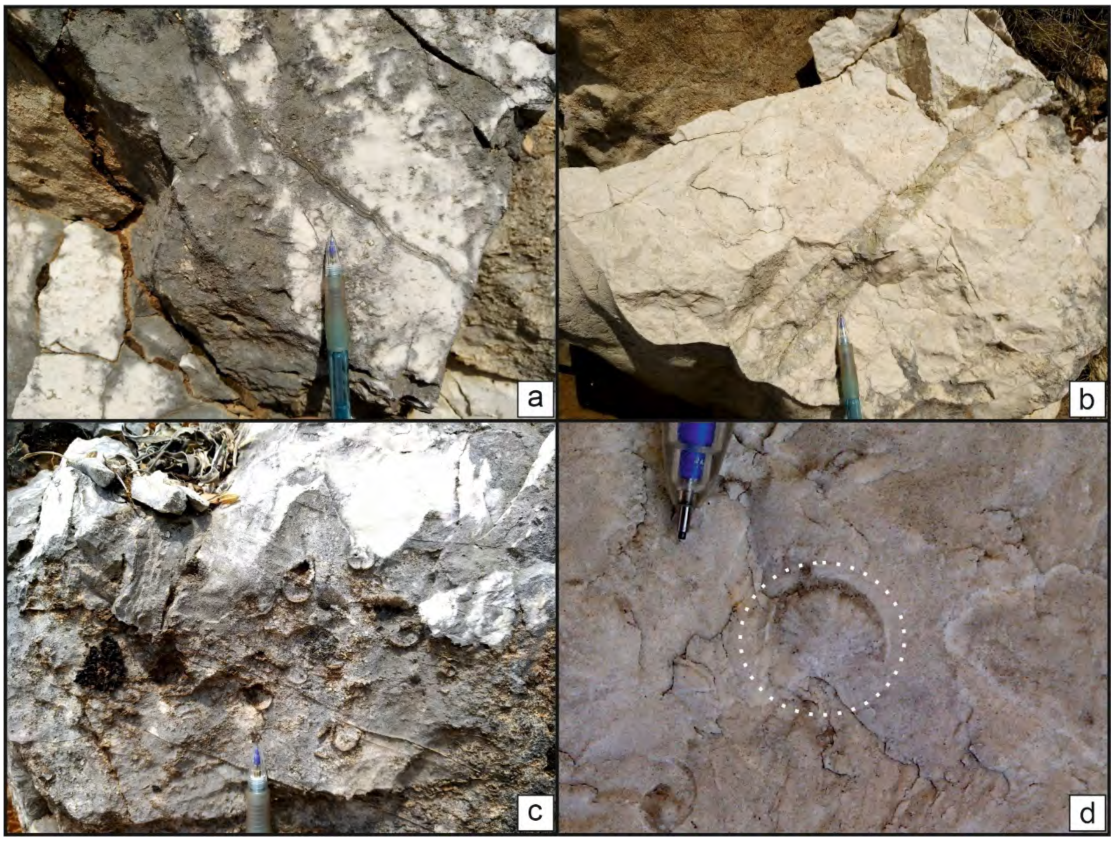

Figure 53. a) Syntaxial growth of fibrous calcite within a vein, b) neptunian dyke, c) gastropods, d) coral section (?*Thecosmillia sp*.)

There are extensive areas demonstrating strikingly different lithologies, corresponding to variations in the depositional setting. In these areas, the above-described lithology is observed in thin (up to 1-2 m) intercalated beds. Three of these sections were studied in detail. These are located a) between the Kefalovryso and Vassiliko villages (northern part of the IZ-C), b) in the Souli-Paramythia Mountains (IZ-C), and c) in the Kouklesi village area. Although they encompass significant lithological features and variations of the Pantokrator Limestones, they are described in detail in Section 5.1.2 as they are present up to the Berriasian stratigraphic level.

4.1.16 Pantokrator Shale

Pantokrator Shale consists mostly of black shale, gray and brown dolomite, and dolomitic sandstone. In the most stratigraphically complete outcrop, it exceeds 20 m in thickness (Figures 54a, b, and c). The uppermost 10–15 meters consist of light ochre to grayish dolomite or dolomitic sandstone, occasionally laminated with a bitumen smell (Figure d). Black carbonaceous beds also occur.

The formation lies within the middlemost parts of the Pantokrator Fm, between the overlying limestones and the underlying dolomites. In many outcrops, it appears to be part of the highest stratigraphic level of the underlying Rhaetian Pantokrator Dolomite, being in direct contact with massive limestone (Figure 54e) belonging to the overlying Liassic Pantokrator Limestone. In one location, the formation appears to lie entirely within the Pantokrator Dolomite (Figure 54a).

The black shale bed thicknesses vary from mm-thick laminae (Figure 54c) to ~70 cm (Figure 54b). The black carbonaceous beds show the same thicknesses. These beds alternate with less dark-colored beds of dolomitic sandstone and dolomite. In the upper parts of the formation, thin (up to 5 cm) white dolomite beds occur, whereas the dark-colored beds become brownish, thinner, and sparser. As a general trend, the formation becomes more light-colored at the top. The maximum thickness of the formation reaches 30 m, including the bituminous dolomitic sandstone.

This formation exhibits some unique physical characteristics compared with the other potential source rock formations observed in Epirus. It emits a very intense bitumen smell, especially after a hammer beating. On one extensive outcrop, the bitumen smell is detected tens of meters away. It ignites and combusts under a weak flame. Hammer strikes leave a deep and hollow sound while most of the impact energy is absorbed by the rock, often making it more difficult to break compared to the other known potential source rocks in Epirus. In one outcrop, structureless black shale appears to be injected within the Pantokrator Limestone.

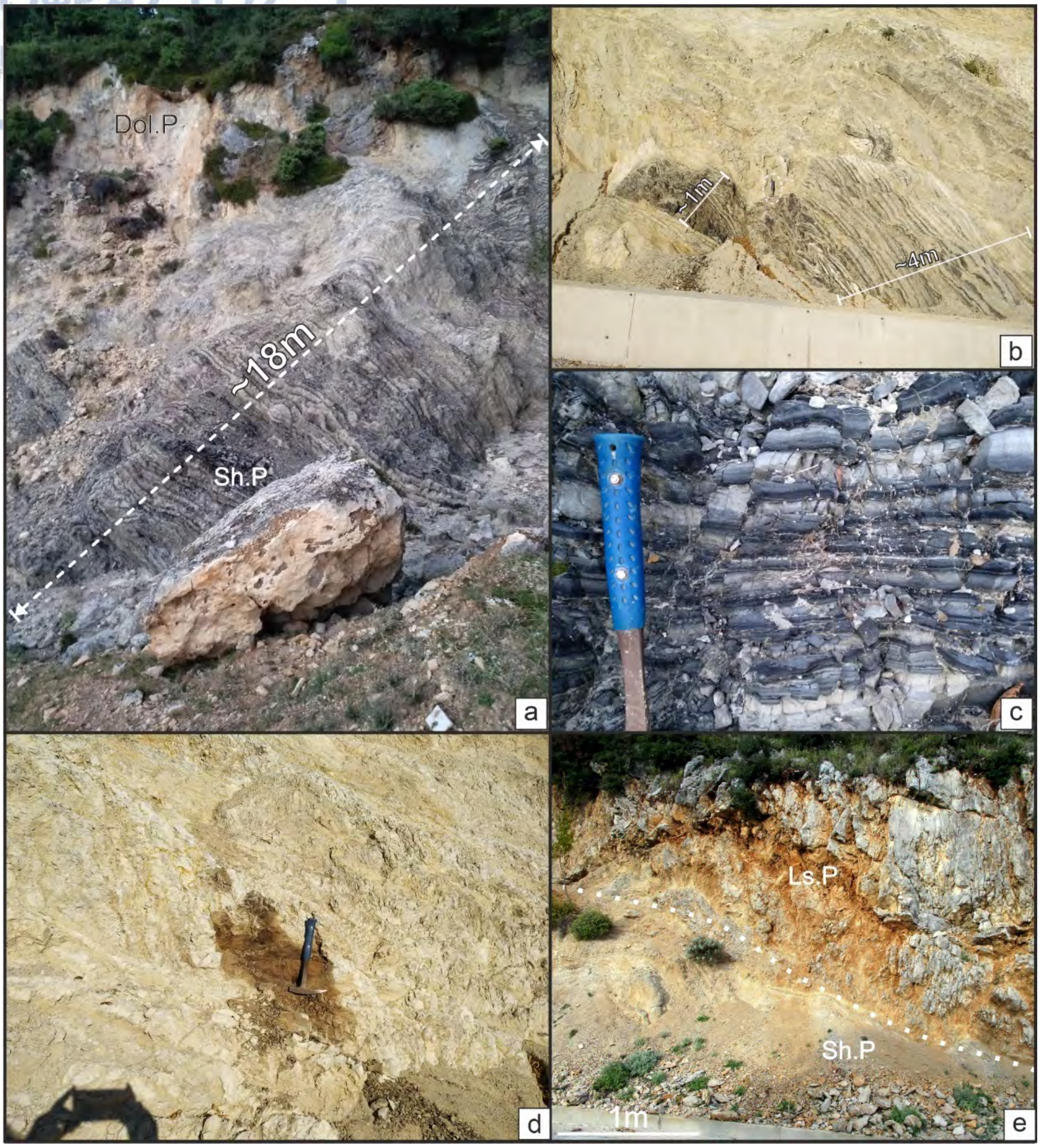

Figure 54. a) the visible approx. 18 m of the formation of the most stratigraphically complete outcrop, b) another outcrop where are visible two lithologically different parts, a lower one with an almost clear black shale block and an upper with successive alternations of black shale and gray dolomitic sandstone, c) close-up image of the formation where the -apparently- rhythmic alternations are visible, d) bituminous dolomitic sandstone from the uppermost 10 meters of the formation, e) the uppermost contact with the Pantokrator Limestone.

The lower contact of the formation appears to be tectonic, abutting steep reverse faults that demonstrate secondary strike-slip movement. The upper contacts in all outcrops with good inspection of the formation are conformable, showing a relatively abrupt termination of the shale-dominated lithology against the carbonate-dominated lithology.

4.1.17 Pantokrator Dolomite

Pantokrator Dolomite demonstrate facies variations among the various locations within the IZ. The Souli Mt. area is mainly observed as massive, often very friable, white to light beige or gray dolomite (Figure 55a). In this section, large (>5 mm) pores are recognized (Figure 55b). In the area between Agia and Parga villages, it is thin-bedded (Figure 55c). The Kefalovryso-Vassiliko area is mainly thin-bedded to laminated in the lower parts (Figure 55d).

Anhydrite nodules are observed within some thick dolomite beds (Figure 55e). The sequence contains thicker dolomite beds upwards (Figure 55f). In the majority of the sections, the boundary between the underlying dolomite and the overlying limestone is obscure, as the dolomitization degree of the strata varies greatly among the sections. Dolomitized algal mats also occur (Figure 55g). The base of the formations is rarely exposed. In the Kefalovryso-Vassiliko section, the passage from the evaporite to the dolomite is substantiated through a thick zone (>150 m) of the laminated dolomite/evaporite (Figure 55h).

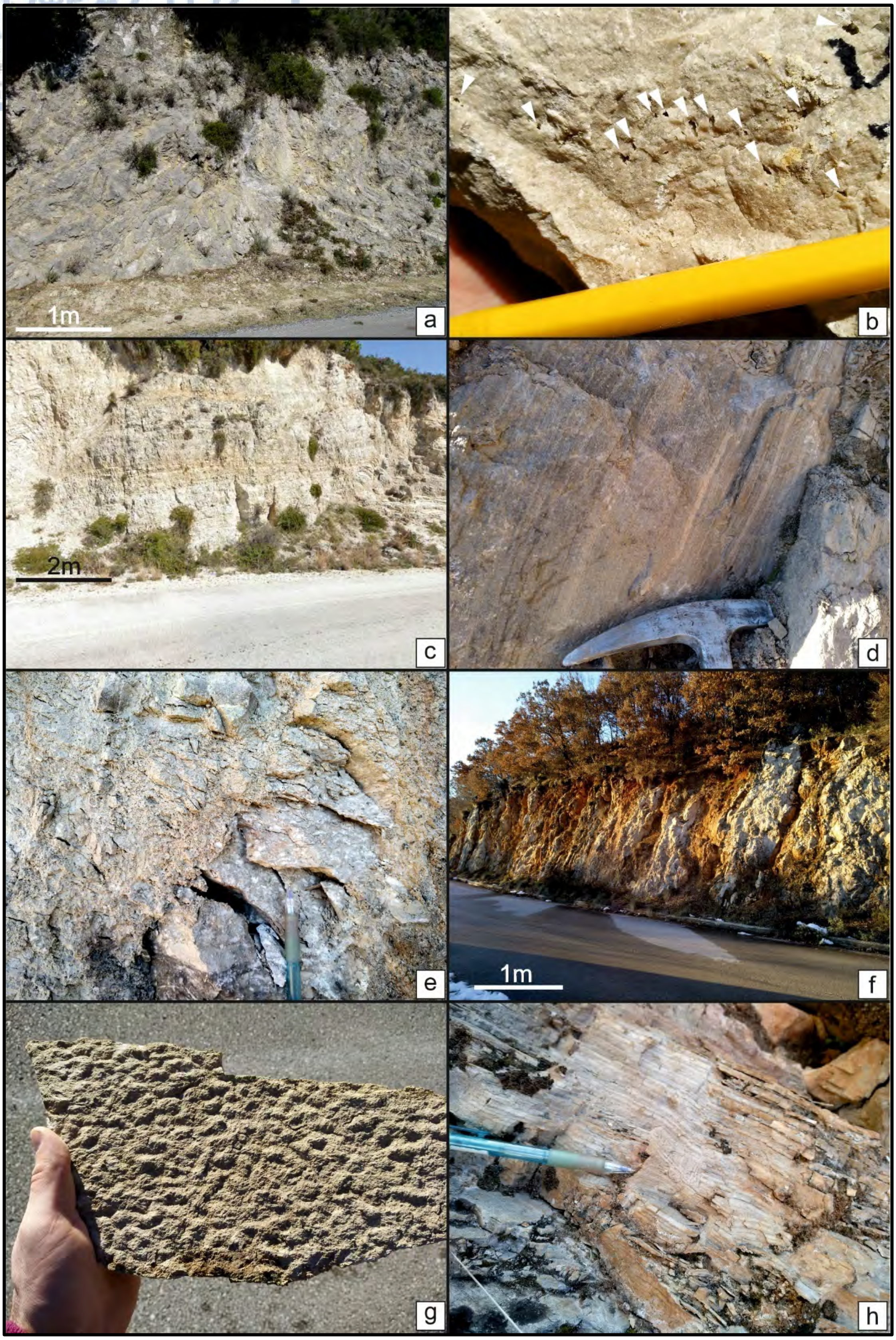

Figure 55. a) Very friable, massive dolomite, b) large pores within massive dolomite, c) thin-to-medium bedded dolomite, d) laminated dolomite at the base of the Pantokrator Fm., e) anhydrite nodules within the dolomite at the top of the evaporite sequence/base of the Pantokrator Fm., f) alternations of massive neritic and bedded dolomite, g) dolomitized algal mats at the base of the Pantokrator Fm., h) dolomite/anhydrite alternation at the base of Pantokrator Fm.

4.1.18 Foustapidima Limestone

The Foustapidima Limestone consist of black micritic, well-bedded limestone. Bed thickness typically ranges between 10 and 15 cm. Its lower 1.5-meter strata are thin-bedded (0.5–1 cm) and consist of carbonaceous shale. At the Igoumenitsa section, a full exposure of the formation occurs. Within the Vrysella diapir, the formation is found lying entirely within the evaporites. Abundant thick-shelled mollusk fauna is observed in various locations where the formation is exposed, such as in outcrops at the Vrysella diapir (Figure 56). The formation thickness reaches 80 m. Its original stratigraphic position is enigmatic as it appears just below the Pantokrator Fm. (but not in direct contact) or within the upper parts of the Evaporite Fm.

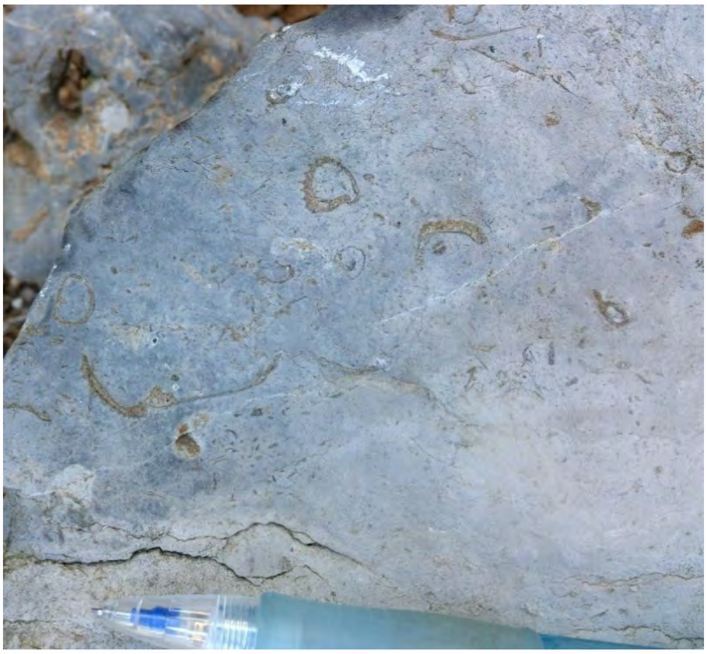

Figure 56. Thick shelled mollusks in Foustapidima limestones

4.1.19 Triassic Collapse Breccia

The Triassic Collapse Breccias are observed in extensive outcrops, mainly in the IZ-E and, to a lesser extent, in the IZ-C. At the outcrop scale, they mainly appear brownish or reddish in fresh road and quarry cuts (Figure a). They demonstrate various lithotypes, such as clast-supported breccia without any apparent matrix (Figure b), sparce clasts within clay/gypsum matrix (Figure c), or structureless mixed carbonate breccia (Figure d) in less weathered outcrops. The clasts in the first lithotype exhibit high sphericity yet a very irregular surface, whereas the clast sizes vary from a few cm up to several dm. In some outcrops, clasts are observed demonstrating more than one cycle of brecciation-lithification (Figure e). The clasts of the two later lithotypes are less rounded. In several sections, abrupt termination of the TCB against fairly dissolved evaporite is observed (Figure f).

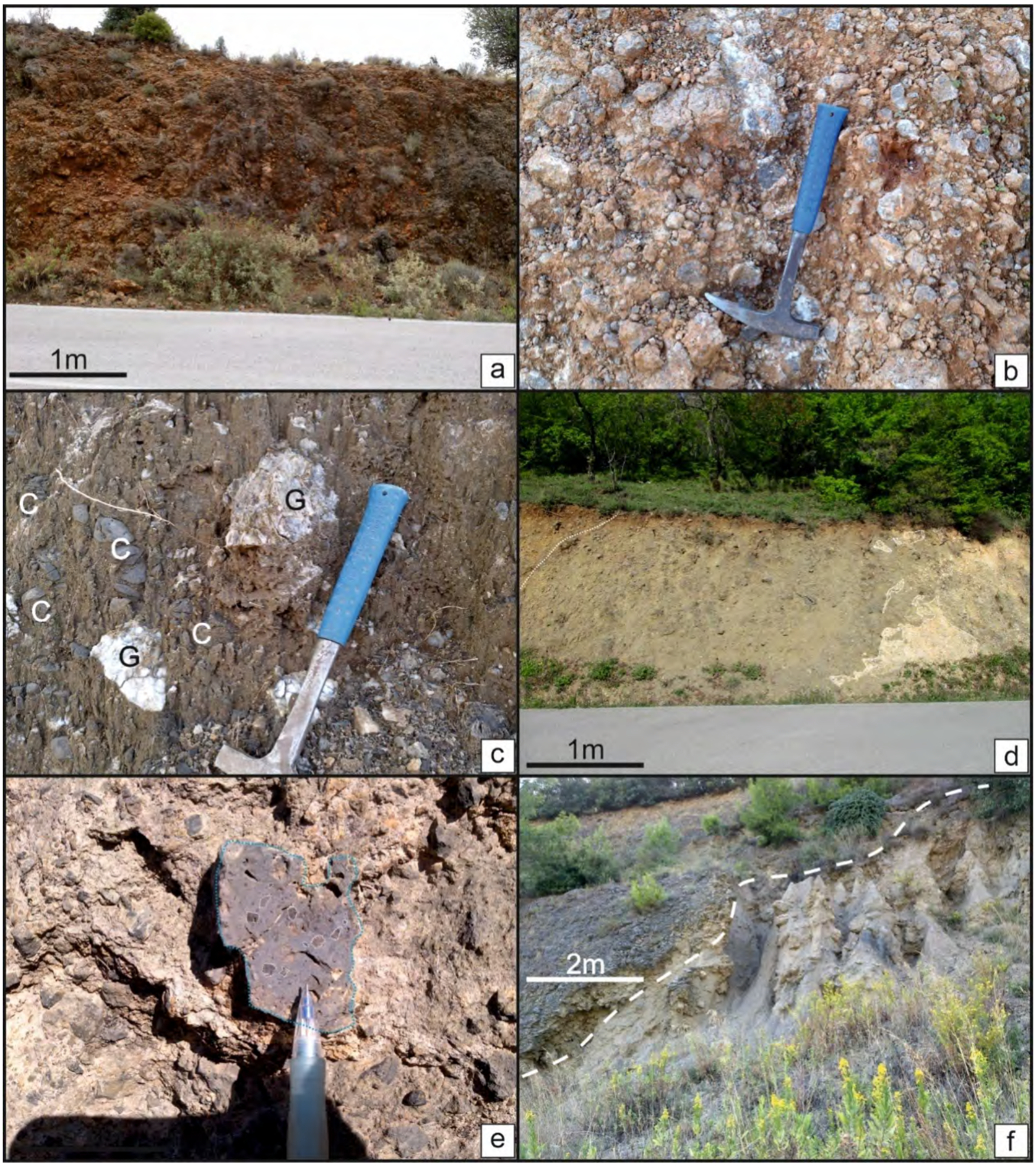

Figure 57. a) Typical image of the Triassic collapse breccia in carbonate-dominated area, b) close-up view of image a, c) clay matrix-supported breccia of undissolved gypsum and carbonate clasts, d) dark color-dominated carbonates chaotically incorporated with light-colored dolomite fragments, e) multiple generations of breccia preserved within a fragment, f) boundary between dissolved (cap) and undissolved (lower part) evaporite.

4.1.20 Triassic evaporites

The Triassic Evaporites are usually exposed in a few restricted outcrops, except for the multi-km Vrysella and Kryovrysi diapirs. On the surface, they consist of black, gray, and white gypsum (Figure 58a), white dolomite beds, and black and brown argillaceous limestone beds up to 2 m thick (Figure 58b).

In sections that exhibit intense shearing, black carbonaceous clasts are observed along with dolomite bed fragments that appear rotated within the gypsum host mass (Figure 58c). Despite the apparent brecciation of the lithological members in some outcrops, gypsum-dominated outcrops are plastically deformed exhibiting isoclinal folds (Figure 58d).

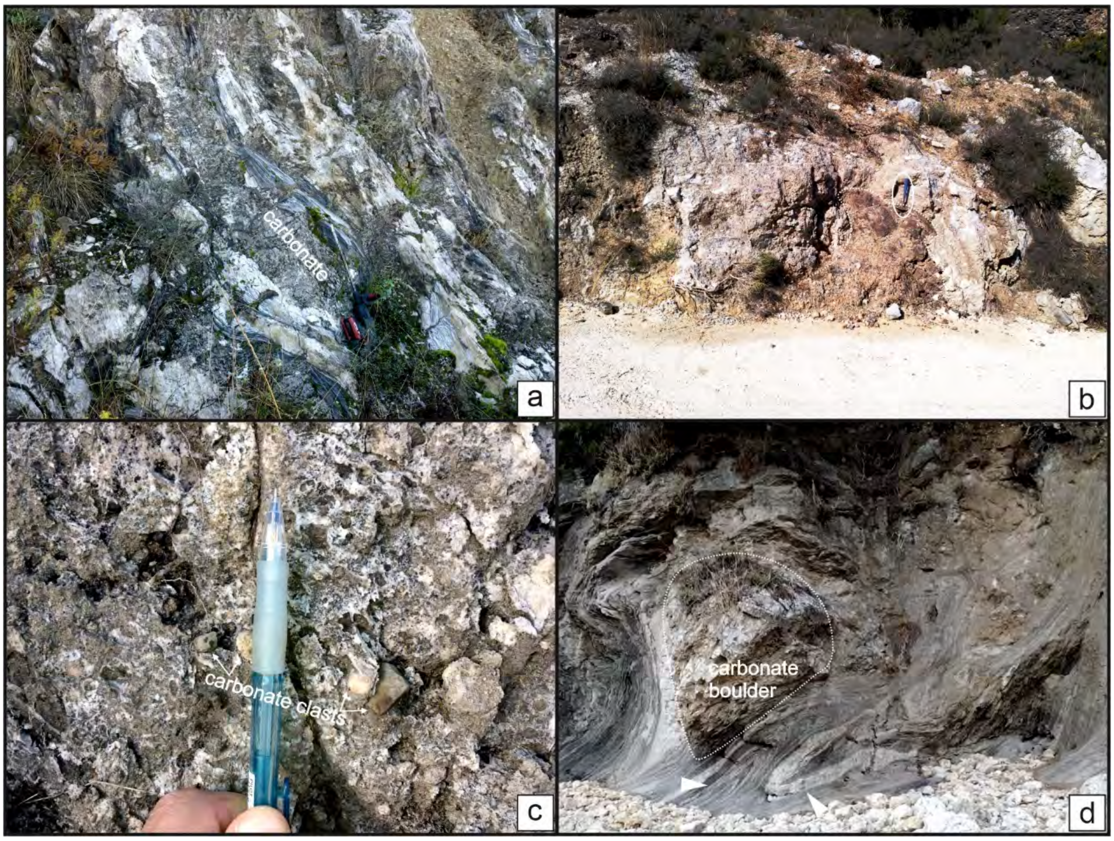

Figure 58. a) Outcrop of unweathered evaporite containing black and white beds of anhydrite, clay and carbonates, b) thick (>1 m) beds of carbonaceous shale and dolomite within the evaporites at the Vrysella diapir, c) common image of black carbonaceous clasts within gypsum host mass, d) a sheared carbonate boulder within gypsum host mass. The white arrow shows an isoclinal fold in gypsum.

4.2 Tectonostratigraphic sections

4.2.1 Koukoulioi

In this section, the stratigraphy of the Lower Posidonia Beds, the stratigraphic transition towards the Upper Posidonia Beds, and the lateral equivalency of the Lower Posidonia Beds to the Ammonitico Rosso are studied in two locations. It is located ~1 km ENE of the Koukoulioi village. Section length is ~700 m in the NNW-SSE direction, parallel to the boundaries of the outcropping formations.

In the northern location, from the bottom to the top of the stratigraphic column are included: ~10 m of thin-bedded Siniais limestones; on top of it, the Lower Posidonia beds are developed with ~4 m of limestone with black shale intercalations and ~8 m of black shales with interbedded thin limestone. Filamentous limestones Fm are not clearly developed; however, above the black shales, there are ~10 m of limestone-dominated lithology containing bedded chert. The Upper Posidonia Fm consists of ~4 m of black bedded chert-dominated lithology with limestone beds, ~5 m of more weathering-resistant limestone-dominated lithology with black bedded chert, ~10 m of thin bedded brown/ochre siliceous and calcareous marls with minor black bedded chert, a 40 cm-thick black chert bed, ~2,5 m of brown thin bedded siliceous and calcareous marl, a 30 cm-thick black chert bed, and 3 m of the brown marls in contact with the Vigla Limestones. In the southern section are observed the topmost parts of the Siniais Limestone, which gradually turns to Ammonitico Rosso facies dominated by red marls and limestone (~3 m).

4.2.2 Pentolakkos

The Pentolakkos Section (Figure 59) is an important area for basin structure understanding during the Upper Cretaceous. The 3-km-long E-W section of the NNE-SSW trending open anticline structure between the Vargiades and Pentolakkos villages demonstrates important stratigraphic differences at its two limbs. The thickness of the Vigla Shales in the western part exceeds 40 m, whereas in the eastern part pinches out, reaching ~1-2 m in thickness. The stratigraphic distance between Sh.V. top and Ls.Sen base is ~1–1.5 m at the western part and ~40 m to the eastern side of the hill. The basal

Senonian strata are differentiated, demonstrating thick, massive limestone with various sizes of bio- and lime-clasts observed in the eastern limb, whereas in the western limb, the beds are thin, and the clasts are fine-grained.

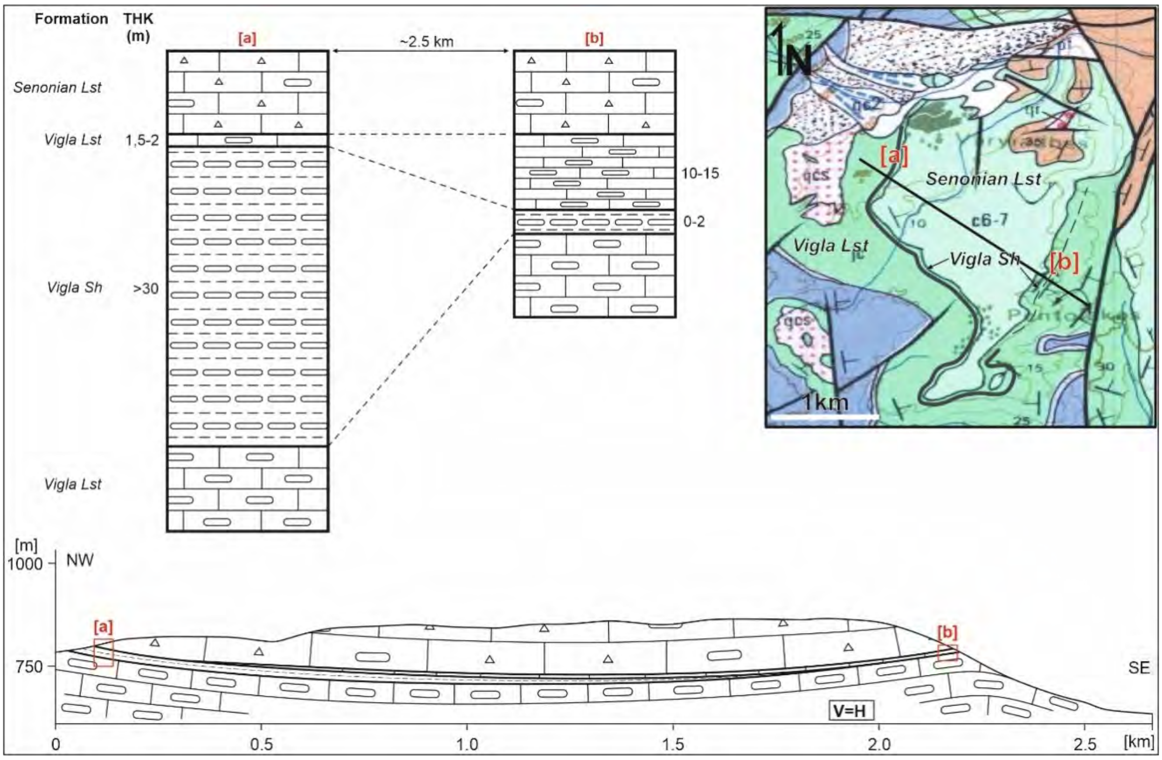

Figure 59. Stratigraphic columns, cross section and geological map of the broader Pentolakkos area with the Vigla shales mapped.

4.2.3 Elataria

The WNW-ESE-oriented, 850 m-long Elataria Section, corresponding to ~400–450 m of stratigraphic extent, is located 1 km ESE of the Elataria village and covers the stratigraphy from the Lower Jurassic (Pantokrator–Lower Posidonia Beds contact) to the Upper Cretaceous (Vigla shales).

The section commences with ~8m of dark gray and bluish laminated argillaceous limestone with a few thin black chert beds. The next 10–15 m are covered by talus slope deposits. Next, we observed ~5m of reddish shales and bedded chert. A sample (sample no. 42) of black chert with a bitumen smell was obtained from a relatively thick (~20 cm) black chert bed; on top of it, abundant Posidonia shells were found. The next 100–120 m belong to the Upper Posidonia Beds. Vigla limestones occupy the next 180–200 m of the section. On top of the Vigla limestone sequence, the Vigla Shales are well developed in a

~60 m section. The stratigraphic extent of this section reaches 45 m, belonging entirely to the shale formation, and from the bottom to the top, it includes: 2.5m of black shales and black bedded chert with a heavy bitumen odor when beaten (lithology A), 15 m of thin-bedded cherty limestone (lithology B), and ~25 m of alternations of various-colored bedded chert and shale (lithology C). The lower parts of the lithology C are well-bedded.

4.2.4 Souli

The area involving the Paramythia and Souli Mountains, as well as the elongated intermontane basin between them, demonstrates high structural and stratigraphic complexity. Concerning the stratigraphy, the well-exposed and relatively easily accessible Upper Triassic (Pantokrator Dolomite) to Eocene (Paleocene–Eocene Limestone) sequence demonstrates great variability of facies and thicknesses. A major thrust fault brings the Pantokrator Fm. over the Flysch. The hanging-wall forelimb is inverted, exposing the Pantokrator Dolomites in the truncated hinge zone at the high and steep drop-off of the WSW Paramythia Mt. face. The mountain ridge and the eastern slopes belong to the backlimb, which is locally intensively folded. A secondary, blind thrust accounts for the development of a flysch-cored recumbent syncline as well as for the uplifting of the Souli Mt.

Five (5) stratigraphic columns (Figure 60 [a] to [e]) from five locations are presented for comparison and stratigraphic correlation. Columns [a] to [d] are located at the backlimb of the blind thrust-related anticline, whereas [e] is located at the steeply dipping forelimb. The backlimb columns demonstrate relatively thick lithostratigraphic unit thicknesses and high facies diversification with all the known Jurassic formations occurring (i.e., Sh.P, Ls.P, Ls.Pl, Mrl.B, Sh.PL, AR, Ls.Fil, and Sh.PU). The forelimb area demonstrates significantly lower lithostratigraphic unit thicknesses, whereas the Mrl.B, Sh.PL, and Ls.Fil are lacking, and the Ls.Pl is very thin (~1-2 m).

Another significant feature of the backlimb stratigraphy is the rapid shallowing of the dolomitization level.

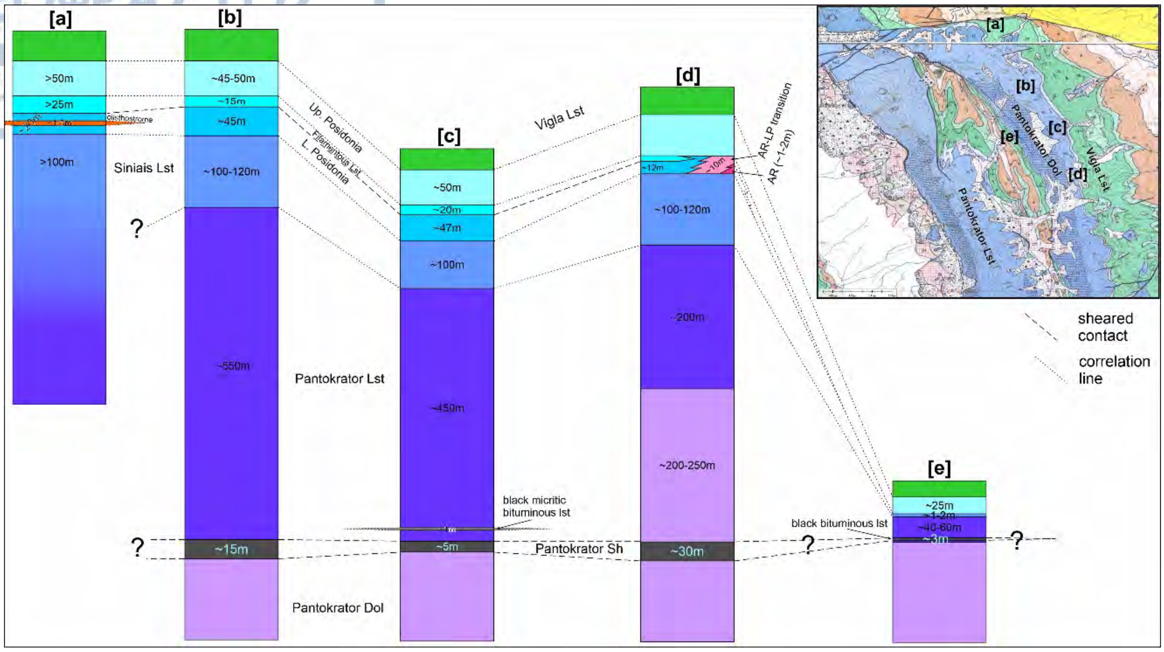

Figure 60. Detailed stratigraphic columns and lithostratigraphic correlation in locations of the broader Souli-Paramythia Mts.

4.2.5 Giromeri

The Giromeri section is important as it encompasses tectonic and stratigraphic features, which can provide detailed insights into the local stratigraphic diversifications as well as the kinematics of the orogenic deformation. The Ls.V contains three distinctively thin intervals with a high clay content, thus having denser vegetation than the surrounding limestone (Fig.). These intervals are separated by a few tens of meters of the typical limestone lithology of the Ls.V Fm. The overall thickness of the Sh.V Fm. is ca. ~90 m, the thickness of the Ls.V. is ca. ~400 m, the stratigraphic distance of the Sh.V. to the Ls.Sen. base is ca. ~20 m, and the base of the Ls.V. is ca. ~270 m. The Sh.PU, the Ls.Fil, and the Sh.PL reach significant thiknesses of around 70–75 m at maximum each.

4.2.6 Thesprotiko Mt

Thesprotiko section (Figure 61) highlights the basin configuration differentiations over short distances. The studied and reconstructed section is ~5 km long, striking E-W and cutting perpendicularly the Thesprotiko Mt. ridge and its tectonic fabric.

The overall structure is represented by an anticline that appears asymmetric and recumbent at parts of Thesprotiko Mt. The deepest interval exposed at the recumbent core of the fold is the Pantokrator Limestones.

The observed stratigraphy involves the Pantokrator Limestones, the Vigla Limestones, the Vigla Shales, represented by three distinct clay/shale/chert intervals, the Senonian and Paleocene-Eocene Limestones, and the flysch. A small, thin outcrop of the Upper Posidonia Shales might occur as well. Nevertheless, its possible occurrence, deduced from the satellite imagery-aided mapping, was not able to be confirmed in the field.

The thickness of the formations varies significantly across the E-W section. The thickness of the Senonian to Eocene limestones rapidly increases towards the east. Moreover, the well-documented Vigla Shales, which extensively outcrop at the eastern limb of the anticline, are absent from the western limb.

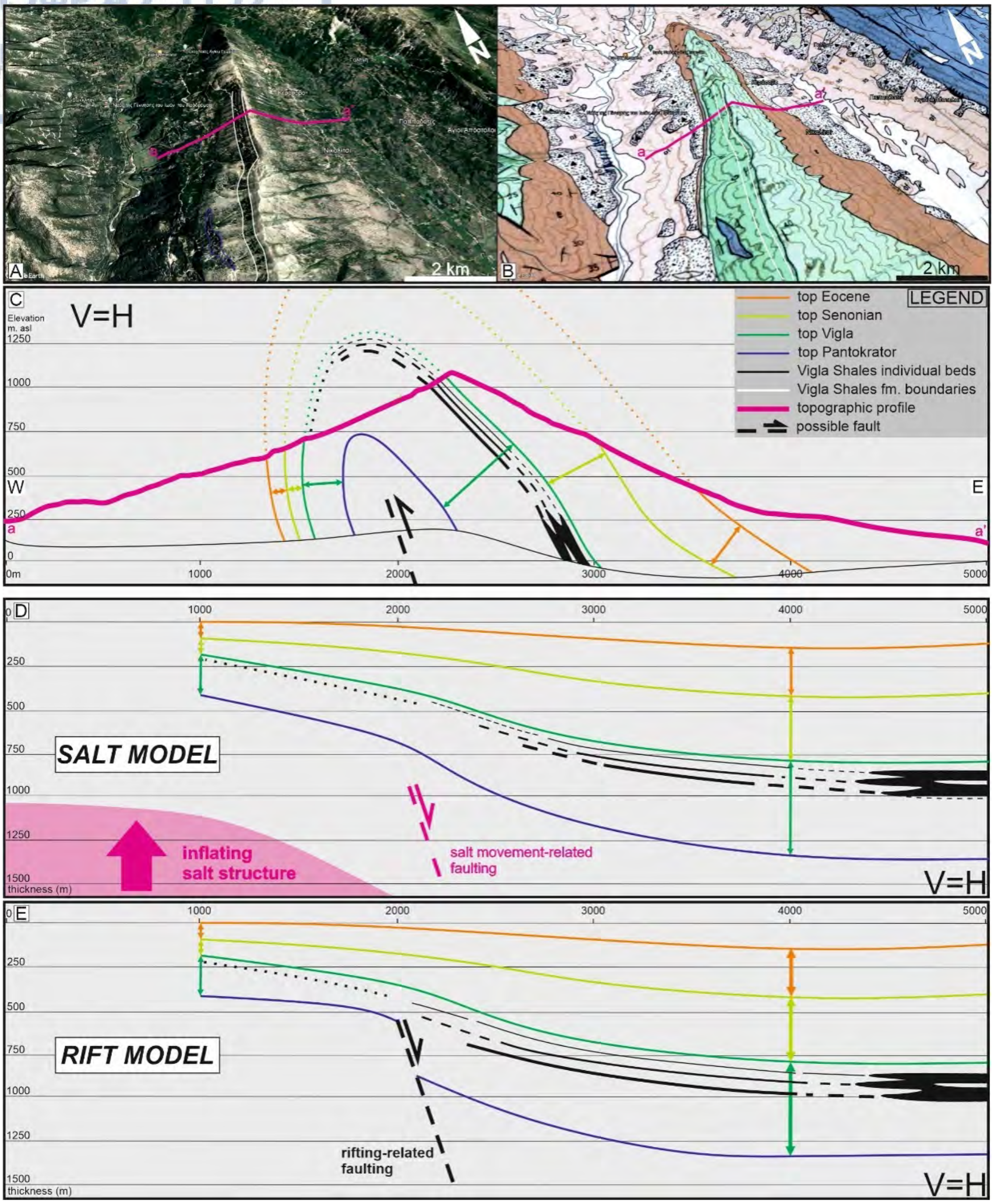

Figure 61. Scheme of the Thesprotiko Mt geological structure with two reconstruction scenarios. A) Satellite image of the area. Vegetation response in the geological substratum is clearly evident. The Vigla shales (verified in outcrops) are enclosed between the white lines. B) Geological map of the area shown in the satellite imagery. C) Cross-section with the carbonate succession shown. D) Reconstruction scenario ("salt model") assuming an inflating structure that controls sedimentation pattern. E) Reconstruction scenario ("rift model") assuming a syn-to-post rift fault controlling sedimentation pattern.

4.2.7 Kefalovryso

The Kefalovryso-Vassiliko section (Figure 62) includes the well-exposed Triassic–Berriasian formations, steeply dipping to reversed in the back-limb position of a thrust-related anticline. In the core of the anticline are exposed formations of the evaporite sequence, summarized herein.

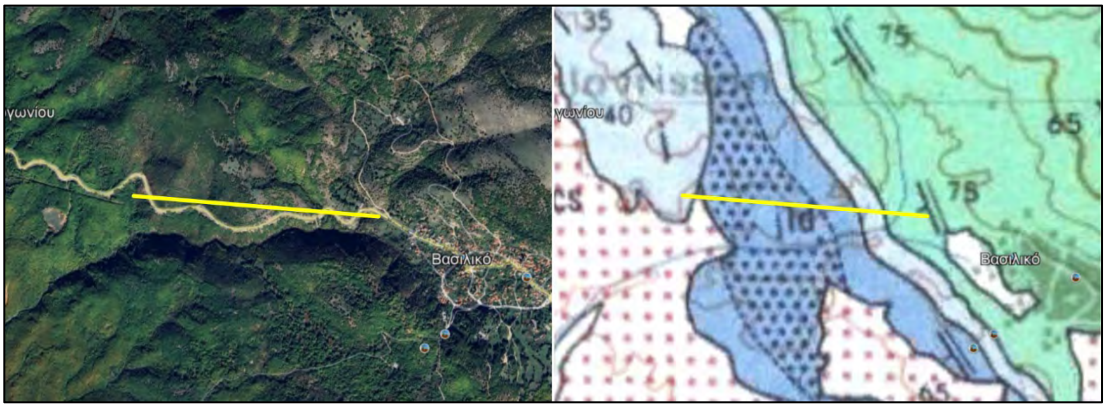

Figure 62. Satellite image and geological map of the Kefalovryso section (yellow line) between the villages of Kefalovryso and Vassiliko. The length of the section is 1,280 m.

The section commences with 250 m of laminated and thin-bedded dolomite/evaporite. Within this section is observed massive dolomite containing anhydrite nodules, thin red clay films, as well as laminated dolomite with possible microbial mat structures (Figure 63 [F]). On top of this succession is observed a 10-m-thick clay-dominated interval showing internal slumping (Figure 63 [E]). The next 80–100 m are dominated by thick-bedded (~1 m) dolomite. On top of it, a 30 m-thick clay-rich, thin-bedded dolomite interval is observed. The next 10 m show a transitional lithology towards a ~200 m-thick sequence of generally thin-bedded limestone. In this 120-meter succession are observed: ~20 m above the base lies the first bed of chert, followed by >10 m of more massive limestone with abundant large vugs (Figure 63 [E], typical of the Pantokrator Limestone lithology). The first black chert bed is located ~80 m above the base of limestone. Above it, ~100 m of thin-bedded limestone with bedded chert occurs. On top of this lies a 4 m-thick formation dominated by thin-bedded limestone and very thin black and white chert beds. The overall color of this formation is red, and it is considered to be a time-equivalent of the Ammonitico Rosso.

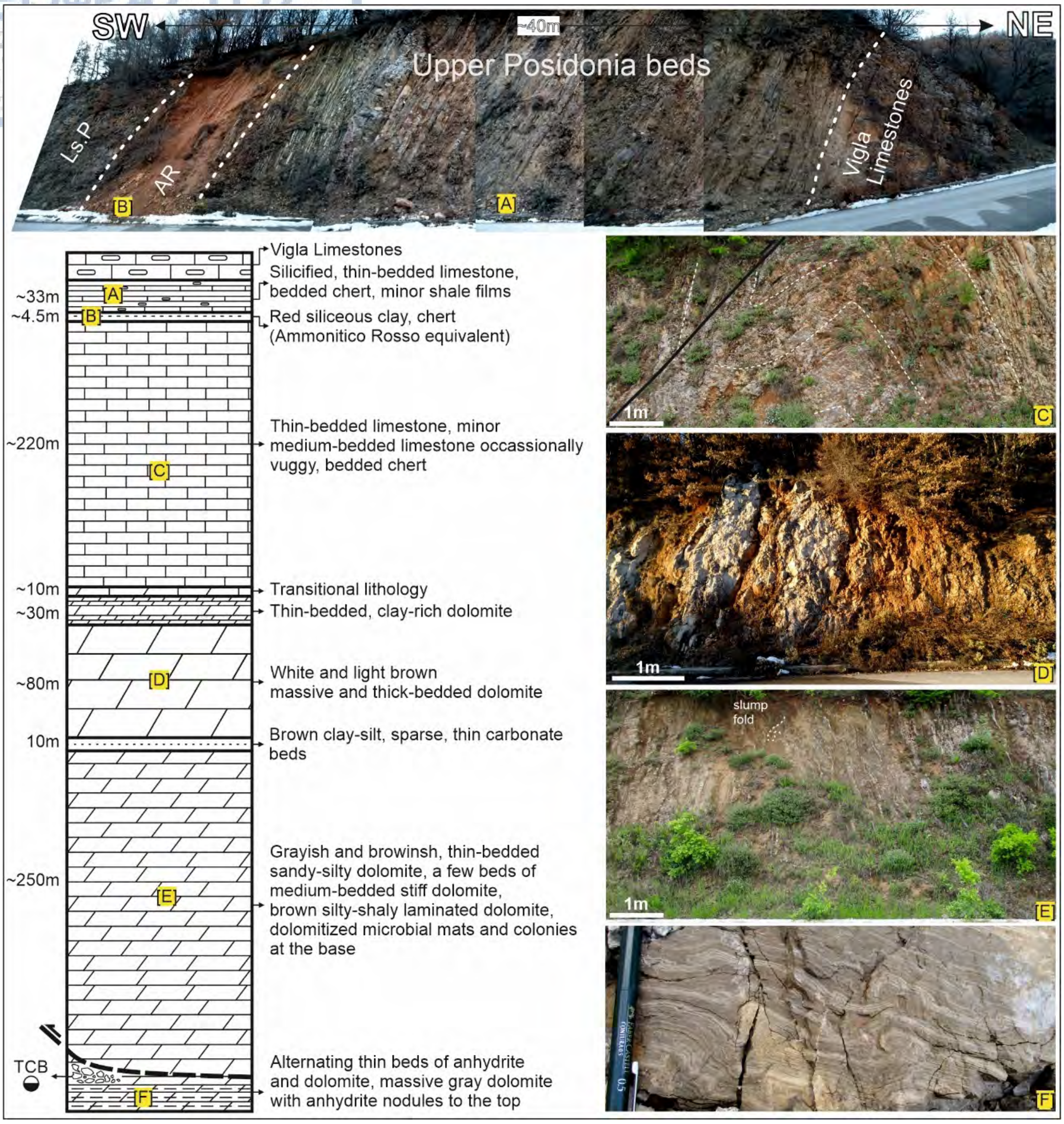

Figure 63. Detailed stratigraphic column of the Kefalovryso section. Lithological descriptions and estimated thicknesses are annotated. On the right hand side and top are provided field photographs with annotation of the stratigraphic position (A-F).

4.2.9 Souli Mt

The Souli-Paramythia Mts. section includes the stratigraphy above the Pantokrator Shales up to the Vigla Limestones (Figure 64). This section is studied in detail as it demonstrates an important deviation from the typical lithology of the Pantokrator Limestones Fm. The base of the section commences above the Pantokrator Shales. It starts with thick or massive limestone for a few meters. Above it, a thick (>500 m) succession of thin-bedded (often laminated) limestone is observed. The lower >150 m of the succession consist of thin limestone and dolomitic limestone beds. A few thicker (~1 m) dark-gray, argillaceous limestone beds occur ~40–50 m stratigraphically above the Pantokrator Shales. These beds emit an intense bitumen smell after hammer beatings. Above this succession is observed a 40 cm-thick single bed consisting of loose white diatomite as well as silicified limestone showing a boudinage form.

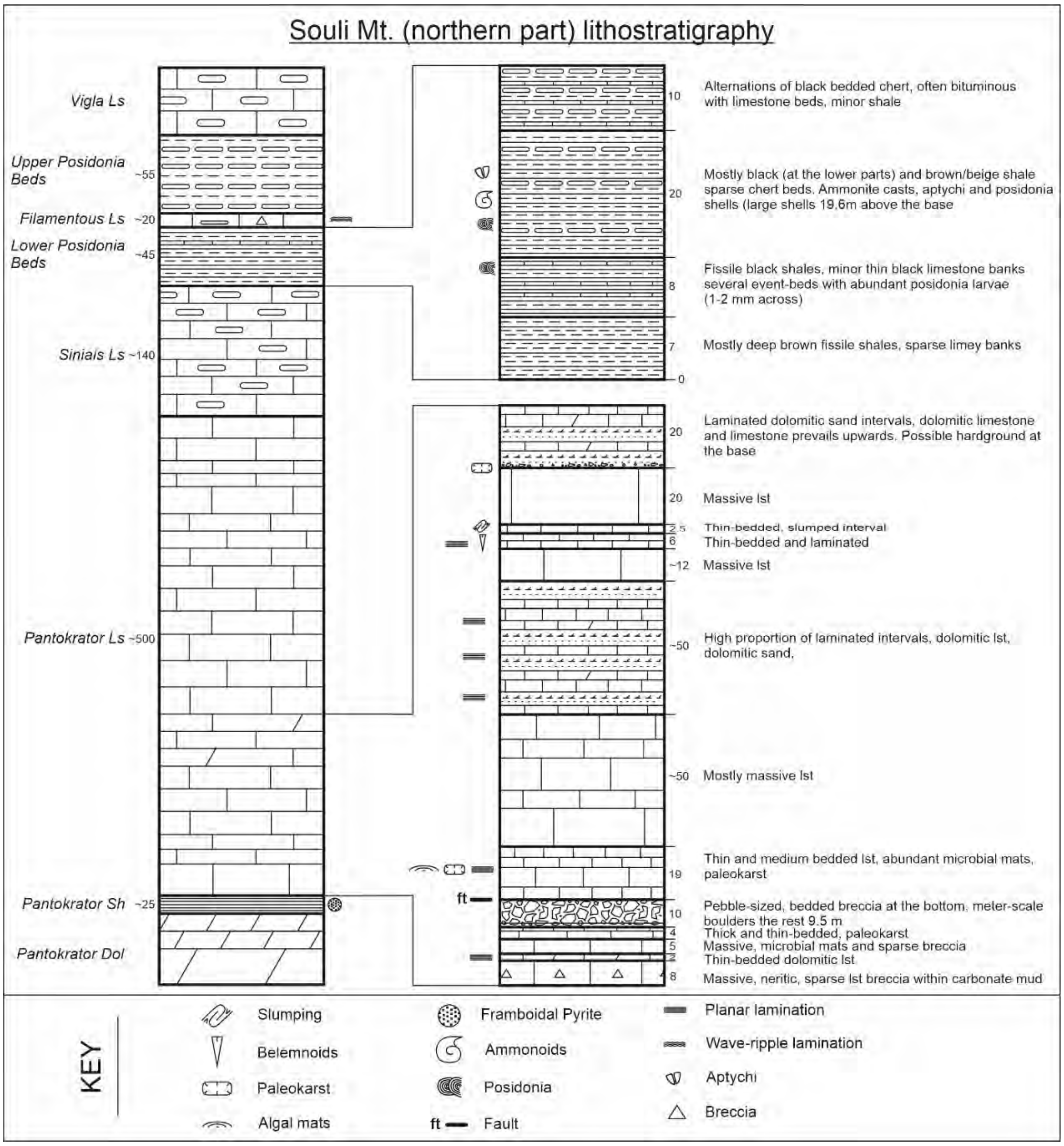

Figure 64. Detailed lithostratigraphic columns at the Souli Mt. Sedimentary features are annotated.

4.2.10 Kouklesi

The broader area around Kouklesi is highly interesting because the syn-rift formations are well exposed in thick sequences while exhibit facies and thicnkness variations. Pantokrator limestones exhibit some interesting lithostratigraphic features as well. In the Figure 65, two cross-sections are shown cutting through the entire structure.

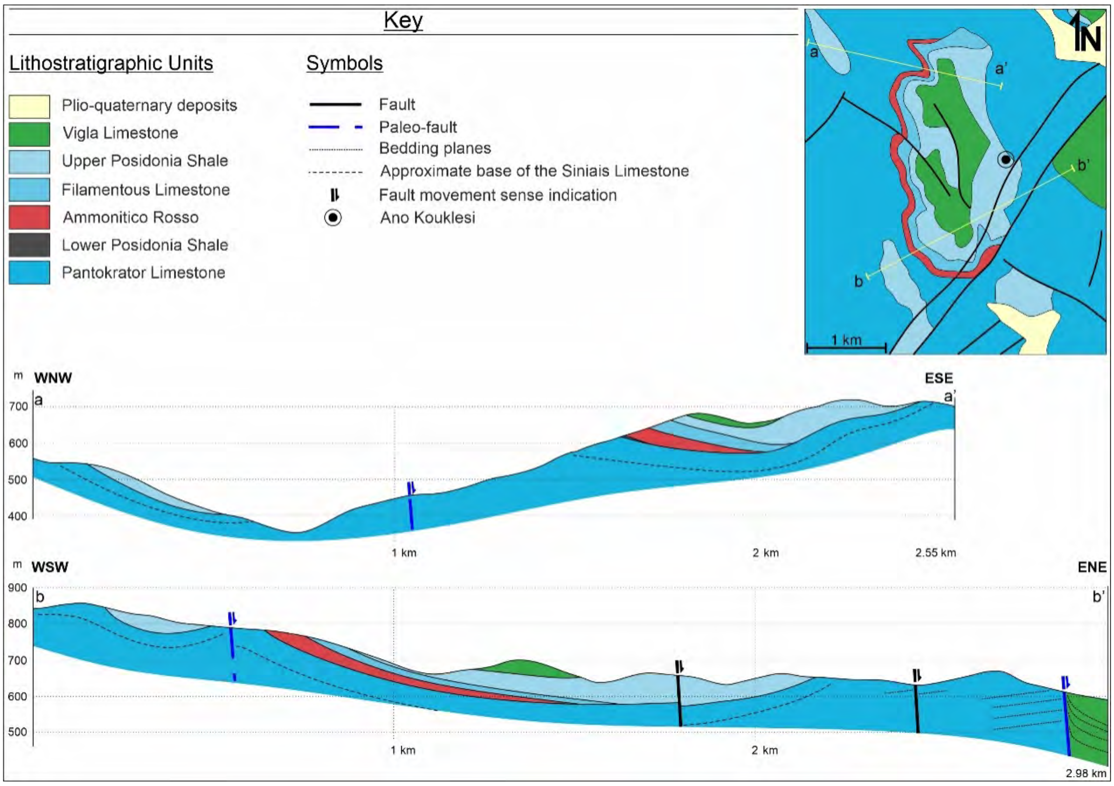

Figure 65. Cross-sections (a-a' and b-b') of the Kouklesi syncline and the surroundings

More detailed, the upper parts of the Pantokrator Limestone Formation are well exposed in gently dipping outcrops. Columnar stromatolites are observed, playing the role of the main framebuilders. Sparce coral fragments, abundant ooids, and thick-shelled benthic mollusk fauna also occur. A very acute contact occurs between the Pantokrator Limestone and the overlying Pliensbachian Siniais Limestone deposits at a 75–80^{o} angle (Figure 66), which is interpreted as a synrift normal fault dissecting the carbonate platform. Alternatively, this contact could be located at the platform edge, where the Pliensbachian deposits represent the onlap over the drowning platform. A similar contact occurs at the Karvounari.

Figure 66. Panorama photo of the acute contact and transition from platform carbonates of the Pantokrator Limestone Fm towards basinal carbonates of Siniais and Vigla Fm

Thick (> 100 m) Upper Posidonia Beds successions occur at the synclinal part of the structure, directly lying over the Siniais Limestone. Ferromanganese nodules are abundant within the Fm in the broader area. Large blocks (>1 m^3) from the underlying Siniais Limestone also occur within the Upper Posidonia. The western part of the structure exhibits a completely different lithology. A thin interval (~2 m) of black shales (Lower Posidonia Beds) directly overlies Siniais Limestone. The Ammonitico Rosso lithofacies overlie the black shales, commencing with ~10 m of red marls or marly limestones in alternations with thinner green marls. The next ~20 m are consistently dominated by pink-red nodular limestones with abundant ammonite fauna, alternating with thin beds of red clay. A white, medium-to-thick bedded limestone succession more than 50m thick directly overlies Ammonitico Rosso. All these relationships are clearly shown in the cross-sections of the Figure 65.

4.3 Lithological contacts

The contact type in the majority of the contacts between lithostratigraphic units is stratigraphic conformity. These are either abrupt, marked by shifts in sedimentation, or gradual. The latter are of gradational and intercalated sub-type. Stratigraphic unconformity between two lithological units was observed only in Kassidiaris Mt., where the Vigla Limestones lie directly over the Upper Posidonia Shales. Between them, a thin (~20 cm) limestone breccia occurs. No change in bedding (DD/DA) is observed;

therefore, the contact represents a disconformity. In several other cases of intraformational oblique contacts of strata, it was not possible to determine whether they were unconformities or soft-sediment deformation structures. In the stratigraphic column of the Figure 67, the contact types are annotated. Indicative outcropping photos of the contact are also apposed next to the column.

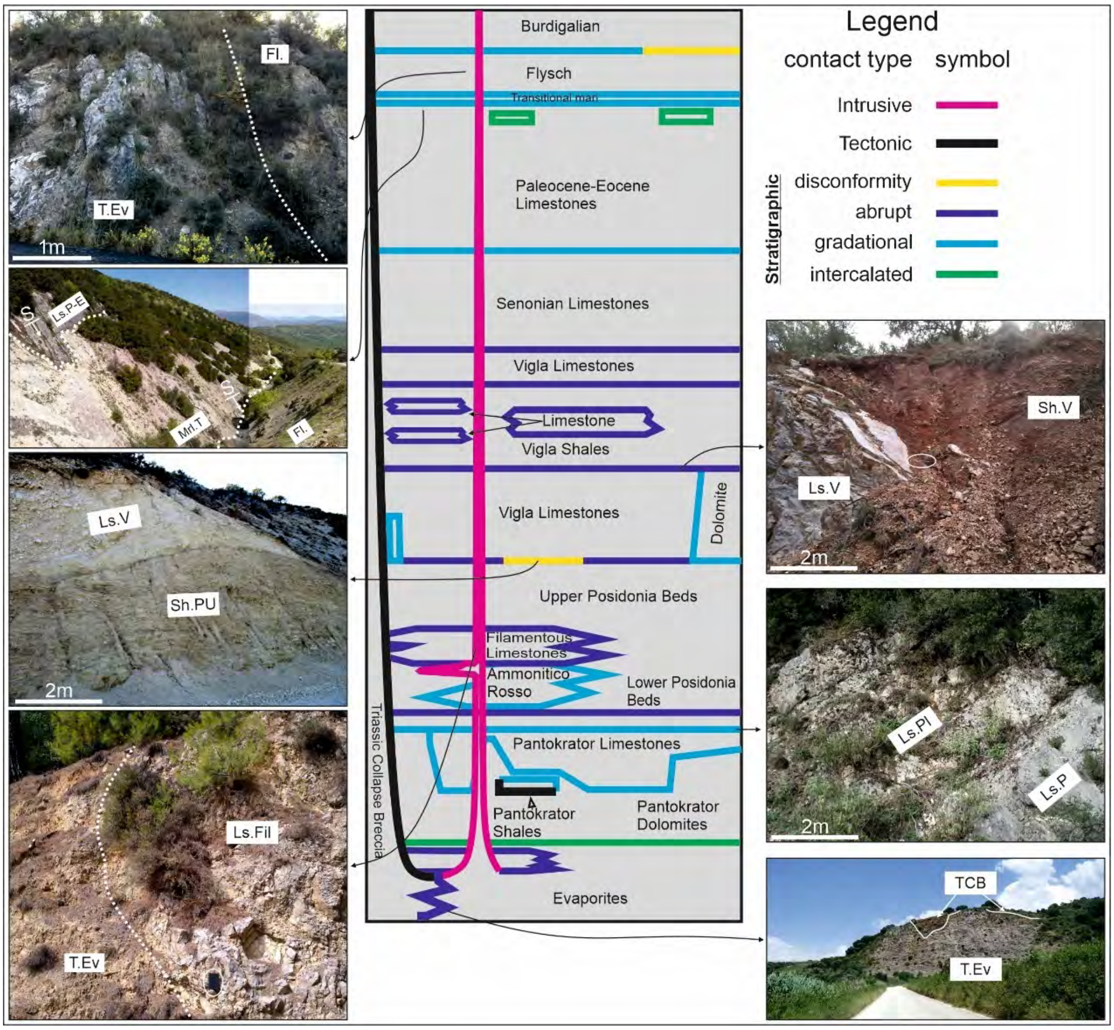

Figure 67. Contact types among lithostratigraphic units annotated with color code. Field photos with reference to the stratigraphic/contact position show characteristic contacts observed.

4.4 Soft-sediment deformation

Slumping is one of the most frequent modes of deformation in incompetent strata. It is commonly represented by folded and truncated strata successions.

Slump folds occur throughout the study area in all the stratigraphic units, from the Pantokrator Shales to the Burdigalian clastic deposits. The thickness of the slumped intervals and individual strata greatly varies among the various formations. A slump fold is observed in the thin-bedded limestone of the Pantokrator Limestone Fm. in the Souli Mt. area (Figure 68). Small (cm-scale) slump folds are sparsely observed in restricted strata in the Pantokrator Shale Fm. (Figure 69).

Figure 68. Slump fold on the top the thin bedded Pantokrator limestones succession.

Extensive slumping is observed in some restricted intervals of the Siniais limestones, demonstrating highly viscous rheological characteristics. The most extensive slumping occurs locally within the Senonian Limestones and is secondary in the Vigla Limestones. Intervals up to ~30 m thick with slumps, often showing an apparent chaotical structure with fold hinges cross-cutting each other, occur within the Senonian successions of the IZ-C. Slump-fold relic hinges also occur locally in the flysch and in Burdigalian. No statistical treatment was applied on slump fold hinge orientation data due to insufficient slump-triggering mechanism understanding for each slumped interval. This is because the author considers the basin bottom inclination angles and directions, are depended on multiple parameters such as inherited fault patterns, faulting and salt withdrawal/inflation. Especially the later phenomenon, although recognized in the area (e.g., Vakalas et al., 2023) is poorly constrained in terms of movement magnitude and salt-structure shapes.

Figure 69. Slump fold within the Pantokrator Shale. Width of view ~40 cm.

4.5 Paleokarst

Emersion events affecting parts of the shallow carbonate platform are evident within the Pantokrator Formation in paleokarst forms. Preferential bedding-parallel dissolution occurs at several stratigraphic levels of the Pantokrator Fm. Vertical to bedding, cemented fractures comprise barriers to the connectivity of the large bed-parallel vugs. This indicates that regional fractures were developed prior to karstification, and fluids saturated with $CaCO_3$, and other less soluble material traveled through them (Figure 70a). These cements were less susceptible to meteoric water dissolution. Small-scale dissolution-collapse with the original bedding preserved was also observed (Figure 70b).

Moreover, dissolution-collapse breccia are present within the lower parts of Pantokrator Limestones. Breccia are commonly “rafting” within carbonate mud matrix, also pointing to emersion shortly after deposition.

Figure 70. a) The red arrows indicate the fractures infilled with more dissolution-resistive cement while blue arrows indicate the open karstic vugs (Pantokrator Limestone). b) small scale collapsed beds with the original bedding preserved (Pantokrator Limestone)

4.6 Structural geology of Epirus

4.6.1 Folding

A total number of 1,659 bedding measurements were obtained from more than 1,200 locations across the study area. Their poles (π) are projected (equal area) on the lower hemisphere of Schmidt net (Figure 71[C]). A π-pole rose diagram and density plot are also shown in Figure 71[A] and 71[B] respectively. The cluster analysis of the π-poles shows two areas of maximum concentration corresponding to the poles of the limbs of a fold. This represents a "mean" fold, characterizing the overall folding style of the area (Figure 71[C]). The mean fold is a non-plunging asymmetric fold gently verging to the WSW. Given that the number of poles in the two clusters (fold limbs) are statistically sufficient to assume that their ratio (nA/nB) represents the fold limb length (L) ratio (L_{LimbA}/L_{LimbB}), the following mean fold was drawn (Figure 72) encompassing all of the main attributes. According to this, enveloping surface of the mean fold gently dips ($62^o/3.13^o$) towards the hinterland. The fold analysis resulting attributes are summarized in the Table 15.

Table 15. Table of the attributes and their values of the basic parameters of the general folding analysis.

Attribute	***Value***
Total bedding measurements (n)	1659
Bedding π-pole cluster analysis	2 principal clusters
Principle cluster: n_A (Limb A - long)	954
Secondary cluster: n_B (Limb B - short)	705
Limb A (dip dir./dip)	61.4°/33.3°
Limb B (dip dir./dip)	242.6°/39.7°
n_A/n_B	1.353
π-circle (common plane of Limb A and Limb B)	152°/89.5°
π &b axis	332°/0.5°
Bisecting plane	62°/86.8°
Interlimb angle	107°
Possible enveloping surface	62°/3.13°

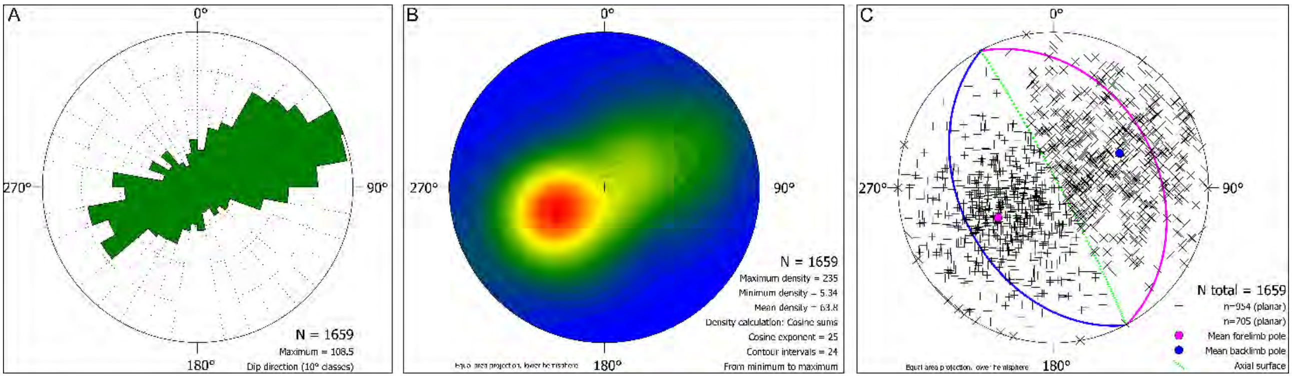

Figure 71. Statistical analysis (N=1659) of the bedding surfaces (S) within the study area. A) Rose diagram with 10° sectors. Maximum density of bedding surfaces at 60°-70° sector with 209 surfaces. B) Bedding π-pole density distribution. A major π-pole concentration is evident (red hues) in the WSW direction (ENE bedding surface). C) The two main π-poles [blue dot and great circle (S=61.4°/33.3°), fuchsia dot and great circle (S=242.6°/39.7°). The green great circle represents the bisecting plane (62°/86.8°) of the two maximum bedding pole concentrations defining a general folding structure.

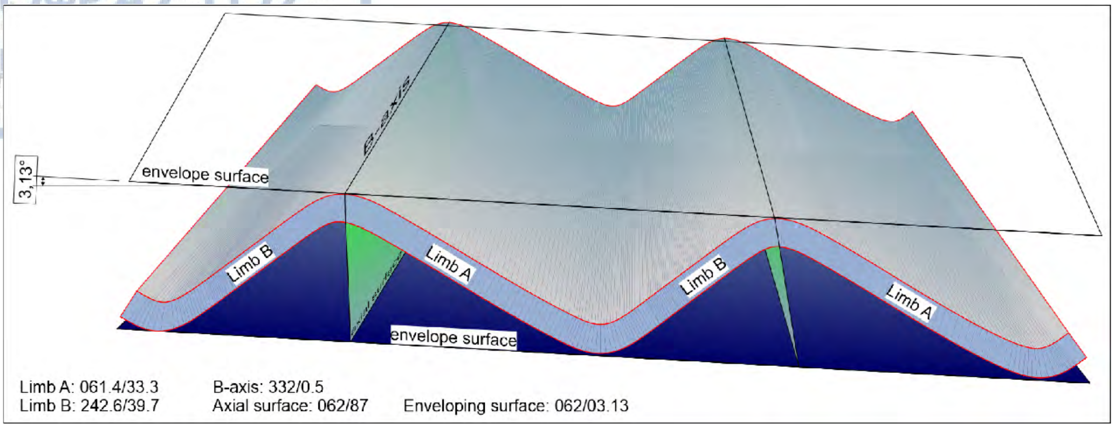

Figure 72. Perspective model of the mean large-scale folding in Epirus. Limb A and limb B define a WSW-verging, NW-SE trending (b-axis: 332°/0.5°) open (interlimb angle=107°) asymmetrical fold. Enveloping plane is gently dipping to ENE (062°/3.13°).

4.6.2 Faulting

Faulting is prominent throughout the study area with all types of fault present i.e., normal, reverse, strike-slip and oblique (normal or reverse component). Limited measurements (N=112) are sufficient for secure statistical analysis. However, it appears that the majority of the faults occurs either in a NW-SE or NE-SW strike (Figure 73). Further separation of the faults with clear kinematic image in the field in the classes of normal, reverse and strike-slip geometry showed that a) the normal faults (N=38) are mainly developed in a NNW-SSE strike and a subordinate class of NE-SW strike, b) the reverse faults show a more persistent NW-SE strike and NE dipping and c) the strike-slip faults show a relatively clear clustering in three strike orientations these of i) NE-SW, ii) WNW-ESE and iii) a subordinate N-S strike. Reverse faults appear to have milder dip angles (~30-40°) than the other types. Normal faults appear to dip around ~55-65°, whereas the strike-slip faults are the steepest with dip angles >65-80° or more especially for the NNW-SSE and NE-SW clusters.

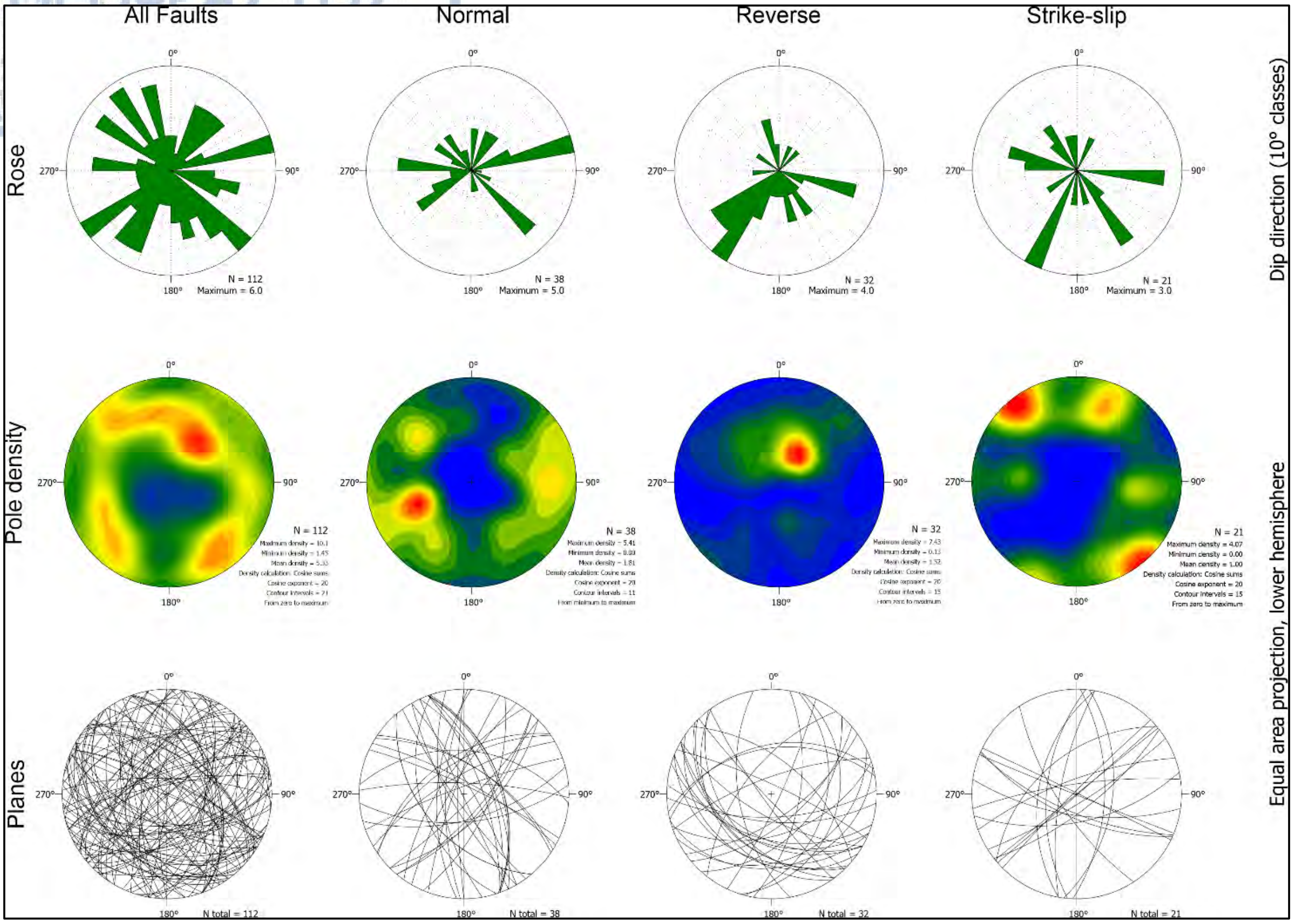

Figure 73. Fault geometrical characteristics statistical analysis. The columns include the sample population (i.e., all faults, normal, reverse and strike-slip) and the rows include the analytical method (i.e., fault surface rose diagram, π-pole density diagram and fault plane plotting). Rose diagram classes are of 10°, while poles and planes are plotted on equal-area diagram.

4.6.3 Jointing

A total number of 434 joint measurements was obtained across Epirus. Statistical analysis (Figure 74) showed a strong cluster of joint surfaces dipping to SSE to SE directions and a second one to NNW directions. A third cluster appears dipping to WNW. The mean joint surface is almost vertical and strikes ENE-WSW (148°/89°). This joint fits well the folding model, likely representing the mean extensive joint (normal to σ1) while the distribution of poles likely reflects the shear fractures (oblique to σ1) developed during folding.

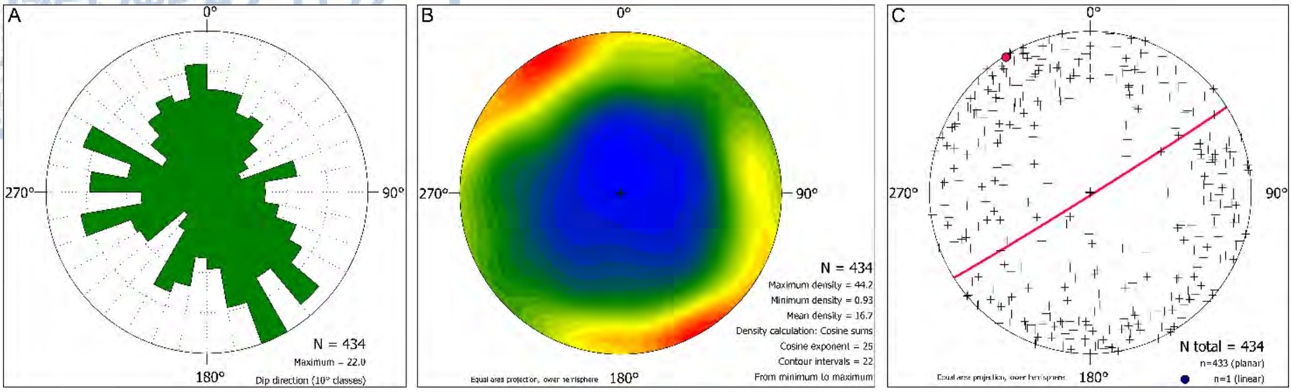

Figure 74. Statistical analysis of the joint (N=434) geometrical attributes (dipping direction and dipping angle). A) Rose diagram (10° sectors). Maximum density of joint surfaces at 150°-160° sector with 22 surfaces. B) Joint π-pole density distribution. C) π-poles and maximum density pole (red dot – 328°/01°) and the associated joint (red great circle – 148°/89°).

4.6.4 Lineations

Measured lineations mainly concern syn-tectonic secondary calcite over faults, folded bedding planes and fibrous calcite. Although measurements are not sufficient for secure statistical implications, a relatively strong cluster occurs in the orogenic direction ENE-WSW (Figure 75). A possible second cluster occurs perpendicular to the main cluster and is mainly linked to faults.

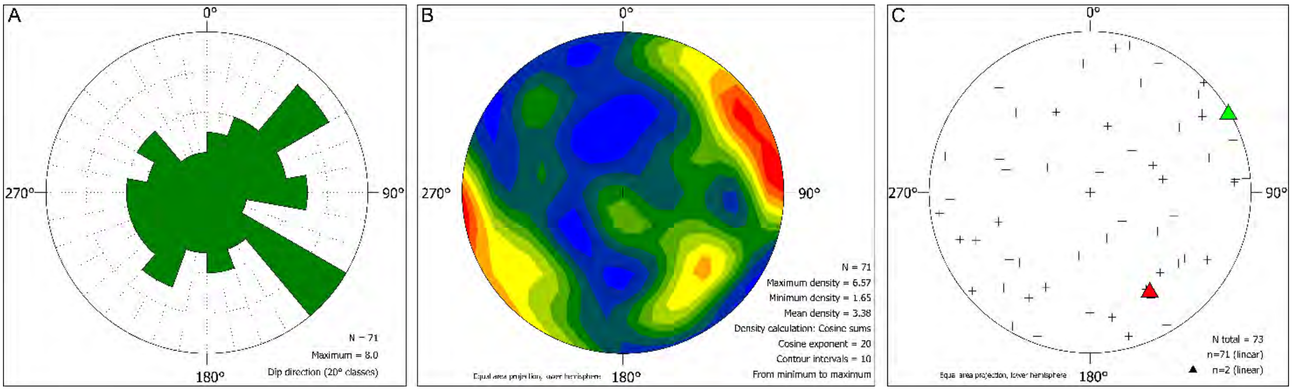

Figure 75. Statistical analysis of the lineation measurements. A) Rose diagram (20° sectors). Although the most populated individual class falls in the 120-140° sector, the majority of the lineations lies in the ENE-WSW direction. This is more evident in the density diagram [B]. Cluster analysis showed two main centers of pole concentration; the main in the ENE-WSW direction and a subordinate in the NNW-SSE direction.

4.7 Detachment levels

The Ionian Zone is comprised of various sedimentary rocks (limestone, shale, chert, dolomite, evaporite, etc.) exhibiting great variability in their mechanical strength profiles. The proportion of the limestone (the mechanically strong intervals) is high compared to the shale (the mechanically weak intervals) in the supra-evaporite succession. These weak intervals occur at specific stratigraphic levels. Their lateral extent, though, is not continuous throughout the entire basin extent.

Moreover, apart from the lithological variations, limestone formations demonstrate various bed thicknesses and corresponding fracture densities, therefore heavily affecting mechanical properties. Chert beds often appear almost pulverized, developing a very dense fracture network and creating sub-mm-size blocks. Large strain amounts appear to be accommodated within the thin-bedded shale/chert-dominated intervals, as is evident by the successive tight chevron folds, kink bands, and folds of dm to m-scale wavelength. These folds are absent from the limestone units. Only in the relatively thin-bedded cherty limestones of Ls.V are observed m-scale wavelength relatively close folds (50–120^{o} interlimb angle). These folds are mainly observed as parasitic folds at the hinges of higher amplitude folds and are not associated to decoupling levels of regional scale.

One of the most contrasted in terms of mechanical properties is the contact between the platform carbonates of the Pantokrator Fm. and the underlying evaporites (or Triassic collapse breccia). In the areas of Anthoussa and Igoumenitsa, it has been observed that the contact between the two formations is zonated, with distinctive zones of different lithological assemblages and tectonic strains (Figure 76).

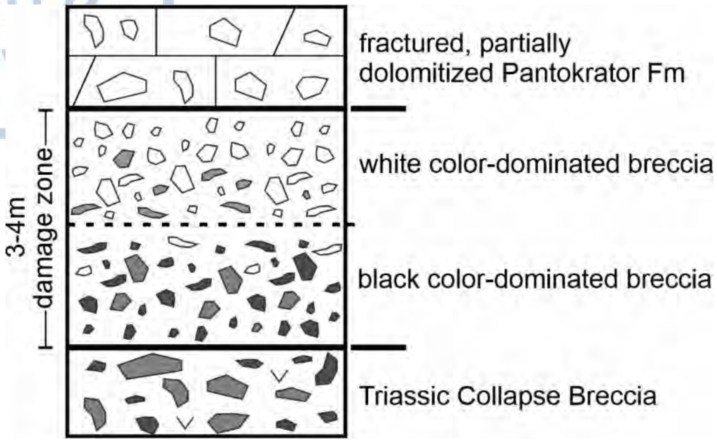

Figure 76. Model of the lithological zonation of the contact between overlying Pantokrator Formation and the underlying Triassic Collapse Breccia.

Nevertheless, the presence of these spatially restricted mechanically weak layers could either serve as local detachments or as potentially inter-connectable nuclei for regional detachments during stress and strain buildup. This phenomenon occurs in the Souli and Paramythia mountains, where a shaly, mechanically weak interval (i.e., Pantokrator Shales) outcrops at the base of a thrust hanging wall, attesting to this hypothesis.

Morley et al. (2021) suggest that "atypical" detachments can be developed at deeper structural levels (late diagenetic to anchimetamorphic conditions) within the carbonate successions when some small lithological variations (i.e., thinner beds, some clay content) occur. This might be the case in the subthrust domain in Epirus; however, the presence of more typical mechanically weak intervals would likely focus and accommodate any strain.

Velaj (1996; 2015) and Mazzoli et al. (2022) suggest that the weak Triassic salt interval in southern Albania effectively decoupled the Tertiary deformation, focusing it only on the sedimentary cover. During this stage (Oligocene-Miocene), break-thrust folds were developed in areas with thick (>> 1km) salt, whereas in areas with thinner salt (<<1 km), the fold-and-thrust belt development was restrained. Moreover, at the latest stages (5-0 Ma), rifting stage-inherited mid-crustal weak levels were reactivated, upthrusting the entire basin and leading to extensive erosion.

Based on extensive field observations on the lithology, the contacts between lithological units, and the preferential deformation patterns in specific thin-bedded and clay-rich intervals, the following mechanical strength profile is proposed for the Epirus (Figure 77).

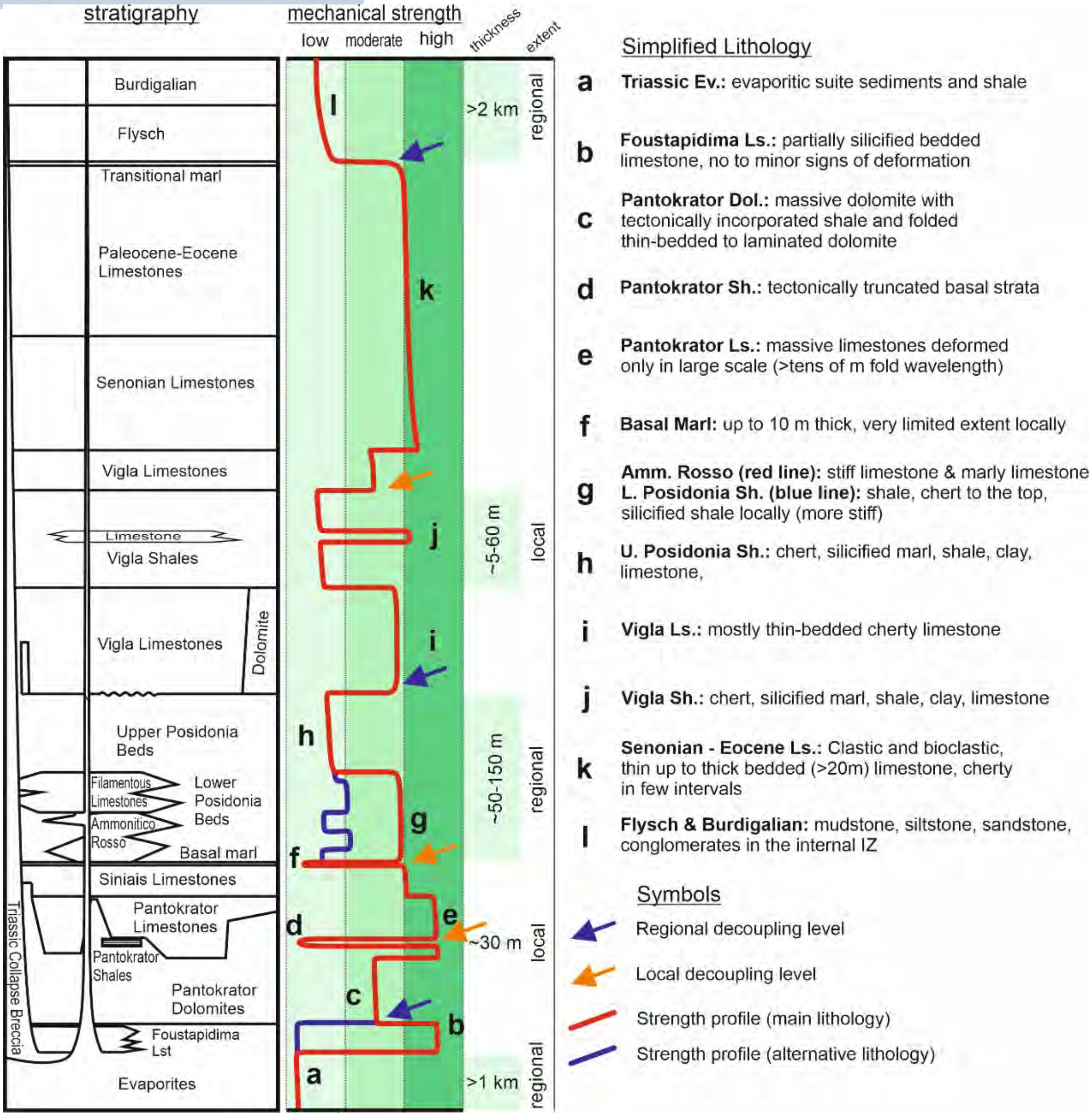

Figure 77. Mechanical stratigraphy profile of the Ionian Zone stratigraphic column in Epirus corresponding to the mechanical strength of the formations (relative deformation susceptibility) from numerous field observations in Epirus.

4.9 Structural style

The overall structural style of the Ionian Zone is characterized by SW-verging km-scale asymmetric thrust-related anticlines and synclines of the NNW-SSE trend, commonly involving the entire Triassic-Tertiary stratigraphic column. The NNW-SSE trending thrusts often cut and transfer the anticlines over kilometers towards the WSW. Successive thrusts create thrust-bounded sheets. Major thrust lengths exceed 30–40 km. Blind thrusts are inferred from the focal mechanisms of numerous earthquakes in the Epirus region, especially in the central and westernmost parts of the Ionian Zone. Back-thrusts and opposite-directed folds often occur, especially in the IZ-I and IZ-C. Long, nearly horizontal, or gently dipping backlimbs occur in many thrust sheets, whereas others exhibit steeper backlimb geometry. Forelimbs are shorter and much steeper. This geometry is attested to by the structural analysis provided in § 4.6.1. Parasitic folds of S, Z, and M types are commonly observed, especially near the hinge zones of thrust-related anticlines. A discrepancy in the aforementioned NNW-SSE trend is most profoundly observed in the area of Thesprotiko Mt, where the main axis of the ridge is developed in a NNE-SSW trend coinciding with the anticlinal axis.

Fold hinges appear very narrow in parts of the flysch deposits, whereas they are gradual in the large-scale folds in limestone-dominated lithologies.

Between the Perdika and Agia villages (IZ-E), a tectonic window occurs where the Corfu Flysch is exposed below the thrusted Mesozoic rocks of the Ionian Zone.

4.10 Rock-Eval 6® Results

The sample locations of the potential source rock intervals are shown in the Figure 78 and the sample identifications are annotated. The RE6 acquired parameters (S1, S2, S3, S3CO) and calculated parameters (TOC, Tmax, S1/TOC, GP, S2/S3, HI, OI) as well as the associated field location identifications, coordinates, age/formations are shown in the Table 16.

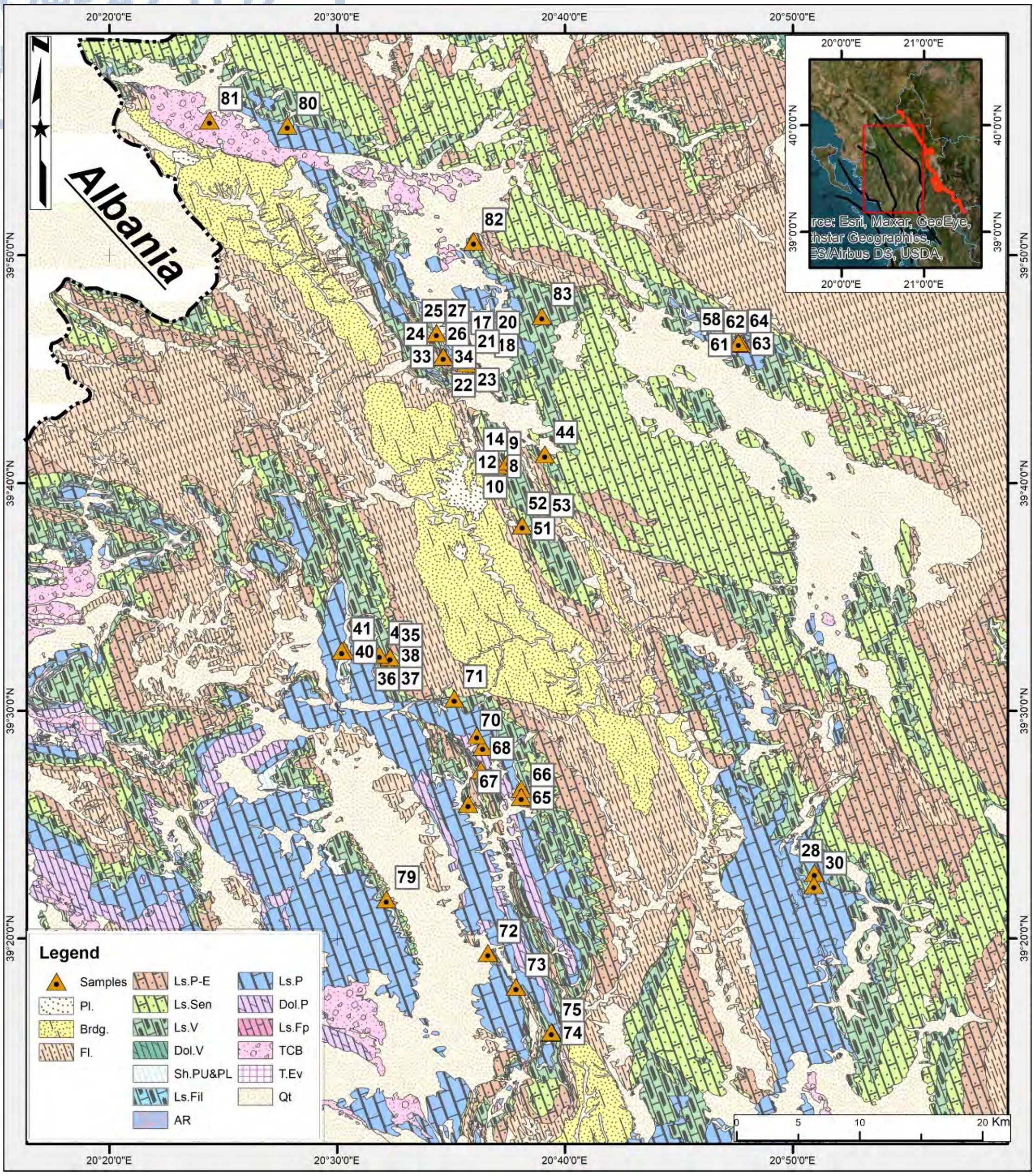

Figure 78. Sample location map. Identification numbers are cited in the Table 14.

Table 16. Table of the Rock-Eval results for all the study samples. Coordinates, identification name and locations are provided. Calculated parameters such as the generation potential (GP), production index (PI), S2/S3 and S1/TOC useful in the evaluation are also provided.

Age	Formation	longitude	latitude	loc.	sample	Qty	S1(mg/g)	S2(mg/g)	Tmax(°C)	S3CO(mg/g)	S3(mg/g)	TOC(%)	HI	OI	GP (S1+S2)	PI = S1/(S1+S2)	S2/S3	S1/TOC
Aptian - Cenomanian	Sh.V	39° 40' 47.1749" N	20° 37' 03.6998" E	#11	8	59	0.03	0.13	391	0.11	0.93	0.11	118	845	0.16	0.01	5.17	0.27
″	Sh.V	39° 40' 47.1749" N	20° 37' 03.6998" E	#11	9	60.1	0.01	0.02	479	0.03	1.81	0.12	17	1508	0.03	0.01	7.49	0.08
″	Sh.V	39° 40' 47.1749" N	20° 37' 03.6998" E	#11	10	60.1	0	0.05	372	0.05	0.36	0.04	125	900	0.05	0.29	0.13	0
″	Sh.V	39° 45' 14.9074" N	20° 35' 40.4997" E	#28	21	59.1	0.02	0.34	429	0.07	0.42	0.16	212	262	0.36	0.056	0.81	0.13
″	Sh.V	39° 45' 14.9074" N	20° 35' 40.4997" E	#28	22	60.8	0.03	2.62	419	0.07	0.35	0.59	444	59	2.65	0.33	0.01	0.05
″	Sh.V	39° 45' 14.9074" N	20° 35' 40.4997" E	#28	23	57.9	0.01	0.11	428	0.01	0.06	0.08	138	75	0.12	0.19	0.14	0.13
″	Sh.V	39° 45' 33.2087" N	20° 34' 39.2160" E	#54	33	58.9	0.07	0.06	397	0.04	0.48	0.06	100	800	0.13	0.08	1.83	1.17
″	Sh.V	39° 45' 33.2087" N	20° 34' 39.2160" E	#54	34	60.1	0.02	0.02	482	0.02	0.2	0.02	100	1000	0.04	0	0.13	1
″	Sh.V	39° 32' 21.0300" N	20° 32' 19.1184" E	#57	35	59.4	0.01	0	483	0.04	1.67	0.05	0	3340	0.01	0.63	0.03	0.20
″	Sh.V	39° 32' 21.0300" N	20° 32' 19.1184" E	#57	36	59.6	0.05	0.03	403	0.05	1.16	0.06	50	1933	0.08	0.30	0.47	0.83
″	Sh.V	39° 32' 21.0300" N	20° 32' 19.1184" E	#57	37	59.8	0.02	0.05	470	0.07	0.39	0.2	25	195	0.07	1	0	0.10
″	Sh.V	39° 32' 21.0300" N	20° 32' 19.1184" E	#57	38	60.5	0.07	8.27	422	0.5	1.6	2.34	353	68	8.34	0	0.14	0.03
″	Sh.V	39° 41' 15.6804" N	20° 39' 06.6708" E	#65	44	59.2	0.02	0.02	477	0.01	0.13	0.01	200	1300	0.04	0.47	0.56	2
″	Sh.V	39° 38' 08.5416" N	20° 38' 07.2528" E	#94	51	59	0	0.01	483	0.01	0.2	0.02	50	1000	0.01	0.50	0.10	0
″	Sh.V	39° 38' 08.5416" N	20° 38' 07.2528" E	#94	52	59.6	0	0.01	481	0.01	0.37	0.01	100	3700	0.01	0	0.05	0
″	Sh.V	39° 50' 36.3408" N	20° 35' 59.0819" E	#203	82	60.6	0.08	0.09	385	0.03	0.16	0.04	225	400	0.17	0.50	0.15	2
″	Sh.V	39° 47' 19.6620" N	20° 38' 59.3233" E	#208	83	60.7	0.03	0.07	410	0.07	0.15	0.06	117	250	0.1	0	0.03	0.50
Oxfordian - Tithonian	Sh.PU	39° 40' 57.3104" N	20° 37' 30.6497" E	#15	12	60.5	0.03	0.01	442	0.01	0.16	0.02	50	800	0.04	0.08	0.30	1.50
″	Sh.PU	39° 40' 57.3104" N	20° 37' 30.6497" E	#15	14	60.4	0.01	0.01	481	0	0.01	0.01	100	100	0.02	0.02	3.85	1
″	Sh.PU	39° 46' 04.6443" N	20° 36' 30.4970" E	#26	17	59.5	0.02	0.22	418	0.14	0.74	0.18	122	411	0.24	0.11	0.40	0.11
″	Sh.PU	39° 46' 04.6443" N	20° 36' 30.4970" E	#26	18	60.9	0.01	0.05	446	0.01	0.22	0.03	167	733	0.06	0	0.47	0.33
″	Sh.PU	39° 46' 35.5210" N	20° 34' 21.5572" E	#29	24	60.9	0	0.01	481		0.01	0	0	0	0.01	0.09	0.67	
″	Sh.PU	39° 46' 35.5210" N	20° 34' 21.5572" E	#29	25	58.9	0.02	0.02	483	0.02	0.44	0.02	100	2200	0.04	0	0.64	1
″	Sh.PU	39° 46' 35.5210" N	20° 34' 21.5572" E	#29	26	60	0	0.01	482	0.01	0.22	0.02	50	1100	0.01	0.17	0.67	0
″	Sh.PU	39° 46' 35.5210" N	20° 34' 21.5572" E	#29	27	60.6	0	0.01	445	0.01	0.09	0.01	100	900	0.01	0.74	0.08	0
″	Sh.PU	39° 22' 53.5080" N	20° 50' 56.7780" E	#41	28	59.4	0	0	483	0.03	0.34	0.01	0	3400	0	0.20	0.44	0
″	Sh.PU	39° 22' 21.0288" N	20° 50' 55.7124" E	#43	30	59.8	0.17	0.06	380	0.07	0.74	0.04	150	1850	0.23	0.17	0.23	4.25
″	Sh.PU	39° 32' 40.6464" N	20° 30' 18.1404" E	#58	40	60.1	0.01	0.05	419	0	0	0.01	500	0	0.06	0.43	0.19	1
″	Sh.PU	39° 38' 02.8212" N	20° 38' 56.6916" E	#95	53	59.2	0.01	0	480	0.04	0.31	0.01	0	3100	0.01	0.75	0.06	1
″	Sh.PU	39° 46' 13.4580" N	20° 46' 56.0208" E	#112	58	59.4	0.02	0.08	433	0.02	0.18	0.04	200	450	0.1	0.50	0.05	0.50
″	Sh.PU	39° 46' 06.8160" N	20° 47' 43.9116" E	#116	61	59	0	0.07	434	0.01	0.15	0.06	117	250	0.07	0	0.05	0
″	Sh.PU	39° 46' 06.8160" N	20° 47' 43.9116" E	#116	62	60.1	0	0.09	434	0.02	0.14	0.05	180	280	0.09	0	0.11	0
″	Sh.PU	39° 46' 06.8160" N	20° 47' 43.9116" E	#116	63	59.5	0.01	0.08	433	0.02	0.2	0.08	100	250	0.09	0	0.06	0.13
″	Sh.PU	39° 46' 09.4944" N	20° 47' 37.0464" E	#117	64	59.1	0.02	0.1	433	0.02	0.15	0.05	200	300	0.12	0	0.05	0.40
″	Sh.PU	39° 26' 34.1844" N	20° 38' 04.5456" E	#131	65	59.6	0	0.01	483	0.01	0.09	0.02	50	450	0.01	0.13	1.75	0
″	Sh.PU	39° 26' 13.4448" N	20° 38' 05.0712" E	#132	66	59.8	0.01	0.5	431	0.03	0.13	0.13	385	100	0.51	0.50	1	0.08
″	Sh.PU	39° 25' 55.1064" N	20° 35' 44.7792" E	#136	67	59.2	0	0.01	481	0.03	0.16	0.02	50	800	0.01	0.50	0.023	0
″	Sh.PU	39° 27' 23.6088" N	20° 36' 18.7596" E	#141	68	59.5	0	0.01	482	0.01	0.22	0.02	50	1100	0.01	0.50	1	0
″	Sh.PU	39° 30' 32.3679" N	20° 35' 08.2442" E	#150	71	59.4	0.06	0.08	381	0.03	0.43	0.03	267	1433	0.14	0	0.11	2
″	Sh.PU	39° 19' 21.5565" N	20° 36' 36.9266" E	#154	72	59.5	0.01	0.07	339	0.01	0.04	0.02	350	200	0.08		0	0.50
″	Sh.PU	39° 17' 52.8612" N	20° 37' 51.3156" E	#157	73	59.5	0.01	0.02	483	0.02	0.05	0.01	200	500	0.03	0.17		1
″	Sh.PU	39° 15' 51.4332" N	20° 39' 26.4996" E	#163	74	60.8	0.01	0.01	483	0.01	0.45	0.01	100	4500	0.02	1	0	1
″	Sh.PU	39° 15' 53.8848" N	20° 39' 24.3972" E	#164	75	59.5	0.03	0.03	419	0.01	0.03	0.02	150	150	0.06	0.33	0.40	1.50
″	Sh.PU	39° 21' 43.2360" N	20° 32' 09.2292" E	#178	79	59.6	0.08	0.03	403	0.03	0.22	0.03	100	733	0.11	0.50	0.02	2.67
″	Sh.PU	39° 55' 42.0132" N	20° 27' 48.5964" E	#193	80	59.1	0.01	0.01	480	0.03	0.44	0.02	50	2200	0.02		0	0.50
Toarcian - Aalenian	Sh.PL	39° 32' 37.9140" N	20° 30' 12.0240" E	#59	41	60.3	0.01	0.1	426	0.03	0.15	0.05	200	300	0.11	0.73	0.14	0.20
″	Sh.PL	39° 32' 27.5964" N	20° 31' 50.8620" E	#60	42	58.2	0.1	2.34	422	0.1	0.24	0.65	360	37	2.44	0.04	9.75	0.15
Pliensbachian	Ls.Pl	39° 46' 05.2606" N	20° 36' 34.9212" E	#27	20	58.3	0.02	0.88	424	0.01	0.08	0.08	1100	100	0.9	0.02	11	0.25
Triassic - Jurassic	Sh.P	39° 28' 25.5180" N	20° 36' 23.3640" E	#144	70A	25.5	2.14	211.06	417	3.98	11.44	27.1	790	43	213.2	0.01	18.45	0.08
″	Sh.P	39° 28' 25.5180" N	20° 36' 23.3640" E	#144	70B	24.3	2.15	170.11	417	2.98	8.53	22.93	773	39	172.26	0.01	19.94	0.09
Triassic	TCB	39° 55' 55.4664" N	20° 24' 24.0156" E	#196	81	60.8	0.25	3.76	417	0.04	0.26	0.85	442	31	4.01	0.06	14.46	0.29

4.10.1 TOC content

The TOC content of the samples varies from 0 to 27.1% wt. The following table (Table 17) summarizes the TOC content characteristics for each formation. The histogram (Figure 79) shows that only 3 samples exceed the 1% of TOC wt. (threshold for good HC potential according to classic screening parameters of Peters and Cassa, 1994).

Table 17. Table of the TOC values of each sampled formation.

Formation	n	Min TOC	Max TOC	Mean TOC
Vigla Shale	17	0.01	2.34	0.23
Upper Posidonia	28	0	0.18	0.03
Lower Posidonia	2	0.05	0.65	0.35
Siniais Limestone	1	0.08	0.08	0.08
Pantokrator Shale	2	22.93	27.1	25.02
Triassic Collapse Breccia	1	0.85	0.85	0.85

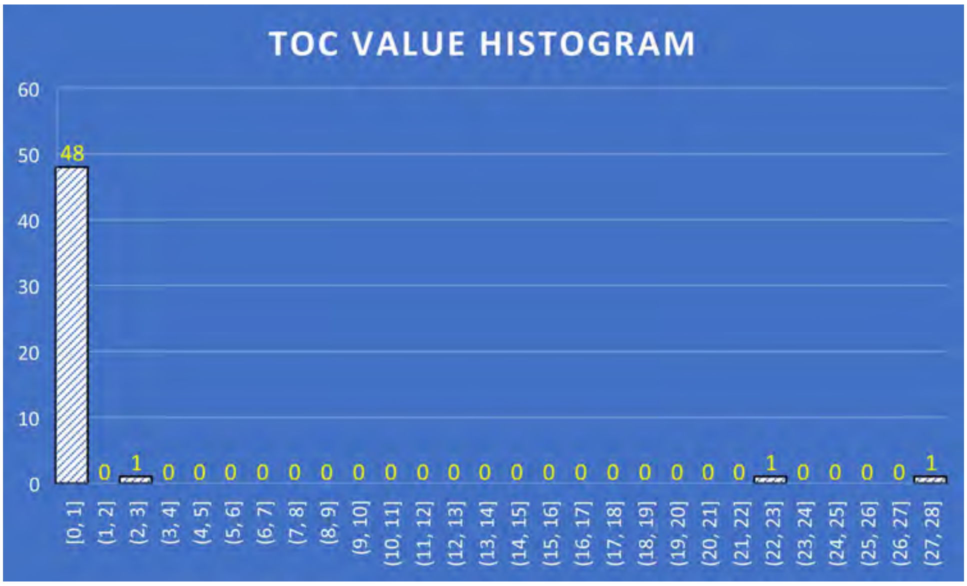

Figure 79. Histogram of the TOC of all the samples. 48/51 samples lie below the 1% TOC threshold.

The distribution of the TOC values is shown in the geological map with the TOC (% wt.) are annotated (Figure 80).

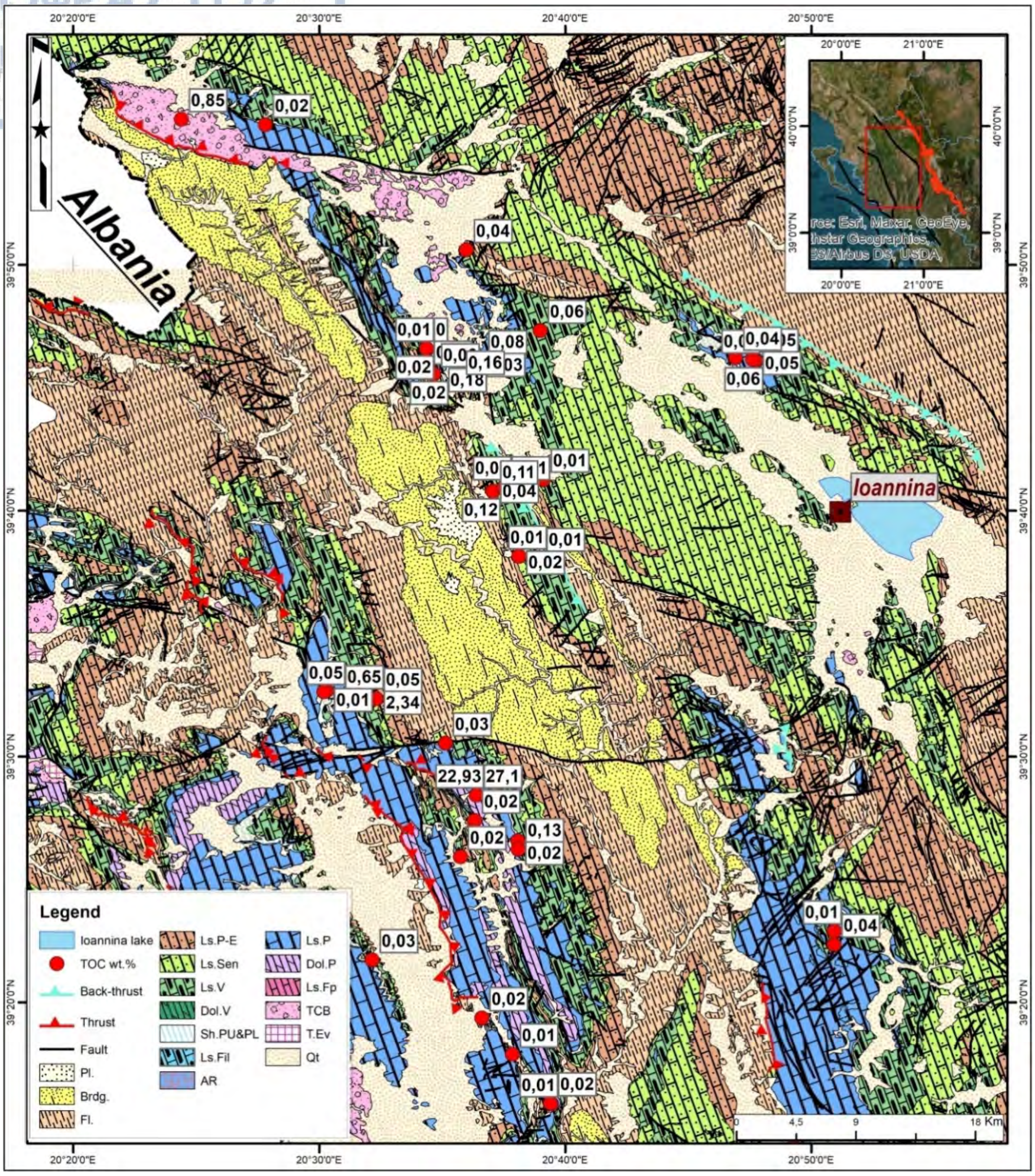

Figure80. TOC content (%wt.) distribution

4.10.2 Hydrogen index

The HI values of the samples vary from 0 to 1100, while the mean HI is 195. The following table (Table 18) summarizes the HI value characteristics for each formation. The histogram (Figure 81) shows that the majority of the samples (n = 38) have gas (remaining or original) or no HC potential (HI<200), 10 samples have mixed oil/gas potential (including 4 unreliable samples with very low TOC content), and only 3 samples are oil-prone, exceeding the HI=600 threshold, with the one being the unreliable Siniais sample. Consequently, only the Pantokrator Shale appears as a dominantly oil-prone potential SR.

Table 18. Table of the HI values of each sampled formation.

Formation	n	Min HI	Max HI	Mean HI
Vigla Shale	17	0	444	140
Upper Posidonia	28	0	500*	139
Lower Posidonia	2	200	360	280
Siniais Limestone	1	1100*`	1100	1100
Pantokrator Shale	2	773	790	782
Triassic Collapse Breccia	1	442	442	442
*Unreliable values due to the very low TOC content				

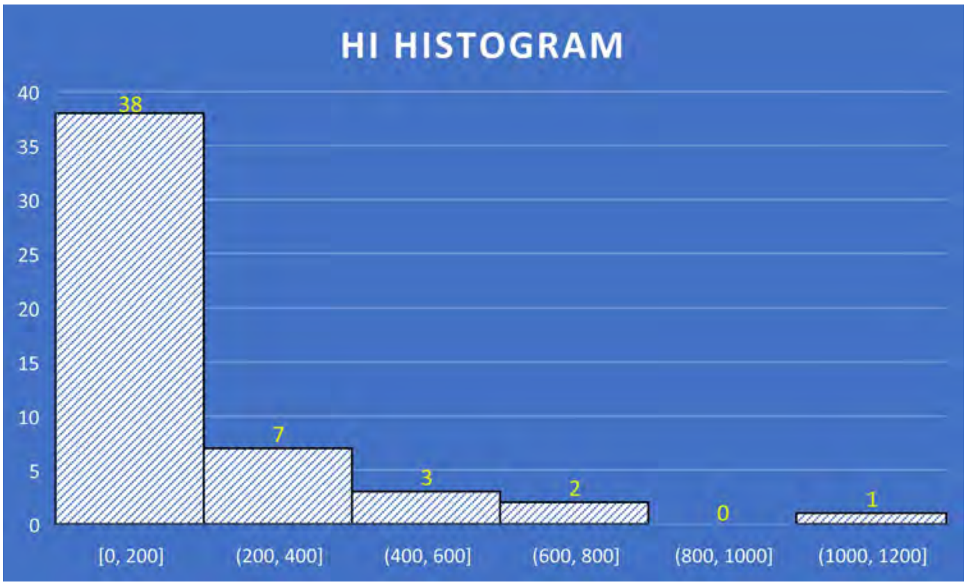

Figure 81. Histogram of the HI of all the samples. 38/51 samples lie below the HI=200.

The distribution of the HI values is shown in the geological map with the HI (g HC/kg TOC) are annotated (Figure 82).

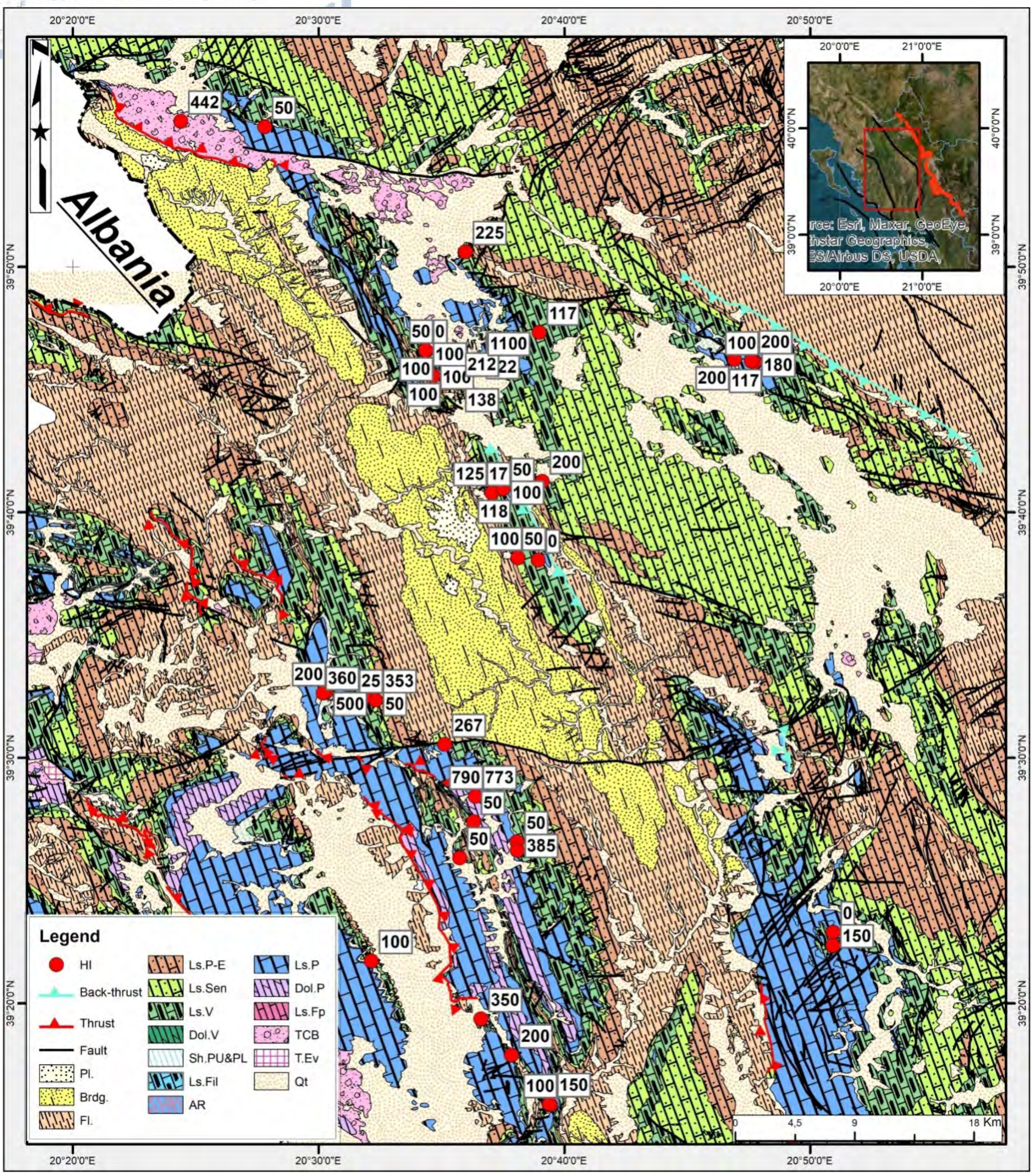

Figure 82. HI (g HC/kg TOC) value distribution

4.10.3 Generation potential

The generation potential (GP=S1+S2) values of the samples vary from 0 to 213.2 g HC/kg rock. The following table (Table 19) summarizes the GP value characteristics for each formation. The histogram (Figure 83) shows that the majority of the samples (n = 4) have no or poor HC potential. Only 5 samples show fair to excellent HC potential. Pantokrator Shale shows exceptionally high GP at ~200 kg HC/ton rock.

Table 19. Table of the HI values of each sampled formation.

Formation	n	Min GP	Max GP	Mean GP
Vigla Shale	17	0.01	8.34	0.73
Upper Posidonia	28	0	0.51	0.08
Lower Posidonia	2	0.11	2.44	1.28
Siniais Limestone	1	0.9	0.9	0.9
Pantokrator Shale	2	172.26	213.2	192.73
Triassic Collapse Breccia	1	4.02	4.02	4.02

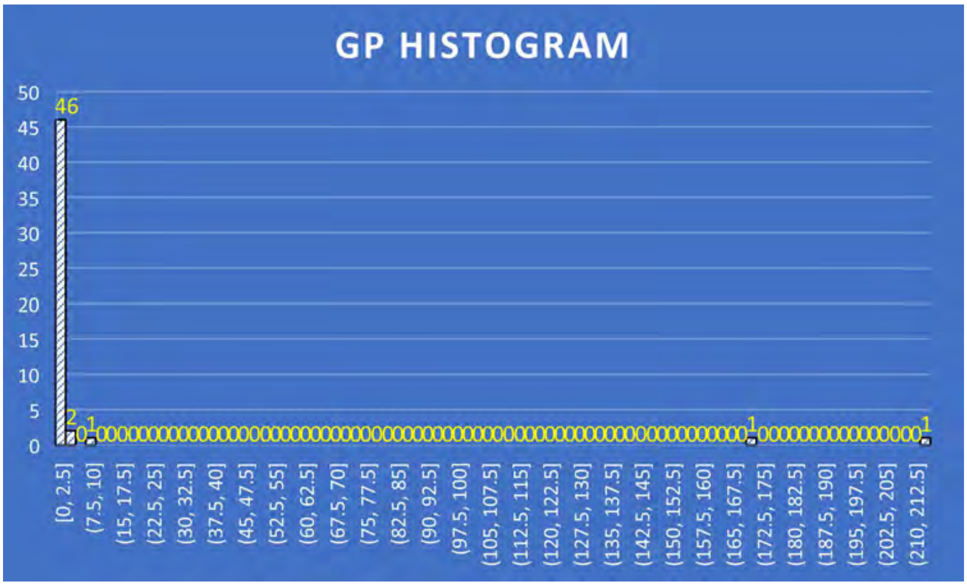

Figure 83. Histogram of the GP of all the samples. 46/51 samples lie below the threshold of 2.5 gr HC/kg rock and are characterized as poor potential SRs.

The distribution of the GP values is shown in the geological map with the GP (kg HC/ton rock) are annotated (Figure 84).

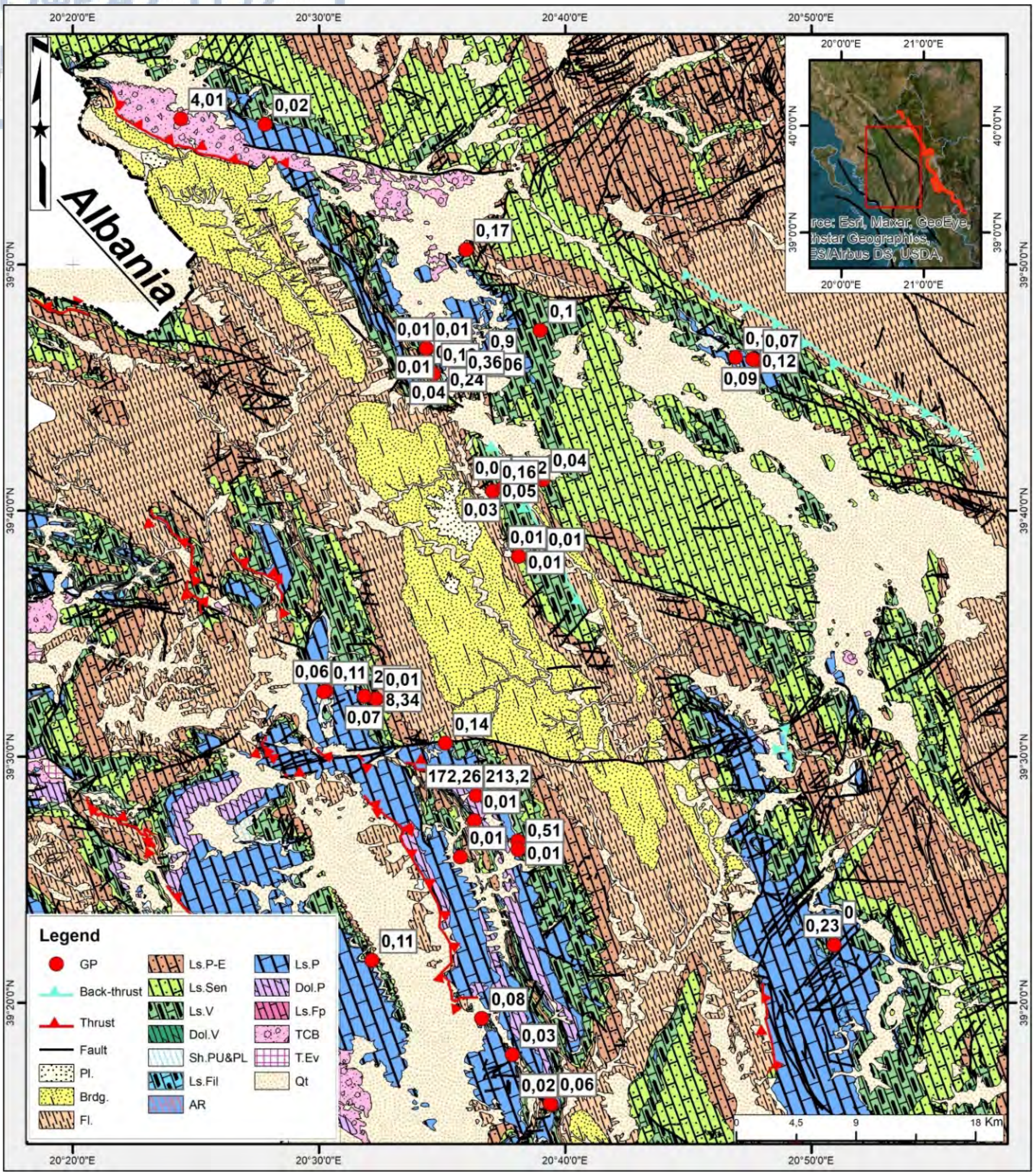

Figure 84. GP (g HC/kg rock) value distribution

4.10.4 Tmax

The T_{max} values of the samples vary from 339 °C to 483 °C, while the mean T_{max} is 439 °C. The following table (Table 20) summarizes the T_{max} value characteristics for each formation. The histogram (Figure 85) shows that only 3 samples fall in the early oil window (T_{max} 435–450 °C). All three of them are unreliable. The majority of the samples (n = 29), including all 17 reliable samples, are immature (T_{max}<435 °C). The remaining 19 samples appear to range from peak mature (T_{max} 450 °C–470 °C) to post-mature (T_{max} > 470 °C).

Therefore, all the reliable samples are thermally immature, with some of them close to the oil window.

Table 20. Table of the T_{max} values of each sampled formation.

Formation	n	Min T_{max}	Max T_{max}	Mean T_{max}	$Mean_R$
Vigla Shale	17	372	483	436	423
Upper Posidonia	28	339	483	445	430*
Lower Posidonia	2	422	426	424	424
Siniais Limestone	1	422	422	422	422*
Pantokrator Shale	2	417	417	417	417
Triassic Collapse Breccia	1	417	417	417	417
$Mean_R$: reliable mean values with the TOC content criterion applied *Tentatively reliable, due to general low TOC values					

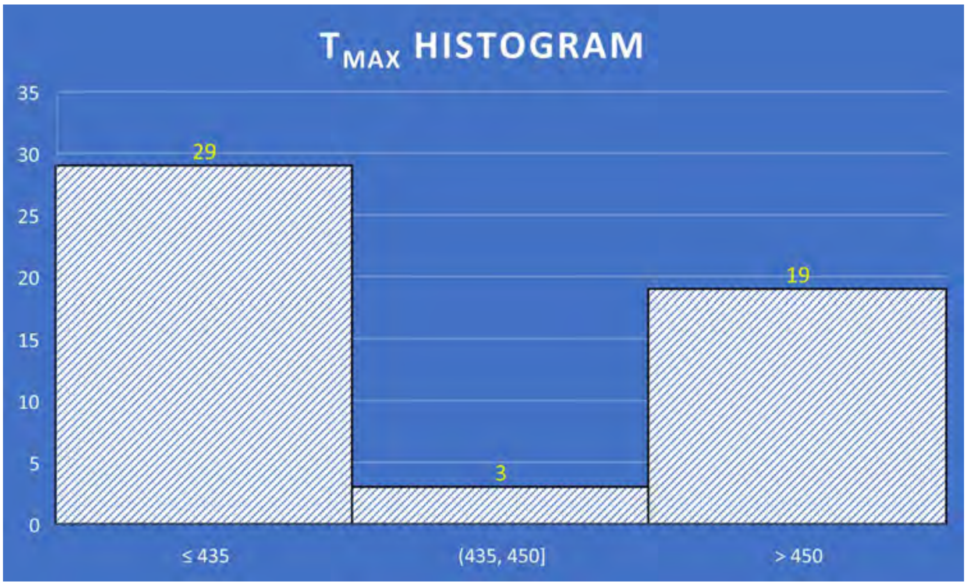

Figure 85. Histogram of the T_{max} of all the samples. 29/51 samples appear thermally immature, 3/51 are in the early oil window and 19/51 are peak mature to post-mature. All the 17 reliable samples are immature.

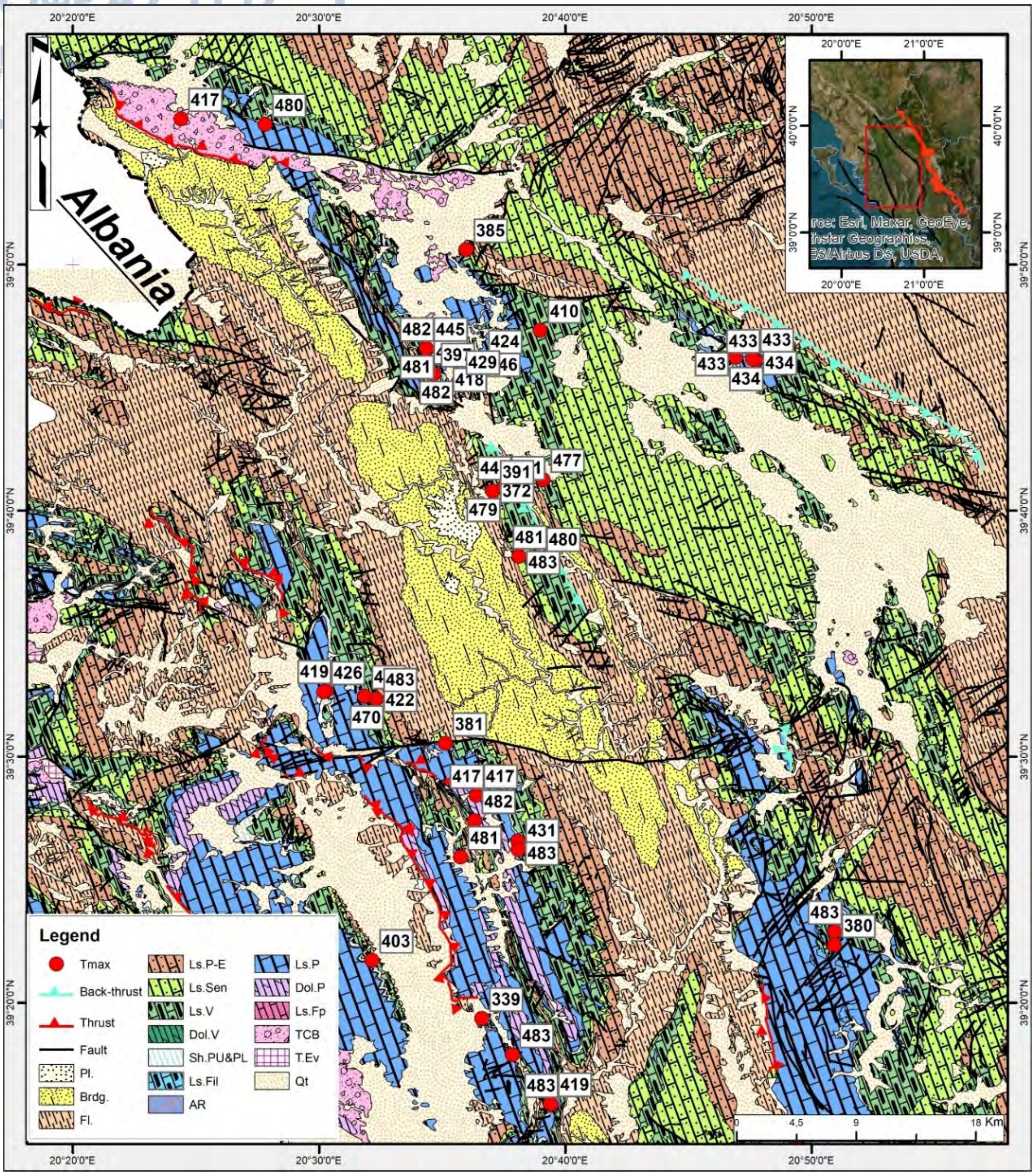

Figure 86. Tmax(°C) value distribution

4.10.5 Oxygen index

The oxygen index (OI) values of the samples varies from 0 to 4500. The following table (Table 21) summarizes the TOC content characteristics for each formation. The histogram (Figure 87) shows that 2 samples show OI=0. These samples also show extremely low TOC and HI, therefore they are statistically unsignificant. In the range of 1-200 OI, 13 samples occur, and they are potentially exploitable, whereas, 36 samples have OI>200. The all these 36 samples belong to the unreliable samples of the survey.

Table 21. Table of the OI values of each sampled formation.

Formation	n	Min OI	Max OI	Mean OI	MeanR
Vigla Shale	17	59	3700	1037	99
Upper Posidonia	28	0	4500	1010	133*
Lower Posidonia	2	37	300	169	37
Siniais Limestone	1	100	100	100	100*
Pantokrator Shale	2	39	43	41	41
Triassic Collapse Breccia	1	31	31	31	31
MeanR: exploitable-meaningful mean values within 0-200 OI range *Tentatively exploitable, due to general low TOC values					

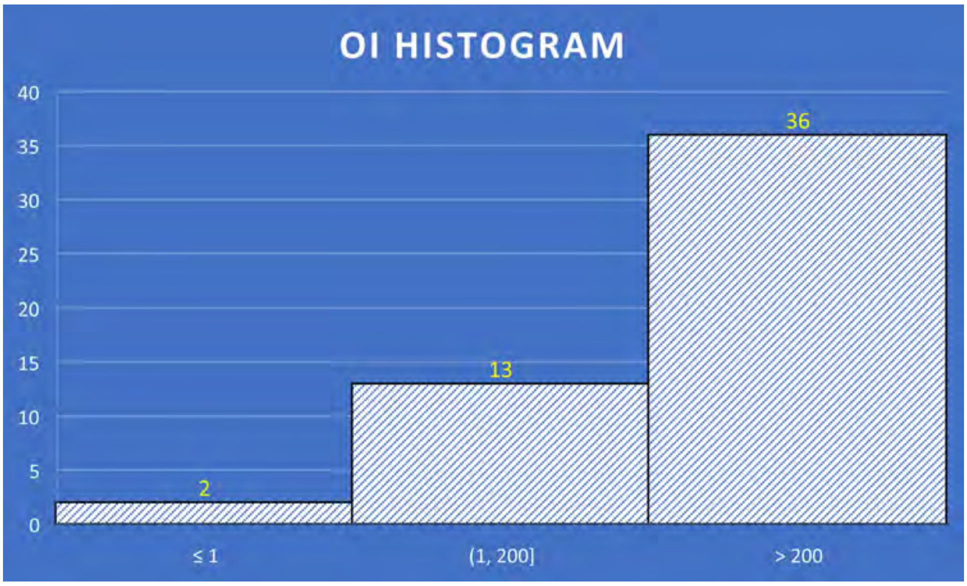

Figure 87. Histogram of the OI of all the samples. 2/51 samples have OI=0 and are excluded from the statistical analysis, 13/51 fall in the 1-200 OI area therefore are potentially exploitable and 36/51 have OI>200.

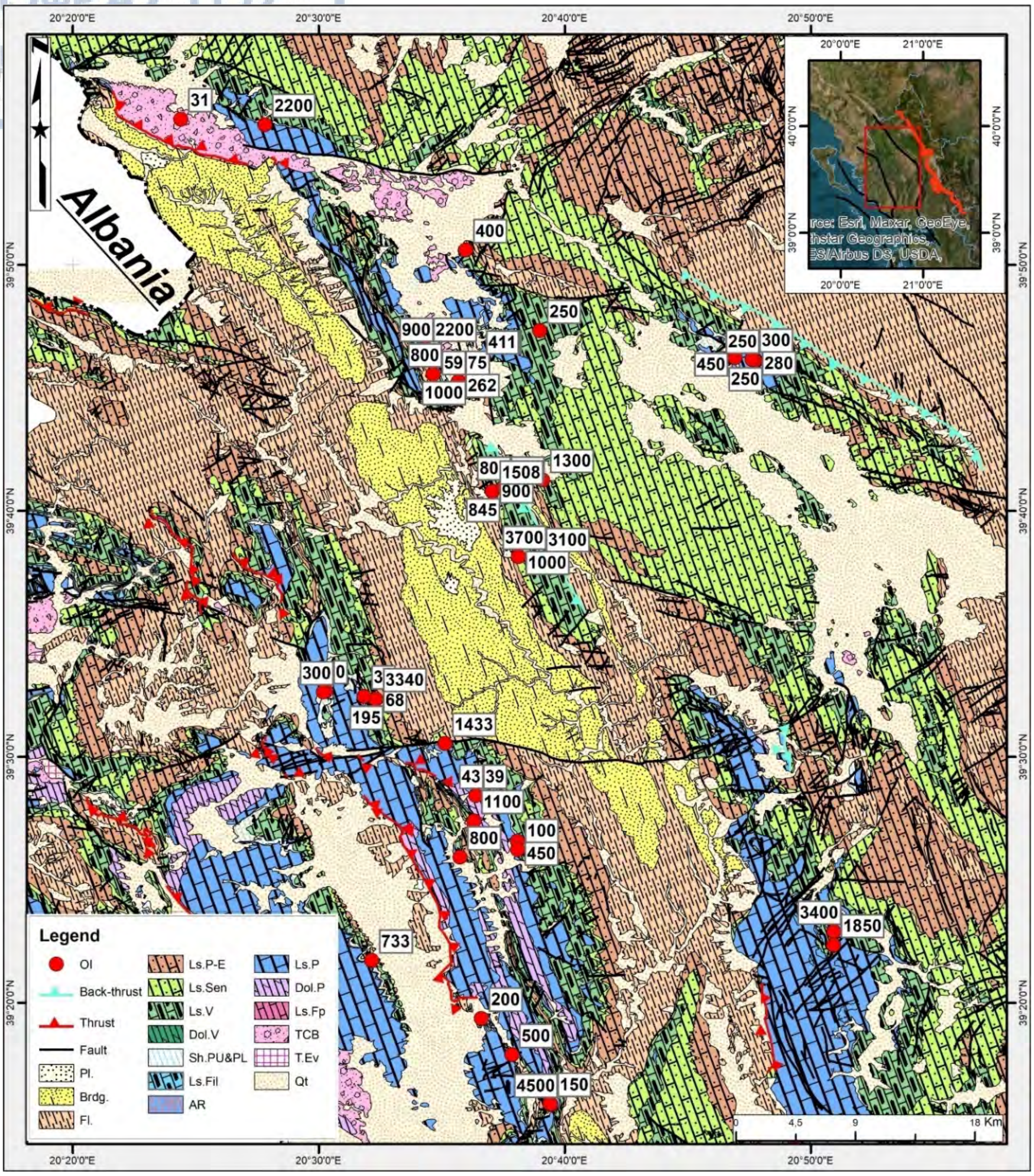

Figure 88. OI value distribution

4.11 Organic petrography

Five polished samples, from four potential SR formations (Table 22) were examined for their organic petrographic properties. These are the five most organic-rich samples of the survey.

Table 22. Table of the samples studied by organic petrographic means and their associated SR attributes

Sample ID	Formation	Area	% TOC	HI	T_{max}	GP
22	Sh.V	Vasilopoulo	0.59	444	419	2.65
38	Sh.V	Elataria	2.34	353	422	8.34

42	Sh.PL	Elataria	0.65	360	422	2.44
70	Sh.P	Souli Mt	27.1	790	417	213.2
81	TCB	Stavrodromi	0.85	442	417	4.01

4.11.1 Vigla Shale

Two Vigla shale samples were studied for their organic petrographic properties. These are sample n. 22 from the Vasilopoulo area and sample n. 38 from the Elataria section. In the samples, alginite, alginite colonies, and migrabitumen are observed. Carbonate crystal aggregates also occur (Figure 89). A few measurements of the bitumen reflectance do not allow for an statistical analysis representative of the formation. However, the mean of these measurements %BRo = 0.233. Using Jacob's (1989) formula [1] this is equal to %VRE = 0.544. This value is in relatively good agreement with the Tmax value of 423^{o}C.

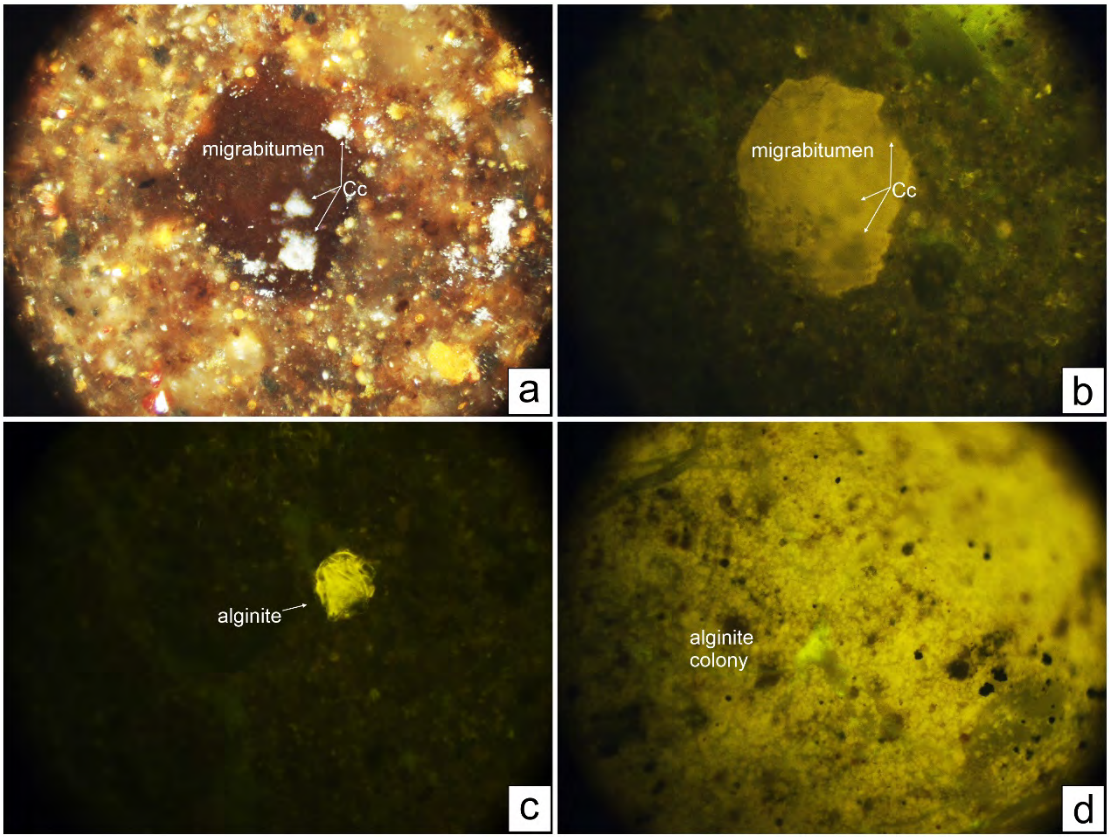

Figure 89. a, b) Pair of photomicrographs (a) under white incident light and (b, c, d) under blue-light excitation. A large migrabitumen and carbonate crystal aggregates at the center of the photomicrograph. c) Alginite, d) Alginite colony

4.11.2 Pantokrator Shale

One sample (no. 70A) from the Souli Mt. section was examined for its organic petrographic properties. The sample is characterized by abundant elongated alginite bands distributed in two distinctive lithologies. One is dominated by silt to fine sand-sized carbonate particles with the alginite bands "wrapped" around them, and one by finely bedded clay with abundant liptinite organic particles. Migrabitumen are abundant and often peated. Inertinite is commonly found. Framboidal pyrite is abundant (Figure 90).

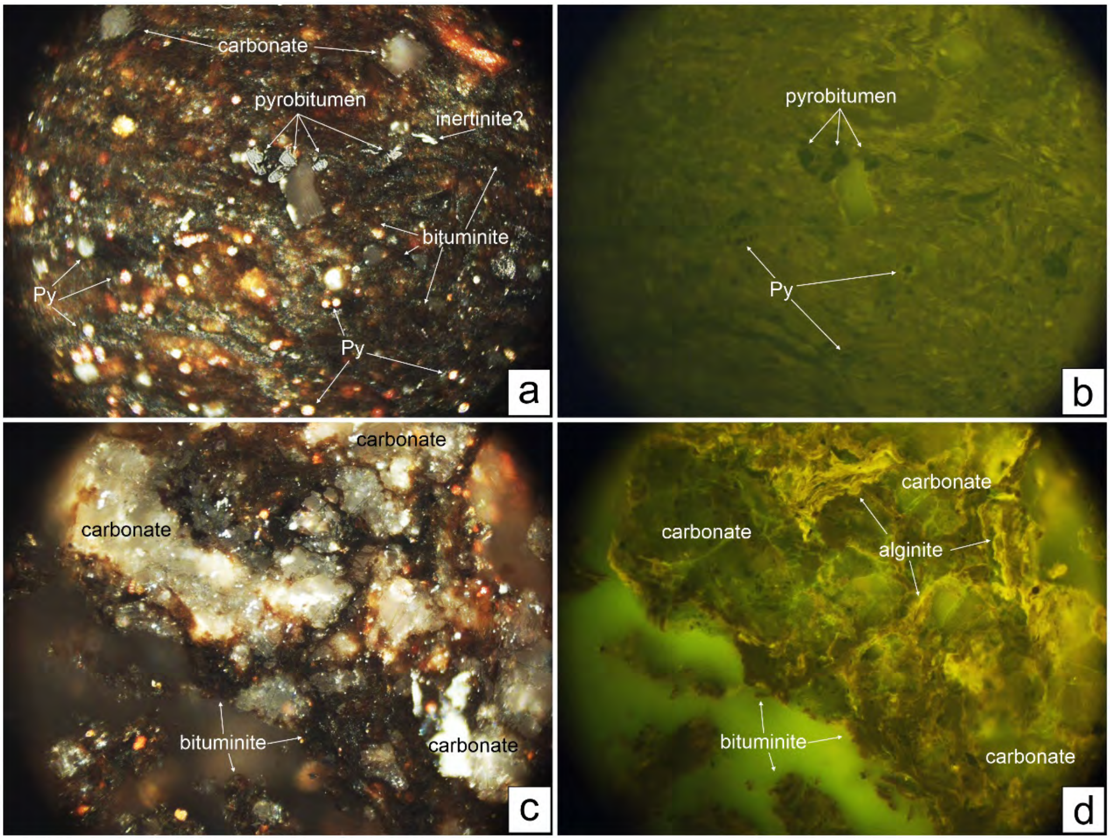

Figure 90. a, b) and c, d) are pairs of photomicrographs, under white incident light (a, c) and under blue-light excitation (b, d). Abundant bituminite, alginite, and pyrobitumen are located around silt-sized carbonate grains. Framboidal pyrite (Py) is also abundant.

Several measurements of bitumen reflectance were statistically evaluated. The histogram distribution showed a clear value concentration in the range of 0.14–0.24% BR_o and a second one in the range of 0.24–0.34% BR_o (Figure 91). This indicates two generations of migrabitumen, whose mean value is 0.236% BR_o, corresponding to 0.55% VRE. This value is in relatively good agreement with the Tmax value of 417 ^oC.

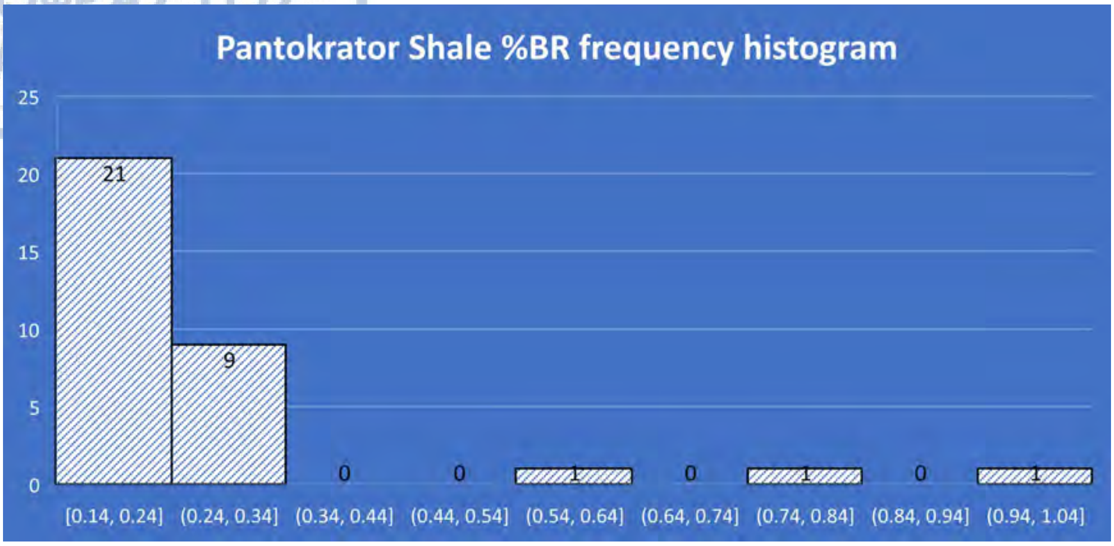

Figure 91. Histogram of the bitumen reflectance of the sample n. &70A of the Pantokrator Shale.

4.11.3 Lower Posidonia shales

One sample (no. 42) from the Elataria section was examined for its organic petrographic properties. In the sample were observed abundant sporinite, alginite, liptodetrinite and large resinite particles (or early oil stains?) (Figure 92). Framboidal pyrite was common.

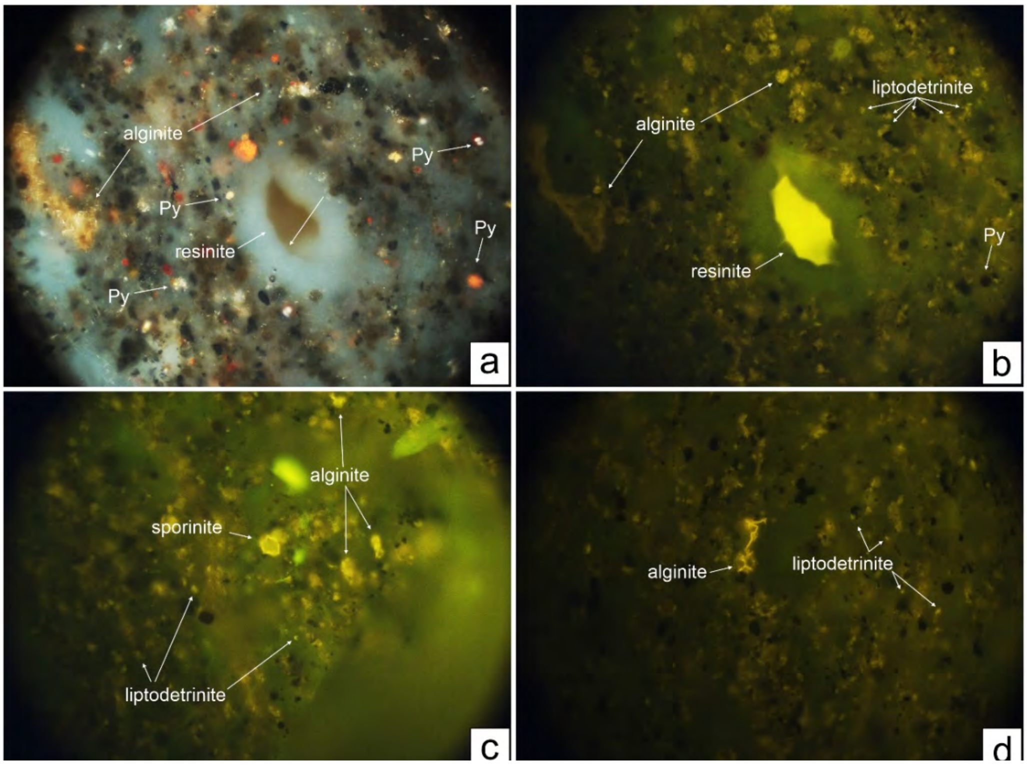

Figure 92. a, b) photomicrograph pair, under white incident light (a) and under blue light excitation (b, c, d). A large resinite particle is observed at the center (a, b) whereas abundant liptodetrinite is observed in all images. A sporinite particle is observed in image (c).

Limited reflectance measurements in bitumen led to the tentative establishment of a %BR value at 0.238 corresponding to ~0.55 %VRE. This value is in relatively good agreement with the T_{max} of 422°C.

4.11.4 Triassic Collapse Breccia

A sample (no. 81) from the TCB near Stavrodromi was examined for its organic petrographic properties. The main petrographic characteristics are the following:

- Tightly-packed silt-size clastic carbonate particles. Long, sutured, and concavo-convex clast boundaries.

- Sparse alginite? particles of 25-35 μm in diameter exhibit vivid green color.

- Possible cutinite and sporinite.

- Nebular background mass with strong fluorescence

- Abundant migrabitumen

- High fluorescence around clastic particles

The most prominent characteristic is the intense fluorescence around the carbonate clasts (Figure 93a). This is likely due to the presence of hydrocarbons within the sample. S1 peak of the RE6 analysis agrees with this observation.

A couple of measurements of the bitumen indicate a mean reflectance of 0.216%. This is equivalent to 0.53% in vitrinite reflectance using the Jacob's formula (1989) and in relatively good agreement with the T_{max} value (417 °C).

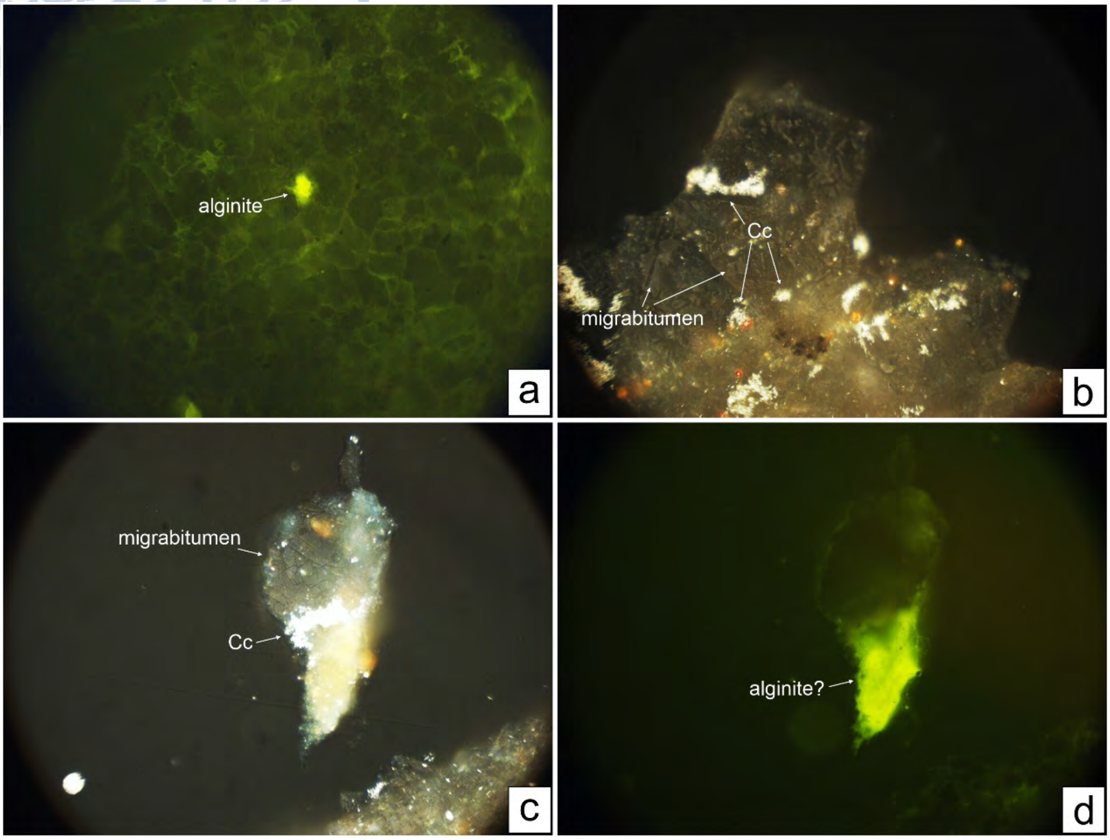

Figure 93. Photomicrographs b and c are under white incident light and the a and d under blue light excitation. c and d are pair. A) an alginite particle in the middle of the photomicrograph and a nebular green background with strong fluorescence, b) migrabitumen and carbonate crystal aggregates, c) and d) a possible alginite particle and migrabitumen.

4.12 Biomarker Results

4.12.1 Bitumen yields

The Pantokrator Shale bitumen yield reached the 52,130 ppm surpassing the well-known Lower Posidonia Shale reaching 2,325 ppm. This shows that the petroleum potential of the Pantokrator Shale well exceeds this of the Lower Posidonia Shale.

4.12.2 Homohopane and sterane side chain isomerization

For the Lower Posidonia Shale, the homohopane side chain isomerization of 0.50 [C22 S/(S+R)] was determined, while a side chain isomerization of 0.15 was determined for C29-steranes. The Pantokrator Shale bitumen showed homohopane isomerization of 0.58 at C22 and a side chain isomerization for C29-steranes of 0.29. These values show that the Lower

Posidonia Shale is below oil window whereas the Pantokrator Shale is in the early oil window.

4.12.3 Pristane/Phytane ratios

Exceptionally low Pr/Ph ratios of 0.29 characterize Pantokrator Shale whereas the Lower Posidonia Shale shows slightly higher Pr/Ph ratio of 0.52. This results indicate strongly anoxic and saline conditions in a stratified water column for the Pantokrator Shale and anoxic conditions for Lower Posidonia Shale, however, likely under normal water salinity.

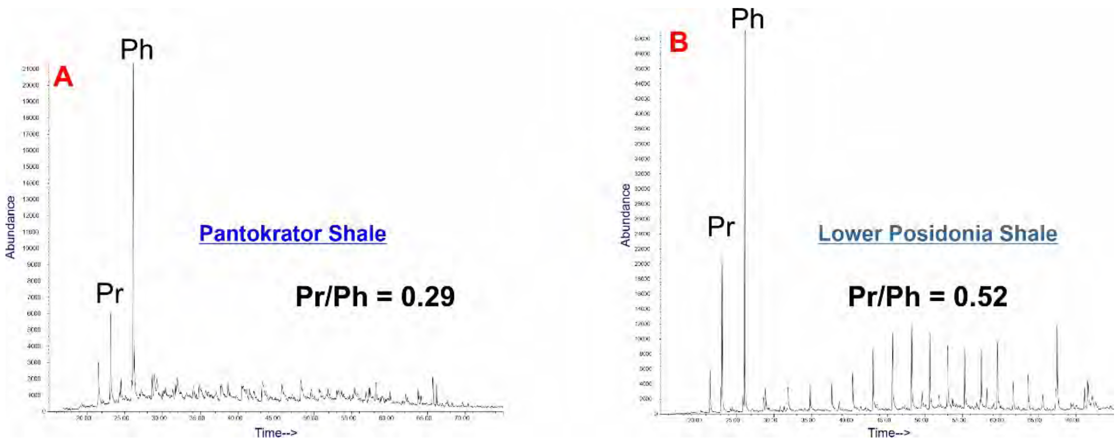

Figure 94. Chromatograms and pristane/phytane ratios in the Pantokrator Shale [A] and the Lower Posidonia Shale [B]

.

4.12.4 Alkylated 2-methyltrimethyltridecyclchromans

The alkylated 2-methyltrimethyltridecyclchromans are salinity-sensitive biomarkers. In the Lower Posidonia Shale the C2 and C3 isomers are of equal abundance indicating saline conditions. In the Pantokrator Shale the C2 are much less abundant than the C3 isomers indicating brackish conditions. These relations are shown in the Figure 95.

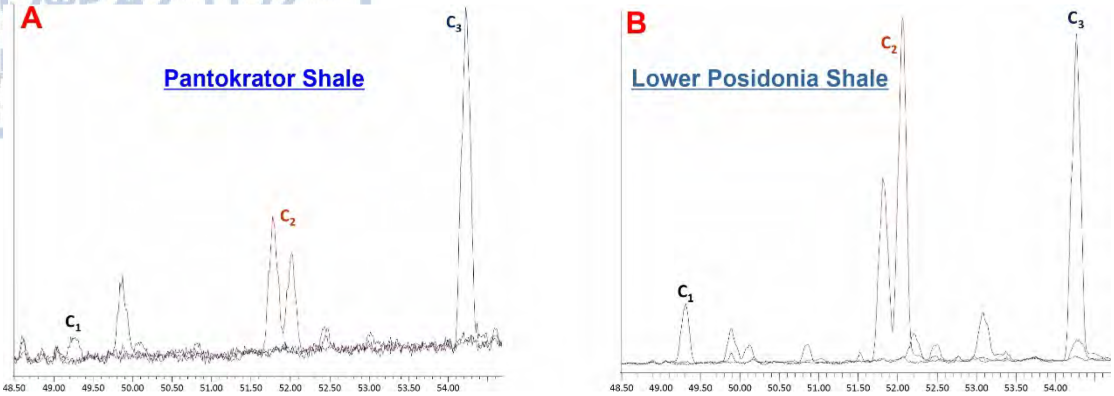

Figure 95. Chromatograms and Alkylated 2-methyltrimethyltridecyclchromans abundance in the Pantokrator Shale [A] and the Lower Posidonia Shale [B].

4.14.5 Biomarkers in solid bitumens (SB)

All the SB samples (i.e., Petousi, Elataria, Vassiliko) are heavily biodegraded (6-7 in Peters & Moldowan Scale) and all acyclic biomarkers (i.e., n-alkanes and the isoprenoids pristane and phytane) have been lost. However, all samples still maintain the cyclic aliphatic and aromatic biomarkers, hence, source allocation is applicable. Evaporative loss and biodegradation degree of the solid bitumen increases from the Elataria and Vassiliko specimens (steranes present) to the Petousi specimen which is characterized by the highest biodegradation (steranes absence). Petousi SB exhibits immature thermal maturity degree, as the extremely low C22-isomerization of homohopanes indicate. Elataria and Vassiliko lie within the early oil window, indicated by the equilibrated C22-isomerization of homohopanes and abundant ββ-steranes. Strongly reducing, sulfur-rich depositional conditions are indicated for all the samples by the extended hopanes up to C36 abundance. 29,30-bisnorhopane and β-carotene in Petousi and Vassiliko SB presence indicates carbonate/evaporitic source rock lithofacies. This is also confirmed by the low relative proportions of rearranged C27 and C29-neohopanes (C27 Ts and C29 Ts), typical indicators of clay-poor depositional environments. The C24 to C26 tetracyclic 17,21-secohopanes to C26 tricyclic triterpenoids (cheilanthanes) ratio is very high, indicating a saline environment. Petousi and Vassiliko SB show a preference for C29 hopanes over C30 hopanes, the existence of gammacerane, and, in the case of Petousi SB, the presence of C32 to C35 hexahydrobenzohopanes. Due to evaporation and biodegradation, the aromatic

HC fractions lost the low molecular weight components (naphthalenes, phenanthrenes, dibenzothiophenes), but retained aromatic steroids and hopanoids. SB from Petousi contains biodegradation-resistant mono- and triaromatic steroids, which lost the aliphatic steranes due to heavy biodegradation. Bitumen has a high concentration of benzohopanes as well as D-ring monoaromatic 8,14-secohopanes stretching from C29 to C35, which corresponds to the distribution of hexahydrobenzohopanes and regular hopanes in Petousi and Vassiliko SB. Elataria SB has fewer aromatic secohopanoids and a lesser amount of benzohopanes, but it contains thiophenic extended hopanes. The abundance of mono- and triaromatic steroids indicates that the initial oil/bitumen mostly originated by eukaryotic algae and was not generated solely from prokaryotic microbial biomass.

4.13 Scanning Electron Microscopy

The results of the SEM elemental analysis over the seven samples are presented in the Table 23.

Table 23. Elemental analysis with SEM. Presence of an element in a sample is annotated with the cross.

No.	***Fm***	***C***	***O***	***Ca***	***Al***	***Si***	***P***	***S***	***K***	***Mn***	***Mg***	***Fe***	***Co***	***Ni***	***Ti***	***Ba***
3	Ls.Sen	+	+	+												
6	TCB	+	+	+	+				+	+	+		+	+	+	
11	Sh.V	+	+	+	+	+	+	+	+			+	+	+	+	
15	Ls./oil	+	+	+	+	+	+	+	+	+		+	+	+		
29	Sh.PU	+	+	+	+	+	+			+		+	+	+	+	
31	Ls.Sen	+	+	+	+	+		+				+				
39	Sh.V	+	+	+	+	+		+	+			+				+

All samples contain carbon, oxygen and calcium likely reflecting the dominant lithology (limestone) and the associated oxides CaO and CO_2. Manganese is present only in the TCB sample, likely reflecting the common presence of dolomite [$CaMg(CO_3)_2$] in Triassic sediments. Barium occurs only in the black shale Vigla Shale sample (no. 39). Black shales often exhibit Ba enrichment due to barite precipitation in ocean water linked to high organic productivity (Paytan and Griffith, 2007). Iron and silica lack in TCB likely reflects the ion's scarcity in the evaporitic/carbonaceous environment where Triassic sediment deposited. Silica is also absent from one Senonian Limestone likely reflecting a pure carbonate deposition whereas the Si presence in the other one agrees with the macroscopic lithologic image of the formation where siliceous nodules are abundant at various intervals.

4.14 Cross-sections

Eight [8] cross-sections (Table 24, Figure 94) were compiled in order to depict part of the complex stratigraphic and structural architecture and their variations in a transverse direction (generally W-E), perpendicular to the NNW-SSE main tectonic fabric. All cross-sections are located within the IZ-C, whereas a couple reach its margins. The geological map used is the 1/100000 IFP-IGRS sheet, over which slight corrections, additions, and modifications concerning the formation boundaries were made.

Table 24. Table of the cross-sections created with annotated the points of interest as well as the total length for each one.

ID	***Cross-section***	***Points of interest***	***Length (km)***
A	Ktismata-Vassiliko	TCB thrust, Koutsokrano backlimb, Kefalovryso back-thrust	22.32
B	Kassidiaris	High tectonic complexity	5.42
C	Langari-Kourenta	Successive thrusts, Kourenta back-thrust, Miocene deposits	22.57
D	Chionistra-Mitsikeli	Successive thrusts, Kourenta back-thrust, Miocene deposits, Ioannina “plateau”, Mitsikeli back-thrust	42.1
E	Zoumbani-Tomaros	Successive thrusts, Chionistra & Tomaros back-thrusts, Miocene deposits	27.8
F	Paramythia-Petousi	Successive thrusts, Jurassic stratigraphy	7.12
G	Kouklesi-Rapsaioi	Jurassic stratigraphy	7.12
H	Tourla-Kerassona	Structural style & complexity, multiple thrusts, Fm. thicknesses variations	24.62

The topographic profiles were extracted from the SRTM GL1 v003 (NASA JPL, 2013) global topographic model. Over this map are shown the traces of the cross-sections (Figure 94).

The cross-sections are correlated in the §5.3 aiming to provide a better understanding of the Ionian Zone structure across the NNW-SSE longitudinal axis.

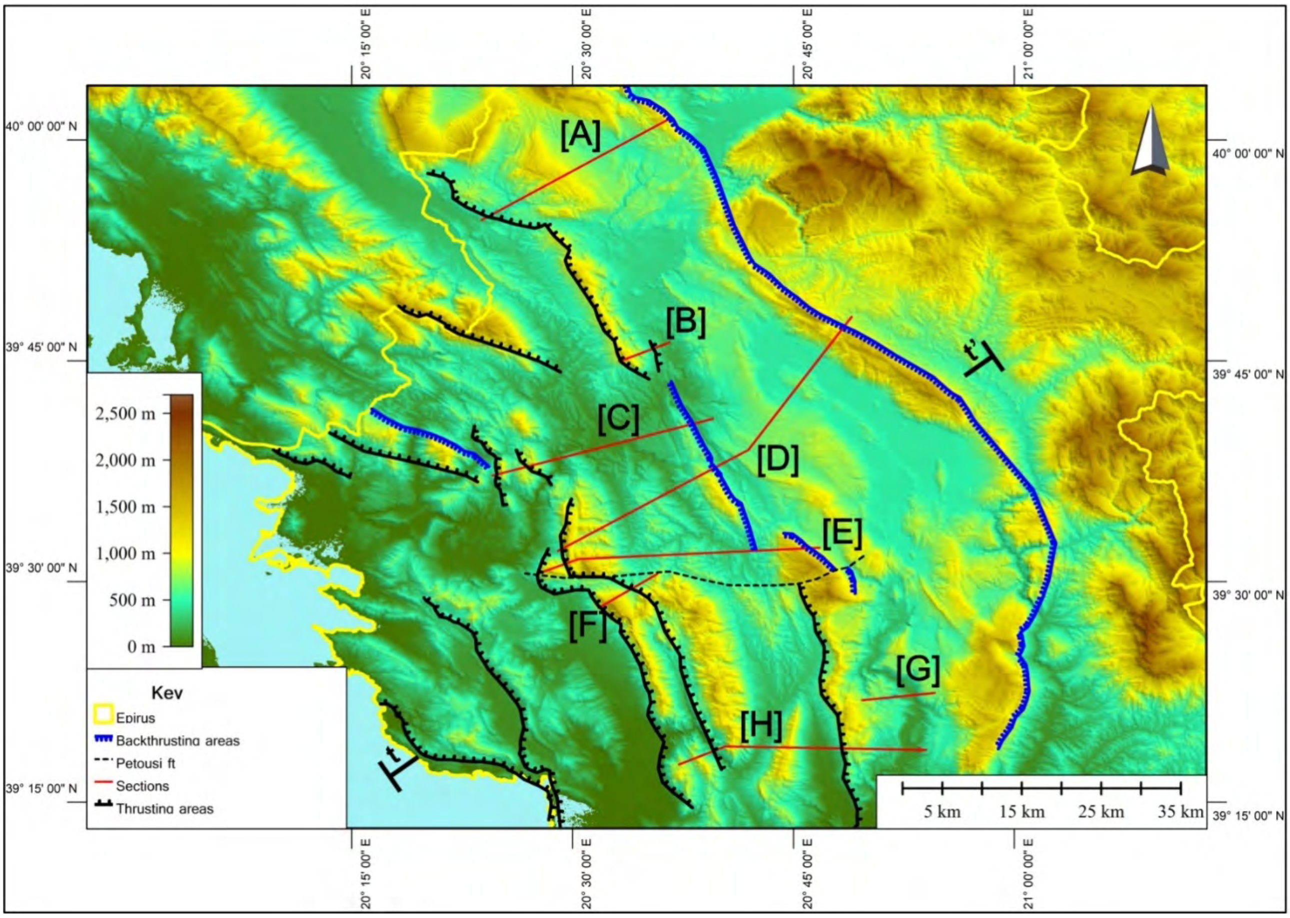

Figure 96. Terrain map with the cross-sections A to H. The major tectonic elements also indicated. Black raked lines represent the traces of the major thrusts whereas the blue raked lines represent the backthrusts and the backthrusting masses. The transect t-t' (Parga-Mitsikeli) is also indicated.

4.14.1 [A] Ktismata – Vassiliko

The Ktismata-Vassiliko cross-section (Figure 95) aims to depict the TCB thrusting over the flysch, the folded zone at the forelimb of the highly asymmetrical Koutsokrano anticline and the back-thrust-related east-verging inverted anticline in the area of Vassiliko. The overall structure corresponds to a structural unit that is double verging.

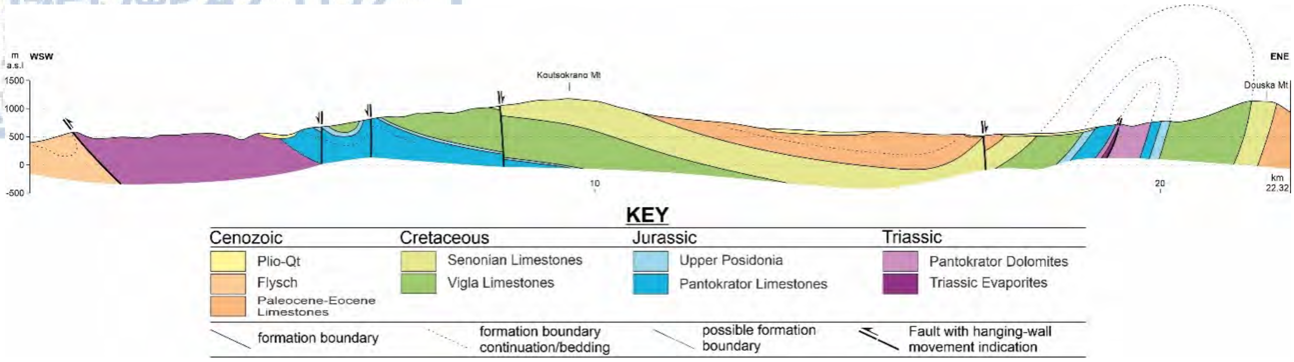

Figure 97. Cross-section [A] Ktismata – Vassiliko

4.14.2 [B] Kassidiaris Mt

The Kassidiaris cross-section (Figure 96) shows the structural complexity that characterizes the Kassidiaris Mt area. It depicts the inverted forelimb at the westernmost part of the section, the shortly-spaced faults at the topographically elevated area, the tight folding and a gently-dipping second thrust. Moreover, the solution of the section demands a rather significant increase of the Ls.V thickness in the NE-facing slopes.

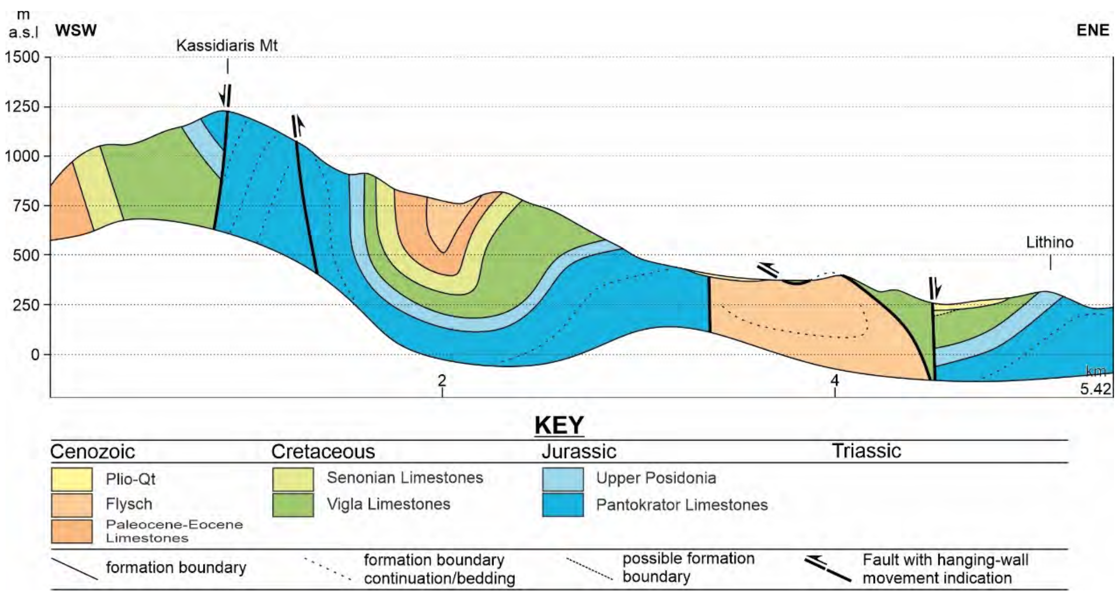

Figure 98. Cross-section [B] Kassidiaris Mt

4.14.3 [C] Langari Mt – Kourenta Mt

The Langari-Kourenta cross-section (Figure 97) depicts the two successive thrusts at the westernmost part and the in-between associated folding pattern, the westward thickening and facies differentiation of the

Miocene deposits, the Kourenta back-thrust, and the associated footwall and hanging wall deformation. The Sh.PU thickness increase towards the east is also visible. It is worth noting the successive open folds starting at the westernmost edge of the Miocene deposits as well as the east-verging and almost recumbent open anticlinal fold at the backlimb of the inner Langari Mt thrust. Concerning the successive folds, they might originate from small-scale blind-thrusting rooted on a decoupling level of the Fl.-Ls.PE boundary or a deeper decoupling level such as the Sh.V. The east-verging anticline might be related to a blind thrust that is correlated to the backthrust located ~10–15 to the south (cross-section [E] in Figures 99 and 111).

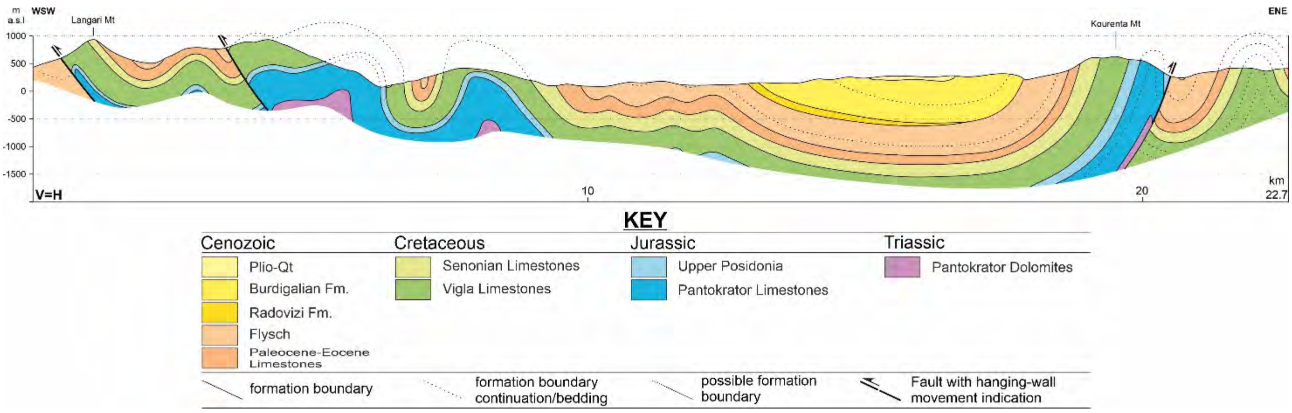

Figure 99. Cross-section [C] Langari Mt – Kourenta Mt

4.14.4 [D] Chionistra Mt – Mitsikeli Mt

The Chionistra-Mitsikeli cross-section (Figure 98) depicts the relatively flat backlimb structure of the so-called “Ioannina plateau” between the backthrusts of Kourenta and Mitsikeli. It also shows details of the Mitsikeli, Chionistra and Kourenta Mts structure and the westward thickening and facies differentiation of the Miocene deposits.

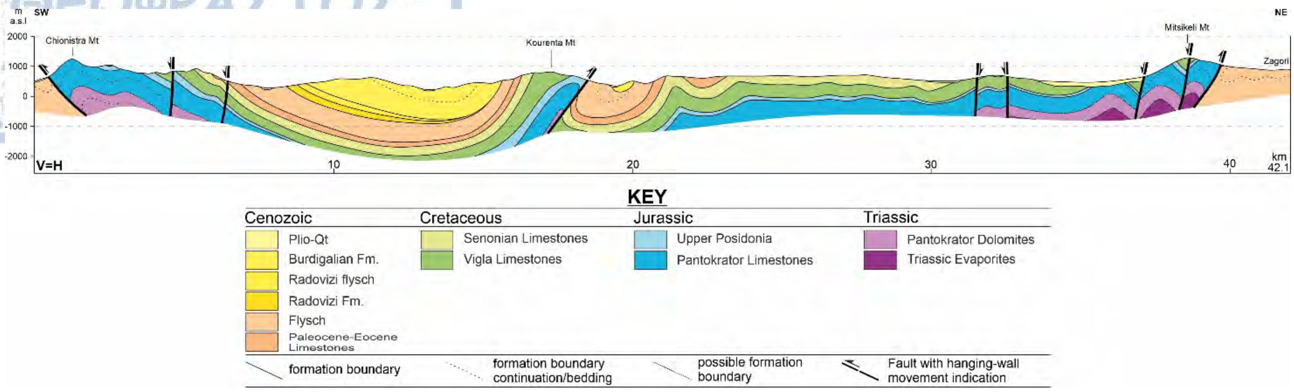

Figure 100. Cross-section [D] Chionistra Mt – Mitsikeli Mt

4.14.5 [E] Zoumbani Mt – Tomaros Mt

The Zoumbani (or Kokkinitsa)-Tomaros cross-section (Figure 99) depicts the two successive thrusts and a backthrust all located in the Chionistra Mt. Moreover, it demonstrates the westward thickening and facies differentiation of the Miocene deposits. In this section the Radovizi Fm. reaches its maximum thickness of ~500-600m. The main structural feature of Tomaros Mt area are the three, closely spaced reverse faults and the leading backthrust. It is worth to notice the successive open folds starting at the easternmost edge of the Miocene deposits. This feature resembles that of Langari-Kourenta section where similar folds occur at the westernmost part of the Miocene deposits.

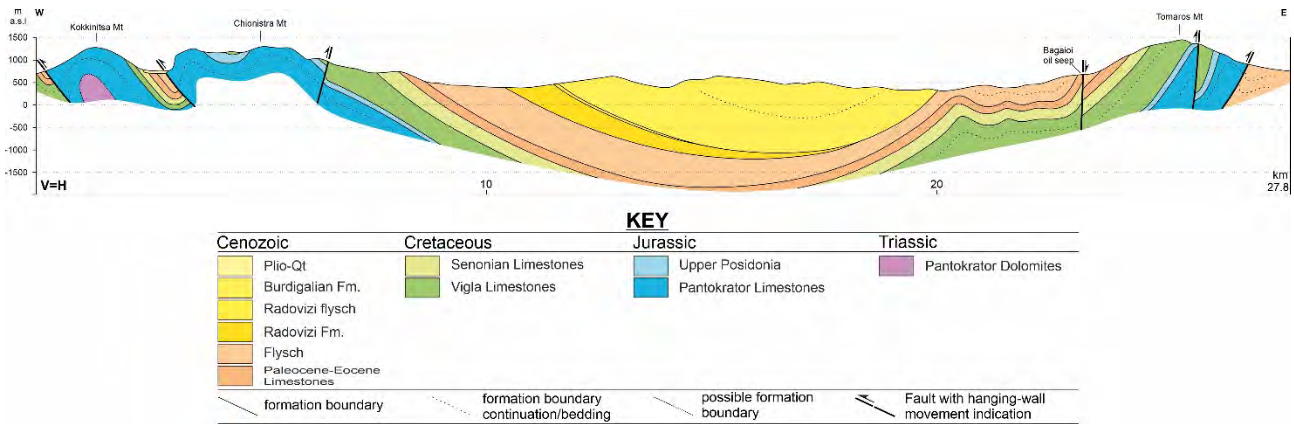

Figure 101. Cross-section [E] Zoumbani Mt – Tomaros Mt

4.14.6 [F] Paramythia Mt – Petousi

The WSW-ENE-directed cross-section (Figure 100) cuts through the frontal thrust of Paramythia Mt., the inverted forelimb, a secondary intra-thrust-sheet blind thrust, the Pantokrator Shales Fm, and the fully developed stratigraphy up to the Lower Cretaceous of the Vigla Limestones. This section involves a good example of the structural style variations that arise from the mechanical properties of the formations. In this way, the thin-bedded, cherty, and, occasionally, shaly formations are prone to accommodating strain in intensively folded zones.

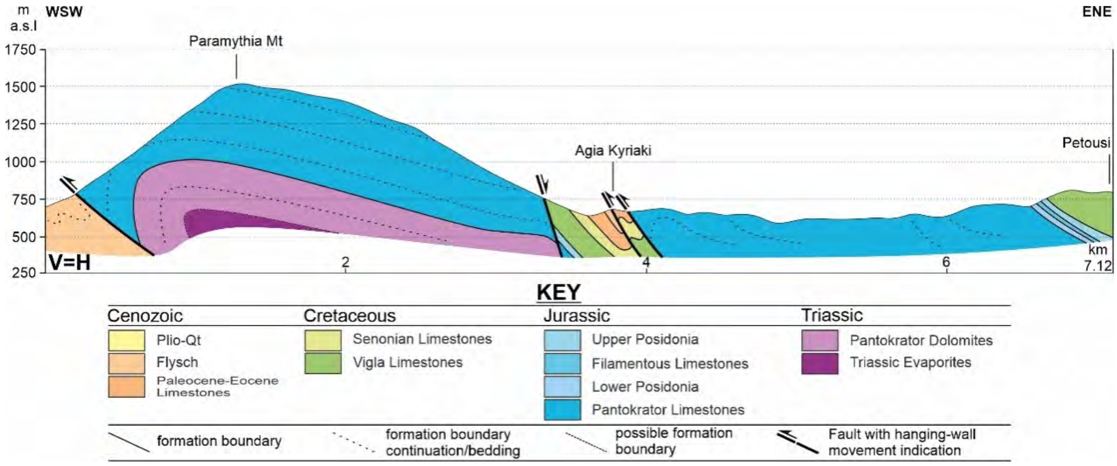

Figure 102. Cross-section [F] Paramythia Mt – Petousi

4.14.7 [G] Kouklesi – Rapsaioi

The Kouklesi-Rapsaioi cross-section (Figure 101) depicts the lateral facies change in short distances from the lower up to the upper Jurassic. 500m to the west of Kouklesi the Ls.P is overlined by the L. Jurassic AR, in Kouklesi, by the Sh.PU and 1km east of Kouklesi by the L. Cretaceous Ls.V.

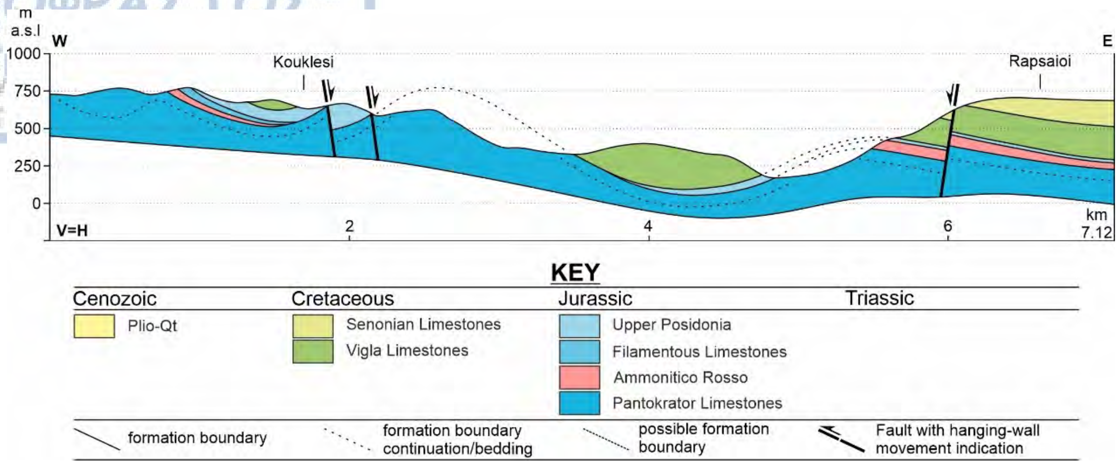

Figure 103. Cross-section [G] Kouklesi – Rapsaioi

4.14.8 [H] Tourla Mt – Kerassona

The WSW-ENE-directed cross-section (Figure 102) cuts through three successive anticline-related hills: "Tourla", "Tsouka" and "Flambouro". The structure is rather complex in the Tourla-Thesprotiko part of the section, deviating from the typical structure of the west-verging asymmetric anticlines by demonstrating tight, almost upright, large amplitude folds. It is important to notice that the formation thickness drastically changes over short distances. Examples of this can be seen in the Ls.V, Ls.Sen, and Ls.PE of the Thesprotiko Mt, where the formations at the forelimb are almost three times thinner than in the backlimb position. Details on the structure of Thesprotiko MT are provided

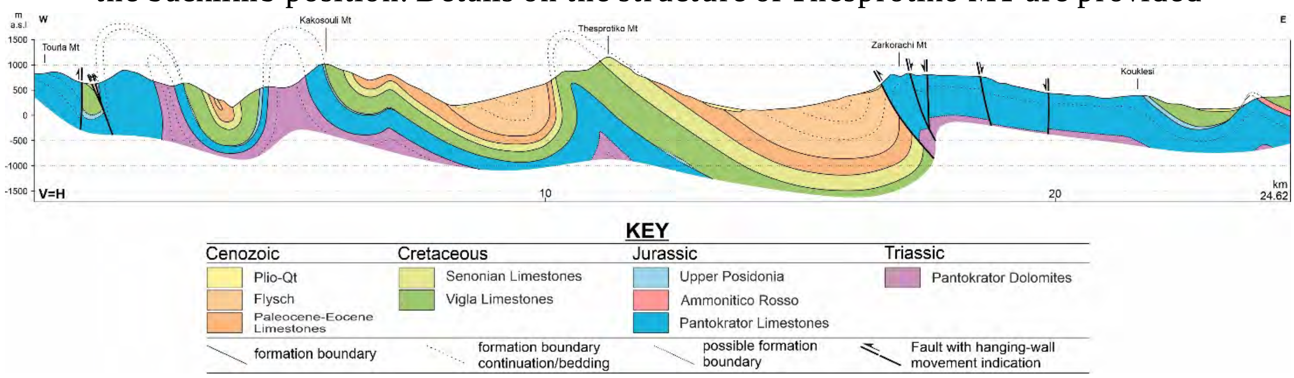

Figure 104. Cross-section [H] Tourla Mt – Kerassona

in §5.1.2.7. The Ls.P. thickness in the area between the Tourla and Kakosouli MTs varies strongly as well. Moreover, it is evident throughout the entire section that the Sh.PU outcrops are scarce. It is worth mentioning the lateral facies change from AR to Sh.PU in the Kouklesi area.

Chapter 5 – Discussion

5.1 Proposed revised stratigraphic column

During the present work, the lithological and stratigraphic characteristics of 20 lithostratigraphic units were documented and are described in detail in § 4.1. Concerning the chronostratigraphic relations of the units, this work mostly follows the time boundaries suggested by the IGRS-IFP (1966) as well as those of various Karakitsios' works (e.g., Karakitsios, 2013).

The following novel suggestions deduced from fieldwork are incorporated in the proposed stratigraphic column of Figure 103.

a. Addition of the Transitional marl is a brown marl interval underlying the AR and the Sh.PL; therefore, its age should lie in the late Pliensbachian to early Toarcian. In some locations under AR, it can contain well-rounded pebble-sized detrital limestone clasts. Its thickness rarely exceeds 7 meters.

b. Addition of the Pantokrator Shale. Pantokrator Shale is found interbedded in the middlemost parts of the Upper Triassic–Liassic platform carbonates, between the Rhaetian Pantokrator Dolomite and the Lower Liassic Pantokrator Limestone. It consists of black shale and bituminous dolomitic sandstone. Thickness is up to 30 m.

c. Triassic salt piercing up to the Burdigalian clastics. This was observed in the area of the Zallongo Mt.

d. Addition of a cherty limestone member within the thick successions of the Vigla Shales

e. Depiction of the dolomitization level variation within the Pantokrator Fm. It was evident during field work that the dolomitization from the Pantokrator platform carbonates fluctuates greatly, even over very short distances. The most characteristic example is found in the area between Souli and Paramythia Mts. In this area, a blind-thrust anticline occurs at its backlimb.

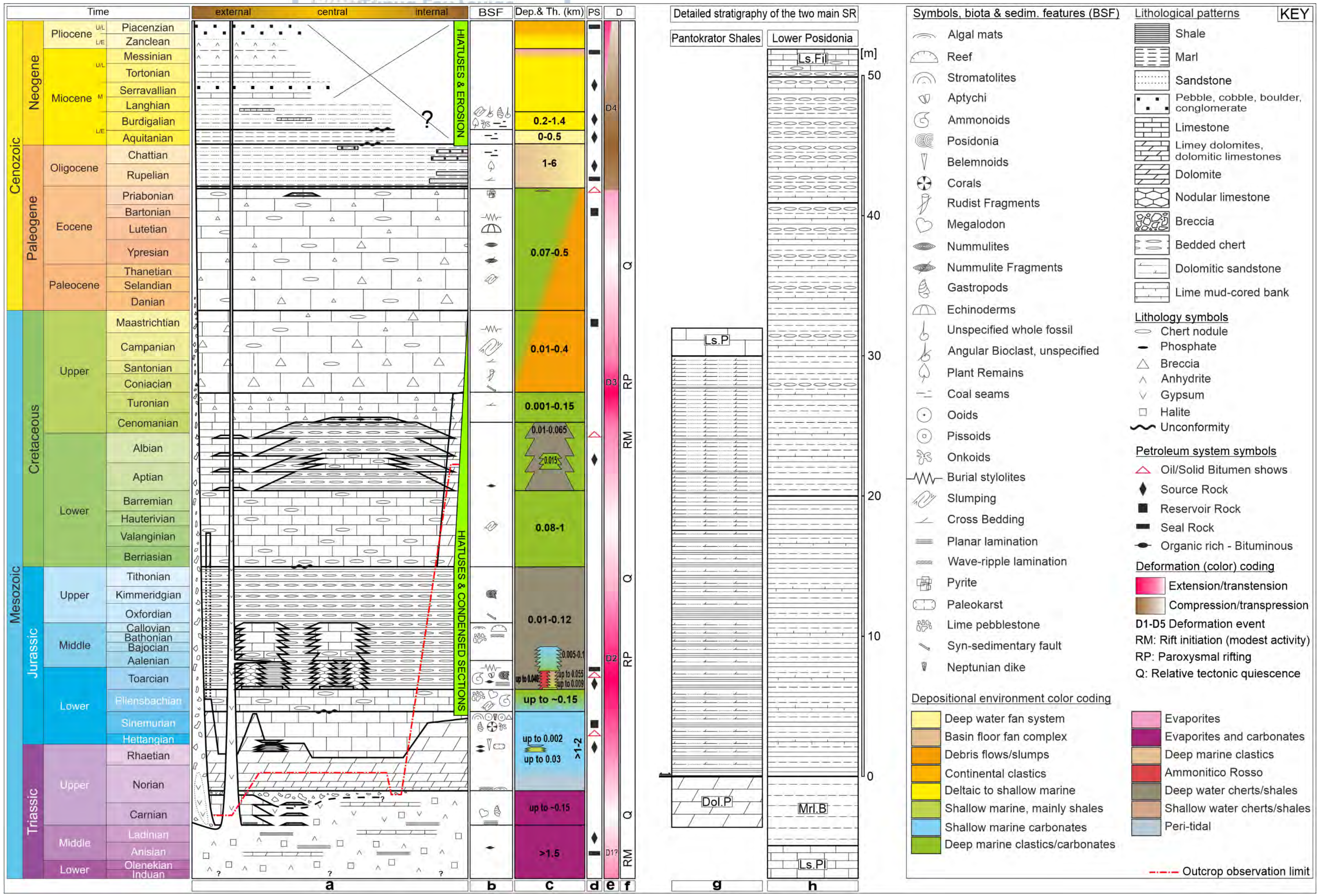

Figure 105. New lithostratigraphic column proposed for the Ionian Zone in Epirus (column a). Lithological/sedimentary characteristics are provided in column b. Estimations of the depositional environments are shown in column c. Petroleum Systems elements are shown in column d. Major geotectonic/deformation events and their estimated duration/magnitude as well as the regional geodynamic status are shown in the columns e and f, respectively. In the columns g and h is shown in detail the lithostratigraphy of the two most important source rocks in Epirus, the Pantokrator Shale and the Lower Posidonia Beds, respectively.

5.2 Tectonic stages and associated depositional settings

5.2.1 D1: Permian – Lower Triassic

This event is associated with the opening of Neo-Tethys and the detachment of the Cimmerian blocks from the northern Gondwana passive continental margin. This event likely affected the northern Gondwana plate domain with far-field stress and faulting, and possibly with thermal cooling-induced subsidence.

During D1, the Ionian Zone was part of an extensive passive margin basin. Permo-Triassic clastics at the base of the Apulian platform (Verrucano Fm.) imply that rifting likely initiated during the late Permian and areas where subaerially exposed and eroded, providing clastic material tectonic depressions. Permo-Triassic volcanosedimentary series of Tyros beds below the Gavrovo platform (ENE of the Ionian Zone) imply that this rift system was active enough to introduce volcanic activity. Therefore, in the in-between area of the Ionian Zone, it is possible that analogous sediments were deposited and early syn-rift structures were developed.

5.2.2 D2: early Upper Triassic – Tithonian

This event is associated with the opening of the East Mediterranean Basin (EMB) and its subsequent development into an oceanic basin and the detachment of the Greater Adriatic Plate (GAP). This changed the geotectonic position of Epirus from part of the northern Gondwana passive margin to the southern part of the GAP passive margin. During this phase, intense block faulting occurred at various stages of paroxysmic activity. Salt movements were enhanced due to extension, leading to inflated and deflated domains. Thermal relaxation of the lithosphere resulted in subsidence at the end of this stage. It is likely, though, that the Ionian basin represents an aulacogen (failed rift). This would explain why Late Jurassic subsidence focused on the Ionian basin domain and not on the astride areas, which remained shallow, since they all together represent part of the GAP passive margin.

Carnian and Sinemurian deposits are dominated by carbonates. The stratigraphically lowest formation of the succession is the "Foustapidima Limestones" Fm., consisting of thin-to-medium-bedded black micritic limestone often rich in thick-shelled mollusk fauna. However, Foustapidima fm. outcrops are small (up to several hundred m) and sparsely distributed in the IZ-E. In cartographic scale as well as in cross sections, Foustapidima fm usually appears to be enclosed within the upper parts of the evaporites. This formation is suggested to have been deposited within the evaporitic basin setting, in a relatively shallow marine basin. These basin types are likely to have been developed in the extended passive continental margin of Gondwana (Mattavelli et al., 1991). The "Pantokrator Dolomites" lie above the Foustapidima Fm.; however, the contact cannot easily be seen in the outcrops. Instead, it is suggested that some tens of meters of evaporite were originally lying between the Pantokrator Dolomites and the Foustapidima. This suggestion is based on a relatively good exposure of these two units in the Igoumenitsa area. Therefore, Foustapidima is considered to be a member of the evaporite sequence.

The Pantokrator Dolomites lithotypes vary greatly within the Ionian Zone. The most distinctive facies are a) the laminated dolomite, such as nearby Vassiliko; b) the thin-bedded dolomite, such as around Parga and Agia; and c) the massive dolomite, such as in Souli Mts. The first type rather indicates a syngenetic origin of the dolomite. Dolomitized microbial mats and colonies attest to this (Figure 104). Microbes play a critical role in dolomitization by catalyzing the formation of dolomite.

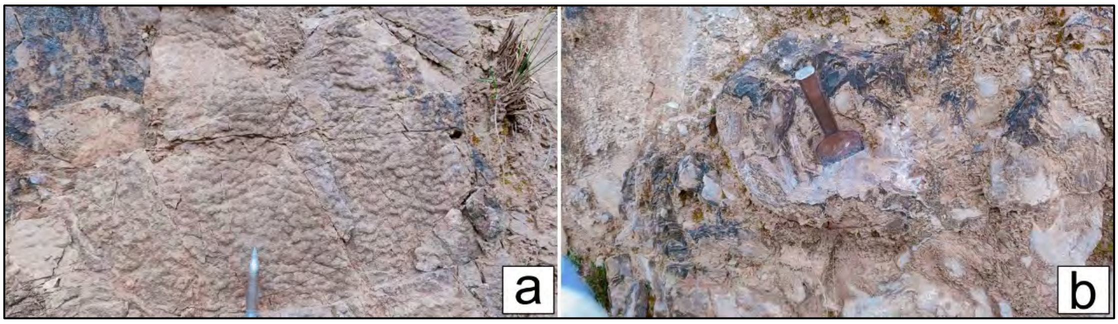

Figure 106. a) dolomitized algal mat, b) dolomitized stromatolite dome

An interesting lithological feature of the Pantokrator Limestone is the presence of zones of bedded and structureless cemented breccia. The clasts vary in size from mm to m. Their contact with the limestone is conformable, with no disruption of the older limestone bedding. This implies that the carbonate platform was exposed to subaerial conditions, and some intervals were dissolved, inducing the creation of these paleokarstic features.

Pantokrator Limestone Fm. is characterized by the prevalence of massive to thick-bedded limestone in neritic facies. However, extensive areas with thin-to-medium-bedded limestone also occur. Although massive limestone can occur at any stratigraphic level of the formation, it commonly exists at the highest stratigraphic levels in several areas. In two sections (Kouklesi and Karvounari), the contact with the overlying Siniais limestones is strongly angular at an angle around 70–80°. This contact likely reflects either the presence of high-angle normal faults (that compartmentalize the platform) or the original platform flanks.

Hence, it is suggested that Pantokrator Fm. rather represents a set of carbonate platforms of various sizes and shapes instead of a single, uniform, Ionian Zone-wide platform. This representation likely explains a part of the observed variations of the Pantokrator Fm. depositional conditions throughout the Ionian Zone in Epirus.

Figure 105 depicts the depositional settings deduced by lithological observations for four intervals: a) Carnian, b) U. Triassic – L. Jurassic, c) Hettangian, d) Rhaetian – Sinemurian.

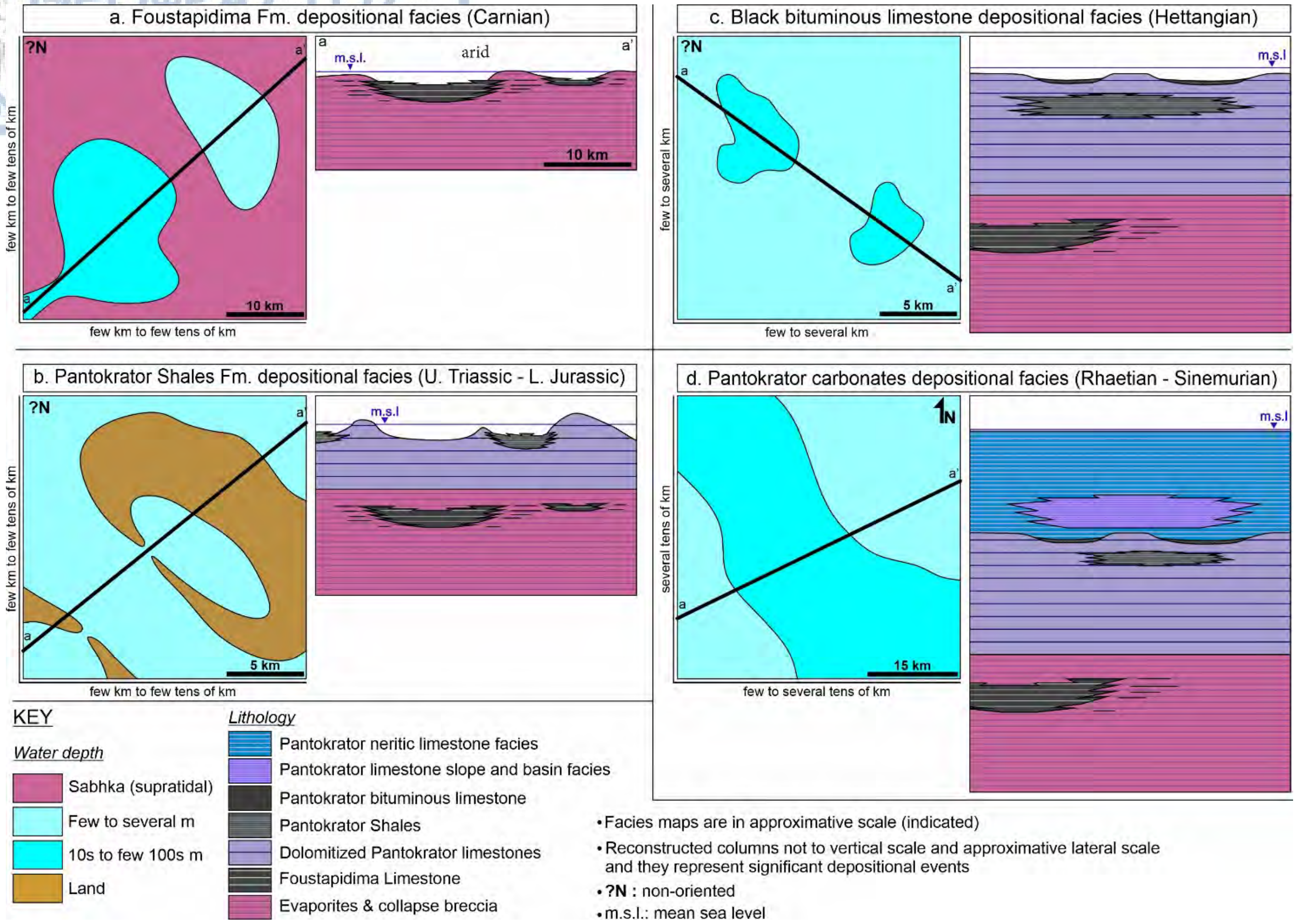

Figure 107. Cartoon sketches tentatively reconstructing the basin configuration during various stages from Carnian to Sinemurian. Reconstruction of the basin during a) Foustapidima Limestone in shallow water depths in a general sabkha setting, b) Pantokrator Shale in a coastal lagoon setting of a carbonate platform, c) black bituminous limestone in relatively deeper water in carbonate platform, d) Pantokrator carbonates (limestones) deposition in widespread neritic conditions with some deeper (slope?) trends.

D2: Pliensbachian - Tithonian

This interval involves three stratigraphic units: the so-called "Lower Posidonia Shales" of Toarcian (and Aalenian?) age, the middle-Jurassic "Filamentous Limestones" and the Upper Jurassic "Upper Posidonia Shales." It is the most extensive and thick siliciclastic, clay/mud/chert-dominated interval within the Upper Triassic-Eocene carbonate succession, exceeding in some sections the 150m cumulative thickness. All three formations demonstrate distinctive lithologies.

Lower Posidonia Shales are mainly composed of fissile black shale and laminated black, blueish, and brown mudstone. Thin limestone beds, black chert beds, and Posidonia shells occur mainly in the middle parts and higher.

Occasionally, mass transport deposits and coarse-grained and usually well-rounded carbonate clasts are found interbedded within shale. This shows the proximity to subaerially exposed blocks (islands). Previous studies attest to the abundant presence of conifer branches and pollen within the shales. Shales are typically laminated and organic-rich. Field evidence shows that this formation was deposited in distinct subbasins, likely tectonically controlled in their origin. However, global climate perturbations leading to changes in sea level, precipitation, erosion, sea water salinity, chemistry and stratification, and halokinesis could also result in the deposition of Lower Posidonia shale. Biomarker data indicate that this formation was deposited under oxygen-deficient and occasionally iron-lean conditions (Alexandridis et al., 2022b).

The lateral counterpart of the Lower Posidonia Shales is the Ammonitico Rosso Fm. There are sections where the interfingering between them is evident by lithological and faunal data. Reddish-pinkish sediments (i.e., clay, shale, and limestone) and generally lower thicknesses of the AR compared to LPS are likely points to a shallower depositional setting with oxygenated waters and occasional base wave action that shaves the top of the deposits and maintains a relatively small thickness. These probably correspond to subsea paleohighs and/or shelf depositional settings.

Below these two units, a brown-reddish-greenish shaly marl locally occurs. The thickness varies from ~1 up to 8 m. Thin, rounded limestone clast intervals are found locally.

Rapid shallowing-upwards facies of the filamentous limestones are likely associated either with a major sea-level drop in a relatively shallow basin or with the presence of faults transposing upwards the tectonic blocks. Carbonate conglomerates interbedded within the filamentous limestones could be associated with both mechanisms. Both cases imply the presence of shallow and emergent areas.

The direct contact of the overlying Upper Posidonia Shales over Pantokrator Limestones is a common stratigraphic feature throughout the Ionian Zone. However, in a few sections, Upper Posidonia Shales are absent from the stratigraphic column, and Vigla Limestones are in contact with

Pantokrator Limestones. In two extreme cases, Eocene limestones are directly placed over Pantokrator in restricted outcrops.

As it has already been pointed out in various Karakitsios' works (e.g., Karakitsios 1995), the roughly wedge-shaped geometry of the Lower Posidonia Beds likely reflects domino-style faulting and half-graben basin geometry. Similar wedge-shaped sedimentary unit geometries are possible to develop in a listric faulting setting as well. The listric faulting model demands a mechanically weak layer for the flat part of the fault to be developed. In Epirus, this interval is the Triassic Evaporite. A problematic aspect of these two basin configuration models is the scarcity (or absence) of convincing field evidence of the basin part where the synrift deposits abut over these faults. These might partially be explained by the tertiary inversion, where the offsets of the formations modified the original synrift contacts. Field evidence of the Upper Posidonia Beds geometry likely indicates that this formation was deposited in a late synrift to post-rift setting. Thicker sequences were deposited in former depocenters, whereas around the shallower areas, the sediment accumulations are much thinner.

Hence, in the Pliensbachian, it is likely documented the rift initiation, and in the late-Pliensbachian–early Toarcian, the rift climax phase was described in Gupta et al. (1998). This is documented in the hiatuses and condensed-sedimentation areas that developed during this period in a rapidly tectonically subsiding basin, which additionally coincided with a rapid global sea-level rise. This shows that the rift magnitude increased, and the strain likely localized in a few faults while other smaller faults ceased. This is reflected in the scarcity of the Lower Posidonia Beds deposits, which occur only in a few asymmetric, silled depocenters.

The Figure 106 demonstrates the basin evolution in six stages, from the end-Pliensbachian to Tithonian-Berriasian. The coupled effect of the tectonic subsidence and the sea-level fluctuations govern the sedimentation.

The deepening directions seem to differ among the various areas. For example, in the area of Chionistra Mt., in the section from the Elataria village to the plateau 1.8km to the south, the deepening direction seems to occur towards the south.

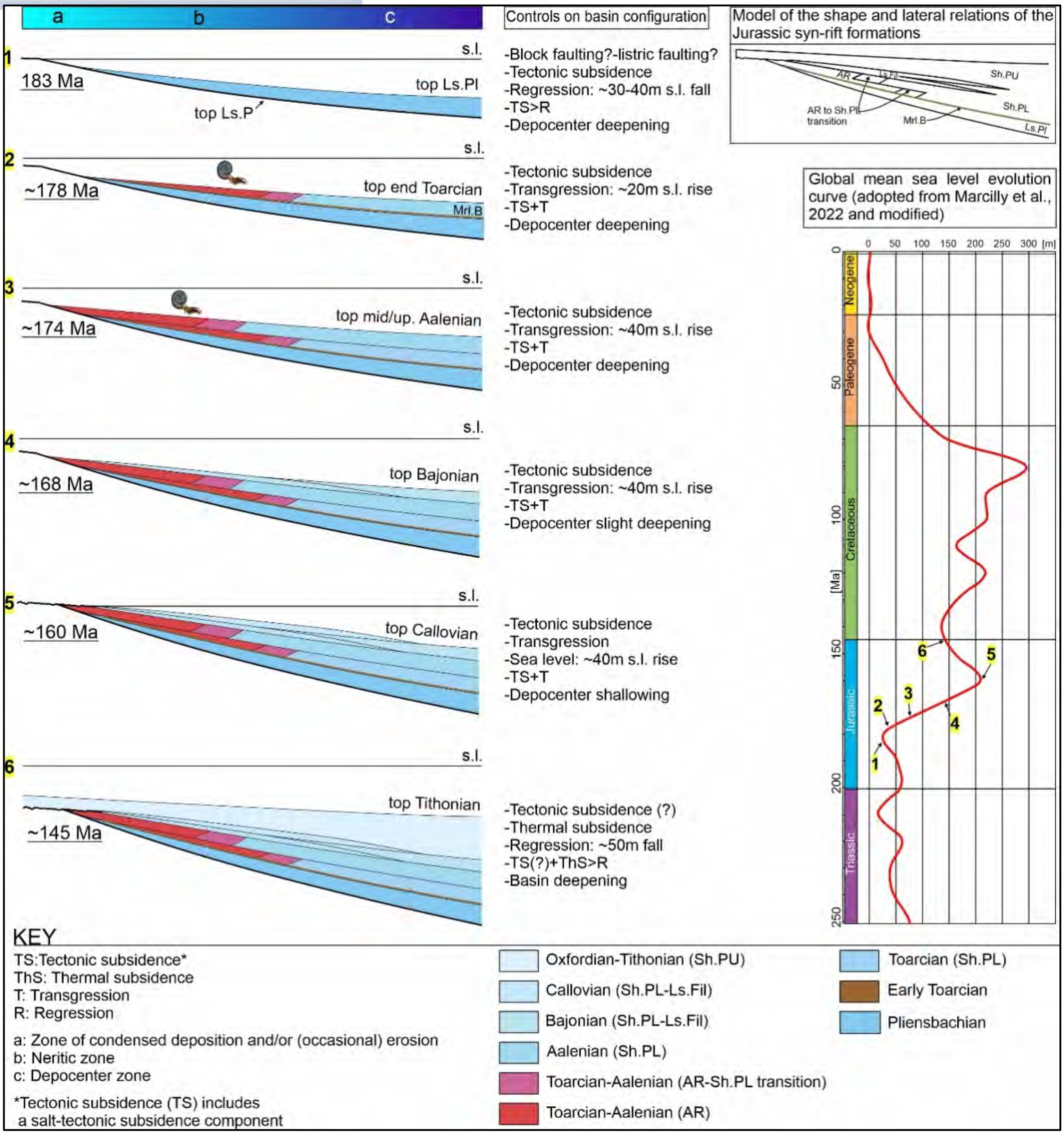

Figure 108. Model of the basin evolution and the deposition of the various lithostratigraphic units from the end-Pliensbachian to Tithonian-Berriasian.

This is because in the Elataria area, an olisthostrome (or a tectonic mélange) consisting of 1.5m in thickness occurs between the Siniais and the Toarcian black shales and cherts. Moreover, thin conglomerate beds are interbedded within the black shales. On the other hand, in the roadcuts of the Sh.PL in the area of the plateau, no clastics are observed, while the thickness of the blueish basal marls is >30m. The lithostratigraphic comparison shows that the Elataria section is near an emergent area (likely fault-related) that provided the clastic material and maintained the area in a relatively high position that condensed the deposition. On the contrary, the plateau section is by an order of magnitude thicker, with the basal strata representing a rather distal portion of the sub-basin. The large (>3cm in diameter) Posidonia shells in the black shales of the plateau are indicators of either oxygenated waters high in the water column or episodes of anoxia that were distant enough to let the Posidonia adult or larvae grow before killing. These perturbations in the oxygen content in the water column are also evident in the red (oxidizing conditions) and green (reducing conditions) alternations observed in the shallower parts where the basal marl was deposited. It is possible that these events are correlated to the occurrence of beds with high (reducing conditions, many deaths) and low (oxidizing conditions, fewer deaths) Posidonia shell content. Also, it is possible to be correlated to higher or lower organic matter preservation in the deeper parts of the basin where the black shale was deposited.

In the area of Kouklesi, a small part of the depocenter is being exposed in the Toka section. In this area, the deepening direction seems to be directed to the northwest part of the subbasin. The broader Kouklesi area is also an excellent area for the Jurassic sub-basin study as it encompasses substantial lithostratigraphic variations.

On Corfu Island, the Jurassic formations are well exposed in the northern part, around Pantokrator Mt. A short review of the lithostratigraphy of the studied sections is presented: In the outcrops of Betrouli, a 1.5-meter-thick conglomerate (Figure 107) occurs between Ls.Sin and Sh.PL, consisting of tightly packed, clast-supported, and mildly sheared white limestone of pebble-to-cobble size clasts. In this area the lower parts of the Sh.PL consist of light-colored, thin bedded limestone, occasionally laminated.

Towards the upper parts of the Formation, the lithology becomes more siliceous and Posidonia shells sparsely occur. On top of the Sh.PL lies the Ls.Fil. Around 300m to the northwest of Betrouli, the Sh.PL is more siliceous, even from lower stratigraphic levels, while the laminated parts are more frequent. A 0.5–1 m-thick conglomerate bed also occurs in the base of the Sh.PL. About

300–500 m to the NW of the previous location, the Sh.PL base lacks the conglomerate, and the lithology is mostly in the lower part of the formation.

Figure 109. Tightly-packed limestone conglomerate at the base of the Lower Posidonia Beds in Corfu (Betrouli section)

The chert beds occur at a higher stratigraphic level. The general color shade of the formation in this area is reddish-ochre. In the area of the abandoned village of Palies Siniais (or Palio Chorio), black shales occur in a relatively extended stratigraphic span of >10m. The geological and lithostratigraphic observations from Corfu imply northward deepening directions.

However, more research effort should be invested in order to document any coincidence or the shifting of the condensed sections and the depocenters.

The presence of conglomerates and/or mélanges in the basal strata of the Lower Posidonia beds is independent of their lithofacies. For example, in the Elataria area, a mélange is observed within a black and gray mud matrix, whereas in Corfu, the conglomerate is below the Posidonia formation, whose basal strata are thin-bedded limestones. Moreover, the high roundness and sphericity degree of the clasts rather indicates a relatively sufficient amount of time in which the clasts worked. This might imply the presence of shorelines where the clastic material has sufficient time to get rounded.

All the aforementioned are summarized in Figure 108, where the regional basin structure is tentatively reconstructed for the Pliensbachian–Toarcian interval.

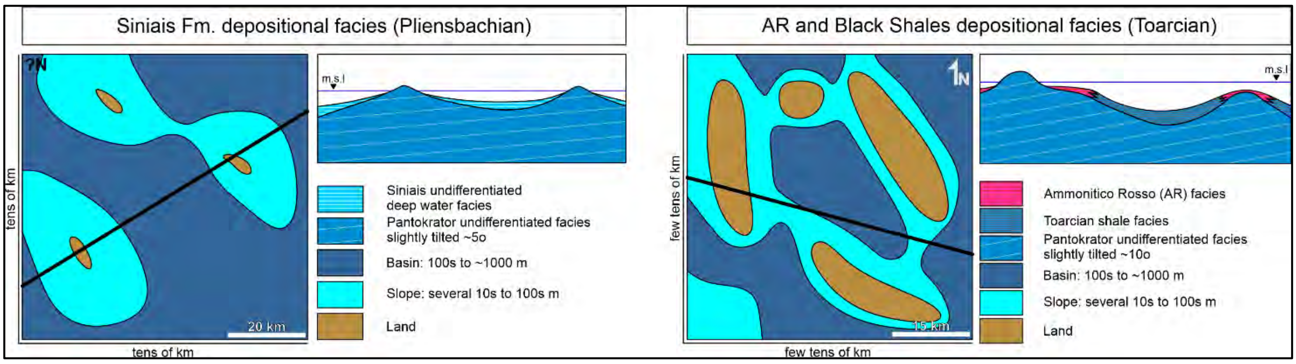

Figure 110. Tentative reconstruction of the basin configuration during Pliensbachian – Toarcian and the associated depositional settings.

5.2.3 D3: Early Senonian – Paleocene

This extensional event is attested by the shift in sedimentation from pelagic micrites to massive bedded rudist bioclastic debris flows, as well as by the presence of syn-sedimentary normal faults extensively occurring at the base of this formation (Figure 109).

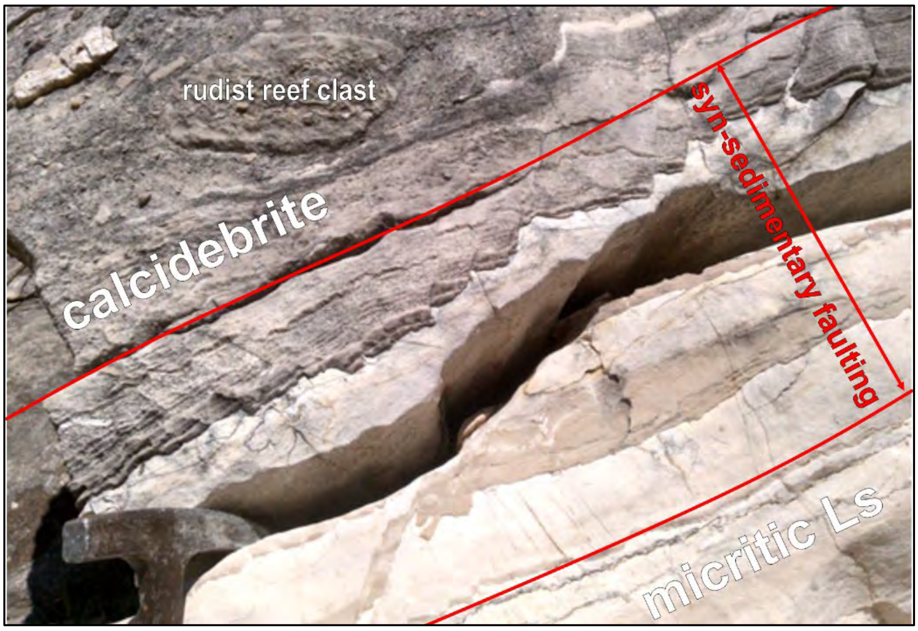

Figure 111. Top Vigla Limestone – Base of the Senonian Limestone. Syn-sedimentary faulting accompanies lithological facies shift from thin-bedded micritic limestone to massive calcidebrite.

This extension probably reactivated older block-bounding faults and, moreover, exposed to erosion parts of the astride Gavrovo and Pre-Apulian neritic platforms. The distribution of the Senonian lobe-complex sediments is controlled by intra-basinal highs and lows (Figure 110). In tectonically quiescent periods, deep basin limestone and chert were deposited. This phase was accompanied by a global rapid regression that further exposed the platforms. Cross-bedding of thin-grained debris below the main pulse of massive-bedded rudist bioclast debris indicates that the extensional phase started shortly after the Sh.V deposition. However, ongoing transgression and, probably, lower extension intensity masked the event until the main phase. This extensional event might be associated with slab pull from the northward intra-oceanic subduction of the oceanic lithosphere attached to the northern margin of the Adria *sensu lato*.

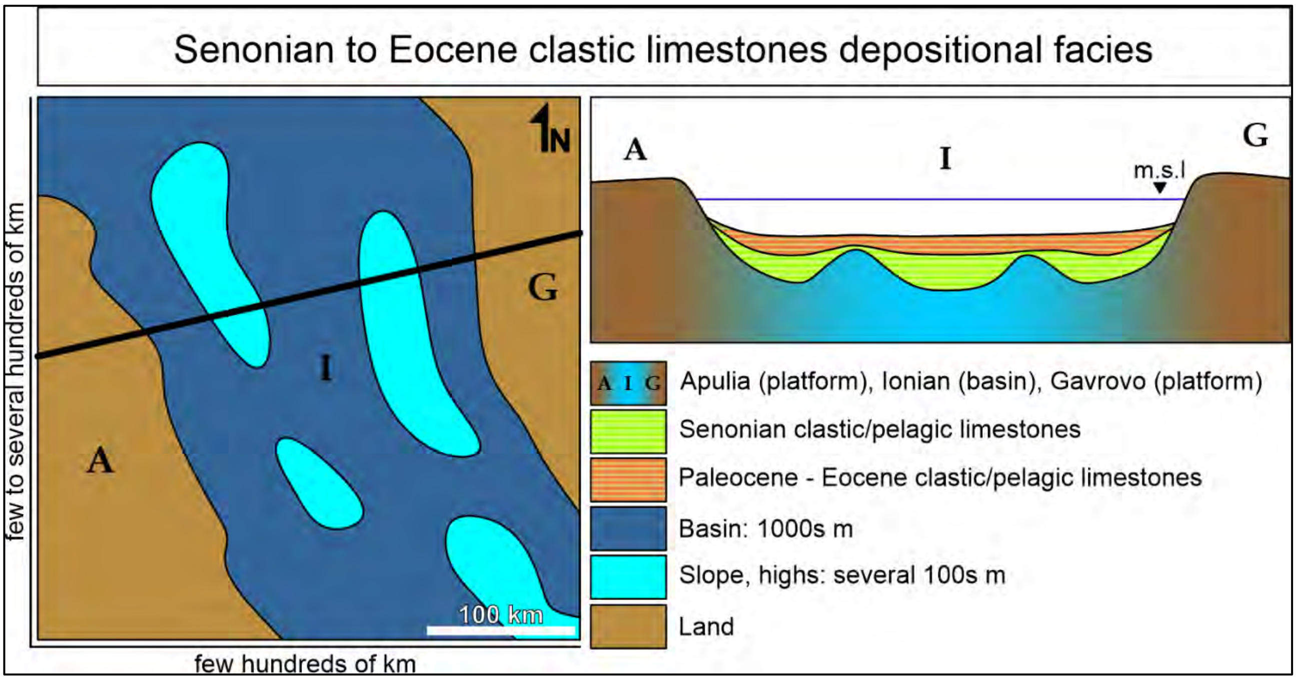

Figure 112. Tentative reconstruction of the basin configuration during Senonian - Eocene and the associated depositional settings.

The Paleocene-Eocene limestones, mainly, and the Senonian limestones, to a lesser degree, show a binary lithological composition. The one end-member, consisting mainly of micritic limestone, chert, and often small bioclast detritus, lithologically demonstrates Deep Shelf Margin (DSM) belt characteristics (based on the Standard Facies Belts model introduced by

Wilson, 1975). The other end-member consists of detrital bioclastic limestone deposited by strong bottom currents, as the cross-bedding suggests. The clast size varies from mm to several dm, pointing to foreslope (FS) belt characteristics. Often observed, cross-bedding relations indicate strong bottom currents. The grains of biological origin consist mainly of rudists (for the Senonian section) and nummulite fragments and whole individuals (in the Eocene section). Clasts of shale and chert are frequently observed, with sizes rarely exceeding 1 cm across. Bed thicknesses vary greatly among various stratigraphic levels and locations. Slumping is a common feature, especially in the Senonian section.

Lithological and stratigraphic characteristics point to a slope to a toe-of-slope setting and probably marginally to an Open Sea Shelf belt. The Senonian shows higher energy characteristics, such as very large fragments (>20 cm across) and cross-bedding, whereas the Eocene shows less energy, reflected in the generally smaller detrital grains and the more frequent micritic beds. There is an exception to this general trend, where in the IZ-I occur massive beds (>20m in thickness) of coarse-grained clastic limestone.

In assessing the problem of the origin of the detrital grains, the following remarks are highlighted:

1) Occurrence of large fragments (~20 cm across) within the Senonian section in the IZ-C and in IZ-I.

2) Occurrence of a large intact part of a rudist in the IZ-E.

3) Angular clasts are dominant

4) The occurrence of breccia within chert beds in the Senonian section indicate high-energy influx, likely in a toe-of-slope setting.

5) The bed thickness

6) Lack of clear evidence for in-situ rudist buildups within the IZ

7) Lack of clear or sufficient evidence of fault escarpments of Senonian – Eocene age within IZ

8) Absence of mega-breccia related to steep fault escarpments

9) Absence of extensive areas of non-deposition or erosion

10) Detrital fauna is time-equivalent to the formations incorporated

11) There is a reducing grain-size trend from the Senonian to Eocene

12) Micritic limestone with chert (locally bedded) is the dominant lithology for tens of meters of the top Eocene section towards the Transitional Marl

Evaluating all the aforementioned lithological and stratigraphic remarks, the following points are suggested as an explanatory conceptual frame for a working hypothesis of basin configuration during the deposition of the Senonian to Eocene formations:

a) A regional event amplified the topographic variations (various basin configurations) occurred on the Adria plate, resulting in widespread deposition of detrital carbonate grains (i.e., Senonian to Eocene Limestones in Greece and Albania, Scaglia Fm. in Italy). This event was likely of tectonic origin or due to a major climatic shift that affected the area. In the first case, topographic features were further amplified by the movements of the Triassic salt. This event is likely linked to the slab pull from the northward intra-oceanic subduction of the oceanic crust and lithosphere attached to the continental northern Adria plate.

b) The detrital input occurred in several events similar to the well-known turbiditic and debris flows. These events varied in terms of sedimentary load and granulometry.

c) The grain size-reducing general trend by time, implies that an abrupt event occurred at the onset of the detrital limestone deposition, whose effect was gradually mitigated and eventually ceased prior to the foreland onset and the flysch deposition.

d) No extensive carbonate platforms existed within the IZ in Epirus area accounting for major supply of the detrital material.

e) Most of the vast volumes of the detrital material originates from the astride Gavrovo and Apulia carbonate platforms, in which are found the mother rocks in situ. In IZ, rudist fauna colonies are not known.

f) The origin of the large fragments in the IZ-C is possibly attributed the reworking of the recent deposits by the high-energy grain flows.

g) The origin of the large fragment (with rudist fauna) in the IZ-I is possibly a large block that was probably larger (olisthostrome) survived the transportation. This is due to the proximity to the Gavrovo platform.

h) The origin of the intact part of a rudist in the IZ-E might be due to the proximity to the Apulia platform.

Therefore, it is suggested that the detrital matter origin is from the two astride carbonate platform areas (i.e., Gavrovo and Apulia). The depositional patterns and thicknesses of the Senonian to Eocene deposits are controlled by the geometric characteristics and distribution of the deep-water subbasins. The coarse-grained detrital clasts of the Senonian age are likely to correspond to a tectonic event that elevated the astride carbonate platforms while submerging the Ionian basin. However, this event might have initiated shortly after the deposition of the Vigla Shales, as the presence of thin-grained detrital material was deposited at the highest stratigraphic levels in the Vigla Limestone. Moreover, the presence of this detrital material deposited under the action of strong bottom currents above the Vigla Shales implies that the Vigla Shales were deposited in basins instead of on top paleotopographic highs. This is also implied in the area of Thesprotiko Mt, where the well-developed Vigla Shale coincided with the thick Senonian–Eocene succession (see Figure 61).

It is suggested that during this event of the sea-floor stretching, the heat flow form the basement towards the basin increased. This might have important impact on the petroleum systems.

5.2.4 D4: Oligocene – Quaternary

This phase was induced by the ongoing continental collision between the GAP and Eurasia. During this phase, the Ionian basin evolved into a foreland basin and accommodated thick flysch successions. Ongoing shortening resulted in the detachment from the supra-evaporite of the Upper Triassic to the Oligocene succession. Individual thrust sheets are likely to represent individual deeply-faulted blocks inherited from the D2 phase. Thrust sheets were stacked in duplexes. During their westward transposition during the Miocene, they locally received thick molassic-type sediments, creating piggyback basins. Because of these upward motions, parts were exposed to erosion, and unconformities were locally observed.

Crustal-scale compression in Epirus is attested by the numerous faults that occur in reverse and thrust faults at depths of ~2–15 km. Extensional faults are related to extensions perpendicular to the main stress tensor (σ1) or to thickened parts of the orogen that collapse due to the gravitational force overcoming the deep-seated compression.

5.3 Tectonic correlation

It is highly likely that parts of the 8 cross-sections can be correlated (Figure 111) on the basis of visible and hidden structural elements such as large-scale synclines and anticlines, thrusts, backthrusts, and blind thrusts. Moreover, some structural elements could be re-evaluated, and spatial variations in kinematics could be deduced.

- In the area of Tomaros Mt, there are three successive, tightly spaced high-angle reverse faults. The easternmost and most gently dipping might constitute a backthrust, while the westernmost is associated with the well-known oil seep in Baousioi. The overall structure might correspond to a pop-up structure.

- The gently-dipping thrust at the eastern part of the Kassidiaris section is considered to constitute an out-of-sequence thrust. This is because the thrusted, outcropping Vigla Shale sediments demonstrate considerably higher thermal maturity than usual, probably indicating that the formation didn’t exhume during the main thrust phase but rather remained buried deeply where it reached higher thermal maturity (VR%: ~0.9, deep yellow alginite colors).

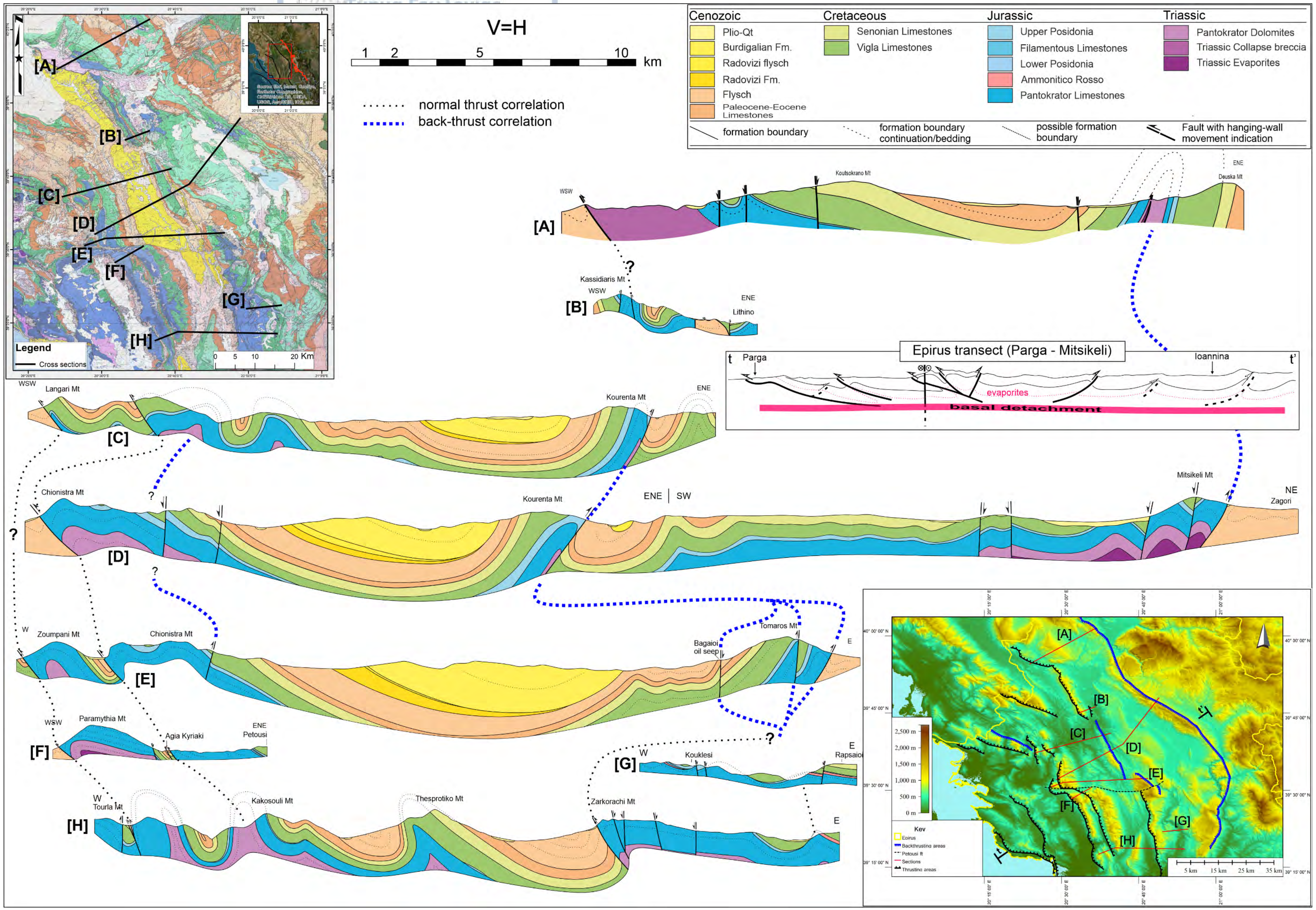

Figure 113. Correlation of the cross-section throughout Epirus. For further information of the geology, tectonics and morphology, notice the inset maps (top-right and bottom-left corner).

5.4 Source rock depositional setting reconstruction based on biomarkers

The biological source of the n-alkanes of the Lower Posidonia Shale shows a contribution of land-plant wax derived long chain analogues (C27 to C37), whereas the Pantokrator Shale lack the long chain analogues. The Pantokrator Shale sediments are assumed to have been deposited in restricted and eventually hypersaline lagoons. Land plant wax input would be expected, however, the exceptionally high aquatic production of short chain n-alkanes will mask any influx from terrigenous sources. The carbonatic lagoon Pantokrator bituminous limestone lacked influx of Fe-rich terrigenous sediments, hence, reduced sulfur released by sulfate reducing bacteria interacted with lipids to form organic sulfur compounds, particularly long-chain alkylated benzothiophenes, common in restricted lagoonal environments. Pantokrator Shale carbonate-poor lagoonal sediments yield less organic sulphur compounds but dominantly show bacterial biological sources, as evidenced by the very strong predominance of hopanes and aromatic hopanoids in the bitumen. In the FPS bitumen aromatic carotenoids including isorenieratane and its biphenylic derivative as well as aryl isoprenoids indicate the presence of *chlorobiaceae*, where the brown strain of the green sulfur bacteria execute photosynthesis under euxinic conditions. This documents an exceptionally low dynamic regime, with strongly stratified water column supporting growth of these highly specialized organisms. Eukaryotic algae steranes are scarce in the Pantokrator Shale, contribute to a slightly higher proportion in the Pantokrator bituminous limestone and are equally abundant to hopanes in the Lower Posidonia Shale. This distribution is indicative of a dominantly microbial organic matter source in the Pantokrator lagoonal sediments and a balanced proportion of algal to microbial producers in the Toarcian shelf settings. The Figure 112 summarizes and demonstrates these results into a water column reconstruction model. and basin reconstruction models.

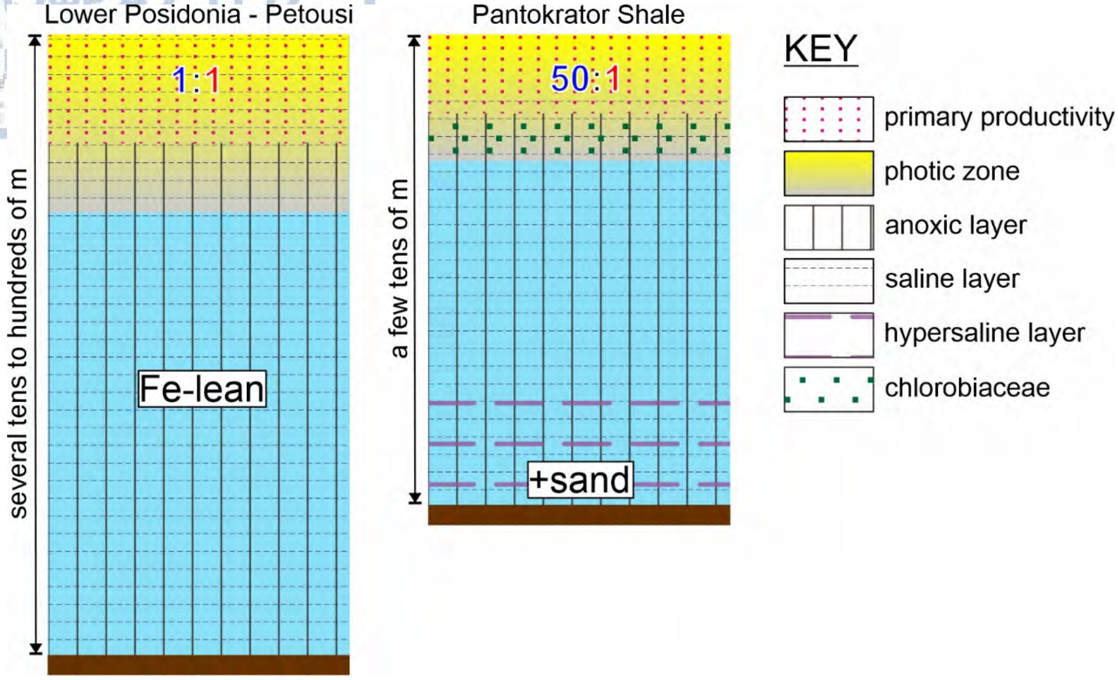

Figure 114. Water column reconstruction model for the Lower Posidonia Shale and the Pantokrator Shale.

The Figure 113 summarizes and demonstrates these results into two basin reconstruction models.

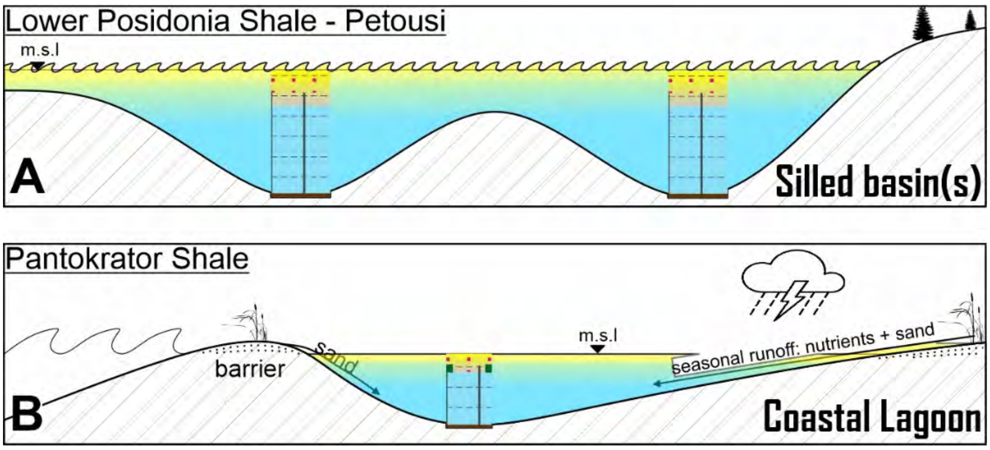

Figure 115. Basin reconstruction model for the Lower Posidonia Shale and The Pantokrator Shale.

5.5 Oil-source correlations

The Lower Posidonia Shale and the Pantokrator Shale extracts may serve as source for the solid bitumens collected in Elataria, Petousi and Vassiliko. The solid bitumens in Petousi and Vassiliko do not exhibit similarity with the Lower Posidonia Shale. In contrast, the solid bitumen in Elataria is more compatible with Lower Posidonia Shale. It has likely derived from the local Elataria kitchen where the Lower Posidonia Shale is present in great thicknesses. Compositions of the Petousi solid bitumen Petousi Lower Posidonia Shale extracts differ substantially, excluding the Posidonia Shale as a source for the solid bitumen. Instead, solid bitumen in Petousi has been likely derived from the Pantokrator Shale or geochemically similar source rock formation (e.g., Triassic formations). The solid bitumen form Vassiliko does not exhibit geochemical similarity to the Lower Posidonia Shale. The solid bitumens in Petousi and Vassiliko exhibit closer affinity to the Pantokrator Shale but do not match perfectly. This might be due to a) lithological/compositional variability within the Pantokrator Shale Fm, b) origin from a different source, e.g., the bituminous Pantokrator limestone or the Triassic evaporite sequence. The Pantokrator Shale extracts contain specific thioaromatic components, all of which will have been missing the solid bitumen due to weathering, oxidation, and evaporative loss. Thus, they are excluded from oil-source correlation. All these results are summarized in and demonstrated in the Figure 114 where the Petroleum System in the adjacent Petousi and Elataria sites is shown.

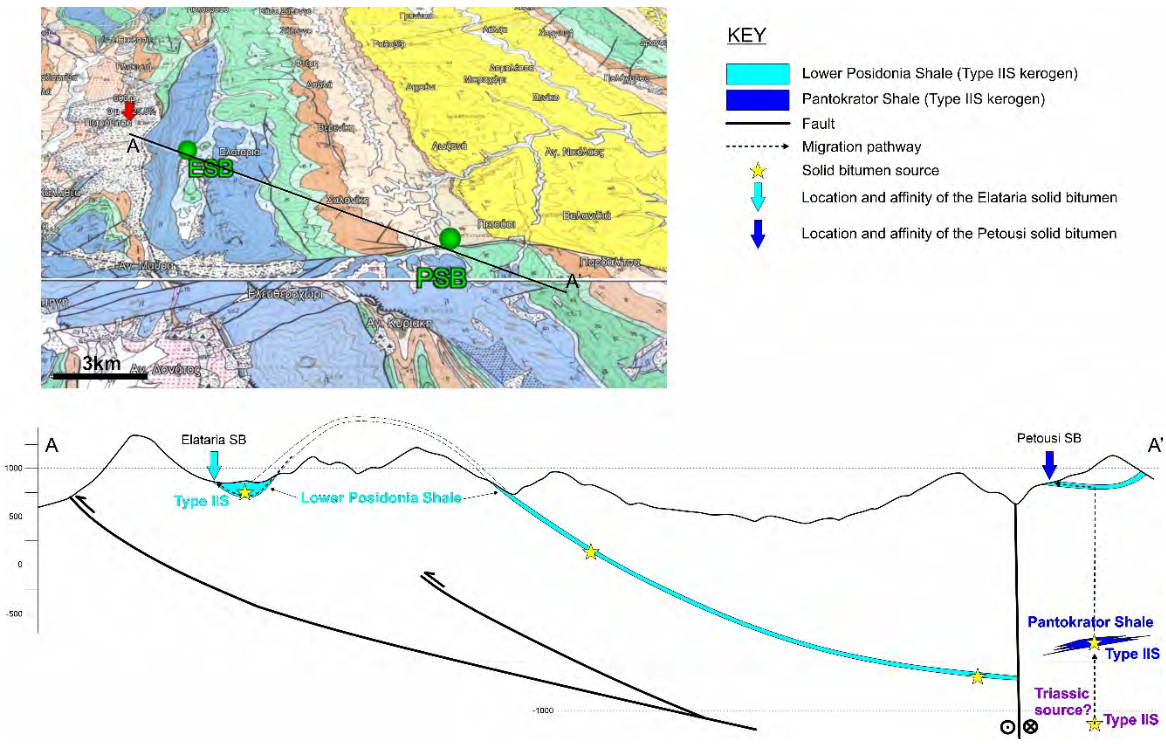

Figure 116. Petroleum System model in the area of Petousi – Elataria describing the affinity of the solid bitumens found in these two locations.

In the Figure 115, the results are summarized and demonstrated providing a petroleum system model that explains the origin of the solid bitumen in the Vassiliko site.

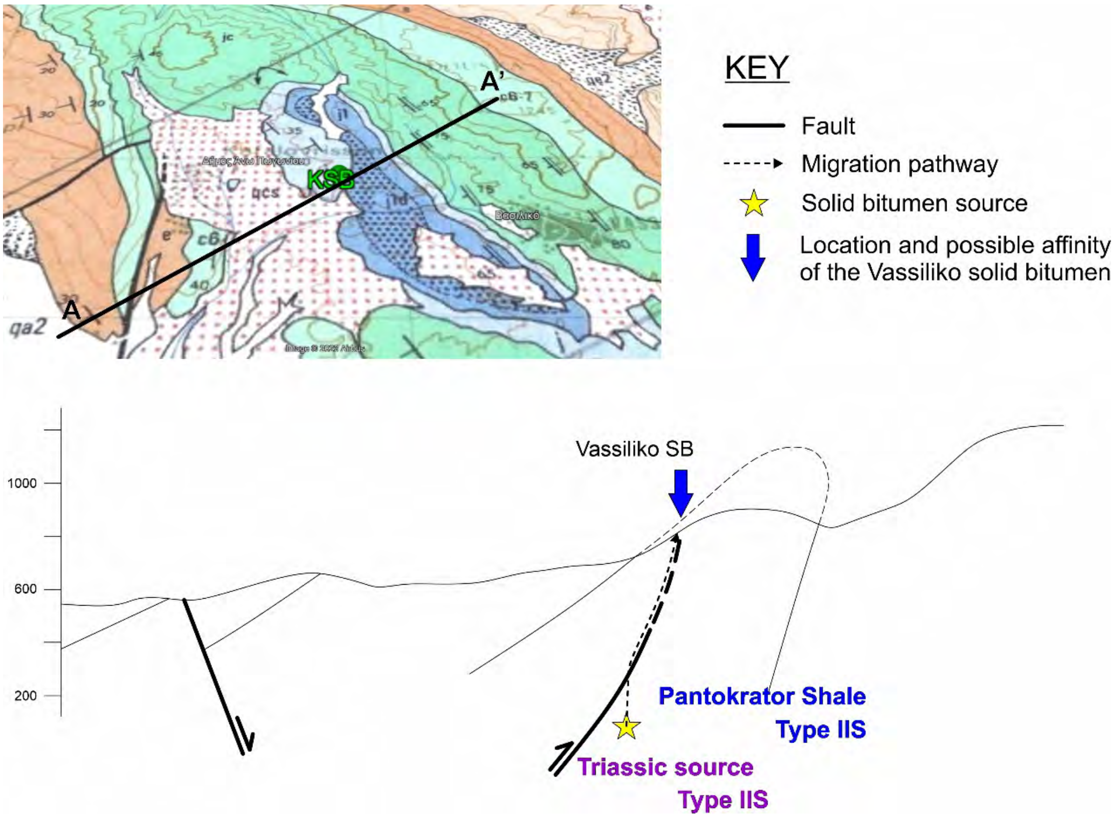

Figure 117. Petroleum System model in the area of Vassiliko describing the affinity of the solid bitumen found in the location.

5.6 Source Rocks

5.6.1 Pantokrator Shale

Pantokrator Shales is a newly identified potential source rock in the Ionian Zone. It was first observed by the author in early March 2017 in a roadcut outcrop located in the Souli Mountain area during PhD fieldwork. Two samples were obtained (70A and 70B), and multiple geological features of the outcrop were documented. Subsequent visits in the area resulted in the identification of more outcrops, uncovering portions of the overall formation, and giving insights into its original extent.

At first glance, the Pantokrator Shale demonstrates oil-prone source rock characteristics of impeccable quality, such as the dark-colored shale-dominated lithology, the very strong bitumen smell, the ignition and combustion of the black shale burning in steady flame, and the significant cumulative thickness (~30 m). Hammer beating on some thick black or brown shale beds leaves a sense of impact absorption, giving the impression of a hollow material, similar to low-rank coal. These characteristics might indicate that the Pantokrator Shales are geological/geochemical equivalent to formations in Italy (e.g., in the Gran Sasso area), which refer to analogous beds as "algal coal" (Stefani and Burchell, 1993).

The formation is located between the overlying Pantokrator Limestone and the underlying uppermost parts of the Pantokrator Dolomites. The formation is separated into two distinctive parts: lower and most organic-rich with >20m thickness (black shales, bituminous gray siltstone, and sandstone), and a less organic-rich upper part ~10m thick (bituminous ochre-brown dolomitic sandstone). Therefore, the total thickness appears to exceed 30 meters. However, internal deformation in both sections as well as the tectonic truncation (fault contact) allow only estimations of the original thickness, which might be even higher.

The lower parts (15–20 m) of the formation include abundant black and brown shale, whereas their abundance is reduced towards the upper parts of the formation. In one location (this is the original discovery), the top of the Pantokrator Shales is found in direct contact with the Pantokrator Limestones. A look at the formations shows that they are comprised of thin (~1 mm to ~2 cm thick) black and dark brown shale, alternating with gray dolomitic sandstone, usually in similar proportion. These mm-scale darker-lighter bed alternations might reflect annual climatic cycles, with the dark ones corresponding to more quiet sedimentation (perhaps fewer storms) and the lighter ones to more energetic events (storm season). Shale-dominated sequences as well as almost-clear-thick (~50–70 cm) black shale beds also occur. Dolomite/dolomitic sandstone-dominated sequences with sparser shale beds mainly occur towards the upper parts of the formation. Geological (Alexandridis et al., 2022a) and organic geochemical (biomarkers) evidence (Alexandridis et al., 2022b) suggests that this formation was deposited in a lagoonal setting.

This formation is important for the petroleum system of Epirus for various reasons, such as:

1) It demonstrates the higher TOC content measured in Epirus (39% wt.) while maintaining the TOC values >20% wt. throughout the entire black shale section (~20 m). The kerogen is highly oil-prone (Type I and II/IIS).
2) The lateral extent (deduced by the distance of the restricted outcrops) testifies that it is not a spatially restricted source rock.
3) Due to the high vertical and lateral extent, and the vast hydrocarbon generation potential (>270 kg HC/ton rock) it is possible that this formation is capable of producing high amounts of hydrocarbons when mature.
4) High organic sulfur content (Alexandridis et al., 2022a) suggests that this source rock is capable of generating hydrocarbons from lower thermal maturity that would normally anticipated.
5) Its efficiency as a source rock has been proven (Alexandridis et al., 2022b).
6) Geological and geochemical similarity with analogous formations in Albania and Italy imply that this formation is of regional importance, hence, it is possible to occur in other parts of the Ionian Zone as well.

5.6.2 Posidonia beds

The term "Posidonia shales" or "Posidonia beds" has been widely used to describe two shaly/cherty Jurassic formations that often bear abundant Posidonia shells. The lithological composition of the formations varies laterally and vertically. However, some lithological characteristics are common and present in many well-developed sections. The summary of these characteristics is shown in the Table 25 and is graphically illustrated in Figure 112. Moreover, characteristic field photographs are also shown in Figure 112.

Table 25. Table of the main attributes that characterize Upper and Lower Posidonia shales and are useful to their characterization.

Attribute	***Lower Posidonia***	***Upper Posidonia***
Age	Toarcian	Upper Jurassic
Thickness*	Up to 50 m	A few m to up to >100m
Dominant hue	Black, gray, blueish, brown	Ochre, reddish, red-brown
Lithology	**Lower part:** black, gray, blue, brown shale, often carbonaceous banks, often fissile. Large and small Posidonia shells. In some sections the base consists of brown marl. In other sections the base contains conglomerate beds and mélange. **Middlemost part:** dark-colored shales, thin and sparce black chert beds, carbonate banks. **Upper part:** Black bedded chert, limestone and shale beds.	Most sections are dominated by alterations of bedded chert and (mainly) silicified shale and siltstone. Limestone beds are frequent. Clay beds occur in some sections. No, significant lithological vertical changes occur in the same section. Angular limestone fragments in some sections, and ferromanganese nodules rarely. Upper Posidonia lithologically resembles the Vigla shales.
Fossils	Posidonia (1mm-4cm across), Ammonites (and aptychi)	Posidonia (rarely below 1 cm across)
Distribution	Restricted in subbasins of few km wide	Regional extent at various thicknesses, local absence
*Outcrop thicknesses		

As the organic geochemical results of the Rock-Eval 6 analysis suggest, the outcrops of Upper Posidonia do not show any petroleum potential. On the other hand, recent outcrop studies (Alexandridis et al., 2021a) and limited data from this study indicate that the lower Posidonia shows good to very good petroleum potential. The lack of detectable organic carbon in Upper Posidonia might be attributed to the lithological composition. More specifically, it is possible that the chert abundancy that demonstrates brittle behavior when stressed has aided the oxidation of the OM by the circulation of meteoric water that has deeply weathered the formation. This might also be applied to the Vigla shales, which have a similar lithological composition to the Upper Posidonia shales. This consideration might partially explain the discrepancy in the OM content in outcrops and wells. Organic geochemical analyses in wells (Rigakis, 1999) indicate that the Upper Posidonia and the Vigla shales contain high amounts of TOC, mainly type II oil-prone kerogen, in high thicknesses in some locations.

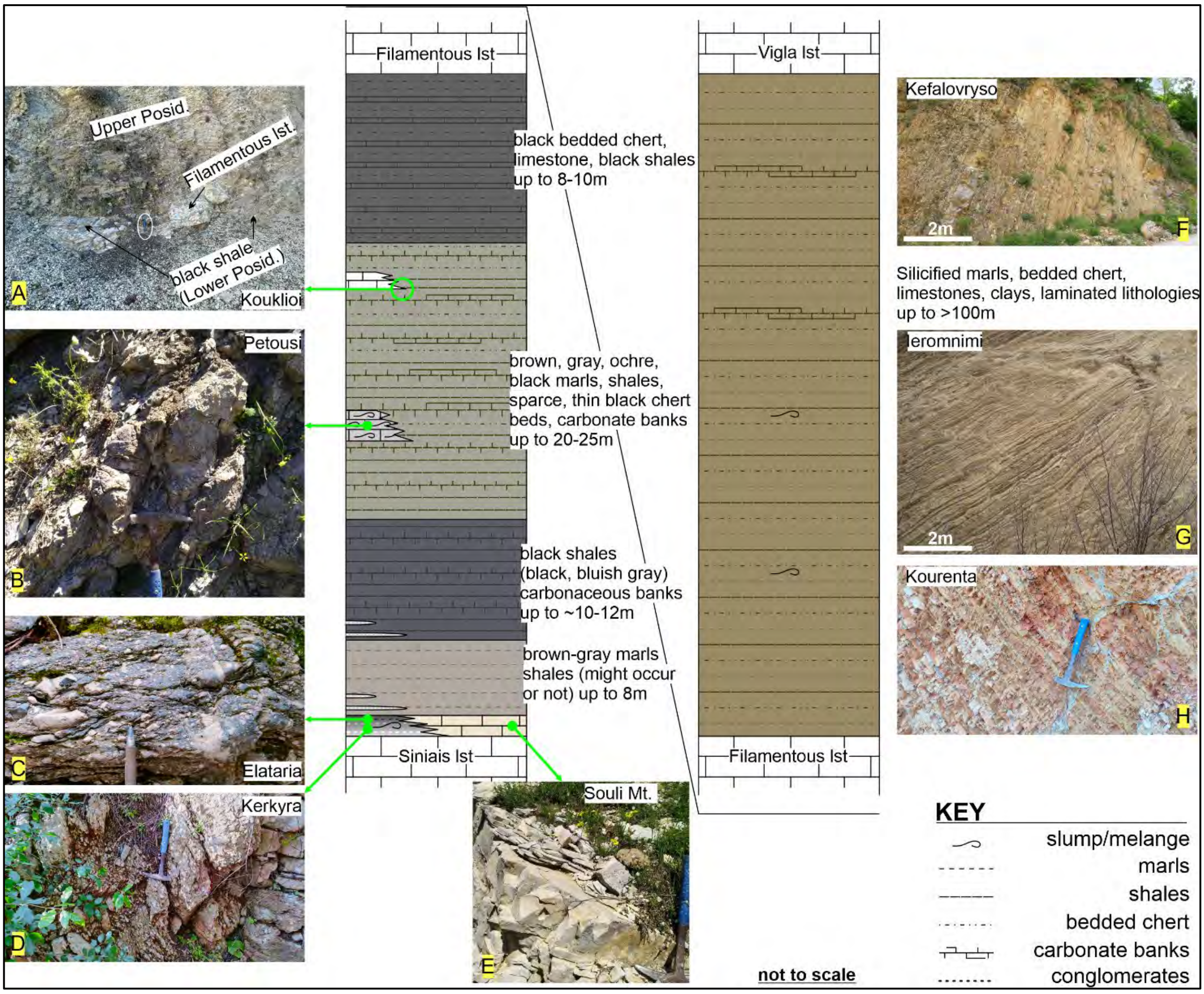

Figure 118. Detailed description and comparison between the Lower and Upper Posidonia Beds. Chromatic palette aims to reflect the true basic colors and hues of the formations in the field. Details of the lithostratigraphy are shown in outcrop photos.

5.6.3 Vigla Shale

The Vigla Shales designation has been given to a thinly-bedded formation consisting of limestone, chert, clay, and shale that lies in the uppermost stratigraphic levels of the Vigla Limestones. The exact stratigraphic position within the Vigla Limestones varies greatly among various sections, even at short distances (see paragraph "Pentolakkos Section" in § 5.1.2). It usually appears a few meters below the base of the Senonian Limestones, whereas in some sections it is ~1 m below the Senonian (e.g., Pentolakkos), and in others it appears 100's of m below the Senonian. The thickness varies from a few meters up to ~50–60 m (e.g., in the Elataria, Kastri, and Krania sections). The formation laterally pinches out in some sections (e.g., Thesprotiko MT). In other sections (e.g., Mitsikeli Mt.), the formation is represented by tens of meters of thin and occasionally laminated limestone with interbedded chert and clay/shale, demonstrating no obvious prominent source rock characteristics such as bitumen odor, dark colors, and clay content. Although several samples were obtained from eight sections, only one section (south of Elataria village) showed some noteworthy petroleum potential up to 8.34 mg HC/g rock (Table).

The results of the formation mapping are shown in the map in Figure 113. The mapping was tentatively performed on a 1:10.000 scale by integrating satellite imagery and field observations.

The depositional setting reconstruction of the Sh.V. is highly risky to be performed as the supportive geological observations per possible scenario vary. For example, in the Kourenta Mt. area, Sh.V. reaches a significant thickness (>45m) over thick undifferentiated Posidonia shales. This implies that the thickness of both might coincide. On the other hand, in the Thesprotiko Mountain area, thick Sh.V. is not accompanied by thick Posidonia beds. Observations like these could be attributed to numerous explanatory basin configuration scenarios. For instance, thick Sh.V was deposited in depocenters, implying that depocenters changed through time.

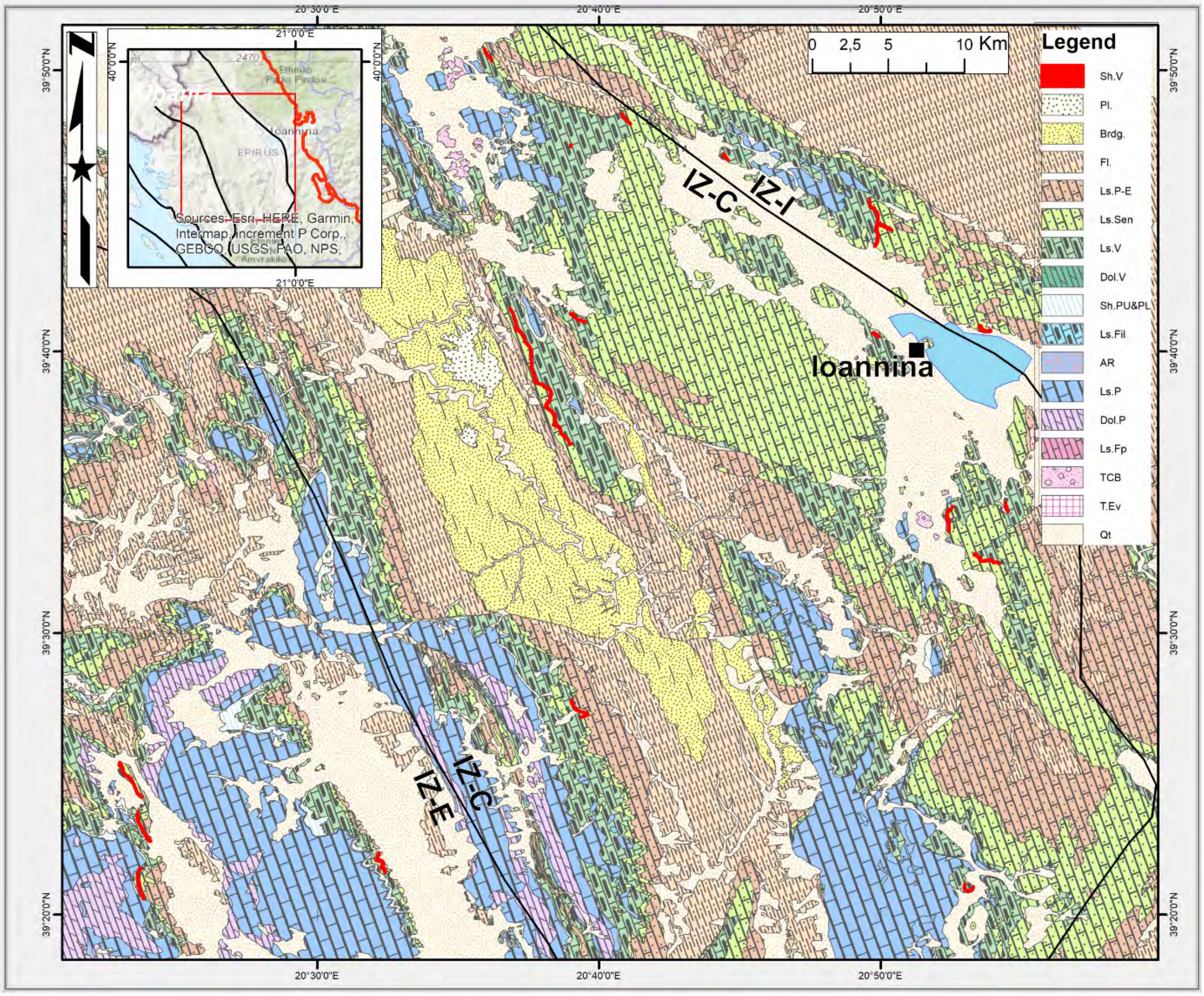

Figure 119. Vigla Shale (tentative) mapping (red traces).

5.6.4 Organic-rich carbonates within Triassic Collapse Breccia

Triassic shallow-water and evaporite deposits are associated with important SR formations in Italy, Albania, and Greece. Specifically for Greece, the occurrence of organic-rich shale fragments within TCB is known from the Dimitra-1 exploration well (Karakitsios and Rigakis, 1996) nearby Kalpaki town. However, during the present study, an organic-rich carbonate clast was obtained between the Teriahi and Stavrodromi villages, approximately in the center of the extensive TCB Fm. (Figure 114), which is roughly exposed among the Delvinaki, Ktismata, and Argyrochori villages nearby the Greek-Albanian borders.

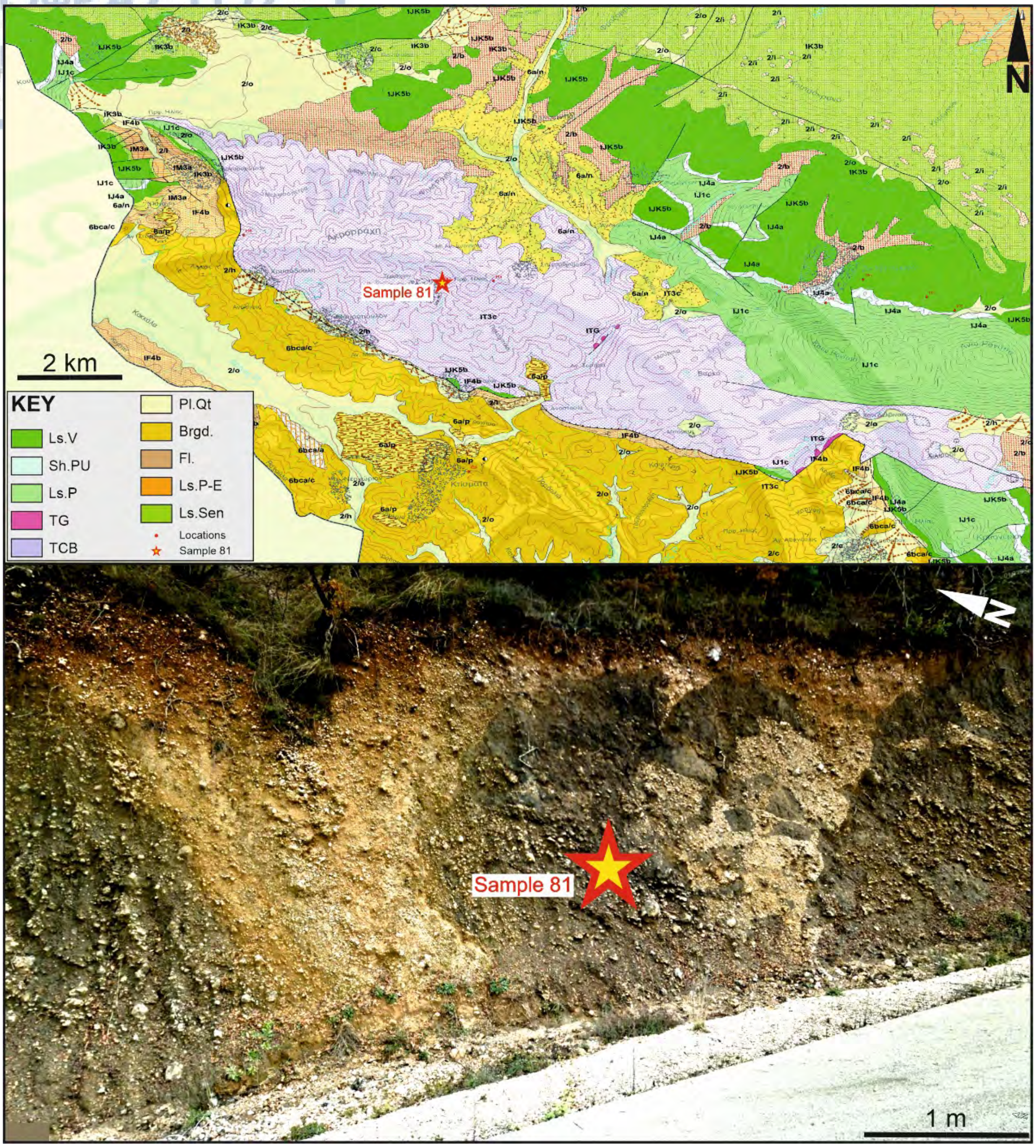

Figure 120. Geological map (part of "Tsamandas" sheet, 1:50.000, IGME) of the broader area of the extensive TCB outcrops. The sample 81 location is annotated with the red-yellow star. The field photograph shows the actual outcrop where the sample 81 was obtained. Notice the sharp contacts between the dolomitic breccia (light-colored) and the bituminous carbonate breccia (dark-colored), as well as the structureless blend of the two lithologies.

The organic geochemical and organic petrographical analyses show an oil-prone SR. The RE6 results show a fair petroleum potential with TOC content at 0.85 wt.%, HI at 442, and a generation potential (S1+S2) at 4.01 mg HC/g rock. The Tmax at 417 ^{o}C, together with the green shades of the alginite in the coal petrography examination, points to an immature SR.

The coal-petrographic examination showed a very well-sorted, densely packed, silt-sized carbonate particle matrix. The grain contacts are mostly concavo-convex and sutured. Fractured grains are also observed. Pyrite is abundant in framboidals and in large aggregates. Possible organo-mineralic aggregates are also observed. Alginite particles are generally as small and sparse as bitumens. Indications of oil are abundant.

Oil likely migrated before the intense diapiric movements brecciated the formation. This is because if the oil migration had taken place later, then probably all the tectonic breccia elements would have oil stains and dark colors, or the light and dark colored lithologies would not be chaotically intermixed.

5.7 Salt tectonics – Salt thermal effect

The presence of salt layer(s) in a stratigraphic sequence has the potential to affect basin evolution in numerous manners (e.g., depositional patterns, heat flow distribution); hence, it can affect the evolution of the petroleum system. The occurrence of a thick salt sequence (i.e., Triassic Evaporite Fm.) is well known in Epirus, both in wells and outcrops. Therefore, in order to provide a geological explanatory context to the new field observations and laboratory results showing unexpected discrepancies, considering them in the established basin evolutionary scheme (i.e., the immature kerogen in the TCB sample), various conceptual salt models were developed.

Unweathered evaporite outcrops are predominantly represented by gypsum with sparse carbonate and shale fragments. On the contrary, gypsum is in subordinate proportion in the subsurface (Nikolaou, 1986), where halite and anhydrite dominate. Gypsum abundance on the surface likely indicates hydration of the anhydrite (gypsification) by meteoric waters. This process results in a 61% volume increase. Confined in the surrounding rocks, excessive volume coupled with the increased fluidity of the damp gypsum might intensify diapiric movements and amplify diapir-related structures. On the other hand, any volume decrease related to the dehydration of any gypsum after deposition might have an important influence on the evaporite formation structure and internal deformation.

Caution is needed in the application of the salt tectonic models to the geology of Epirus. This is because the knowledge of the Triassic evaporites is limited, concerning the lithological assemblages and their spatial distribution.

Alexandridis et al. (2020 proposed a simple, first-order new tentative conceptual salt tectonic model for the Epirus (Figure). The model was based on field observations such as the multiple generations of breccia, the thickness of formations, and the occurrence of interbedded evaporites within the Jurassic. Also, it was based on the discovery of immature kerogen within Triassic Collapse Breccia. Concerning that, and given that simulations suggested that Triassic should be mature to overmature, the following question emerged· How did this sample escaped oil window?

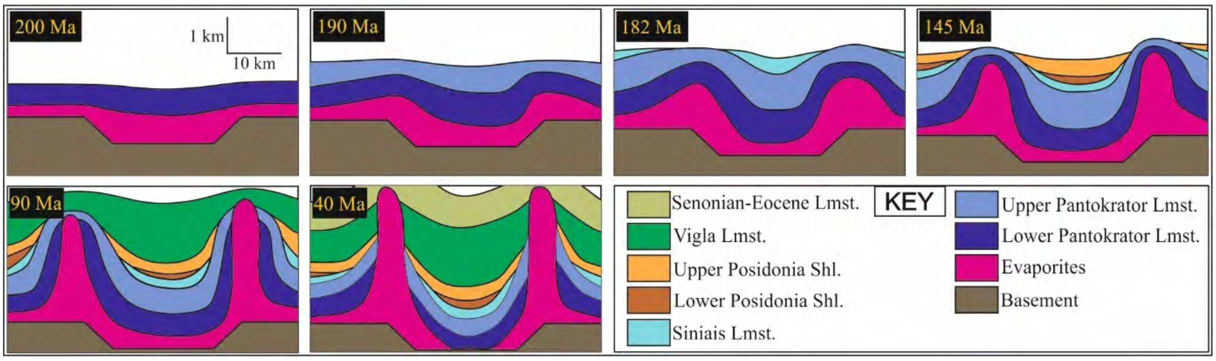

Figure 121. A first-order approximative conceptual salt-tectonic model for the Ionian Zone in Epirus (adopted from Alexandridis et al., 2020).

Fitting all these observations into the explanatory context required to question the classic simple evolutionary model, i.e., the rift model. Hence, it was proposed that many of the tectonostratigraphic elements could be controlled by early salt movements (e.g., inflations, withdrawals, and expulsions). This model can work independently and describe the majority of the tectonostratigraphic observations, but it can also work coupled to the rift model, providing a more pragmatic approach to basin evolution understanding.

5.8 Controls on the Ionian Zone structural style

The general structural outline of the Ionian Zone in Epirus is characterized by the westward thrust and the eastward back-thrust mass movements. The main mechanically weak layer that decouples the deformation below and above it is the Triassic salt layer.

Surface expressions of the thrusts exist in the uplifted areas in the form of NW-SE and NNW-SSE trending hill ranges. These geomorphological features demonstrate a slope inclination asymmetry, with the west-facing slopes being much steeper than the east-facing ones, reflecting the structure of asymmetrical folds related to thrusting. On the other hand, these geomorphological and structural features related to back thrusts show the opposite asymmetry (Figure 116). Therefore, mountain and hill range geomorphological profiles can be used as proxies for thrust- and back-thrust-impacted areas. In this manner, blind thrusts and back thrusts can be concluded, and their edges can be extrapolated further than the surface mapping.

Blind thrusts and back-thrusts can also be inferred by large-scale folds developed within thrust sheets (or between successive thrusts and back-thrusts) as well as from the earthquake foci and focal mechanisms. The fold direction (or the axial surface dip direction) can also be kinematically associated with thrusts and back-thrusts. This relation is evident in several locations where the associated strata maintain the associated folding along the prolongation of the strike of the fault for many kilometers away from the surficial tip of the thrust or back thrust.

The thickness variations of the supra-salt formations are evident when correlating lithological columns throughout Epirus and building cross-sections. However, the factors controlling the magnitude and distribution of these variations may vary among areas and within each formation.

In particular, Pantokrator Limestone Fm. is the first supra-salt formation that fully outcrops in many sections; hence, the lithostratigraphic correlation can be performed with a high degree of confidence. This formation demonstrates important thickness variations over short distances of a few km, especially in the broader area of Souli and Paramythia Mts.

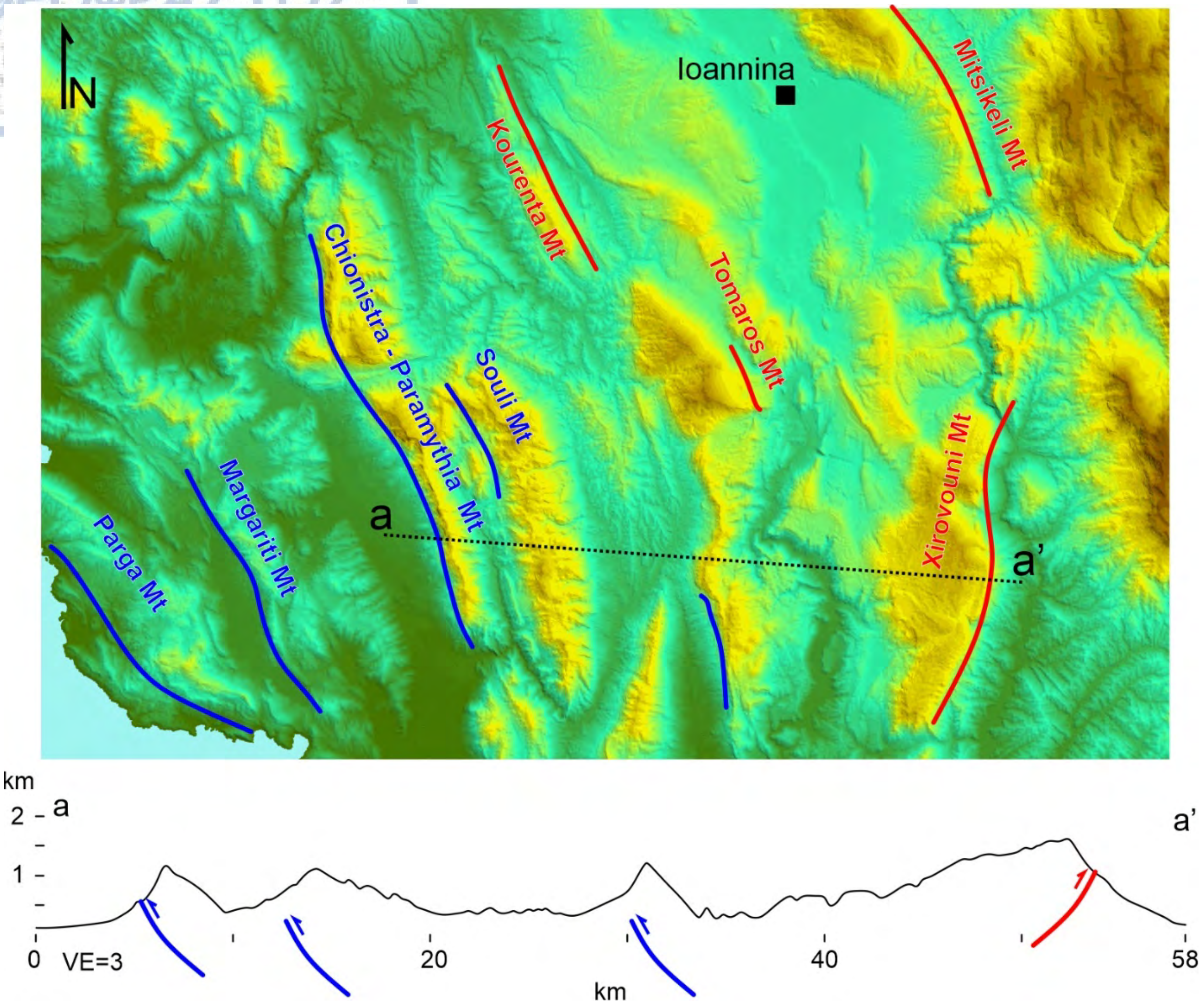

Figure 122. DEM model map with the thrusts (blue lines) and the back-thrusts (red lines) annotated. The a-a' morphological section is vertically exaggerated by 3 times. Positions of thrusts, blind thrusts and back thrusts are shown on the morphological profile.

In this area, the maximum limestone thickness exceeds 600 m in the backlimb area of a thrust-related anticline, whereas the minimum thickness is ~60 m in the forelimb area, less than 2 km away. These variations could be attributed to three main possible factors:

a) Early (late Triassic–early Jurassic) salt movements resulting in salt culminations (domes) and depressions This could have resulted in thicker sequences in the depression areas and thinner sequences in the culmination areas. The thick Pantokrator Limestone part in the area appears to be mainly of margin and slope facies (Belemnite rostra, slump folds).

b) Late Triassic–early Jurassic rift-related depressions and highs This could have resulted in thicker sequences in the tectonic depressions and thinner sequences in the elevated parts of the fault blocks.

c) Variations in the dolomitization level and the associated differences in the mechanical and rheological properties.

All three factors are capable of impacting the structural style in the following manners:

a) The thrust development during Tertiary collision would have “preferred” the *minimum energy path* namely cutting through the thin instead of the thick carbonate successions. Moreover, faults developed on the hinges of the salt anticlines, might reactivated during compression as reverse faults.

Hence, it is suggested that the evaporites and the associated collapse breccia at the soles of the thrust sheets, might have originated from such anticline structures.

b) The Souli-Paramythia thrust sheet and the associated anticlinal large-scale structures demonstrate important structural arrangement variations. These characteristic intra-sheet structures are revealing of the regional stratigraphic and tectonic components.

It is suggested that the highly folded zone in the “Paramythia-Souli North” cross-section originates (at least partially) from the restraining bend of the Petousi strike-slip fault in the area between Pardalitsa and Valanidia villages.

5.9 Discussion of the Rock Eval results

Within the study area, 13 sub-areas (Figure 107, Table 26) have been distinguished in order for the RE6 results to be evaluated on a local basis. This is because tectonic segregation of the Ionian Zone by the Tertiary thrusts produced individual thrust sheets demonstrating lithostratigraphic differences. It is possible that the thrusts represent reactivated extensive faults, occasionally active during Mesozoic-Cenozoic sedimentation, hence being capable of significantly affecting the lithostratigraphy and subsequent thermal evolution. This is quite evident in some sections, such as the Thesprotiko Mt, which is analyzed and reconstructed in §5.1.2.7. Therefore, these 13 sub-areas likely encompass comparable RE6 parameters.

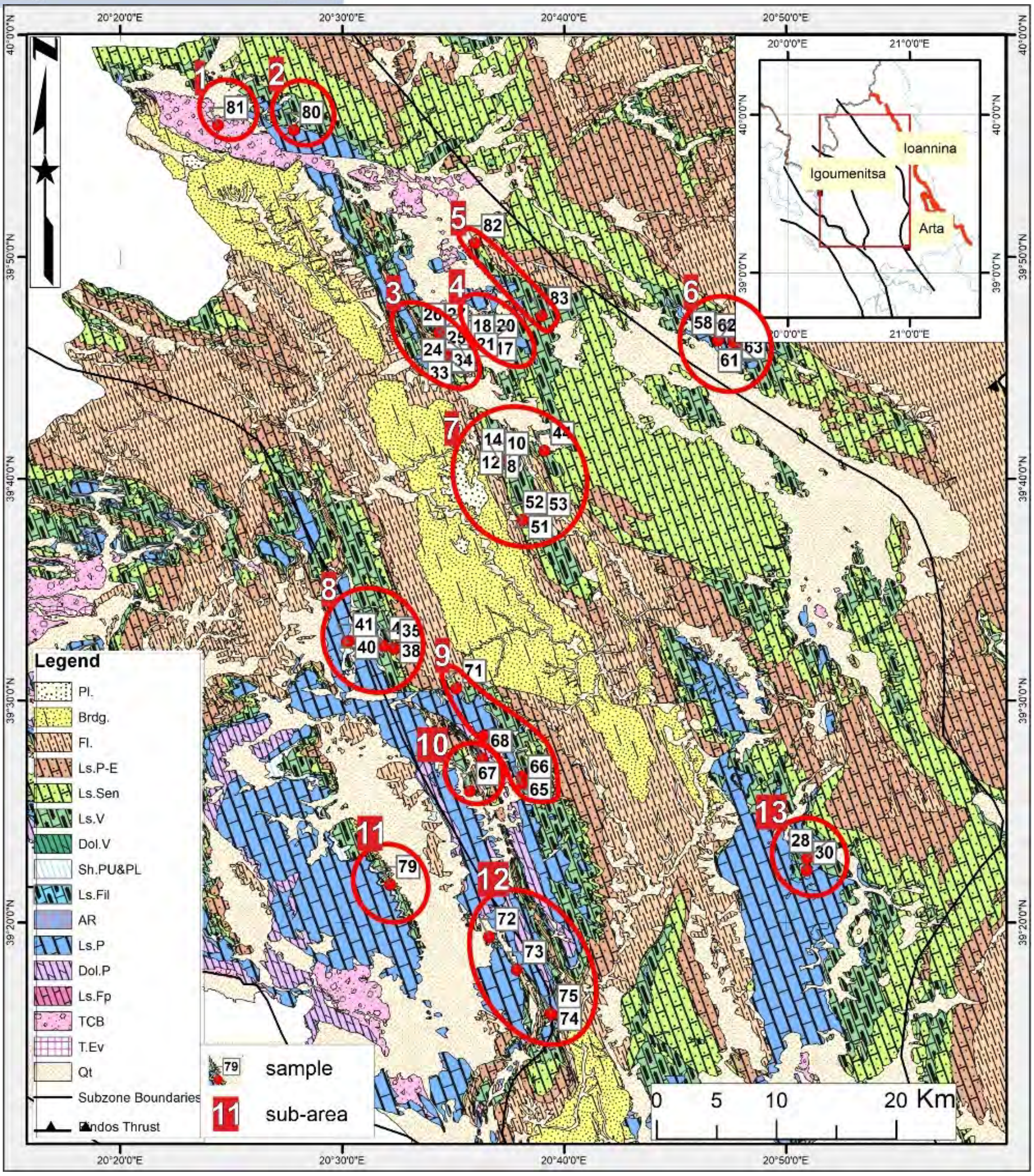

Figure 123. Subareas (1-13) for evaluation of the RE6 results in a local basis.

Table 26. Table of the sub-areas with the associated samples.

Sub-Area	***Name***	***Sample(s)***
1	Stavrodromi	81 (TCB)
2	Delvinaki	80 (Sh.PU)
3	Ieromnimi-Kastri	24, 25, 26, 27 (Sh.PU) - 33, 34 (Sh.V)
4	Vasilopoulo	17, 18 (Sh. PU) - Ls.Fil (20) - 21, 22, 23 (Sh.V)
5	Vrondismeni	82, 83 (Sh.V)
6	Mitsikeli	58, 61, 62, 63, 64 (Sh.PU)
7	Kourenta	8, 9, 10, 44, 51, 52 (Sh.V) - 12, 14, 53 (Sh. PU)
8	Chionistra	35, 36, 37, 38 (Sh.V) - 40, 41, 42 (Sh. PU)
9	Souli Mt (north)	65, 66 (Sh. PU) - 70A, 70B (Sh. P)
10	Frosyni	67, 68 (Sh. PU)
11	Skandalo	79 (Sh.PU)
12	Souli Mt (south)	72, 73 ,74, 75 (Sh. PU)
13	Kouklesi	28, 30 (Sh. PU)

5.9.1 Sub-area 1 (Stavrodromi)

Sub-area 1 is located within an extensive diapir where TCB dominates the lithology. The sample no. 81 was obtained from dark-colored bituminous carbonate clasts which are chaotically incorporated within light-colored dolomitic breccia. Rock-Eval 6 results indicate that the sample contains a fair amount of TOC (0.85%). The kerogen is immature based both on Tmax (417 ^{o}C) and organic petrography. The HI is 442 mg HC/g TOC. Tmax and HI point to a thermally immature Type II oil-prone kerogen. Organic petrography is in agreement with this. On the other hand, according to basin modeling, Triassic kerogen is expected to be thermally mature to over-mature. Therefore, this part of the Triassic formation likely remained shallowly buried throughout the basin evolution history. This might be indicative of a long-lived, inflated salt structure such as a salt pillow or wall. The high S1/TOC ratio (0.29) suggests that the sample is contaminated with oil. This likely implies that deeper parts of the formation contain oil-prone kerogen in sufficient quantities to successfully migrate oil, and they have reached the oil window. However, given that these organic-rich intervals have likely developed in an iron-poor carbonate/evaporitic setting, they might contain a high amount of organic sulfur; therefore, it is possible to have generated oil at a lower thermal maturity than the typical oil window of 0.6%.

Interestingly, compared with the results of the extensive source rock study by Alexandridis et al. (2021a), sample no. 81 is the only Triassic sample containing immature kerogen.

5.9.2 Sub-area 2 (Delvinaki)

In this sub-area, a relatively thick (>30m) Sh.PU succession dominated by brownish marls and black bedded chert is found. A bulk sample [no. 80] of black chert and brown marl was obtained. The RE6 results indicate high oxidation (OI = 2,200), while the TOC content is very low (0.02%); therefore, the results cannot reliably characterize the HC potential of this formation in this area.

5.9.3 Sub-area 3 (Ieromnimi-Kastri)

This area is located on the east-facing slopes of Kassidiaris Mt., nearby Ieromnimi and Kastri. Six samples were obtained. Four samples were obtained from the lower 40m of the Sh.PU Fm. (no. 24, 25, 26, and 27) from favorable lithologies such as black clay and chert. Two bulk chert and shale samples were obtained from the Sh.V (no. 33 and 34). The thicknesses for both formations are particularly high in this area. The total Sh.PU exceeds 80 m, whereas the Ls.Fil apparently lacks stratigraphy in the Ieromnimi section. The lower 30–40 m of the formation appear much darker than the upper 40m.

The Sh.V. appears particularly well-developed in two shaly/cherty intervals. The lower is ~10m and the upper ~30m thick, separated by a ~15m thick, thin-bedded cherty limestone. The sample no. 33 was obtained from the lower part of the lower shale/chert interval, whereas the sample no. 34 was obtained from the lower part of the shale/chert upper interval (Figure 118).

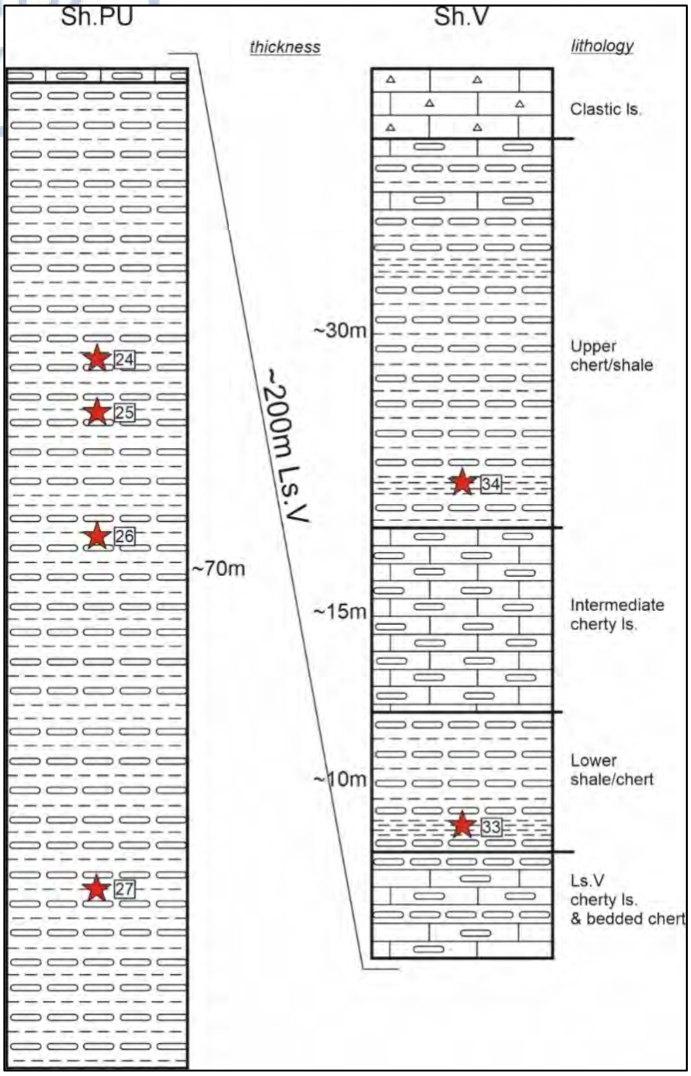

Figure 124. Detailed stratigraphic columns of the Upper Posidonia Beds (Sh.PU) in the area of Ieromnimi and Vigla Shale (Sh.V) in the area of Kastri. Red stars represent the sample levels. Sample Id numbers are annotated.

The RE results for the Sh.V cannot reliably characterize the formation in this location as the TOC is very low (0.02% and 0.06%), the OI are very high (800 and 1,000) the Tmax values show 90°C difference (397°C and 482°C) respectively. The RE results for the Sh.PU are unreliable for the characterization of the formation in this section as the TOC is very low (0.01% to 0.02%), the OI are very high (900 to 2,200) or zero.

5.9.4 Sub-area 4 (Vasilopoulo)

The sub-area includes six samples: three from the Sh.V. (no. 21, 22, and 23) nearby Vasilopoulo and three from the Sh.PU (no. 17, 18, and 19) nearby

Lithino. The Sh.V. samples crop out at the hanging wall of the thrust of the Vigla formation over the Oligocene flysch. The three samples from the Sh.V. were obtained at three intervals with a stratigraphic span of about 2m. Sample no. 21 is from a 10 cm-thick black chert lens; sample no. 22 is from a brecciated bituminous black chert bed with a strong bitumen smell just above the fault surface; and sample no. 23 is from a thick black chert bed. The dominant lithology of the Sh.V. is the black or dark-colored bedded chert (>50% v/v) for about 15-20 m, while upwards the lithology is dominated by white limestone. Although sub-area 4 is located closely between sub-areas 3 and 5, it was separated as the organic petrography of the Sh.V. sample suggests slightly higher thermal maturity than the other outcrops. Hence, the thrust that puts the Vigla Shale over Flysch might constitute an out-of-sequence thrust. The implications for the thermal maturity of the potential SR intervals in such a structural arrangement might be substantial as the SR intervals stay subsurface longer. Moreover, the decoupling level might be the Sh.V level, which appears to be thicker in the broader area.

5.9.5 Sub-area 5 (Vrondismeni)

In the area of Vrondismeni, two samples were obtained from the Vigla Shale (n. 82 and 83), which in the area reaches a significant thickness >30 m. Promising lithologies in terms of source rock potential occur in the sections and consist of laminated marls, clays, and limestones. The distance between the two samples is ~10 km; however, both lie on a rather linear and undisrupted stringer of Vigla Shale. Both samples have very low TOC (0.04% and 0.06%, respectively). Therefore, Tmax values are not reliable.

5.9.6 Sub-area 6 (Mitsikeli)

The studied parts of the Mitsikeli mountain include the areas around the Karyes, Perivleptos, Dikorfo, Lighiades, and Mazi villages. The analyzed samples (no. 58, 61, 62, 63, and 64) were obtained from Sh.PU outcropping throughout Mitsikeli Mt. In the Karyes section, the Sh.PU lies unconformably over karstified Siniais limestones (Figure 119). The section is heavily weathered, and the collected samples eventually excluded from further analysis of their organic geochemical properties.

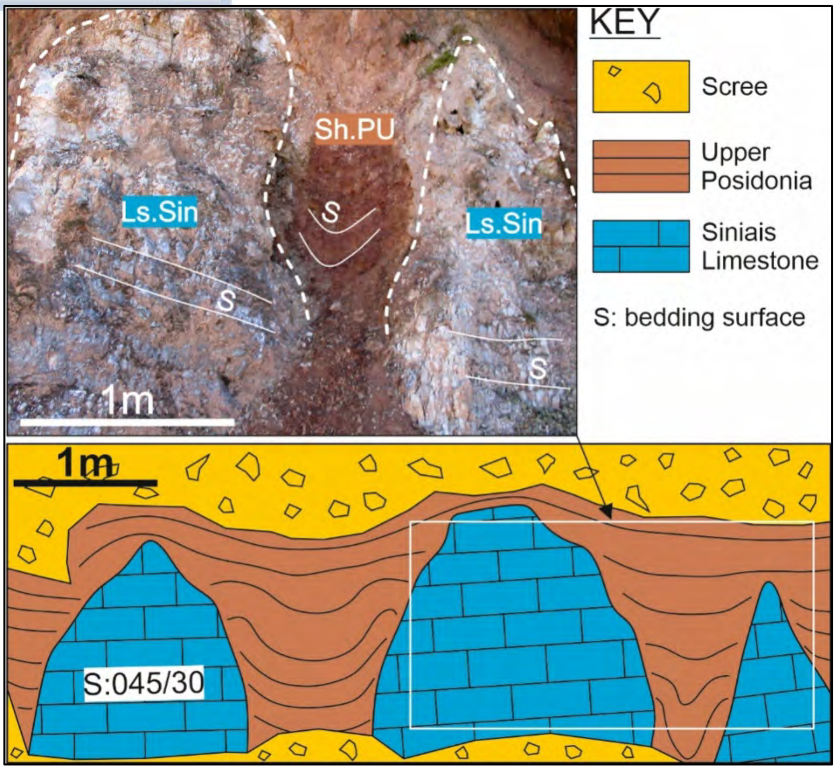

Figure 125. Field photograph and sketch of the unconformable (erosional unconformity) contact between the Upper Posidonia Beds and the karstified Siniais Limestone.

On the roadcuts from Perivleptos to "Panagia Stoupaina" monastery and later on to Dikorfo, the Sh.PU is often exposed to a great extent. However, complex tectonics with successive faults and folds did not allow for detailed stratigraphic observations.

The Rock-Eval results of the Mitsikeli area show an organic-lean source (TOC <0.1% wt.). Although Tmax temperatures show constant values (433–434 ^{o}C), the low S2 (<0.2) indicates that these values are unreliable for further evaluation (Peters, 1986).

5.9.7 Sub-area 7 (Kourenta)

Kourenta Mt. is an NNW-SSE-striking elongated hill that demonstrates important tectonic and stratigraphic characteristics. The overall structure corresponds to a back-thrust-related anticline, in whose core are exposed deeper stratigraphic formations such as the Posidonia shales and the Pantokrator limestones. However, the presence of a normal thrust (Figure 120) on the west-facing flanks of the hill range makes the determination of the main thrust dubious.

The thickness of the potential source rock formations is particularly large, well exceeding 100 m for the Sh.PU and >35m for the Sh.V. Nine samples were obtained from the area, six of them from the Vigla Shales (no. 8, 9, 10, 44, 51, and 52) and three from the Upper Posidonia Shales (no. 12, 14, and 53).

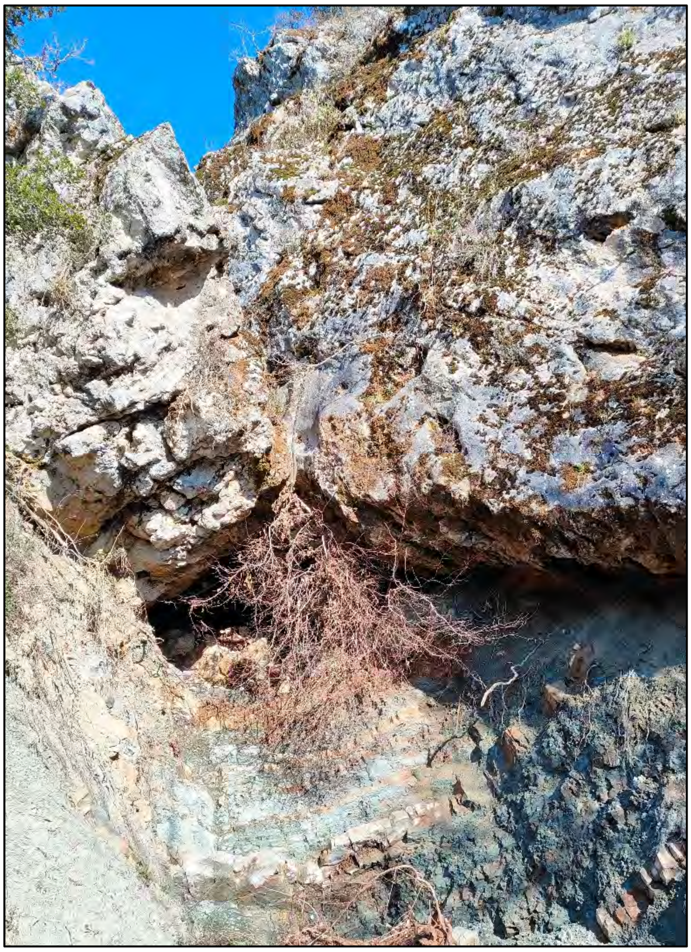

Figure 126. Eocene limestones thrusted on the Oligocene flysch nearby the old village of Giourganista (Ag. Christoforos).

All the Vigla shales samples are strongly oxidized, with OI ranging from 845 to 3700. TOC values are very low, and only two surpass the 0.1% wt. (samples 8 and 9). Tmax values are unreliable due to very low S2 (<0.2).

Samples of the Upper Posidonia shales are strongly oxidized, and the TOC values are extremely low (0.01-0.02% wt.); therefore, the results cannot characterize the formation in the area.

5.9.8 Sub-area 8 (Chionistra)

Chionistra Mt. is a very important area for the study of Jurassic and Cretaceous source rocks. This is because there are extensive outcrops of the Sh. PL, the Sh. PU, and the Sh.V.

From the Chionistra area were analyzed the samples obtained by the Vigla shales (no. 35, 36, 37, and 38) and the Upper (no. 40) and Lower Posidonia shales (no. 41 and 42). Their relative stratigraphic positions are given in the stratigraphic column in Figure 127.

The Vigla Shale samples are strongly oxidized except sample no. 38, which is the most organic-rich sample from Vigla Shale of the entire study (TOC = 2.34% wt., OI = 68, and HI = 353).

Due to the lack of filamentous limestones, the Upper and Lower Posidonia shales have been separated on a stratigraphic basis; namely, the lowest 25–30 m of the Posidonia formation were attributed to the Lower Posidonia. In the sampled section, ~10m of blueish-grayish laminated argillaceous limestone from the Lower Posidonia Beds conformably overlies the Siniais limestones (~10m thick). The next ~10m of the sequence are missing due to erosion, and the sequence continues with red siliceous silts and black bedded chert. In other well-developed sequences, chert occurs in abundance at the higher stratigraphic levels of the Lower Posidonia. Therefore, the samples taken from this level (no. 41, 42) are considered to belong to the Lower Posidonia. The Rock-Eval results suggest a poor hydrocarbon potential (TOC wt. 0.05% and 0.65%, respectively). Especially for the more organically rich sample (no. 42), the HI of 360 and the Tmax of 422 ^{o}C indicate an immature kerogen of Type II. The Tmax value is in agreement with the organic petrographic and VR% results.

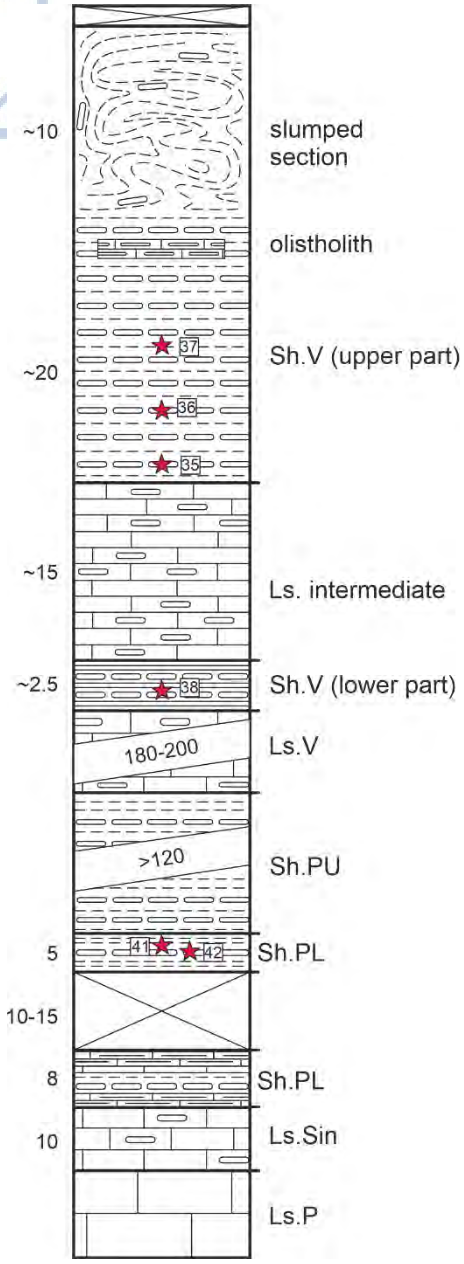

Figure 127. Stratigraphic column of the Elataria section.

5.9.9 Sub-area 9 (Souli Mt. north)

In the northern portions of Souli Mt., all the known Jurassic potential source rocks (BM, Sh. PL, and Sh.PU) are very well exposed along strike in outcrops exceeding 5 km in length. Moreover, during this study, one of the most significant potential source rocks of the Ionian Zone was discovered, i.e., the Pantokrator Shale.

Two samples were obtained from the Upper Posidonia Beds (no. 65 and 66) and two samples from the Pantokrator Shale (no. 70A and 70B).

Although the Upper Posidonia demonstrates very low TOC content (0.02 and 0.13% wt., respectively), the rest of the Rock-Eval parameters for sample no. 66 are in ranges that allow us to characterize it as reliable both in terms of result validity and usage.

On the other hand, pyrolysis results of the Pantokrator Shale indicate an excellent source rock in terms of hydrocarbon potential (TOC up to 27.1% wt., GP up to 213 g HC/kg rock), capable of generating substantial amounts of liquid hydrocarbons (HI = 790). A recent study on the sulfur speciation of the Pantokrator Shale suggested that the formation is capable of generating oil with relatively low thermal maturity in analogy with other organic sulfur-rich formations, e.g., Bazhenov Fm., Kimmeridge Clay Fm., Monterey Shale Fm., etc. (Alexandridis et al., 2022a).

5.9.10 Sub-area 10 (Frosyni)

The Frosyni area is located between Souli and Paramythia mountains. The area is well exposed in the Upper Posidonia Beds. Two samples were obtained from two locations (no. 67 and 68). The TOC content is very low (0.02% wt.) for both samples, while the OI is very high (>800). Therefore, these samples are not reliable enough to characterize the petroleum potential of the formation in this area.

5.9.11 Sub-area 11 (Skandalo)

The Skandalo area lies on the back limb of the asymmetric thrust-related anticline of the Margariti thrust sheet. The Upper Posidonia Beds are relatively thick in the area (>30 m). Only one sample was obtained from the Upper Posidonia Beds (no. 79). The TOC content is very low (0.03% wt.); therefore, this sample cannot characterize the hydrocarbon potential of the formation in this area.

5.9.12 Sub-area 12 (Souli Mt. south)

In this area, the Upper Posidonia Beds are particularly thick (>100 m). Four samples (no. 72, 73, 74, and 75) were obtained from four locations and stratigraphic levels from favorable lithologies such as black shale and black chert. All of them showed very low TOC content (0.01-0.02% wt.). Therefore, they can't characterize the hydrocarbon potential of the formation in the area.

5.9.13 Sub-area 13 (Kouklesi)

The area of Kouklesi where the outcropping Jurassic strata were studied and samples (no. 28, 30) from the Sh.PU were obtained. Both samples are located in the eastern part of the deeply eroded syncline that exposes all the Jurassic formations. The stratigraphic column includes the upper part of the Ls.P, the Ls.Pl, the AR, the Ls.Fil, the Sh.PU, and the Ls.V, whereas a small outcrop of the Ls.PL is located 1.6 km to the NW of Kouklesi.

The main remarks about the lithostratigraphy in the broader area include:

- The upper parts of the Ls.P exposed at the eastern parts demonstrate shallow neritic characteristics such as thick-shelled mollusk fauna, oolithic shoal complexes, and columnar stromatolites, while Neptunian dikes and syntaxial fiber veins occur sporadically.
- In one location, the exposed contact between the Ls.P and the overlying Ls.Pl is substantiated at an angle of ~85o–90o. In this contact area, there are no outcropping Upper or Lower Posidonia shales and cherts. The lithological transition from Ls.Pl. towards Ls.V. is very gradual, and no apparent contact or boundary is observed between the two formations.
- The Sh.PU is found in direct contact with Ls.P. at the eastern part of the syncline, whereas at the western part, the sedimentary succession involves the AR overlined by Ls.Fil and Sh.PU. Sh.PL also occurs in one spatially restricted outcrop.
- The thickness of the syn-rift formations increases westward.

- Large angular blocks (m3-volume) and smaller pebble-to-cobble-sized angular fragments from the Sl.Pl are found within Sh.PU.
- Ferromanganese and polymetallic nodules occur within Sh.PU.
- Ammonite and belemnite casts occur at the western part of the anticline at the AR stratigraphic level.

The Kouklesi area lithostratigraphy likely assimilates the proposed basin evolution scheme presented in the §6.9.4 about the Pliensbachian-Tithonian tectonosedimentary basin evolution. The eastern flanks of the syncline likely represents the structurally elevated parts of a half-graben whereas the western parts experienced gradual tectonic subsidence. The large Ls.Pl blocks likely represent the talus-like deposits nearby the base of tectonic escarpment(s). The western termination of the syncline is substantiated by an anticline. This anticline marks an abrupt transition in the sedimentation as the syn-rift lithologies represented only by the Sh.PU. This anticline might be attributed to a reactivated half-graben fault. However, farther to the east of the anticline, the syn-rift basin deepening direction is opposite than in Kouklesi and the formation geometry is mirror image. This likely eventually indicates that the basin geometry was not solely attributed to domino fault block half-grabens, but also horst-and-graben or even salt-related inflations. Polymetallic nodules likely indicate a very intense basin deepening in depths likely exceeding the 3,000 m where these nodules are formed.

5.9.14 Remarks on the source rock Evaluation

During this study, it was discovered that the Pantokrator Shale contains up to 39% wt. TOC of Type I, II, and IIS highly oil-prone kerogen. This discovery has very important implications for the petroleum systems of Epirus and western Greece in general.

Moreover, during this study, a thermally immature Triassic sample was discovered. This finding might constitute a basis for the reconstruction of the Triassic source rocks. It has also contributed to the conceptualization of the salt tectonic model for the Epirus.

The samples from the Vigla Shale (n = 17) showed some interesting results, but only in the area of Elataria.

The samples of the Upper Posidonia Beds (n = 28) show no hydrocarbon potential.

One of the two samples of the Lower Posidonia Beds showed some interesting results; however, the sample number is very low for any implication to be made.

This study showed that the Upper Posidonia Beds, which are widely considered one of the most important source rocks, have no hydrocarbon potential. However, since the OI was systematically extremely high, it should be considered whether these results reflect the heavy oxidation of the organic matter in depths of at least 30 cm (the maximum sampling depth). The same applies for the majority of the Vigla Shale samples that demonstrate almost identical macroscopic lithological assemblages with the Upper Posidonia Beds.

Moreover, it appears that surficial conditions might not intensively alter the shaly formations (i.e., Pantokrator Shale). This might occur because fracturing in these formations is significantly less intense than in the siliceous and cherty formations (e.g., Vigla Shale and Upper Posidonia).

5.9.15 RE6 cross-plots

Pyrolysis results were plotted on cross-plots of i) HI *vs.* OI, ii) S1 *vs.* TOC, iii) HI *vs.* Tmax and iv) S2 *vs.* TOC in order to evaluate the kerogen type, maturity and source richness (Figure 122).

In order for the evaluation to be meaningful and reliable, several samples were screened-out. The remaining 17 samples (Table 27) include: a) the 6 samples with the highest TOC content and generally reliable results (no. 22, 38, 42, 70A, 70B and 81), b) samples with low TOC but with T_{max} around the expected (~420-435^{o}C range) and relatively low OI (not heavily oxidized), and c) samples from specific areas that show strong consistency of some of their values (i.e., the samples no. 61 to 64 from the Mitsikeli Mt that all show T_{max} 433-434^{o}C).

From these 17 samples, 13 were plotted on the HI/OI cross plot (Figure 122A), as the rest 4 have an OI > 200 (fall outside the plot boundaries). Moreover, of these 13 samples, 8 were plotted with filled symbols (reliable to characterize the kerogen type) and 5 with hollow symbols (unreliable to characterize the kerogen type). 12 out of the 17 samples plotted on the S1/TOC (Figure 122B) are all considered reliable in terms of determining whether their free hydrocarbons are indigenous or not. All 51 samples were plotted on the HI/Tmax plot (Figure 122ºC). Only 10 of them were plotted with a filled symbol, as they are considered reliable to characterize the kerogen type and thermal maturity of their formations. All 51 samples were plotted on the S2/TOC with HI diagram, all with the filled symbol, as they reliably reflect the sample status in terms of hydrocarbon potential at the sampling locations and depths.

Table 27. Table of 17, tentatively reliable samples selected for the cross-plots of Figure 122 A

Age	*Formation*	*location*	*ID*	*Qty*	*S1*	*S2*	*Tmax*	*S3CO*	*S3*	*TOC*	*HI*	*OI*	*S1/TOC*
Aptian-Turonian	*Vigla Shale*	#28	21	59	0.02	0.34	429	0.07	0.42	0.16	212	262	0.13
		#28	22	61	0.03	2.62	419	0.07	0.35	0.59	444	59	0.05
		#28	23	58	0.01	0.11	428	0.01	0.06	0.08	138	75	0.13
		#57	38	61	0.07	8.27	422	0.5	1.6	2.34	353	68	0.03
Oxfordian-Tithonian	*Upper Posidonia Beds*	#26	17	60	0.02	0.22	418	0.14	0.74	0.18	122	411	0.11
		#112	58	59	0.02	0.08	433	0.02	0.18	0.04	200	450	0.50
		#116	61	59	0	0.07	434	0.01	0.15	0.06	117	250	0
		#116	62	60	0	0.09	434	0.02	0.14	0.05	180	280	0
		#116	63	60	0.01	0.08	433	0.02	0.2	0.08	100	250	0.13
		#117	64	59	0.02	0.1	433	0.02	0.15	0.05	200	300	0.40
		#132	66	60	0.01	0.5	431	0.03	0.13	0.13	385	100	0.08
Toarcian-Aalenian	*Lower Posidonia Beds*	#60	42	58	0.1	2.34	422	0.1	0.24	0.65	360	37	0.15
		#59	41	60	0.01	0.1	426	0.03	0.15	0.05	200	300	
Pliensbachian	*Siniais Limestone*	#27	20	58	0.02	0.88	424	0.01	0.08	0.08	1100	100	0.25
Rhaetian-Hettangian	*Pantokrator Shale*	#144	70A	26	2.14	211.06	417	3.98	11.44	27.1	790	43	0.08
		#144	70B	24	2.15	170.11	417	2.98	8.53	22.93	773	39	0.09
Triassic	*Triassic collapse breccia*	#196	81	61	0.25	3.76	417	0.04	0.26	0.85	442	31	0.29

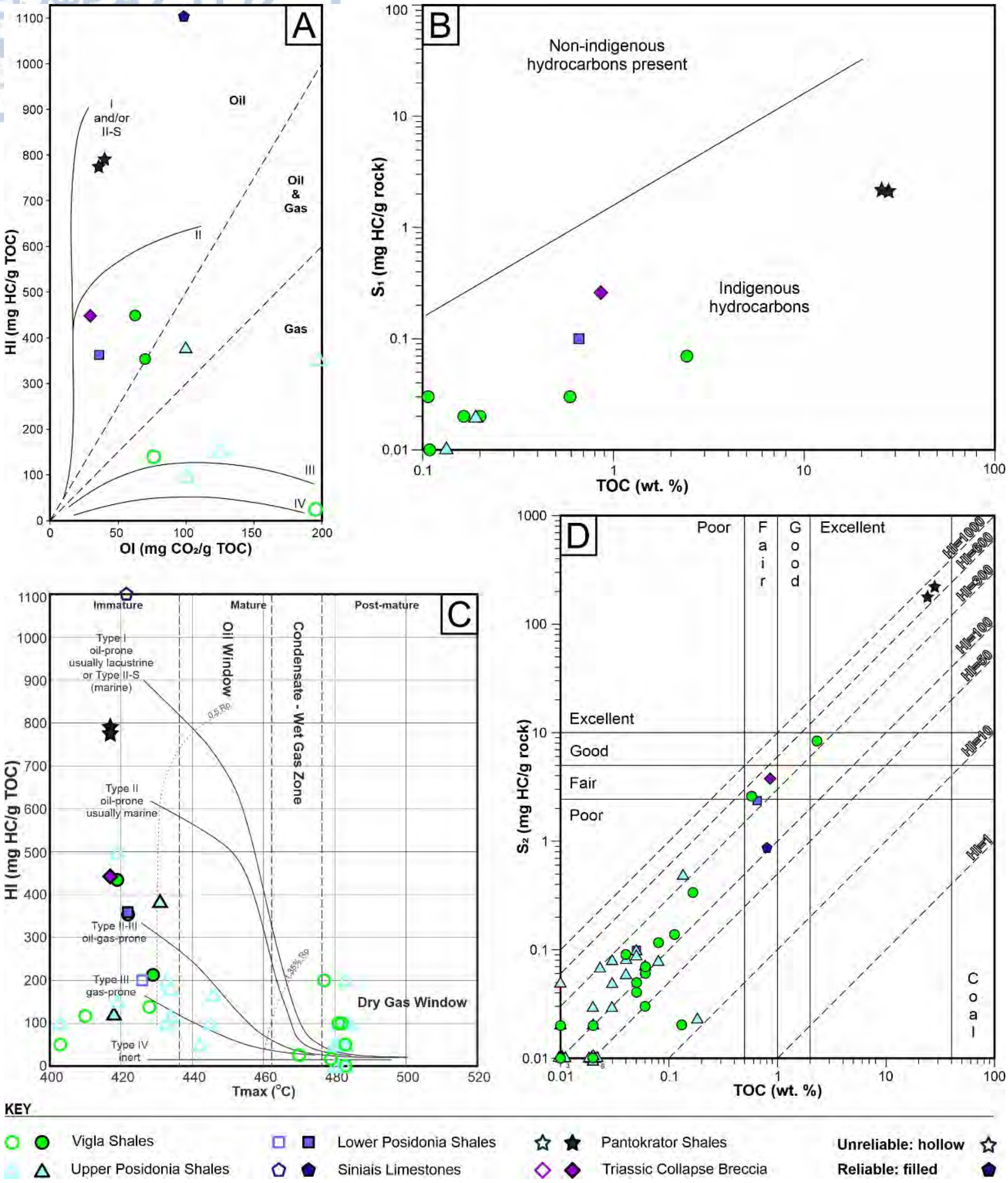

Figure 128. A-D) Cross plots of pyrolysis results and calculated parameters. Notice the color/shape coding; green circles: Vigla Shale, azure triangles: Upper Posidonia Beds, blue squares: Lower Posidonia Beds, deep blue pentagons: Siniais Limestone, black stars: Pantokrator Shale and purple diamond: Triassic Collapse Breccia. A) HI vs. OI cross-plot, B) S_1 vs. TOC cross-plot, C) HI vs. T_{max} cross-plot, D) S_2 vs. cross-plot.

5.10 Anoxic Conditions

Oxygen-depleted conditions at the bottom of the water column are arguably the most important control factor for organic matter preservation in the sediments below it. Anoxia in a mass of water can be attributed to several possible reasons. Demaison and Moore (1980) proposed four types of anoxic settings based on modern analogs. Potential source rocks in Epirus show that anoxic conditions were established locally at specific time intervals. Pantokrator Shale was shown (Alexandridis et al., 2022b) to have been deposited under strongly reducing and euxinic conditions in a restricted shallow basin (lagoon). Lower Posidonia Beds were shown (Alexandridis et al., 2022b) to have been deposited in deeper water in reducing and occasionally euxinic, silled basins.

5.11 Heat Flow Evolution Estimations

Utilizing the lithostratigraphic and structural information into a potential conceptual explanatory context concerning the heat flow evolution within the basin, provides valuable insights in HC exploration.

The basic geological information employed in the proposed conceptual heat flow model for the IZ (Figure 123) is summarized as follows:

1) The Lower-Middle Triassic rifting event and the associated elevated heat flow is inferred by the regional geotectonic models which suggest that a rift phase occurred in the region during at this time resulting in half-graben faulted block geometries that infilled with thick sedimentary successions. The majority of the geotectonic models suggest that the adjacent to the Ionian Zone (s.l.) areas were part of large passive margin. Therefore, although there are no sufficient geological data (outcrops) to support this hypothesis, the uniformity of the basin during and after this event (evaporitic basin throughout the region) may imply for the rifting scenario in Ionian region.
2) The second and main rift and associated elevated heat flow event for the Ionian Zone initiated in Pliensbachian and resulted a) in the submersion of the Ionian Zone area relatively to the astride areas that remained platform areas (i.e., Apulia, Gavrovo), and b) in the tectonism of the Ionian basin developing a persistent half-graben geometry that led in the deposition of wedge-shaped sedimentary

bodies and source rocks in the deeper anoxic/euxinic parts of silled basins. The rotated block tips emerged and eroded/karstified. This study suggests that this event ended before the late Jurassic, based on the perception of the Upper Posidonia beds to represent the first post-rift sediments. This is because this formation is developed almost uniformly throughout IZ and covers the older formations, suggesting that tectonic subsidence and faulted-block rotation generally ceased and only some block tips remained emerged or were still uplifted due to halokinesis.

3) This study suggests that a third extension and associated elevated heat flow event occurred during early Senonian. This elevated heat flow event suggestion arises from a) the widespread synsedimentary normal faulting across IZ and b) in the emersion and erosion of the astride carbonate platforms. This event accounts for the calciturbiditic and calcidebritic sedimentation occurred in Senonian and partly in Paleocene-Eocene. It was likely triggered by the slab pull of the oceanic subduction of the greater Adria plate under Eurasian plate.

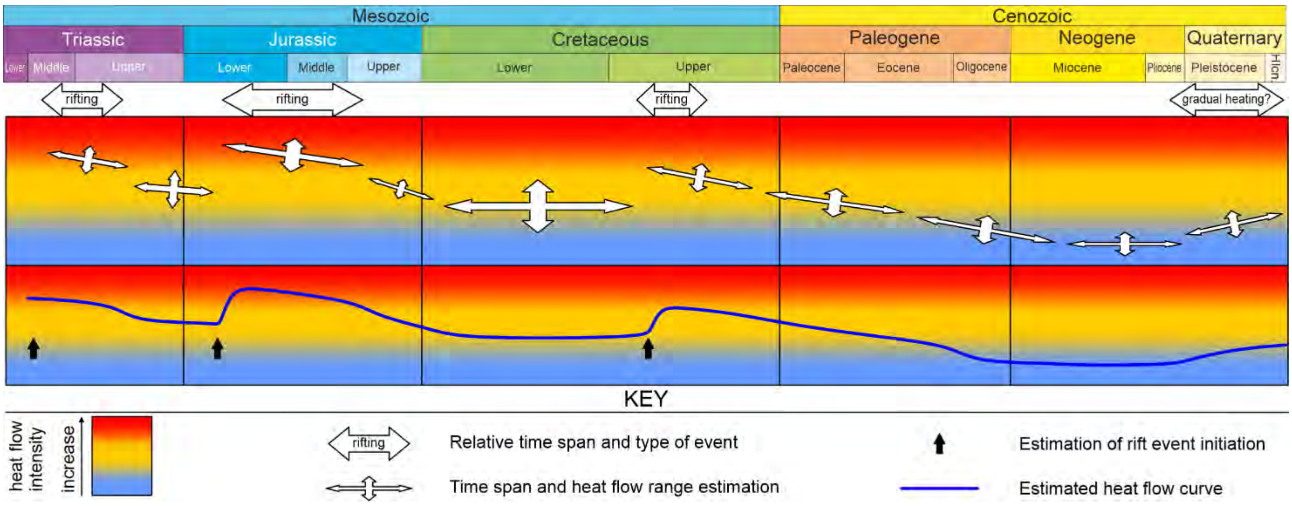

Figure 129. Heat flow evolution (Triassic-Qt) estimations based on geological observations and basin evolution reconstructions.

5.12 Petroleum Systems definition and function

5.12.1 Source Rocks

One of the outcomes of this study is the identification of two new potential SRs: the Rhaetian-Hettangian Pantokrator Shales and the organic-rich clastic-carbonate clasts within the TCB. Moreover, the Upper Posidonia Shales showed no HC potential. In the following Table 28, the SR attributes are annotated as well as a general characterization of each interval concerning its HC potentiality. The characterization is based upon organic geochemical, organic petrographic, and abundant field observations.

Table 28. Source rock potential in Epirus. Includes the findings form this study and is further enriched with the outcomes of the SR study by Alexandridis et al. (2021a).

attribute / Fm	oil	gas	thickness (m)	org. rich thickn. cumul. (m)	extent (km)
Brdg.	–	○			
Fl.gen.	–	○○	1000s	1 -10s	10s
Fl.Rad	●		200	0,5	<10
Fl.Ram	●		4	0,5	<1
Vigla Sh	●/●●		10-70	1-2	10s
Up.Posid	–	–	up to 100	–	10s
Low.Posid	●●/●●●		~30-50	~30	>10
AR	–	–	~2-10	–	
Pantkr.Sh	●●●		~30	~30	>5
TR	●●/●●●				100s

● Low oil potential
●● Good oil potential
●●● High oil potential
○ Fair gas potential
○○ Good gas potential

5.12.2 Seal Rocks

Triassic evaporites are the most efficient seal rock formation as they contain thick successions of halite and anhydrite, which demonstrate excellent sealing properties. However, the exploration risk within the evaporite series is high due to uncertainty about the potential SR extent, their thermal maturity, and the intense Cenozoic halokinesis that might affect any HC accumulation. Alternatively, flysch constitutes the main seal rock in the majority of the Albanian oil fields. Chert/shale formations (Lower and Upper Posidonia Beds, Vigla Shales) have good seal rock properties due to the high clay content. Tight limestone intervals (Lower Posidonia Beds, Vigla Limestones) might have acted as local and temporary seals prior to the development of regional tectonic fractures that diminished their seal capability.

The presence of faults within a sedimentary basin has been identified as a key risk factor concerning HC trapping, preservation, and migration, as well as during production (Knipe et al., 1997). Therefore, it is critical to calibrate in the laboratory the faults’ sealing properties to understand their hydraulic behavior in order to predict whether they act as fluid conduits or barriers.

This is more imperative in the Epirus, as it represents an area that underwent multiple or prolonged deformation stages, each capable of causing intense faulting or fracturing. Cross-sections and geophysical interpretations of the Ionian Zone show that thrust faulting (and the accompanying folding) is extensive and characterizes the overall structure. Hence, it is critical to understand the fault hydraulic behavior around possible HC accumulations (prospects) as well as their function (conduits or barriers) to the migrating HC (Yielding et al., 1997). Moreover, current thrust-related seismicity indicates extant compression, at least in some portions of Epirus and at structural levels. These recent movements are capable of modifying the pre-existing hydraulic properties along the faults. These temporally-evolved parameters should be evaluated for important, specific time intervals, e.g., during the main HC expulsion pulse or after accumulation in a trap.

Clay/shale smearing, diagenesis, cataclasis, and juxtaposition have been proposed by various authors as key mechanisms for fault sealing (e.g., Knipe, 1992). In Epirus, all of these probably occur. More detailed, shaly intervals (e.g., Sh.P., Sh.PL, Sh.PU, Sh.V., Fl.) cut by faults might provide the thin-grained material smeared between the hanging wall and footwall. Diagenesis resulting from fluid circulation through fault planes is highly likely. However, ongoing tectonism might disturb fault sealing potential formerly achieved by diagenesis, resulting in a "collapse seal" (Knipe, 1992). Field observations and cross-sections clearly show potential reservoir intervals abutting low-permeability formations. Cataclasis of the rocks astride of a fault surface can create a fault gouge, which is a fault rock with low permeability and good seal potential, especially when it involves siliciclastic formations.

Practically, these properties may spatiotemporally be altered. Hence, detailed studies are necessary to assess their barrier/conduit abilities through space and time.

5.12.3 Reservoir Rocks

The possible reservoirs should be defined with respect to the possible seal intervals and/or structures (i.e., faults). They can be further divided into two categories: those belonging to the Upper Triassic–Eocene carbonate sequence and those belonging to the Cenozoic clastic sequence (foreland flysch and piggyback molasse type deposits). For all the possible carbonate reservoirs, it is assumed that favorable places occur where the total porosity is enhanced by natural fractures (i.e., in fold hinge zones); otherwise, primary porosity and permeability are low, and they are not considered to be efficient reservoirs.

Hence, reservoirs in the carbonate series can occur at any stratigraphic level that is capped by an efficient seal interval. These possible reservoir intervals are presented in the Figure 124.

5.12.4 Overburden Rocks

According to Magoon's definition (2004), the overburden rock is defined in relation to a specific source rock. It provides the burden that compresses and buries the source rock beneath it, contributing to the thermal maturation. In this sense, the sedimentary column that overlies each source rock comprises its overburden rock, regardless of the way this column was assembled (i.e., depositionally or tectonically).

The stratigraphic column in Epirus contains six source rock intervals (e.g., Karakitsios and Rigakis, 1996; Rigakis and Karakitsios, 1998; Alexandridis et al., 2021a). Their overburden rocks are shown in Figure 124, and their thicknesses are annotated.

5.12.5 Trap Formation – Charging

Although the intense Tertiary orogenic movements have overprinted the preexisting structures, the complex tectono-sedimentary evolution of the Ionian Zone has allowed the development of various trap types throughout the basin's history. Trap structures of the pre-collisional stage have been destroyed or masked by the collisional stage compressional structures, which are currently dominant. Therefore, these older trap structures are to some degree hypothetical and/or conceptual, but nevertheless geologically pragmatic, based on well-established geological models.

5.12.6 Generation – Expulsion – Migration – Accumulation – Preservation

Several oil/bitumen surficial shows throughout Epirus prove that HCs have been generated, effectively expelled from SRs of the evaporitic-carbonate sequence and migrated up to the surface through effective migration pathways. However, it remains questionable whether these HCs accumulated in traps and were preserved there or not, and if yes, in what quantities.

Concerning preservation, it is important to understand the physical properties of the reservoir and the seal rock. That is because seal rock might a) be eroded after HC accumulation, b) not be a good gas seal (as gas is much more mobile than oil), while oil in the reservoir may thermally convert to gas (and escape or not). However, the gas/condensate Delvina field (reservoir: Senonian-Eocene lst., seal: Oligocene flysch) in southern Albania indicates that the flysch can comprise an effective seal even for the highly mobile gaseous HCs.

It should be noticed that in Plio-Pleistocene tectonic depressions (such as the Arta-Preveza basin and the Sarandaporos river area) that demonstrate high heat flow (thermal fluids), the source rock formations are expected to have reached higher thermal maturity, therefore producing lighter HCs, condensates, and thermogenic gas. Part of the HC accumulations in such reservoirs might have been thermally degraded to methane. Such processes are known to occur in the oilfields of Po Valley, northern Italy (Mattavelli et al., 1993).

5.13 Basin and Petroleum System modelling

For the basin and petroleum system modelling, it was decided to perform burial/thermal simulations for two stratigraphic columns; one in a paleo-anticline and one in a paleo-syncline position. This is because it is evident by the field work and the cross-sections and stratigraphic columns created that there “well-developed” and “condensed” stratigraphic sections due to the paleographic and paleotectonic configuration of the basin. They are named accordingly after the location name of the sections that were used for the stratigraphic columns for the simulation, i.e., the “Botsara syncline” and the “Paramythia anticline”. Moreover, two heat-flow scenarios were tested, the one with a modest rifting magnitude and the other with more intense rifting magnitude. These are the “basic” and the “hot” scenarios, respectively.

Moreover, the modelling of the source rock response in the burial/thermal evolution of the basin was based on TOC and HI values that were derived from the present study and previous studies. Two kerogen kinetic models were picked for two kerogen scenarios, this of Type II and for IIS. For the Type II kerogen was picked the “Tissot_in_Waples(1992)_TII_Crack” model and for the Type IIS kerogen the “Lewan(2002)_TII-S(MontSh)”.

For the heat flow simulation, the initial conditions for the basic scenario include a value of 2.5 of the β-factor for the crust and rifting period from the 19oMa to 160 Ma. This resulted to a peak heat flow of ~82 Mw/m^2 at 160 Ma. For the “hot” scenario, β-factor was 3.5, rifting was from 190Ma to 160Ma and the resulting peak heat flow at the 160Ma reached the 98 Mw/m^2.

In the burial plots of the Figures 130 and 131 are shown the burial, burial-thermal and burial-transformation ratio plots for the Botsara syncline and Paramythia anticline respectively.

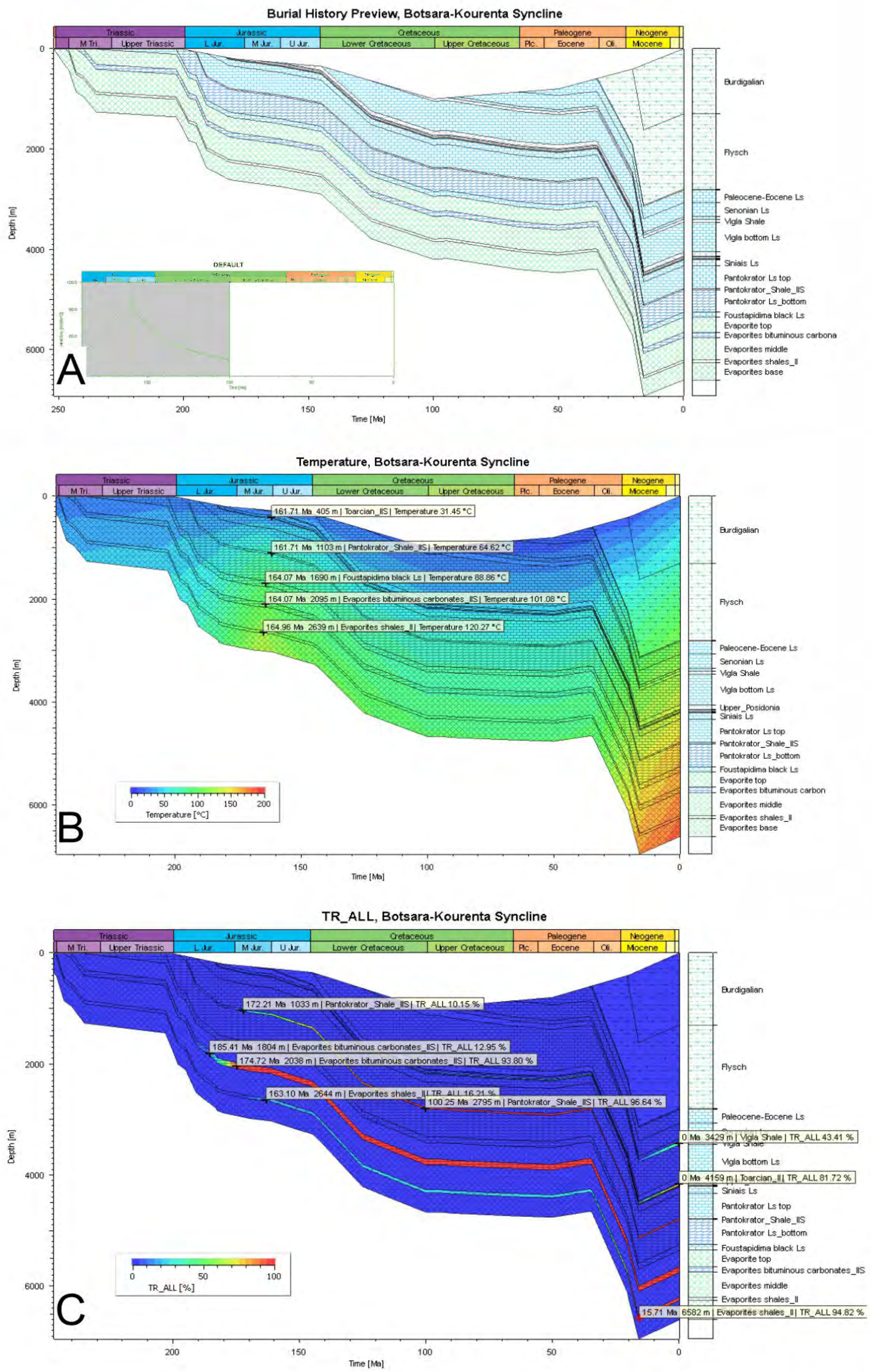

Figure 130. [A] Burial, [B] burial-thermal and [C] burial-transformation ratio plots for the Botsara syncline and the basic heat-flow scenario.

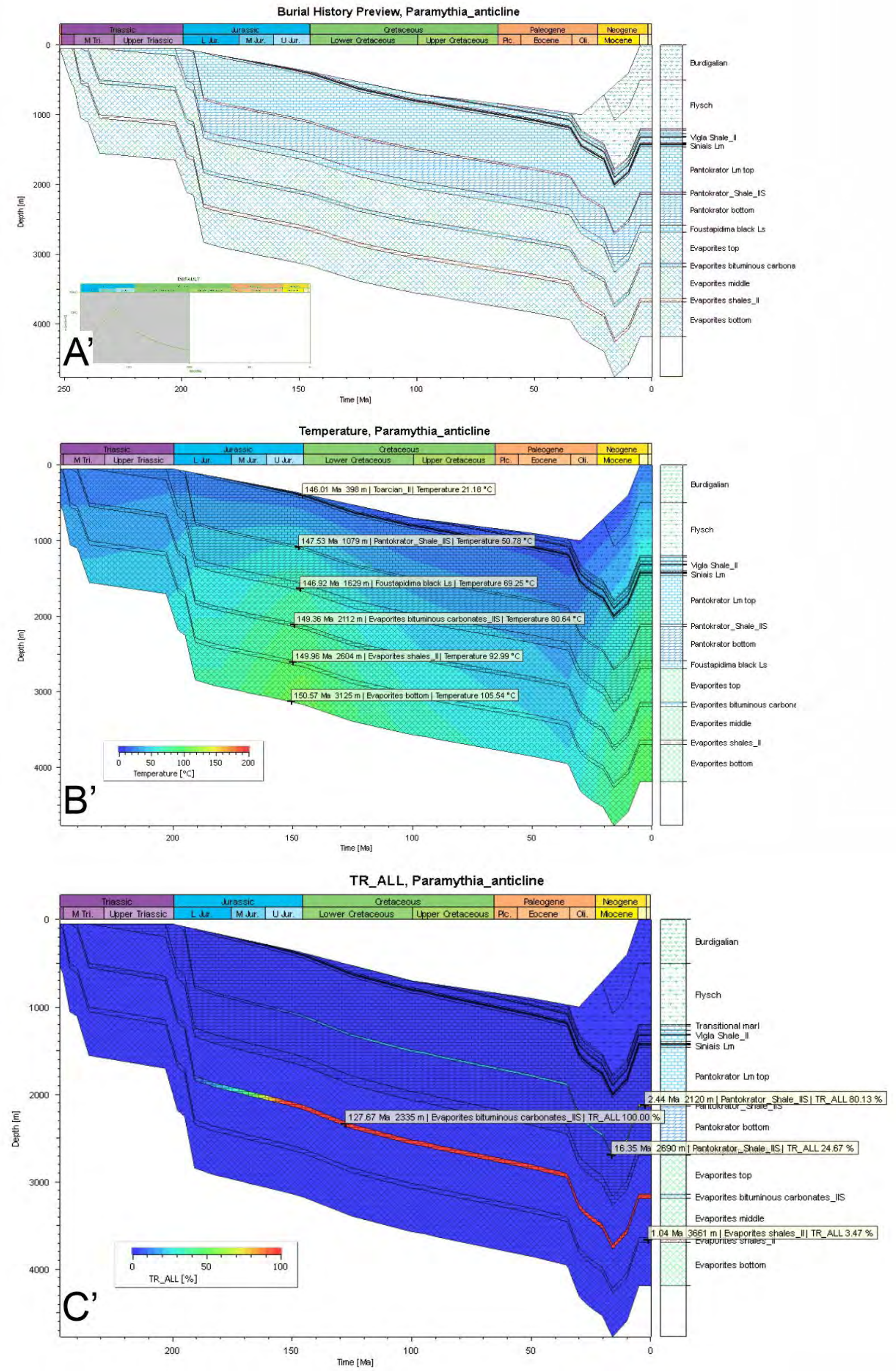

Figure 131. [A] Burial, [B] burial-thermal and [C] burial-transformation ratio plots for the Botsara syncline and the basic heat-flow scenario.

The basic comparison between the two stratigraphic column scenarios with respect to the petroleum system function is shown in the Figures 132 and 133. More specifically, in the Figure 132 is shown the transformation ratio and the vitrinite reflectance for both stratigraphic column scenarios and for the basic heat flow scenario while in the Figure 133 are shown the results for the hot scenario.

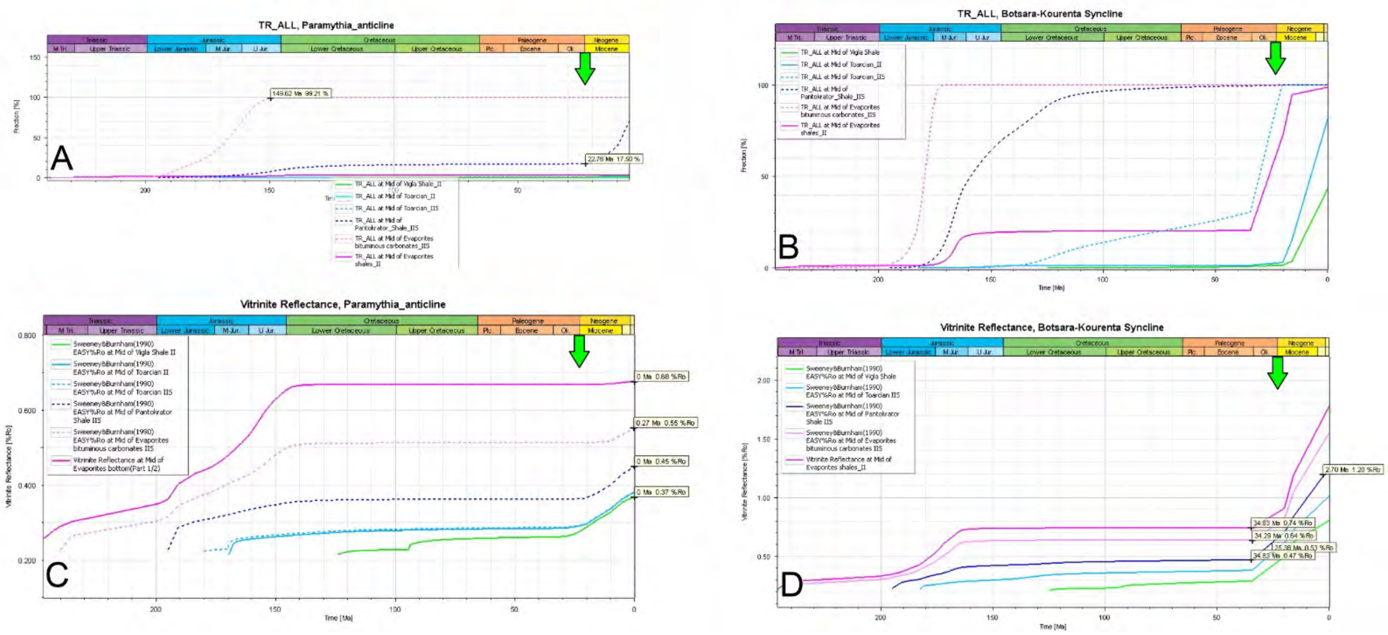

Figure 132. Basic heat flow scenario. [A], [B] Transformation ratios for the SRs in the Paramythia and Botsara columns respectively, [C], [D] Vitrinite reflectance for the SRs in the Paramythia and Botsara columns respectively. The green arrows indicate the trap formation timing (Late Oligocene – Early Miocene). Dashed lines represent the Type IIS kerogens (i.e., Upper Triassic bituminous carbonates, Pantokrator Shale and an interval of the Toarcian Shale) whereas the solid lines represent the Type II kerogen (i.e., the Triassic shales, the Toarcian Shale and the Vigla Shale). Color coding corresponds to ages (i.e., deep magenta is for the Triassic, blue shades for the Jurassic and green for the Cretaceous).

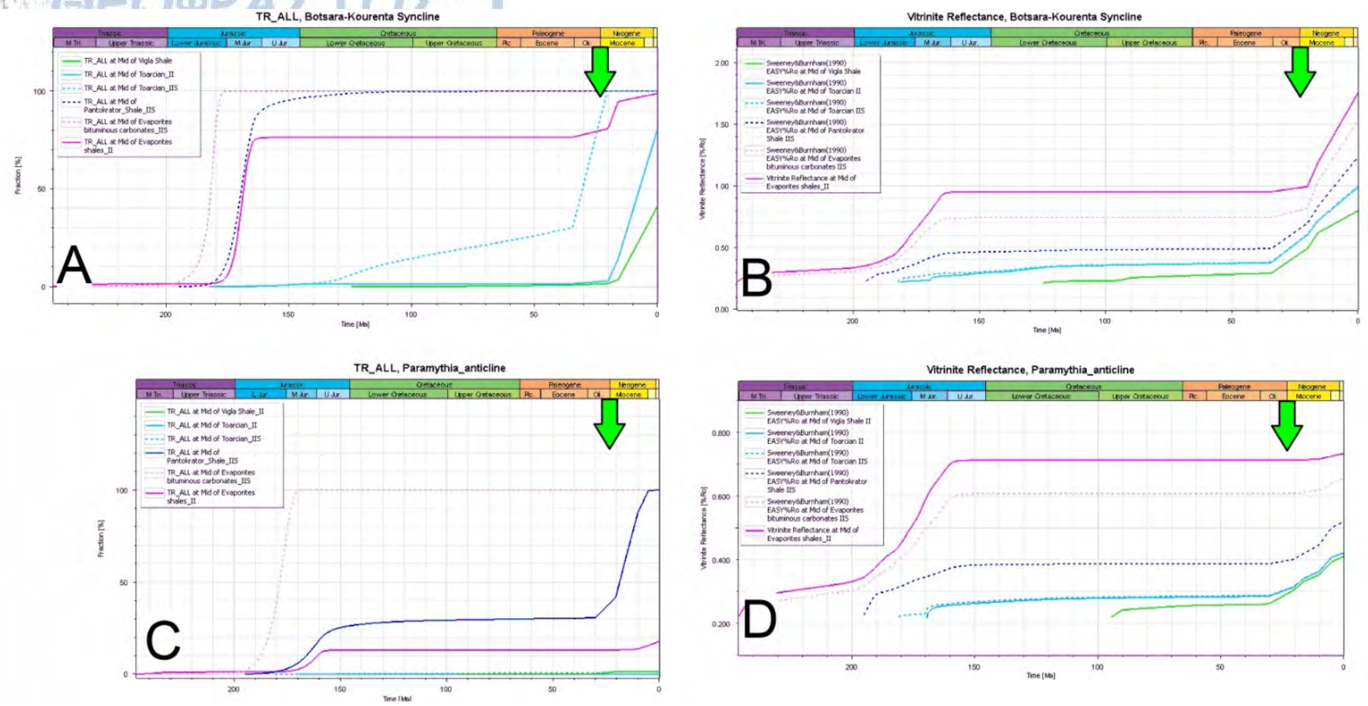

Figure 133. “Hot” heat flow scenario. [A], [C] Transformation ratios for the SRs in the Botsara and Paramythia columns respectively, [B], [D] Vitrinite reflectance for the SRs in the Botsara and Paramythia columns respectively. The green arrows indicate the trap formation timing (Late Oligocene – Early Miocene). Dashed lines represent the Type IIS kerogens (i.e., Upper Triassic bituminous carbonates, Pantokrator Shale and an interval of the Toarcian Shale) whereas the solid lines represent the Type II kerogen (i.e., the Triassic shales, the Toarcian Shale and the Vigla Shale). Color coding corresponds to ages (i.e., deep magenta is for the Triassic, blue shades for the Jurassic and green for the Cretaceous).

Evaluating the two different stratigraphic scenarios and the two heat-flow scenarios, the following remarks can be drawn:

1) The Type II Triassic kerogen might demonstrate a minor remaining potential in both Botsara’s scenarios whereas it remains at low transformation ratio in both Paramythia’s scenarios. In these low ratios it is possible that the expulsion of liquid HCs is very limited.
2) Any hydrocarbons produced from the Triassic bituminous Type IIS carbonates are not expected to have been trapped except for minor intra-evaporite stratigraphic traps. This is because this formation in all 4 combinations of scenarios (basic, hot, syncline, anticline) it has generated its HCs more than 100Ma before the main trap formation in Oligocene.
3) The Type IIs Pantokrator Shale has cannot account for any HC accumulation in both of the Botsara scenarios (basic, hot) while it has

a remaining potential in the Paramythia scenarios. Trap formation timing (Oligocene) occurred >50Ma after the burnout in Botsara scenarios.

4) The Type IIS Toarcian has a small remaining potential in Botsara's scenarios whereas remains immature in both Paramythia's scenarios.
5) The Type II Toarcian Shale generates the majority of its HCs after trap formation in both Botsara's scenarios whereas it remains immature in both Paramythia's scenarios.
6) Basin modelling indicates that some of the Triassic formations is possible to have "escaped" oil-window. This is in agreement with the discovery of the immature kerogen (i.e., sample no. 81).

5.14 Hydrocarbons in reservoirs

To estimate the likely anticipated hydrocarbon types within a reservoir interval, a number of fundamental factors are taken into account. These include the:

- kerogen type(s) in the SR intervals
- kerogen thermal maturity per SR interval
- depth of the reservoir (pressure and temperature)
- seal effectiveness
- migration VS trapping timing
- reservoir temperature (oil thermal cracking)

It is well known that some kerogen types (i.e., Types I, II, and IIS) are oil-prone, whereas others (i.e., Type III) are gas-prone. Moreover, as the kerogen matures, its structure and chemical composition change, mainly by losing hydrogen and oxygen, resulting in a relative increase in carbon. This is clearly shown in the van Krevelen diagram. This practically means that an oil-prone kerogen will peak its liquid HC production at the peak-oil stage, whereas its gas peak follows and occurs after the phase-out stage. Hence, an oil-prone kerogen becomes gas-prone after the oil peak and eventually becomes inert in the overmature stage.

It has been shown (Alexandridis et al., 2022a; 2022b) that intervals of the Sh.P., of the Sh.PL, and of the bituminous limestone above the Sh.P. contain sulfur-bonded kerogen, mainly of Type IIS. These sulfur-rich formations are known to generate and expel HCs at considerably lower thermal maturity (e.g., Kimmeridgian Clay, Monterey Shale, etc.).

The likelihood of HCs specifically associated with each one of the source rock intervals occurring within particular potential traps, as well as their types and relative abundance, is analyzed here. In order for specific HCs to be associated with a specific SR interval and occur in a specific reservoir, the HCs must have migrated after the trap formation. In Epirus, the major trap-forming process is considered the tertiary compression that created asymmetric anticlines, typically associated with thrusts and backthrusts. Additionally, the nearby Albanian analogs show that the thrust-related duplication of the stratigraphic column resulted in the development of subthrust traps sealed by flysch or by the Triassic evaporites. Another prospect type should be analogous to the Katakolon oil and gas field (discovered in 1981), where the eroded, folded pre-Neogene strata are overburdened and capped by thick Neogene clastics. This evolution leads not only to the sealing of the pre-Neogene formations but also to another generation-expulsion-migration-accumulation round. The results are schematically presented in Figure 124.

The main pairs of potential seals and the associated underlying reservoirs with the possible anticipated HC proportionate mixtures are analyzed herein:

a. R1 reservoir: Senonian-Eocene limestones (S1 seal: Oligocene flysch)

Flysch sealing efficiency, both for liquid and gaseous HCs, is proven in the nearby Albanian oil and gas fields. This is probably due to the fact that its lowest stratigraphic levels are dominated by clays, which have very low porosity and permeability, and its response to stress shows plasticity instead of fragility. This means that any fractures are healed.

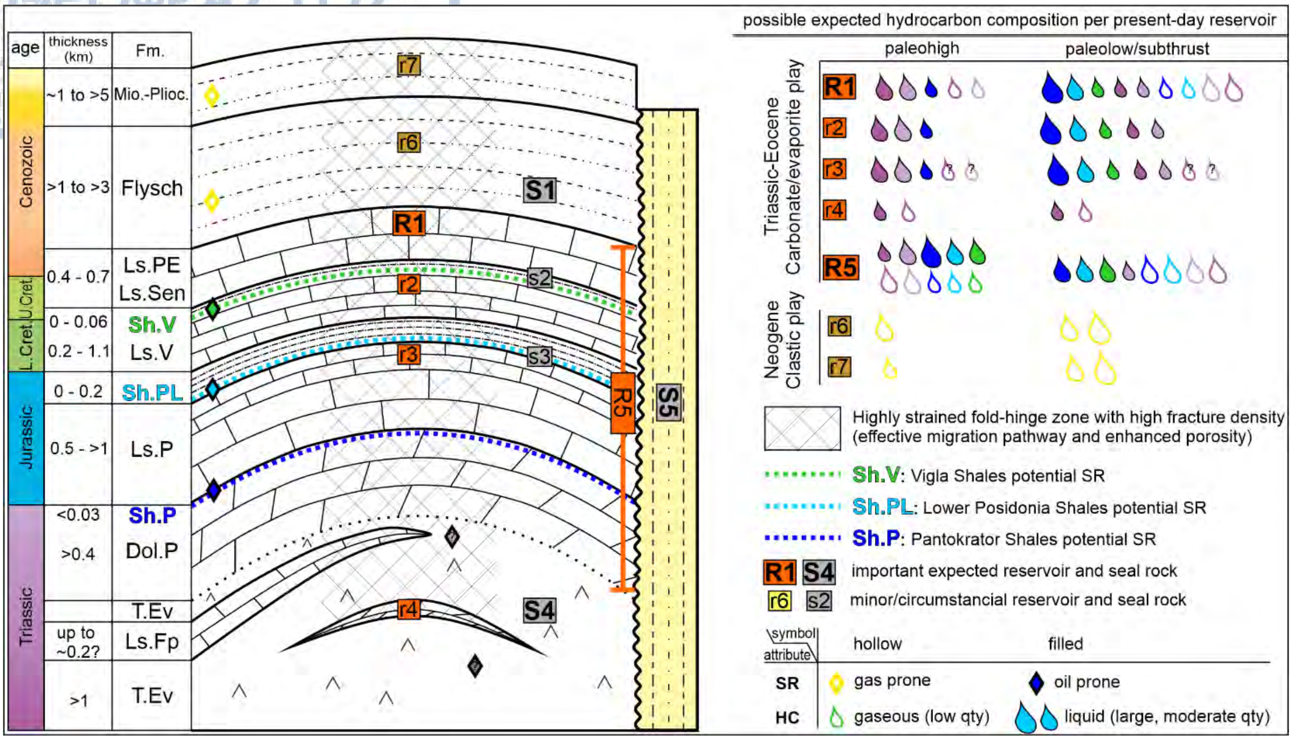

Figure 134. Conceptual model of the possible expected composition in terms of source-rock affinity of the hydrocarbons for each potential reservoir interval. R-r stands for "reservoir" major and minor respectively, S-s stands for "seal" major and minor respectively, rhombs and dashed lines symbolize source rocks. The hydrocarbons are accumulated in anticlinal traps. Color coding corresponds to the ages of each component for example, the light-purple hue drop represents oil derived from the upper Triassic source rocks.

The underlying Senonian-Eocene reservoir is efficient in terms of HC production, even though it is often silty. Naturally-induced fractures enhance the primary intergranular and moldic porosity. Due to the high lateral extent and the great thickness of both the seal and reservoir, the seal-reservoir pairs of these prospects are expected (and are concerned by the present study) to be the most efficient in the carbonate/evaporite play (Triassic–Eocene).

This regional seal is expected to have trapped both oil and gas (as it does in the Albanian oilfields) derived from all the underlying SR intervals in the case of the "paleolow" position, where the accumulated sediments reached high thickness, as well as in the subthrust plays. However, in "paleohigh" positions, the anticipated HCs likely originate from the deeper potential SRs such as Sh.P. and Triassic organic-rich intervals and not from the Sh.PL and Sh.V.

b. r2 reservoir: L. Cretaceous Vigla Limestones (s2 seal: L. Cretaceous Vigla Shales)

Vigla Shales are expected to demonstrate some sealing efficiency; however, the lateral extent, the relatively small thickness, and the high chert content (very friable) imply that this would be limited. In addition, the high lateral lithological variability makes this potential seal highly risky. The underlying micritic limestones of the Vigla Limestones Fm. are expected to have some reservoir efficiency in highly strained zones, such as in fold hinges. However, the very low primary porosity and permeability indicate that this prospect type is highly risky. Due to the anticipated low-quality sealing properties of the Vigla shales, these prospects might contain only some fair quantities of liquid HCs, as the gaseous would readily escape the trap due to their high mobility.

c. r3 reservoir: L. Jurassic Pliensbachian and/or Pantokrator Limestones (s3 seal: L. Jurassic Posidonia Shales)

It has been suggested (Alexandridis et al., 2022b) that the Lower Posidonia Shales may demonstrate sealing capabilities. This is due to the high clay content, the significant thickness (up to ~50 m), and the lateral extent that exceeds the 10km in outcrops running parallel to the orogen direction. However, the lateral extent right to the main orogenic axis is unclear. Alexandridis et al. (2022b) suggested that the origin of the solid bitumen staining the pores and fractures of an olisthostrome interbedded within the Lower Posidonia Shales originates from the Pantokrator Shales. Possible geological models explaining the bitumen staining the upper part of the formation but not the lower involve scenarios where the lower, highly clayey part acts as a local seal of anticlinal trap(s).

It is possible, though, that in areas where the lithology is dominated by silicified shales (such as in the Mavroudi section), sealing efficiency will be much lower in highly fractured zones as the shale creep rates might be substantially lower. Creeping of shale is a well-known and studied phenomenon that is associated with fracture self-healing (Cerasi et al., 2017; Rybacki et al., 2017).

The underlying Pliensbachian limestones are expected to have some reservoir potential in highly fractured zones. In areas where the Pliensbachian limestones are missing from the stratigraphy and the reservoir is the Pantokrator limestones, it is expected that the primary porosity is substantially higher. However, the secondary porosity induced by fracturing is questionably a positive factor, as the very thick beds tend to produce much sparser fractures than their thin-bedded counterparts.

In this reservoir, both liquid and gaseous HCs from various sources might be encounter. However, due to the limited thickness, the frequent facies changes, and the general tectonic strain, it is less likely for gaseous HCs to be preserved in these traps.

d. r4 reservoir: Triassic Dolomites (S4 seal: Triassic Evaporites)

Dolomite bodies incorporated within the evaporites could likely be fueled with liquid and gaseous HCs derived from the possible organic-rich intervals within the evaporitic series. Preservation of fair HC amounts is possible; however, due to the high and prolonged heating, it might contain thermogenic methane.

e. R5 reservoir: U. Triassic–Eocene carbonates (S5 seal: Plio-Pleistocene)

This prospect type is likely mainly in offshore areas where thick series of Plio-Pleistocene clastics have been accumulated after the emersion and partial erosion of the topographically high parts of thrust sheets, sealing them. Katakolon discovery (1981) and analogues in the Gulf of Valencia and in the Pannonian basin (Strata Georesearch, 2018) suggest that this play type is possible in parts of western Greece.

f. r6 reservoir: Oligocene flysch (S4 seal: Oligocene flysch ± Mio-Pliocene deposits)

Alexandridis et al. (2021a) reports Type III kerogen in the flysch. This kerogen is possible to have generated HC in the deeper parts of the Flysch FM, especially in the Epirus-Akarnania syncline or in subthrust plays. Being highly mobile, gaseous HCs might have migrated through all the flysch lithologies and accumulated in more porous lithologies (e.g., fractured sandstones). Moreover, it is possible that leakage of accumulated HCs through the lower part of the flysch has migrated to traps of adequate lithology within the flysch. Important thermogenic gas fields occur in Italy within this succession (Bertello, 2008).

g. r7 reservoir: Mio-Pliocene molassic (S4 seal: Mio-Pliocene deposits)

Thick clastic accumulations in syn- and post- main-thrusting-pulse basins may contain organic-rich intervals (Maravelis et al., 2014; Alexandridis et al., 2021a). These are capable to generate limited amounts of mainly gaseous HCs in their deepest parts. This is evident in Albania, where large oil and gas fields occur in the peri-Adriatic depression (Curi, 1993; Sejdini et al., 1994).

In summary, the main reservoir is considered the Senonian-Eocene limestones [R1], and the main seal the Oligocene flysch [S1]. The reservoirs r2 and r3 with their associated s2 and s3 seals are considered as local or circumstantial reservoirs of generally high leakage risk. The r4 reservoir is considered possible, as small amounts of oil (a few barrels) have been produced (Nikolaou, personal communication). The geological configuration for the scenario of the R5 reservoir is promising in areas with high Plio-Pleistocene sediment accumulations as they provide the overburden for a dynamic HC generation pulse in the underlying source rocks. The S4 seal is a major highly effective seal, mainly for the subthrust plays.

The R1, r4, R5, r6 and r7 are highly likely to contain gaseous HCs. This probability is lower for the r3 reservoir and even lower for the r2 reservoir. These estimations for the gas content are analogous to the sealing capacity of the associated seal rocks. These capacities are higher in the clayey and evaporitic lithologies that exhibit high self-healing rates. Liquid HCs being less mobile are possible to be found in all reservoirs of the carbonate/evaporite play; however, less possible in r2.

Concerning the petroleum types, the Type I and II/S kerogens of the Sh.P are expected to have generated amounts of waxy, naphthenic oil and gas, whereas the Type II kerogens of the Sh.PL and Sh.V are capable of generating naphthenic oil and gas. Based on the immature sample from the Triassic collapse breccia, these formations are expected to have generated naphthenic oil and gas. The sparse organic-rich intervals in the clastic sequence are expected to have generated biogenic gas and some thermogenic gas in the subthrust plays. Liquid hydrocarbons are expected to have been generated from restricted H-rich kerogens; however, migration to traps is unlikely due to the limited volumes.

Although significant gas fields occur in Italy and Albania within the Mio-Pliocene successions, current exploration status in Greece does not allow for optimistic scenarios for the clastic play. Further exploration is needed to establish the HC potential of the Greek analogs.

5.15 Migration Pathways

The cartoon of the Petroleum System in Epirus (Figure 125) demonstrates the geological and structural arrangement of the petroleum system around the critical moment. Over this conceptual model, the source rocks, reservoirs and sealing rocks are shown, as well as the migration pathways area annotated. The possible trap arrangements are coupled with the trapping/preservation risk. This is why only two reservoir/trap arrangements are promoted as possible/effective for the carbonate sequence, whereas the conceptual reservoir “r2” (see chapter 5.13) is not included in this sketch.

The basic considerations for the HC migration paths include the sealing efficiency of the Lower Posidonia Shale as well as of the thrust. Flysch seal is de-risked in this model because it comprises the main seal in numerous Albanian oilfields. No HC phase separation is applied, however, there should always be taken into account that the Posidonia shales might constitute efficient seal for heavy liquid HCs but not that efficient for gaseous HCs.

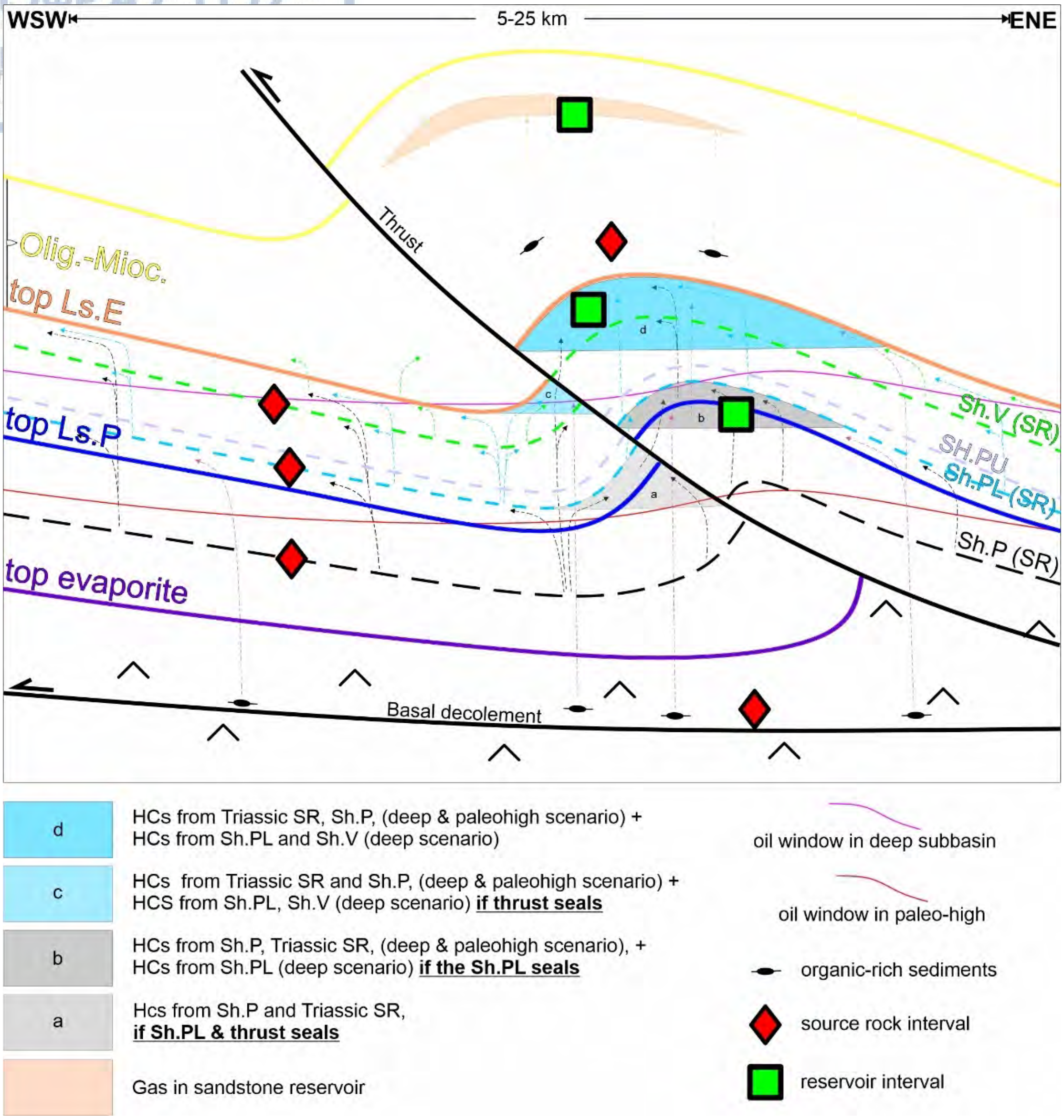

Figure 135. Petroleum System cartoon illustrating the way this study envisages the most representative tectonic and stratigraphic architecture, the petroleum system's elements and processes, as well as the migration pathways and the possible accumulation/preservation geological arrangements.

5.16 Geological and Petroleum Geological History of Epirus

In the following paragraphs, a narration of the geological evolution and the associated petroleum geology of the sedimentary basin is attempted, which is now preserved as the Ionian Zone in western Greece and southern Albania. It is presented in distinctive stages, each one corresponding to the creation or activity timeframe of a major known petroleum system element and/or process.

The name of the sedimentary basin is "Ionian Basin" and is irrelevant to the well-known, present-day Ionian Basin located in the sea area southwestern to the Greek and southeastern to the Italian peninsulas, respectively. Moreover, narration refers to the Epirus' part of the Ionian Zone/Basin.

During the Triassic, Epirus was part of the northern Gondwanan rifted passive margin. Arid conditions prevailed over an extensive peri-tidal basin setting, resulting in the deposition of a thick evaporite series in Greece, Italy, and Albania. Local variations in the basin configuration due to early rifting and seafloor spreading resulted in the deposition of lithological facies often associated with euxinic conditions and organic matter preservation in shale and carbonate rocks. Pervasive dolomitization might have also resulted in the development of intervals with reservoir potential. On top of the evaporites, a carbonate platform sequence was developed, reaching great thicknesses from the Rhaetian to the Sinemurian. The lower parts of the sequence are pervasively dolomitized, probably indicating the ongoing aridity in the broader area. Around the Triassic/Jurassic boundary, black shale was locally deposited in small, restricted basins (likely coastal lagoons) in Italy, Albania, and Greece. These deposits demonstrate the most exceptional, high-quality source rock characteristics of any other formation in the peri-Adriatic region. Moreover, vulcanization of the organic matter in a highly reducing, Fe-poor, and S-rich environment created a kerogen capable of generating liquid HC from lower thermal maturities. The overlying sequence consists mainly of shallow-water limestone, often demonstrating very high primary porosity attributed to shelly fauna; however, the very high thickness of the beds does not allow the development of a dense fracture network (secondary enhanced porosity). Nevertheless, these fractures may serve as migration conduits. In the beginning of the Pliensbachian, the deposition of micritic, cherty hemi-pelagic limestones, occasionally organic-rich, demonstrating great thickness variations throughout the basin, likely pointed to the differential subsidence of faulted blocks. Neptunian dikes and neritic limestone breccia incorporated within lime mud likely show tectonic activity (faulting). However, it is difficult to accurately constrain the basin configuration controls at this stage, as the observations can also be attributed to alternative explanations such as halokinesis, isostatic adjustments, and rapid sea-level changes. The present work suggests that all these factors combined (i.e., block faulting, halokinesis, isostacy, and sea level) controlled the basin architecture and associated depositional patterns. Subsequent Toarcian sedimentation of Ammonitico Rosso in relatively shallow water and thin-grained organic-rich clastics (Basal Marl and Lower Posidonia Shales) in the depocenters suggests erosion of adjacent land. This is further supported by the presence of abundant conifer pollen and resinite among Sh.PL macerals. Anoxic and periodically euxinic conditions were established in the silled depocenter areas, resulting in OM preservation. T-OAE might affect the water column oxygenation profile. Given that the sea level rapidly rises during this stage, the emersion of land should be attributed to the further rotation of faulted blocks, likely enhanced by evaporite movement. Evaporite mobilization during this period is likely attested by the presence of intercalated evaporites locally in the deep-water upper Liassic to middle Jurassic successions. During the late stages of the Liassic towards the middle Jurassic, shales and cherts, often organic-rich, were deposited in the depocenters, whereas in the shallower parts were successively deposited white hemi-pelagic limestone with black-bedded chert intercalated, laminar biohermal limestone with filaments, and proximal stromatolite breccia. Tightly packed, pebble-sized, rounded limestone conglomerate beds are intercalated at various levels. Upper Jurassic is marked by the relatively uniform deposition of alternating, thinly-bedded shales, silts, marls, and bedded-chert (Upper Posidonia Shales). This sequence likely corresponds to the late syn-rift to post-rift sequence, where the crustal cooling uniformly submerged the entire basin. Direct onlap of the Sh.PU and/or Vigla Limestones on top of Pantokrator Limestones shows the occurrence of areas with condensed deposition or non-deposition, reflecting the cessation of the tectonically active period. This multistage rift phase of the Triassic–Tithonian age and the Ionian basin subsidence were likely developed as an aulacogen (failed rift) branch of the localized rift that created the east Mediterranean oceanic basin. During this stage, the heat flow was likely elevated and might result in the first oil generation pulse of the deeper Triassic organic-rich intervals. From the Berriasian to the Aptian, hemi-pelagic to pelagic limestones with chert nodules and bedded-chert were almost uniformly deposited throughout the basin. Thickness variations reflect the inherited basin floor topography attributed to the former rift phase as well as the ongoing halokinesis. The establishment of local shale and chert deposition, often rich in OM, indicates the development of restricted silled depocenters during the Aptian to Cenomanian. This mild reactivation of the former rift structures is likely due to far-field stresses from the onset of the subduction system to the north (see more details). During this period, the coincidence of global ocean anoxic events (i.e., Bonarelli, Paquier, etc.) enhanced the OM preservation, which is found in well-documented thin intervals (a few cm). Ocean circulation bringing nutrient- and phosphate-rich water up to shelf break resulted in the deposition of phosphorite locally on top of the Sh.V. A few tens of meters of pelagic micritic limestone with thin-grained limestone debris, often with cross-bedding stratification. However, Sh.V. and Posidonia basin depocenters do not always coincide. This is indicative of the complex basin evolution, synchronously affected by tectonic stresses and halokinesis. A dramatic shift in sedimentation occurred in the early Senonian when massive-bedded, coarse-grained bioclastic limestone debris deposited almost uniformly throughout the basin. The transition is usually clearly evident by the occurrence of a massive bed exhibiting mechanical strength in contrast to the underlying beds. This event likely corresponds to an abrupt rift rejuvenation likely induced by the subducted northern Adria plate slab rheological interactions with the upper mantle, capable of affecting the overlying crust where Epirus was situated. Hence, it is possible for a second phase of intense heat flow to have occurred during this stage. This might have affected the entire Triassic and perhaps the Pantokrator Shales at particular favorable locations, namely at the subsequent syn-rift depocenters where accumulated sediments reached elevated thicknesses. A second oil generation phase might have occurred during this stage, from the Triassic and Sh.P. kerogen. Similar to Senonian, Paleogene and Eocene limestones are bioclastic, detrital, and frequently correspond to mass transport deposits. However, gradual clastic grain thinning (with the exception of the IZ-I, where massive beds of coarse-grained bioclastic limestone occur) and the prevalence of micritic limestone, mudstone, and thin-grained wackestone. Therefore, it is likely that after the first early Senonian paroxysmal extensional phase, tectonic intensity progressively decreased and possibly intensified in short-lived events responsible for the occasional coarse-grained clastic influx. This event lasted up to the end of the Eocene. The ongoing continental collision of the Adria plate over the Eurasian active margin placed the wider Epirus area in a foreland basin position. This basin configuration is responsible for the vast amounts of clastics (flysch) deposited in the migrating foredeep over the carbonate succession. Flysch accumulation (>2-4 km) is responsible for the rapid burial of the underlying successions, including the potential source rock intervals in greater depths where temperatures reached the oil window for the Sh.V, Sh.PL, and Sh.P and the gas window for the Triassic. This event likely accounts for the major oil accumulations of the Mesozoic period in Albania. At the same time, Flysch sealed any anticlinal structures developed by the compression. However, rapid progression of the stress front resulted in break thrusts and thrust sheet development. This affected the petroleum system in numerous ways. First, large parts of the thrust sheets escaped the oil window, and the supra-Triassic source rocks remained immature almost in all outcrops. Second, emersion resulted in erosion deep enough to destroy traps and possible HC accumulations. Third, parts of the thrusts were overridden by other thrust sheets. This implies that the SRs of the lower thrusts are in the oil window. Seismic images from Albania suggest intense thrust sheet stacking with 3 and 4 thrust sheets. These have been buried deep, up to 15km or more, surpassing the dry gas zone and reaching the anchimetamorphic zone.

5.17 Geological Risk Assessment

The assessment of geological uncertainties is the co-evaluation of numerous geological variables, aiming to forecast optimal drilling outcome scenarios by reducing the risk of geological success.

Epirus demonstrates a rather complex geological superstructure in terms of tectonic structure and stratigraphic assemblage. It has undergone composite, multistage tectonosedimentary evolution that has promoted great lateral and vertical variability of the petroleum system elements and processes. Hence, the geological evaluation and de-risking should include multiple scenarios for each play or prospect. This primarily involves the identification or occurrence of each one of these and, later on, the estimation of their effectiveness.

Epirus is a salt-based, inverted sedimentary basin that forms a fold-and-thrust belt. The spatial variability of the stratigraphic units (e.g., the regional detachment Triassic evaporite thickness and distribution, the lithostratigraphic unit thickness, and lithology variability) induce spatial structural style variability that in turn defines the structural play type. Moreover, the distribution of source, overburden, seal, and reservoir rocks, as well as tertiary thrusting, rotation, faulting, diapirism, uplift/erosion, and Neogene sedimentation, strongly control the occurrence and preservation of HCs in various trap types.

Risk mitigation also includes the evaluation of the successes and failures of the exploration drilling on a regional scale, which for Epirus are the Italian and Albanian analogs. These well-known petroliferous areas show striking similarities in lithostratigraphy, basin evolution, and deformation with Epirus. Therefore, they are used as a de-risk component, indicating that HCs have indeed been successfully entrapped in commercial quantities. Petroleum-geological characteristics for these regional analogs are provided for comparison in the next section.

5.18 Regional Analogs

The study of the petroleum geology of oil-prolific and well-explored areas adjacent to western Greece can provide a fundamental understanding of the situation in their Greek geological counterparts. Two neighboring countries display many decades of systematic exploration activities and many decades of oil production from large oil fields. These countries are Albania and Italy, whose petroleum geology and the obvious similarity with Greek petroleum geology are discussed in the next paragraphs.

5.18.1 Albania

Albania hosts several onshore oil fields, including the Patos-Marinza oil field, the largest in Europe with recoverable reserves of ~200 MMbbl of oil. The structure contains ~2 billion bbl. of oil initially in place (OIIP), being a single-phase oil HC system. It was the first oil field discovered in Albania in 1928, and it has been operating since the 1930s at low recovery rates of around 5%. The main reservoirs are six; five of them are unconsolidated sand of the Tortonian age, and one is an interval of Senonian-Eocene-age limestone. The trap structure (~5 km WSW-ENE by ~14 km NNW-SSE) is a monocline fold of late Miocene–Pliocene sediments unconformably overlying an eroded anticline of the Ionian zone carbonate succession. The primary SR is considered the Upper Triassic–Lower Cretaceous succession, and the seal rock is the Tortonian fine-grained terrigenous clastics.

Exploration activities in the Albanian part of the Ionian Zone resulted in the identification of seven (7) SR intervals spanning from the Rhaetian up to the late Miocene–Pliocene (e.g., Curi, 1993; Sejdini et al., 1994). The comparison with the SR intervals of the Greek Ionian Zone counterparts shows striking similarities between the SR stratigraphic distribution.

5.18.2 Italy

Italy demonstrates numerous oil and gas fields of various play types corresponding to different tectonic domains (Mattavelli and Novelli, 1988). Oilfields of the fold-and-thrust belt mainly host oil, whereas foreland contains thermogenic gas and the foredeep domain contains biogenic gas. The main source rocks fueling the oil fields (fold-and-thrust belt domain) are the Triassic to lowest Liassic source rocks containing Type I and II kerogen (e.g., Katz et al., 2000). Analogous to their Greek and Albanian counterparts, thin organic-rich intervals occur in the Toarcian and Lower Cretaceous. However, the Toarcian does not account for significant oil accumulations in reservoirs, whereas the Lower Cretaceous has not been correlated to any known oil accumulation. Moreover, the fold-and-thrust belt exerts thermogenic gas almost exclusively (97%). Biogenic gas is dominantly (82%) occurring in the Plio-Pleistocene foredeep deposits, originating from organic-rich beds of this age. Foreland gas is mainly biogenic, derived from the Cenozoic clastics (e.g., Bertello et al., 2010).

Chapter 6 – Conclusions

1) A new SR (Pantokrator Shale) was discovered in the area of Paramythia and Souli Mts. The organic geochemical, organic petrographic and geological (i.e., thickness, extent) characteristics suggest that it is an important source rock in terms of generation potential and defines a new petroleum system for the Ionian Zone. The comparison of the geological and geochemical characteristics with time-equivalent formations in Albania and Italy suggests that this formation even though restricted in sparce subbasins, plays a critical role in the petroleum systems of the peri-Adriatic region. Therefore, its discovery in Greece, strengthens the overall SR potential HC performance of Epirus and, by extension, western Greece.
2) The Rock Eval and organic petrographic results show that the dispersed organic matter is particularly abundant in the Pantokrator Shale, whereas in the other potential SR formations (i.e., Lower Posidonia Shale, Vigla Shale, Triassic) although present, it is in much lower abundance. Additionally, the bitumen yield of the Lower Posidonia Shale is well below of that of the Pantokrator Shale. All these results suggest that the Most prolific, oil-prone potential SR in Epirus is the newly discovered Pantokrator Shale.
3) The Rock Eval and organic petrographic results show that the outcrops of the Mesozoic source rocks are below oil window.
4) Based on the organic geochemical, organic petrographic and biomarker data, the kerogen Type of a) the Pantokrator Shale is I, II and IIS and the Lower Posidonia Shale is II, IIS and II/III. This shows that the IIS kerogen-dominated intervals of these formations can be early-oil generators (i.e., generate HCs at Tmax<430°C or VR%<0.6). Hence, HCs have been generated from such intervals before their uplifting. Hydrocarbons are expected to be generated in deeper parts of the basins.
5) The presence of the immature kerogen (Tmax=417°C, vivid green, fluorescent maceral hues) in a sample from the TCB Fm. (no. 81),

contradicting to every other Triassic sample analyzed in Alexandridis et al., 2021a, indicates a different thermal evolution for the Triassic of this area. This observation in addition to the lateral variation of the supra-salt formation thickness implies that synsedimentary diapiric salt movements resulted in the “escape” of parts of the evaporites from the oil window. Therefore, a first-order, conceptual salt tectonic-model suggesting early salt movements was developed, providing an explanatory context for the immature Triassic kerogen and other geological observations.

6) Numerous geological observations resulted to the suggestion of a new basal heat flow scheme for the Ionian Zone in Epirus. This scheme suggests that the area experienced a) a first elevated heat flow phase during the middle Triassic rift phase that is known to have affected the northern Gondwana passive margin, b) the second and dominant heat flow pulse associated with the Jurassic rifting that ceased before the Upper Jurassic and c) a possible third, weaker heat flow pulse of during the early Senonian associated to the extensional tectonics of that time.
7) Numerous field observations (e.g., lithology, bedding, sedimentary features, contacts) of the lithostratigraphic units resulted to a new, detailed lithostratigraphic column that includes a) the new formation of the Pantokrator Shale, b) detailed dolomitizations level per each Ionian sub-zone, c) details of the Toarcian-Tithonian formations, d) a stratigraphic position for the Foustapidima limestones, e) details of the Vigla Shale lithostratigraphy, f) the Triassic salt piercement up to Burdigalian level, g) an observation limit of the lithostratigraphic units exposure in outcrops, h) depositional environments, i) detailed stratigraphic columns of the two most important source rocks (i.e., Pantokrator Shale and Lower Posidonia Shale) and j) sedimentary features per lithostratigraphic unit.
8) A rock strength profile is proposed for the IZ in Epirus and the potential detachment levels are shown in two classes; the potentially regional decollement intervals and the potentially local ones.

9) This study differentiated the Lower Posidonia Shale and the Upper Posidonia Shale in terms of lithology and Rock Eval properties. According to this, the general lithostratigraphic characteristics for the Lower Posidonia Shale demonstrate that this formation is generally silica-poor and clay-rich in the lower third of the formation, it contains high amounts of type II, II/III and IIS kerogen and its color shades are among black, gray and blueish. The Upper Posidonia Shale lithology is dominated by chert beds, silicified marls and limestones while the shales are much less frequent and of red/brown color shades. No HC potential detected in this formation during this study.

10) Detailed depositional environment models were developed for the lithostratigraphic units from Triassic to Eocene, utilizing the numerous lithological observations. Especially for the Pliensbachian-Tithonian interval, the reconstruction showed that the interplay between tectonic subsidence, faulted block rotation and global sea-level fluctuation defines the rather complex lithostratigraphy of this interval.

11) Biomarker results were utilized conjointly with geological observations, for depositional setting reconstructions. In this way, the reconstructed depositional setting model of the Pantokrator Shale shows deposition in a lagoon with strongly stratified brackish water column where specialized sulfur bacteria (*chlorobiaceae*) were thrived, executing photosynthesis in a strongly euxinic, low dynamic, photic zone. For the Lower Posidonia Shale, the conditions appear anoxic and periodically euxinic, the salinity was normal, and the organic organisms thrived were bacteria and algae in almost equal proportions. Thus, the lower parts of silled marine basins account for the preservation of the organic matter.

12) Comparisons and correlations among biomarkers from bitumen extracts from the Lower Posidonia Shale and the Pantokrator Shale with those from solid bitumen from surficial oil/bitumen shows imply that these SRs may account for the solid bitumen in these seeps. More detailed, solid bitumens in Vassiliko and Petousi are

likely derived from the Pantokrator Shale or geochemically similar SRs (e.g., Triassic SR). Solid bitumen in Elataria has likely derived from the Lower Posidonia Shale. Interestingly, solid bitumen in Petousi and Elataria is found within the Lower Posidonia beds. This shows that the formation was the carrier bed (or part of the tertiary migration system) in the Petousi, whereas in Elataria the solid bitumen found likely in a primary migration stage, without having migrated outside the SR. These conclusions provide new valuable insights for the petroleum system function in Epirus.

13) The map of the Vigla Shale in Epirus is the first map of the formation outcrops publicly available, was composed with conjoint work of satellite imagery analysis and fieldwork.
14) The structural outline of the IZ in Epirus is characterized by the westward thrusts and blind-thrusts, and the eastward back-thrust mass movements. The main mechanically weak layer that decouples the deformation below and above it is the Triassic salt layer.
15) The tectonic analysis indicates that the main deformation event related to the continental collision between Adria plate and Eurasia plate accounts for the ENE-WSW-directed σ1 principal stress axis that is perpendicular to fold β-axes and thrust strikes. Moreover, the σ1 is related to the two main joint sets, being in the orientation of their bisector.
16) The cross-sections highlight the thickness variation of formations across the section. The correlation of the cross-sections indicates that several thrusts can be correlated indicating thrusting structures that exceed their mapped portions. Moreover, cross-section comparison suggests that some thrusts can be correlated to nearly vertical faults and/or backthrusts, suggesting that the structural style along a compression lineament may vary.
17) Evaluating three scenarios of SR burial [i.e., a) a basin with thick sedimentation or tectonic duplication of the stratigraphic column, b) a basin with thin sedimentation and c) an eroded Alpine structural high reburied by post-Alpine sedimentation], it was possible to estimate the HC phase per scenario and per each potential reservoir.

18) The main migration pathway (in lithology terms) for HCs produced from the Mesozoic source rocks is the generally vertical through the various limestone intervals while the sub-horizontal should be dominant below the clay-rich formations such as the Lower Posidonia Shale and, locally, the Vigla Shale. The regionally effective sub-horizontal migration pathway is the base of the flysch.

19) Concerning the geotectonic evolutionary scheme of the Ionian Zone it is suggested that it can be analyzed as follows: a) a (likely) prolonged stage (Permian-Early Triassic) where the IZ was part of the extensive passive margin of Gondwana, b) an initial rift event during Early-Middle Triassic related to the gradual opening of the Eastern Mediterranean oceanic basin and the detachment of the Greater Adria plate from Gondwana, c) a drifting stage that started in Middle-Late Triassic and related to the East Mediterranean ocean spreading which lasted up to Lower Jurassic, d) a Lower-Middle Jurassic rift rejuvenation that obliquely cut the southern passive margin of the Greater Adria plate, created the Ionian basin and allowed the water influx form the East Mediterranean ocean, e) a drifting phase of the entire Grater Adria plate and northward subduction during Early Cretaceous that resulted in slab pull in Early Senonian and a brief, minor rift rejuvenation, f) an Upper Senonian to Eocene phase that the Greater Adria plate continuously subducting below Eurasian plate, and, g) an Oligocene to Lower Miocene stage that the area became the flexural basin (foreland) area of the progressing orogenic front which progressively squeezed initiating the FTB developed and the basin inversion which is still ongoing in the westernmost parts of Epirus where the compression is still ongoing.

20) The Mesozoic Ionian basin constitutes an aulacogen (a failed-rift branch where the crustal separation was not completed) of the East Mediterranean Ocean, therefore a regional breakup unconformity is not possible to occur. Instead, it is suggested that all the Mesozoic unconformities are related to the emerged parts of the horst-graben or the half-graben geometry basins.

21) The salt tectonic model is proposed as an end-member model showing that all the scenarios concerning the tectonostratigraphic architecture and the associated petroleum geological implications are possible, independently from the rift model.

Ελληνική Περίληψη

«Συμβολή στην κατανόηση της γεωλογικής δομής και των πετρελαϊκών συστημάτων της Ηπείρου με συνδυασμό μεθόδων γεωλογίας πεδίου και οργανικής γεωχημείας»

Ιωάννης Αλεξανδρίδης

Ένα πλήθος ενδείξεων πετρελαίου στην Ήπειρο αποδεικνύει την ύπαρξη πετρελαϊκού συστήματος. Βασικός σκοπός της παρούσας διδακτορικής διατριβής είναι η κατανόηση της λειτουργίας αυτού του πετρελαϊκού συστήματος. Προς τον σκοπό αυτό πραγματοποιήθηκε εκτεταμένη και λεπτομερής έρευνα πεδίου σε όλη την Ήπειρο προκειμένου να επανεκτιμηθούν τα πετρελαιογεωλογικά στοιχεία με έμφαση στον χαρακτηρισμό των μητρικών πετρωμάτων με μεθόδους οργανικής γεωχημείας. Μελετήθηκαν πολλές εκατοντάδες τομές ως προς την λιθοστρωματογραφία και τη δομή τους ενώ συλλέχθηκαν και αναλύθηκαν δεκάδες δείγματα πιθανών μητρικών πετρωμάτων, επιτρέποντας μια ενοποιητική αναπαράσταση της λεκάνης και του πετρελαϊκού συστήματος. Ορισμένα αξιοσημείωτα αποτελέσματα περιλαμβάνουν α) την ανακάλυψη ενός νέου σχηματισμού, με χαρακτηριστικά μητρικού πετρώματος παγκοσμίου κλάσης (ήτοι οι σχίστες Παντοκράτορα), β) την ανάπτυξη μοντέλων τεκτονικής άλατος, γ) την σύνθεση λεπτομερούς στρωματογραφικής στήλης της Ηπείρου, δ) τον συσχετισμό επιφανειακών ενδείξεων πετρελαίου με γνωστούς μητρικούς σχηματισμούς, ε) την αναπαραστάσεις παλαιοπεριβαλλοντικών συνθηκών απόθεσης μητρικών σχηματισμών και στ) αναπαραστάσεις της λεκάνης. Συνεπώς, η διατριβή αυτή βελτιώνει σημαντικά την κατανόηση του γεωλογικού οικοδομήματος και της λειτουργίας του πετρελαϊκού συστήματος στην Ήπειρο.

ABSTRACT

"Contribution to the understanding of the geological structure and petroleum systems of Epirus with integration of field geology and organic geochemistry methods"

Ioannis Alexandridis

A multitude of oil seeps in Epirus proves the occurrence of a petroleum system. The core aim of the present doctoral thesis is to enhance the understanding regarding the function of this petroleum system. To that end, an extensive field-based study was meticulously carried out throughout Epirus to re-assess the petroleum-geological elements focusing on source rock characterization with organic geochemistry methods. Several hundreds of sections were studied in terms of lithostratigraphy and structure, while numerous potential source rock samples were collected and analyzed allowing for an integrated basin and petroleum system reconstruction. Some of the remarks of the study include a) the discovery of a new potential source rock exhibiting world-class source characteristics (i.e., the Pantokrator Shale), b) the development of salt-tectonic models, c) the construction of a detailed lithostratigraphic column for Epirus, d) the correlation of surficial oil shows to known sources, e) reconstructions of source rock paleoenvironmental depositional conditions and f) basin reconstructions. Hence, this thesis significantly improves the understanding of the geological structure and petroleum system function in Epirus.

References

Alexandridis, I., Georgakopoulos, A., 2020. A first-order approximative conceptual salt-tectonic model for the Ionian zone (NW Greece). In: AAPG Europe Regional Conference 2020 the Last 50 Years of Exploration in Europe and the Mediterranean: Lessons Learned for Future E&P Efforts AAPG. Athens, Greece.

Alexandridis, I., Georgakopoulos, A., Carvajal-Ortiz, H., Gentzis, T., Oikonomopoulos, I., 2021a. Source Rocks in Ionian Zone, western Greece. Discoveries and revisions from an outcrop study. In: Third EAGE Eastern Mediterranean Workshop. EAGE, pp. 1–3. https://doi.org/10.3997/2214-4609.202137019.

Alexandridis, I., Oikonomopoulos, I., Carvajal-Ortiz, H., Gentzis, T., Kalaitzidis, S., Georgakopoulos, A., Christanis, K., 2021b. Organic petrography, geochemistry, and sulfur speciation of a new potential Mesozoic source rock in Western Greece. Third EAGE Eastern Mediterranean Workshop. https://doi.org/10.3997/2214-4609.202137020.

Alexandridis, I., Oikonomopoulos, I. K., Carvajal-Ortiz, H., Gentzis, T., Kalaitzidis, S., Georgakopoulos, A. N., Christanis, K., 2022. Discovery of a new source-rock interval within the Pantokrator Formation, Ionian Zone, Western Greece: Insights from sulfur speciation and kinetics analyses. Marine and Petroleum Geology, 145, 105918. https://doi.org/10.1016/j.marpetgeo.2022.105918.

Alexandridis, I., Schwark, L. 2022b. Preliminary Results of a Biomarker Study of the Upper Triassic -Lower Jurassic Source Rocks in Ionian Zone, Epirus, NW Greece. Basin and depositional setting implications. In: 16th world congress of the Geological Society of Greece. ISBN: 978-960-98709-8-6, Vol. 10, pp. 728-729.

Alexandridis, I., Schwark, L., 2023a. Molecular geochemistry characterization of upper-Triassic to Toarcian source rocks in the Ionian Zone, Greece. IMOG 2023. https://doi.org/10.3997/2214-4609.202333022.

Alexandridis, I., Schwark, L., 2023c. Biomarkers in source-rock and solid bitumen in Epirus, Western Greece. Implications for oil-source correlations. Fourth EAGE Eastern Mediterranean Workshop. https://doi.org/10.3997/2214-4609.202330024.

Allen, P. A., Allen, J. R., 2013. Basin Analysis Principles and application to Petroleum Play Assessment. Wiley-Blackwell.

Alsop, G. I., Marco, S. 2014. Fold and fabric relationships in temporally and spatially evolving slump systems: A multi-cell flow model. Journal of Structural Geology, 63, 27–49. https://doi.org/10.1016/j.jsg.2014.02.007

ASTMD 7708, 2014. Standard Test Method for Microscopical Determination of the Reflectance of Vitrinite Dispersed in Sedimentary Rocks. ASTM International, West Conshohochen, PA. www.astm.org.

Auboin, J., Brunn, J. H., Celet ,P., Dercourt, J., Godfriaux, I., Mercier, J., 1963. Esquisse de la Geologie de la Grece: Livre Memoire Professeur Fallot, Memoires Societe geologique de France, p. 383-610.

Barrier, E., Vrielynck, B., Brouillet, J., Brunet, M., 2018. Paleotectonic Reconstruction of the Central Tethyan Realm. Tectonono-Sedimentary-Palinspastic maps from Late Permian to Pliocene. In: CCGM/CGMW, Paris. CCGM/CGMW Paris: France.

Baskin, D.K., Peters, K.E., 1992. Early generation characteristics of a sulfur-rich Monterey kerogen. AAPG (Am. Assoc. Pet. Geol.) Bull. 76, 1–13.

Behar, F., Vandenbroucke, M., 1987. Chemical modelling of kerogens. Organic Geochemistry, 11(1), 15–24. https://doi.org/10.1016/0146-6380(87)90047-7.

Behar, F., Beaumont, Y., De, B., Penteado, H.I., 2001. Rock-eval 6 technology: performances and developments. Oil and gas science and technology. Review nstitut Français du P´etrole Energ. Nouv. 56, 111–134.

Bertello, F., Fantoni, R., Franciosi, R., Gatti, V., Ghielmi, M., Pugliese, A., 2010. From thrust-and-fold belt to foreland: hydrocarbon occurrences in

Italy. Geological Society, London, Petroleum Geology Conference series 7 (1), 113–126.

Bohacs, K. M., Grabowski, G. J., Carroll, A. R., Mankiewicz, P. J., Miskell-Gerhardt, K. J., Schwalbach, J. R., Wegner, M. B., & Simo, J. A. 2005. Production, destruction, and dilution—the many paths to source-rock development. Deposition of Organic-Carbon-Rich Sediments: Models, 61–101. https://doi.org/10.2110/pec.05.82.0061.

Bosellini, A., Hsu, K. J., 1973. Mediterranean plate tectonics and Triassic palaeogeography. Nature, 244(5412), 144–146. https://doi.org/10.1038/244144a0.

Brune, S., Williams, S. E., Müller, R. D., 2018. Oblique rifting: The rule, not the exception. Solid Earth, 9(5), 1187–1206. https://doi.org/10.5194/se-9-1187-2018.

Callot, J.-P., Salel, J.-F., Letouzey, J., Daniel, J.-M., Ringenbach, J.-C., 2016. Three-dimensional evolution of salt-controlled minibasins: interactions, folding, and megaflap development. AAPG Bull. 100, 1419-1442. doi:10.1306/03101614087.

Casero, P., 2004. Structural setting of petroleum exploration plays in Italy. In: Crescenti, V., D'Offizi, S., Merlino, S., Sacchi, L. (Eds.), Geology of Italy, Special Volume of the Italian Geological Society for the IGC 32 Florence-2004, pp. 189–199.

Catalano, R., Doglioni, C., Merlini, S., 2001. On the mesozoic Ionian basin. Geophys. J. Int. 144, 49e64.

Curi, F., 1993. Oil generation and accumulation in the albanide Ionian basin. In: Spencer, A.M. (Ed.), Generation, Accumulation and Production of Europe's Hydrocarbons III, Special Publication of the European Association of Petroleum Geoscientists No.3. © Springer· Verlag Berlin Heidelberg.

Cooper, M., 2007. Structural style and hydrocarbon prospectivity in fold and Thrust Belts: A global review. Geological Society, London, Special

Publications, 272(1), 447–472. https://doi.org/10.1144/gsl.sp.2007.272.01.23.

Dembicki, H., 1992. The effects of the mineral matrix on the determination of kinetic parameters using modified rock eval pyrolysis. Organic Geochemistry, 18(4), 531–539. https://doi.org/10.1016/0146-6380(92)90116-f.

Dembicki Jr., H., 2009. Three common source rock evaluation errors made by geologists during prospect or play appraisals. American Association of Petroleum Geologists Bulletin 93, 341–356.

Dembicki, H.,2017. Practical petroleum geochemistry for exploration and production. Elsevier.

Dercourt, J., Zonenshain, L. P., Ricou, L.-E., Kazmin, V. G., Le Pichon, X., Knipper, A. L., Grandjacquet, C., Sbortshikov, I. M., Geyssant, J., Lepvrier, C., Pechersky, D. H., Boulin, J., Sibuet, J.-C., Savostin, L. A., Sorokhtin, O., Westphal, M., Bazhenov, M. L., Lauer, J. P., Biju-Duval, B., 1986. Geological evolution of the Tethys Belt from the Atlantic to the Pamirs since the lias. Tectonophysics, 123(1–4), 241–315. https://doi.org/10.1016/0040-1951(86)90199-x.

Dercourt, J., Gaetani, M., Vrielynck, B., 2000. Atlas Peri-Tethys Palaeogeographical Maps. CCGM.

Duffy, O.B., Dooley, T.P., Hudec, M.R., Jackson, M.P.A., Fernandez, N., Jackson, C.A.-L., Soto, J.I., 2018. Structural evolution of salt-influenced fold-and-thrust belts: a synthesis and new insights from basins containing isolated salt diapirs. J. Struct. Geol. 114, 206-221. doi:10.1016/j.jsg.2018.06.024.

Dunham, R. J., 1962. Classification of carbonate rocks according to depositional texture, in W. E. Ham, ed., Classification of Carbonate Rocks: AAPG Memoir 1, p. 108–121.

Energy Information Administration, 2015. Lower 48 States shale plays. http://www.eia.gov/oil_gas/rpd/shale_gas.pdf.

Finch, E., Gawthorpe, R., 2017. Growth and interaction of normal faults and fault network evolution in Rifts: Insights from three-dimensional discrete element modelling. Geological Society, London, Special Publications, 439(1), 219–248. https://doi.org/10.1144/sp439.23.

Flügel, E., 2009. Carbonate depositional environments. Microfacies of Carbonate Rocks, 7–52. https://doi.org/10.1007/978-3-642-03796-2_2.

Folk, R. L., 1959. Practical petrographic classification of limestones. AAPG Bulletin, v. 43, p. 1–38.

Fossen, H., 2010. Structural geology. Cambridge University Press.

Gawthorpe, R. L., Leeder, M. R., 2000. Tectono-sedimentary evolution of active extensional basins. Basin Research, 12(3–4), 195–218. https://doi.org/10.1046/j.1365-2117.2000.00121.x.

Gealey, W., 1988. Plate tectonic evolution of the Mediterranean-Middle East region. Tectonophysics 155, 285e306.

Gupta, S., Cowie, P. A., Dawers, N. H., Underhill, J. R., 1998. A mechanism to explain rift-basin subsidence and stratigraphic patterns through fault-array evolution. Geology, 26(7), 595. 10.1130/0091-7613(1998)026<0595:amterb>2.3.co;2.

Herodotus, 484–430 B.C. Histories: Book D, verse 195.

Hudec, M. R., & Jackson, M. P. A. (2007). Terra infirma: Understanding salt tectonics. Earth-Science Reviews, 82(1–2), 1–28. https://doi.org/10.1016/j.earscirev.2007.01.001.

Horsfield, B., Rullkotter, J., 1994. Diagenesis, catagenesis, and metagenesis of organic matter. In: Magoon, L.B., Dow, W.G. (Eds.), The Petroleum System–From Source to Trap, vol. 60. American Association of Petroleum Geologists Memoir, pp. 189–199.

IEA, 2023. World total energy supply by source, 1971-2019, IEA, Paris https://www.iea.org/data-and-statistics/charts/world-total-energy-supply-by-source-1971-2019, IEA. License: CC BY 4.0.

IEA, 2023. Global share of total energy supply by source, 1973, IEA, Paris https://www.iea.org/data-and-statistics/charts/global-share-of-total-energy-supply-by-source-1973-2, IEA. License: CC BY 4.0.

IEA, 2023. Global share of total energy supply by source, 2019, IEA, Paris https://www.iea.org/data-and-statistics/charts/global-share-of-total-energy-supply-by-source-2019, IEA. License: CC BY 4.0.

IGRS-IFP (Institut de Géologie et Recherches du Sous-sol Institut Français du Pétrole), 1966. Etude géologique de l'Epire (Grèce nord-occidentale): Technip eds., Paris, 306 p.

Ingersoll, R. V., 2011. Tectonics of sedimentary basins, with revised nomenclature. Tectonics of Sedimentary Basins, 1–43. https://doi.org/10.1002/9781444347166.ch1

Issler, D. R., Beaumont, C., 1989. A finite element model of the subsidence and thermal evolution of extensional basins: Application to the Labrador Continental margin. Thermal History of Sedimentary Basins, 239–267. https://doi.org/10.1007/978-1-4612-3492-0_14

Iso 7404-2, 2009. Methods for the Petrographic analysis of coal – Part 2: methods of preparing coal samples. In: International Organization for Standardization. ISO 7404-2: 2009(en). www.iso.org/standard/42798.html.

Iso 7404-5, 2009. Methods for the petrographic analysis of coal – Part 5: method of determining microscopically the reflectance of vitrinite. In: International Organization for Standardization. ISO 7404–5: 2009(en). www.iso.org/standard/4 2832.html.

Jackson, M. P. A., Talbot, C. J., 1991. A glossary of salt tectonics. Geological Circulars. https://doi.org/10.23867/gc9104d.

Jacob, H., 1989. Classification, structure, Genesis and practical importance of natural solid oil bitumen ("migrabitumen"). International Journal of Coal Geology, 11(1), 65–79. https://doi.org/10.1016/0166-5162(89)90113-4.

Jarvie, D.M., 1991. Total organic carbon (TOC) analysis. In: American Association of Petroleum Geologists Treatise of Petroleum Geology: Source and Migration Processes and Evaluation Techniques, pp. 113e118.

Johnson Ibach L., E. 1982. Relationship between sedimentation rate and total organic carbon content in ancient marine sediments. AAPG Bulletin, 66. https://doi.org/10.1306/03b59a5d-16d1-11d7-8645000102c1865d

Karakitsios, V., 1995. The influence of preexisting structure and halokinesis on organic matter preservation and thrust system evolution in the Ionian basin, northwest Greece. AAPG (Am. Assoc. Pet. Geol.) Bull. 79, 960–980.

Karakitsios, V., Rigakis, N. 1996. New oil source rocks cut in Greek Ionian basin. Oil & Gas Journal, 97(7), 56–59.

Karakitsios, V., Pomoni-Papaioannou, F., 1998. Sedimentological study of the Triassic solution-collapse Breccias of the Ionian zone (NW Greece). Carbonates Evaporites 13 (2), 207–218.

Karakitsios, V., 2003. Evolution and Petroleum Potential of the Ionian Basin (Northwestern Greece). International Conference & Exhibition, AAPG, p. 47.

Karakitsios, V., H. Tsikos, Y. van Breugel, I. Bakopoulos, L. Koletti, 2004. Cretaceous oceanic anoxic events in western continental Greece: Bulletin of the Geological Society of Greece, v. 34, no. 2, p. 846–855.

Karakitsios, V., and N. Rigakis, 2007, Evolution and petroleum potential of western Greece: Journal of Petroleum Geology, v. 30, no. 3, p. 197–218, doi:10.1111/j.1747-5457.2007.00197.x.

Karakitsios, V., 2013. Western Greece and ionian sea petroleum systems. AAPG (Am. Assoc. Pet. Geol.) Bull. 97, 1567–1595.

Karakitsios, V., Kvacek, Z., Mantzouka, D., 2015. The first plant megafossil in the early jurassic of Greece: brachyphyllum (coniferales) from the lower Posidonia beds (toarcian) in the ionian zone (NW Greece) and its palaeogeographic implications. Neues Jahrbuch Geol. Palaontol. Abhand. 278 (1), 79–94.

Katz, B., Dittmar, E., Ehret, G., 2000. A geochemical review of the carbonate source rocks in Italy. J. Petrol. Geol. 23 (4), 399–424.

Katz, B.J., Lin, F., 2021. Consideration of the limitations of thermal maturity with respect to vitrinite reflectance, Tmax, and other proxies. AAPG (Am. Assoc. Pet. Geol.) Bull. 105, 695–720.

Kazmin, V.G., Natapov, L.M. (Eds.), 1998. Paleogeographic Atlas of Northern Eurasia. Institute of Tectonics of Lithospheric Plates, Moscow (CD-ROM).

Kim, Y. -S., Sanderson, D. J., 2005. The relationship between displacement and length of faults: A Review. Earth-Science Reviews, 68(3–4), 317–334. https://doi.org/10.1016/j.earscirev.2004.06.003.

Kontakiotis, G., Moforis, L., Karakitsios, V., Antonarakou, A., 2020. Sedimentary Facies Analysis, Reservoir Characteristics and Paleogeography Significance of the Early Jurassic to Eocene Carbonates in Epirus (Ionian Zone, Western Greece). Journal of Marine Science and Engineering. 8(9):706. https://doi.org/10.3390/jmse8090706.

Le Pichon, X., Şengör, A. M. C., & İmren, C., 2019. A new approach to the opening of the Eastern Mediterranean Sea and the origin of the Hellenic subduction zone. part 1: The Eastern Mediterranean Sea. Canadian Journal of Earth Sciences, 56(11), 1119–1143. https://doi.org/10.1139/cjes-2018-0128.

Lewan M., D., 1987. Petrographic study of primary petroleum migration in the Woodford Shale and related rock units. In Migration of Hydrocarbons in Sedimentary Basins (ed. B. DOLIGEZ), pp. 113-130. I.F.P., Editions Technip, Paris.

Magoon, L.B., Dow, W.G., 1994. The petroleum system. In: Magoon, L.B., Dow, W.G. (Eds.), The Petroleum System—From Source to Trap, vol. 60. AAPG Memoir, pp. 3–24.

Makris, J., Papoulia, J., 2011. Velocity Modeling and Mapping of Sub-salt Structures in Sedimentary Basins of Western Greece Using Node Technology. 73rd EAGE Conference & Exhibition incorporating SPE EUROPEC 2011, Vienna, Austria, 23-26 May 2011.

Makris, J., Papoulia, J., 2019. Triassic Evaporites On- and Offshore Western Greece and their Significance in Hydrocarbon Exploration. Second EAGE Eastern Mediterranean Workshop 19-21 November 2019, Athens, Greece.

Maravelis, A., Koukounya, A., Tserolas, P., Pasadakis, N., Zelilidis, A., 2014. Geochemistry of upper miocene–lower Pliocene source rocks in the Hellenic Fold and thrust belt, Zakynthos island, ionian sea, western Greece. Mar. Petrol. Geol. 66, 217–230.

Marrett, R., Allmendinger, R. W. 1990. Kinematic analysis of fault-slip data. Journal of Structural Geology, 12(8), 973–986. https://doi.org/10.1016/0191-8141(90)90093-e.

Masini, E., Manatschal, G., Mohn, G., 2013. The Alpine Tethys rifted margins: reconciling old and new ideas to understand the stratigraphic architecture of magma-poor rifted margins. Sedimentology 60 (1), 174–196. https://doi.org/10.1111/sed.12017.

Mattavelli, L., Novelli, L., 1990. Geochemistry and habitat of the oils in Italy. AAPG (Am. Assoc. Pet. Geol.) Bull. 74, 1623–1639.

Mattavelli, L., Pieri, M., Groppi, G., 1993. Petroleum exploration in Italy: a review. Mar. Petrol. Geol. 10, 410–425. https://doi.org/10.1016/0264-8172(93)90044-S.

McKenzie, D., 1978. Some remarks on the development of sedimentary basins. Earth and Planetary Science Letters, 40(1), 25–32. https://doi.org/10.1016/0012-821x(78)90071-7.

Mello, U. T., Karner, G. D., Anderson, R. N., 1995. Role of salt in restraining the maturation of Subsalt Source Rocks. Marine and Petroleum Geology, 12(7), 697–716. https://doi.org/10.1016/0264-8172(95)93596-v.

Meyer, B.L., Nederlof, M.H., 1984. Identification of source rocks on wireline logs by density/resistivity and sonic transit time/resistivity crossplots. American Association of Petroleum Geologists Bulletin 68, 121e129.

Monopolis, D., Bruneton, A., 1982. Ionian Sea (western Greece): Its structural outline deduced from drilling and Geophysical Data. Tectonophysics, 83(3–4), 227–242. https://doi.org/10.1016/0040-1951(82)90020-8.

Morley, C. K., Jitmahantakul, S., von Hagke, C., Warren, J., Linares, F., 2021. Development of an intra-carbonate detachment during thrusting: The variable influence of pressure solution on deformation style, Khao Khwang fold and thrust belt, Thailand. Geosphere, 17(2), 602–625. https://doi.org/10.1130/ges02267.1.

Moscardelli, L., Wood, L., 2008. New Classification system for mass transport complexes in offshore Trinidad. Basin Research, 20(1), 73–98. https://doi.org/10.1111/j.1365-2117.2007.00340.x.

Nikolaou, K., 1986. Contribution to the knowledge of the Neogene, the geology of the Ionian and Pre-Apulian zone boundaries. In: Relation to the Petroleum Geology Observations in Strofades, Zakynthos and Kefallonia Islands. Doctoral thesis. University of Athens, Athens, Greece, p. 228.

Nikolaou, K. A., 2001. Origin and migration mechanism of the main hydrocarbon seeps in Western Greece [in Greek]. Bulletin of the Geological Society of Greece, 34(3), 1213–1219. https://doi.org/10.12681/bgsg.17185.

Palacas, J.G., D. Monopolis, C. A. Nicolaou, D. E. Anders, 1986. Geochemical correlation of surface and subsurface oils, western Greece, in D. Leythaeuser and J. Rullkotter, eds., Advances in organic geochemistry 1985: Organic Geochemistry, v. 10, p. 417–423, doi:10.1016/0146-6380(86)90041-0.

Papanikolaou, D., 2013. Tectonostratigraphic models of the Alpine terranes and subduction history of the Hellenides. Tectonophysics, 595–596, 1–24. https://doi.org/10.1016/j.tecto.2012.08.008.

Payton, A. Griffith, E.M., 2007. Marine Barite: Recorder of Variations in Ocean Export Productivity, Deep Sea Resources, Part II. Study of Oceanography, 54 (5-7): 687-705.

Peters, K.E., 1986. Guidelines for evaluating petroleum source rock using programmed pyrolysis. AAPG (Am. Assoc. Pet. Geol.) Bull. 70 (3), 318–329. https://doi.org/10.1306/94885688-1704-11d7-8645000102c1865d.

Peters, K.E., Moldowan, J.M., 1993. The Biomarker Guide, first ed. Prentice Hall, Englewood Cliffs, New Jersey, p. 363.

Peters, K.E., Cassa, M.R., 1994. Applied source rock geochemistry. The Petroleum System - from Source to Trap 93–120. January 1994.

Peron-Pinvidic, G., Manatschal, G., 2019. Rifted Margins: State of the art and future challenges. Frontiers in Earth Science, 7. https://doi.org/10.3389/feart.2019.00218.

Pieri, M., 2001. Italian petroleum geology. In: Vai, G.B., Martini, P.I. (Eds.), Anatomy of an Orogen. The Apennines and Adjacent Mediterranean Basins. Kluwer Academic, Dordrecht, pp. 533–549.

Prifti, I., Muska, K., 2013. Hydrocarbon occurrences and petroleum geochemistry of Albanian oils. Italian Journal of Geosciences 132 (2), 228–235.

Prifti, I., Mehmeti, N., Dauti, S., 2014. Petroleum system of east part of ionian zone in Albania. Online International Interdisciplinary Research Journal, {Bi-Monthly} ume- IV (III). ISSN2249-9598.

Rahman, H. M., Kennedy, M., Löhr, S., Dewhurst, D. N., 2017. Clay-Organic Association as a control on hydrocarbon generation in shale. Organic Geochemistry, 105, 42–55. https://doi.org/10.1016/j.orggeochem.2017.01.011.

Rahman, H. M., Kennedy, M., Löhr, S., Dewhurst, D. N., Sherwood, N., Yang, S., Horsfield, B., 2018. The influence of shale depositional fabric on the kinetics of hydrocarbon generation through control of mineral surface contact area on clay catalysis. Geochimica et Cosmochimica Acta, 220, 429–448. https://doi.org/10.1016/j.gca.2017.10.012.

Ramberg, H., 1963. Strain distribution and geometry of folds. Bulletin of the Geological Institution of the University of Uppsala 42: 1–20.

Ramsay, J. G., Huber, M. I., 1987. The Techniques of Modern Structural Geology. 2: Folds and Fractures. London: Academic Press.

Reston, T.J., 2005. Polyphase faulting during the development of the west Galicia rifted margin. Earth and Planetary Science Letters, 237, 561–576.

Rigakis, N., Karakitsios, V., 1998. The source rock horizons of the Ionian Basin (NW Greece). Mar. Petrol. Geol. 15, 593–617.

Rigakis, N., 1999. Contribution to stratigraphy research on wells and outcrops of the Alpine formations in Western Greece. In: Relation to the Petroleum Generation Efficiency of Their Organic Matter. Ph.D. Thesis, Athens University, p. 255.

Rigakis, N., Nikolaou, K., Marnelis, F., Pakos, Th, 2007. The utility of oil shows in the hydrocarbon exploration of western Greece. Bull. Geol. Soc. Greece 40, 959–971.

Rigakis, N., Karakitsios, V., Marnelis, F., Sotiropoulos, S., 2013. Geological solutions concluded by petroleum geochemical data in Western Greece. Bull. Geol. Soc. Greece 47 (4), 2131.

Rønnevik, C., H., 2015. Exploration strategy. Petroleum Geoscience, 639–651. https://doi.org/10.1007/978-3-642-34132-8_26.

Robertson, Alastair H., Mountrakis, D., 2006. Tectonic development of the Eastern Mediterranean Region: An introduction. Geological Society, London, Special Publications, 260(1), 1–9. https://doi.org/10.1144/gsl.sp.2006.260.01.01.

Robertson, A. H., 2007. Overview of tectonic settings related to the rifting and opening of Mesozoic ocean basins in the Eastern Tethys: Oman, Himalayas and eastern Mediterranean regions. Geological Society, London, Special Publications, 282(1), 325–388. https://doi.org/10.1144/sp282.15.

Ronov, A.B., 1958. Organic carbon in sedimentary rocks (in relation to the presence of petroleum). Geochemistry 5, 497e509.

Rowan, M.G., Giles, K.A., Hearon, T.E. IV, Fiduk, J.C., 2016. Megaflaps adjacent to salt diapirs. AAPG Bull. 100, 1723-1747. doi:10.1306/05241616009.

Sanei, H., 2020. Genesis of solid bitumen. Scientific Reports, 10(1). https://doi.org/10.1038/s41598-020-72692-2.

Schmid, S. M., Fügenschuh, B., Kounov, A., Maţenco, L., Nievergelt, P., Oberhänsli, R., Pleuger, J., Schefer, S., Schuster, R., Tomljenović, B., Ustaszewski, K., van Hinsbergen, D. J. J., 2020. Tectonic units of the Alpine Collision Zone between Eastern Alps and Western Turkey. Gondwana Research, 78, 308–374. https://doi.org/10.1016/j.gr.2019.07.005.

Scotese, C., 2016. Paleomap Paleoatlas for GPLATES and the paleodata plotter program. Geological Society of America Abstracts with Programs. https://doi.org/10.1130/abs/2016nc-275387.

Seifert, W., Moldowan, M.J., Demaison, G., 1984. Source correlation of biodegraded oils. Org. Geochem. 6, 633–643.

Sejdini, B., Constantinescu, P., Piperi, T., 1994. Petroleum exploration in Albania. In: Popescu, B. (Ed.), Hydrocarbons of Eastern Central Europe. Springer-Verlag, Heidelberg, pp. 1–28.

Shanmugam, G., 2020. Gravity flows: Types, definitions, origins, identification markers, and Problems. Journal of The Indian Association of Sedimentologists, 37(2), 61–90. doi: 10.51710/jias.v37i2.117.

Smith, A. G., Moores, E, M., 1974. The Hellenides, in Spencer, A. M., ed., Mesozoic-Cenozoic orogenic belts, data for orogenic studies: Geol. Soc. London Spec. Pub. 4, p. 159-185.

Spalluto, L., Moretti, M., Festa, V., Tropeano, M. 2007. Seismically-induced slumps in lower-Maastrichtian peritidal carbonates of the Apulian platform (southern Italy). Sedimentary Geology, 196(1–4), 81–98. https://doi.org/10.1016/j.sedgeo.2006.06.009.

Tissot, B. P., Welte, D. H., 1984. Petroleum Formation and occurrence. Springer.

Tsikos, H., et al., 2004. Organic carbon deposition in the Cretaceous of the Ionian basin, NW Greece: The Paquier Event (OAE1b) revisited: Geological Magazine, v. 141, no. 4, p. 401–416.

Underhill, J. R., 1988. Triassic evaporites and Plio-Quaternary diapirism in western Greece: Journal of the Geological Society, v. 145, p. 269–282, doi:10.1144/gsjgs.145.2.0269.

Underhill, J. R., 1989. Late Cenozoic deformation of the Hellenide foreland, western Greece: Geological Society of America Bulletin, v. 101, p. 613–634, doi:10.1130/0016-7606(1989)101<0613:LCDOTH>2.3.CO;2.

USGS 2000. US Geological Survey World Petroleum Assessment 2000-Description and Results. USGS Digital Data Series DDS-60 (CD ROMs).

Vakalas, I., Kokkalas, S., Konstantopoulos, P., Tzimeas, C., Kampolis, I., Tsiglifi, H., Pérez-Martin, R., Hernandez-Jiménez, P., Pita-Gutierrez, J. P., 2023. Implications of salt diapirism in syn-depositional architecture of a carbonate margin-to-edge transition: An example from Plataria Syncline, Ionian Zone, NW Greece. Applied Sciences, 13(12), 7043. https://doi.org/10.3390/app13127043.

van Hinsbergen, D. J. J., Torsvik, T. H., Schmid, S. M., Maţenco, L. C., Maffione, M., Vissers, R. L. M., Gürer, D., Spakman, W., 2020. Orogenic architecture of the Mediterranean region and kinematic reconstruction of its tectonic evolution since the Triassic. Gondwana Research, 81, 79–229. https://doi.org/10.1016/j.gr.2019.07.009.

Velaj, T., 1996. Triassic evaporitic role in the evolution of the Ionian Zone of Albanides. Proceedings. https://doi.org/10.3997/2214-4609.201409099.

Velaj, T., 2015. New ideas on the tectonic of the Kurveleshi Anticlinal Belt in Albania, and the perspective for exploration in its subthrust. Petroleum, 1(4), 269–288. DOI: 10.1016/j.petlm.2015.10.013.

Withjack, M. O., Schlische, R. W., Olsen, P. E., 2002. Rift-basin structure and its influence on sedimentary systems. Sedimentation in Continental Rifts, 57–81. https://doi.org/10.2110/pec.02.73.0057.

Zappaterra, E., 1994, Source rock distribution model of the peri-Adriatic region: AAPG Bulletin, v. 78, no. 3, p. 333–354.

ANNEX

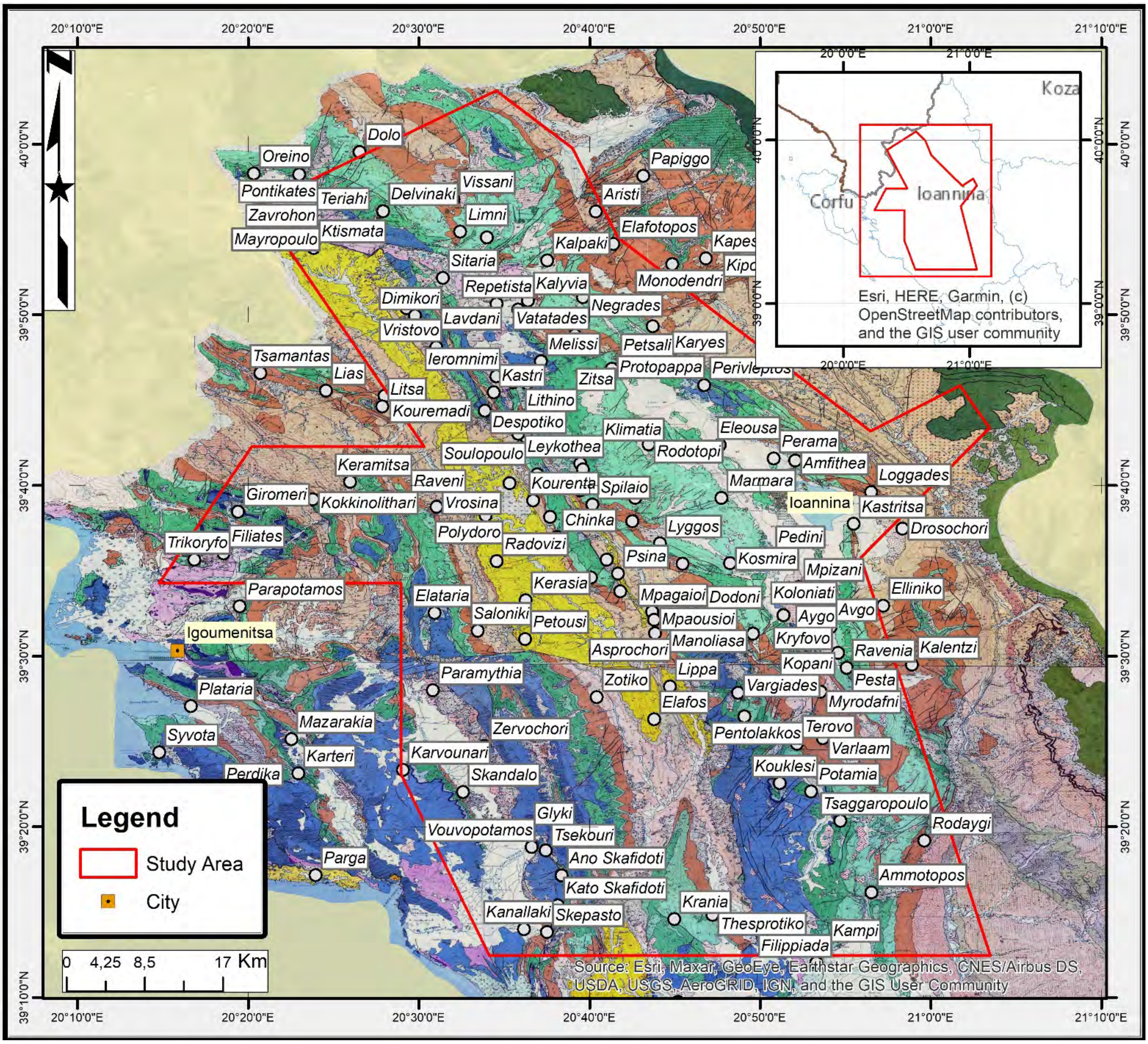

Geological Map of the study area (1/100000, IGRS-IFP, 1966) with the main villages and towns annotated.

Table of the locations where the photos of the lithostratigraphic formatioons of the section 4.1 were taken.

Figure		location	Figure		location	Figure		location
33	a	Botsara	42	a	Ieromnimi	52	a	Delvinaki
33	b	Rhadovizi	42	b	Frosyni	52	b	Rodotopi
33	c	Tyria	42	c	Ieromnimi	52	c	Mavronoros
33	d	Elafos	42	d	Kassidiaris	52	d	Ano Kouklesi
33	e	Kerasia	43	a	Ano Kouklesi	52	e	Ano Kouklesi
33	f	Zallongo	43	b	Ano Kouklesi	52	f	Ano Kouklesi
34	a	Syncline Epirus-Akarnania	43	c	Ano Kouklesi	53	a	Ano Kouklesi
34	b	Syncline Epirus-Akarnania	43	d	Ano Kouklesi	53	b	Mavronoros
34	c	Syncline Epirus-Akarnania	43	e	Ano Kouklesi	53	c	Ano Kouklesi
34	d	Syncline Epirus-Akarnania	44	a	Souli Mt	53	d	Ano Kouklesi
35	a	Syncline Epirus-Akarnania	44	b	Souli Mt	54	a	Koukoulioi
35	b	Syncline Epirus-Akarnania	44	c	Souli Mt	54	b	Souli Mt
36	a	Lyggos	44	d	Souli Mt	54	c	Koukoulioi
36	b	Linghiades	44	e	Rapio	54	d	Souli Mt
36	c	Saloniki	44	f	Souli Mt	54	e	Souli Mt
36	d	Syncline Epirus-Akarnania	45	a	Elataria	55	a	Paramythia
37	a	Kalentzi	45	b	Koukoulioi	55	b	Souli Mt
37	b1	Chrysorrachi	46	a	Souli Mt	55	c	Parga
37	b2	Saloniki	46	b	Souli Mt	55	d	Kefalovryso
37	c	Ravenia	46	c	Souli Mt	55	e	Kefalovryso
37	d	Syncline Epirus-Akarnania	47	a	Mavroudi	55	f	Kefalovryso
37	e	Saloniki	47	b	Mavroudi	55	g	Kefalovryso
37	f	Syncline Epirus-Akarnania	47	c	Mavroudi	55	h	Kefalovryso
38	a	Syncline Epirus-Akarnania	47	d	Mavroudi	56	a	Vrissela
38	b	Kokkinolithari	48	a	Elataria	57	a	Parapotamos
38	c	Keramitsa	48	b	Elataria	57	b	Igoumenitsa
38	d	Klimatia	49	a	Skandalo	57	c	Kryovrysi
38	e	Lippa	49	b	Ano Kouklesi	57	d	Delvinaki
38	f	Rodaygi	49	c	Ano Kouklesi	57	e	Igoumenitsa
39	a	Pentolakkos	49	d	Ano Kouklesi	57	f	Parga
39	b	Kastri	49	e	Karvounari	58	a	Ekklisia
39	c	Tsangaropoulo	49	f	Karvounari	58	b	Zallongo
40	a	Despotiko	50	a	Ano Kouklesi	58	c	Kryovrysi
40	b	Kourenta	50	b	Petousi	58	d	Alonaki
40	c	Linghiades	51	a	Lithino			
40	d	Kopani	51	b	Varlaam			
40	e	Kefalovryso	51	c	Mavronoros			
41	a	Konitsa	51	d	Mavronoros			
41	b	Elliniko	51	e	Mavronoros			
			51	f	Mavronoros			